frontiers | Research Topics

Metal homeostasis in microbial physiology and virulence

Edited by
José F. da Silva Neto, Mauricio H. Pontes and Charley Staats

Published in
Frontiers in Cellular and Infection Microbiology

ISSN 1664-8714
ISBN 978-2-8325-4264-4
DOI 10.3389/978-2-8325-4264-4

About Frontiers

Frontiers is more than just an open access publisher of scholarly articles: it is a pioneering approach to the world of academia, radically improving the way scholarly research is managed. The grand vision of Frontiers is a world where all people have an equal opportunity to seek, share and generate knowledge. Frontiers provides immediate and permanent online open access to all its publications, but this alone is not enough to realize our grand goals.

Frontiers journal series

The Frontiers journal series is a multi-tier and interdisciplinary set of open-access, online journals, promising a paradigm shift from the current review, selection and dissemination processes in academic publishing. All Frontiers journals are driven by researchers for researchers; therefore, they constitute a service to the scholarly community. At the same time, the *Frontiers journal series* operates on a revolutionary invention, the tiered publishing system, initially addressing specific communities of scholars, and gradually climbing up to broader public understanding, thus serving the interests of the lay society, too.

Dedication to quality

Each Frontiers article is a landmark of the highest quality, thanks to genuinely collaborative interactions between authors and review editors, who include some of the world's best academicians. Research must be certified by peers before entering a stream of knowledge that may eventually reach the public - and shape society; therefore, Frontiers only applies the most rigorous and unbiased reviews. Frontiers revolutionizes research publishing by freely delivering the most outstanding research, evaluated with no bias from both the academic and social point of view. By applying the most advanced information technologies, Frontiers is catapulting scholarly publishing into a new generation.

What are Frontiers Research Topics?

Frontiers Research Topics are very popular trademarks of the *Frontiers journals series*: they are collections of at least ten articles, all centered on a particular subject. With their unique mix of varied contributions from Original Research to Review Articles, Frontiers Research Topics unify the most influential researchers, the latest key findings and historical advances in a hot research area.

Find out more on how to host your own Frontiers Research Topic or contribute to one as an author by contacting the Frontiers editorial office: frontiersin.org/about/contact

Metal homeostasis in microbial physiology and virulence

Topic editors

José F. da Silva Neto — University of Sao Paulo, Brazil

Mauricio H. Pontes — The Pennsylvania State University, United States

Charley Staats — Federal University of Rio Grande do Sul, Brazil

Citation

da Silva Neto, J. F., Pontes, M. H., Staats, C., eds. (2024). *Metal homeostasis in microbial physiology and virulence*. Lausanne: Frontiers Media SA.

doi: 10.3389/978-2-8325-4264-4

Table of contents

frontiers | Frontiers in Cellular and Infection Microbiology

TYPE Editorial
PUBLISHED 22 March 2023
DOI 10.3389/fcimb.2023.1183137

OPEN ACCESS

EDITED AND REVIEWED BY
Thomas Rudel,
Julius Maximilian University of Würzburg, Germany

*CORRESPONDENCE
José F. da Silva Neto
jfsneto@usp.br
Charley C. Staats
staats@ufrgs.br
Mauricio H. Pontes
mpontes@pennstatehealth.psu.edu

SPECIALTY SECTION
This article was submitted to Bacteria and Host, a section of the journal Frontiers in Cellular and Infection Microbiology

RECEIVED 09 March 2023
ACCEPTED 14 March 2023
PUBLISHED 22 March 2023

CITATION
da Silva Neto JF, Staats CC and Pontes MH (2023) Editorial: Metal homeostasis in microbial physiology and virulence. *Front. Cell. Infect. Microbiol.* 13:1183137. doi: 10.3389/fcimb.2023.1183137

Editorial: Metal homeostasis in microbial physiology and virulence

José F. da Silva Neto[1]*, Charley C. Staats[2]* and Mauricio H. Pontes[3,4]*

[1]Departamento de Biologia Celular e Molecular e Bioagentes Patogênicos, Faculdade de Medicina de Ribeirão Preto, Universidade de São Paulo, Ribeirão Preto, Brazil, [2]Programa de Pós-Graduação em Biologia Celular e Molecular, Centro de Biotecnologia, Universidade Federal do Rio Grande do Sul, Porto Alegre, Brazil, [3]Department of Pathology and Laboratory Medicine, Penn State College of Medicine, Hershey, PA, United States, [4]Department of Microbiology and Immunology, Penn State College of Medicine, Hershey, PA, United States

KEYWORDS

transition metals, metal acquisition systems, metal efflux systems, nutritional immunity, siderophores, metalloregulators, bacterial and fungal virulence, iron homeostasis

Editorial on the Research Topic
Metal homeostasis in microbial physiology and virulence

Biological-relevant transition metals such as iron, zinc, manganese, and copper are at the center of a battle between pathogens and hosts, playing a major role in the outcome of bacterial and fungal infections. Hosts withhold metals from invading microbes or attempt to intoxicate them with metal overload. Microbes may employ numerous strategies to circumvent these host-imposed nutritional immunity mechanisms and ensure an appropriate metal supply for their physiological demands. In this Research Topic, a series of Review and Original Research Articles presents distinct facets of metal homeostasis in the context of microbe-host interactions.

Mycobacterium tuberculosis, one of the most important human pathogens, causes millions of tuberculosis cases worldwide. Rodriguez et al. provided an overview of the response of *M. tuberculosis* to changes in iron availability, emphasizing the relevance of iron to tuberculosis pathogenesis. The authors summarize the multiple mechanisms used by *M. tuberculosis* for iron uptake, focusing on the pathways involving the siderophores mycobactin and carboxymycobactin. The impact of iron limitation on many other aspects of *M. tuberculosis* physiology is also discussed, including upregulation of virulence factors, modification of the cell surface, increase of extracellular vesicle release, and metabolic switches toward quiescent, antibiotic tolerant states. Given the prominent role of iron for *M. tuberculosis* virulence, the authors suggest that key proteins involved in iron utilization could be new targets for therapeutic intervention. The Cornelissen group contributes two interesting Reviews on metal homeostasis in *Neisseria meningitidis* and *Neisseria gonorrhoeae*, two human-specific pathogens adapted to steal metals directly from host metal-binding proteins. Branch et al. provide a broad perspective of how these two pathogenic *Neisseria* that cause so distinct human diseases have evolved similar mechanisms to manage zinc, manganese, and copper in the context of human infections. The authors emphasize how the human host restricts these metals in the infection sites by increasing the

release of calprotectin and how the pathogenic *Neisseria* sense and respond to such alterations by expressing surface transporters that pirate zinc from calprotectin. The authors also discuss the emergent field of host-mediated metal intoxication in the context of *Neisseria* infections. Stoudenmire et al. present a focused review of how *N. gonorrhoeae*, the bacterium that causes gonorrhea, bypasses human nutritional immunity by utilizing iron from host metalloproteins. As a pathogen unable to synthesize its own siderophores, *N. gonorrhoeae* relies on multiple iron-regulated TonB-dependent transporters to steal iron directly from host proteins such as hemoglobin (HpuAB), transferrin (TbpA), and lactoferrin (LbpA).

Heme is an abundant iron reservoir in humans, and many pathogens can use heme from host hemoproteins like hemoglobin. de Lima et al. established that the ChuPRSTUV system is required for heme and hemoglobin utilization in *Chromobacterium violaceum*, a Gram-negative environmental bacterium that causes severe human infections. Using a mouse model of acute infection, the authors demonstrate that *C. violaceum* requires the combined activities of Chu and its siderophores to acquired iron and display full virulence. Interestingly, the authors also discovered that the ChuP protein regulates siderophore utilization, providing an integrated mechanism by which *C. violaceum* may control iron acquisition *via* siderophore and heme during infection. Unlike *C. violaceum*, the obligate human pathogen *Streptococcus pyogenes* prefers heme as an iron source. Lyles et al. investigated the role of the protein HupZ in the heme metabolism of *S. pyogenes*. They showed that HupZ binds heme, but it has a weak heme degradation activity, suggesting that this protein may function as a heme chaperone and/or detoxifying protein. Using a murine model of vaginal infection, the authors demonstrated that HupZ contributes to *S. pyogenes* colonization of the host.

Two Original Research Articles reported particular aspects of the host nutritional immunity in response to bacterial infection. Grubwieser et al. investigated how alveolar epithelial cells adapt their cellular iron homeostasis in response to *in vitro* infection by *Klebsiella pneumoniae* and *Escherichia coli*, two species that frequently cause hospital-acquired pneumonia. The authors found that the extracellular pathogen *E. coli* induces an iron retention phenotype in A549 cells. In contrast, infection by the facultative intracellular bacterium *K. pneumoniae* promotes an iron export phenotype. These findings suggest that human alveolar cells can employ distinct iron-based nutritional immunity mechanisms as a defense against invading pathogenic bacteria. Baishya et al. explored novel roles of calprotectin in the biofilms of *Pseudomonas aeruginosa* and *Staphylococcus aureus*, during growth in laboratory culture medium and in a mouse model of chronic wound infection. Whereas the innate immune protein calprotectin has been primarily studied in the context of its metal chelating activities, little is known about its metal-independent antimicrobial activity. Using a number of microscopy techniques, the authors found that calprotectin stimulates bacterial encapsulation in mesh-like structures, an effect that seems to be independent of calprotectin's ability to bind metals. These findings provide new clues about how calprotectin inhibits bacterial growth.

Metal homeostasis in the context of fungal-host interaction is the theme of two Original Research Articles. Souza et al. investigated the exoproteome of the fungus *Paracoccidioides brasiliensis* in response to iron deprivation by mass spectrometry. In previous works, the group has demonstrated that this human pathogen responds to iron deprivation by increasing production of siderophores and the activity of cell surface associated ferric reductases. In the current work, the authors identified 141 proteins, 64 of which were predicted to be secreted. The exoproteome data was validated by the demonstration that Cyb5 is a secreted iron-binding protein. Another important fungal pathogen, the airborne human mold *Aspergillus fumigatus*, has complex systems for maintaining copper homeostasis, which are required for *A. fumigatus* pathogenicity. Yap et al. reported that the availability of certain amino acids (especially histidine) and proteins increases resistance to copper in *A. fumigatus*. The authors provide several lines of evidence that the mechanism of protection involves histidine inhibition of low-affinity copper acquisition systems by extracellular copper complexation, and demonstrate that iron limitation decreases copper resistance. As copper resistance of *A. fumigatus* is crucial to its survival during infection, this work provides novel insights into how this pathogen may avoid nutritional immunity strategies that are imposed by the host.

This Research Topic sheds light on the complex mechanisms used by bacterial and fungal pathogens to scavenge essential metals from their hosts, as well as how the host can employ nutritional immunity to restrict access to these metals. By understanding such mechanisms, we will be able to develop new strategies to combat these pathogens and reduce the prevalence of diseases they cause.

Author contributions

JN, CS, and MP edited the topic and wrote the manuscript. All authors contributed to the article and approved the submitted version.

Conflict of interest

The authors declare that the research was conducted in the absence of any commercial or financial relationships that could be construed as a potential conflict of interest.

Publisher's note

frontiers | Frontiers in Cellular and Infection Microbiology

ORIGINAL RESEARCH
published: 22 April 2022
doi: 10.3389/fcimb.2022.847846

Ambient Availability of Amino Acids, Proteins, and Iron Impacts Copper Resistance of *Aspergillus fumigatus*

Annie Yap[1], *Heribert Talasz*[2], *Herbert Lindner*[2], *Reinhard Würzner*[3] *and Hubertus Haas*[1]*

[1] Institute of Molecular Biology, Biocenter, Medical University of Innsbruck, Innsbruck, Austria, [2] Protein Micro-Analysis Facility, Institute of Medical Biochemistry, Biocenter, Medical University of Innsbruck, Innsbruck, Austria, [3] Institute of Hygiene and Medical Microbiology, Department of Hygiene, Microbiology, and Public Health, Medical University of Innsbruck, Innsbruck, Austria

The transition metals iron and copper are required by virtually all organisms but are toxic in excess. Acquisition of both metals and resistance to copper excess have previously been shown to be important for virulence of the most common airborne human mold pathogen, *Aspergillus fumigatus*. Here we demonstrate that the ambient availability of amino acids and proteins increases the copper resistance of *A. fumigatus* wild type and particularly of the Δ*crpA* mutant that lacks export-mediated copper detoxification. The highest-protecting activity was found for L-histidine followed by L-asparagine, L-aspartate, L-serine, L-threonine, and L-tyrosine. Other amino acids and proteins also displayed significant but lower protection. The protecting activity of non-proteinogenic D-histidine, L-histidine-mediated growth inhibition in the absence of high-affinity copper uptake, determination of cellular metal contents, and expression analysis of copper-regulated genes suggested that histidine inhibits low-affinity but not high-affinity copper acquisition by extracellular copper complexation. An increase in the cellular copper content was found to be accompanied by an increase in the iron content, and, in agreement, iron starvation increased copper susceptibility, which underlines the importance of cellular metal balancing. Due to the role of iron and copper in nutritional immunity, these findings are likely to play an important role in the host niche.

Keywords: fungi, molds, *Aspergillus fumigatus*, copper, toxicity, amino acids, histidine, iron

OPEN ACCESS

Edited by:
Charley Staats,
Federal University of Rio Grande do Sul, Brazil

Reviewed by:
Val Culotta,
Johns Hopkins University, United States
Alexandre Melo Bailao,
Universidade Federal de Goiás, Brazil

***Correspondence:**
Hubertus Haas
hubertus.haas@i-med.ac.at

Specialty section:
This article was submitted to Bacteria and Host, a section of the journal Frontiers in Cellular and Infection Microbiology

Received: *03 January 2022*
Accepted: *23 March 2022*
Published: *22 April 2022*

Citation:
Yap A, Talasz H, Lindner H, Würzner R and Haas H (2022) Ambient Availability of Amino Acids, Proteins, and Iron Impacts Copper Resistance of Aspergillus fumigatus. Front. Cell. Infect. Microbiol. 12:847846. doi: 10.3389/fcimb.2022.847846

INTRODUCTION

The mold *Aspergillus fumigatus*' arsenal of nutrient-acquiring mechanisms allows its survival in the environment and diverse host niches, which makes this opportunistic pathogen the major cause of invasive pulmonary aspergillosis in immunocompromised patients worldwide (Latgé and Chamilos, 2019). In particular, the redox-active metals iron (Fe) and copper (Cu) have been previously shown to be important for its survival and virulence (Gerwien et al., 2018; Raffa et al., 2019; Misslinger et al., 2021). On the one hand, the redox potential makes Cu an excellent cofactor for many enzymes such as cytochrome oxidase (CoxB), superoxide dismutase (SodA), or laccases such as ferroxidase

(FetC), which is involved in reductive Fe assimilation (Oberegger et al., 2000; Blatzer et al., 2011; Anabosi et al., 2021). On the other hand, the very same redox potential of Cu can result in toxicity as Cu catalyzes the formation of reactive oxygen species (ROS) *via* Fenton-like chemistry or cause mismetallation such as displacement of Fe in Fe–sulfur cluster-containing enzymes leading to their inactivation (Gerwien et al., 2018; Raffa et al., 2019).

Owing to this toxicity, Cu has been used for centuries in different chemical combinations as an antimicrobial agent against plant pathogens, as "self-sanitizing" Cu-alloy surfaces to prevent nosocomial infections, or as ointments to treat superficial infections of animals and humans (Festa and Thiele, 2011; Besold et al., 2016). Remarkably, Cu toxicity is also employed by the mammalian innate immune system to fight invading pathogens because massive amounts of Cu are pumped into the phagolysosome to support killing of phagocytosed pathogens (Gerwien et al., 2018).

Maintenance of Cu homeostasis in *A. fumigatus*, which has to ensure sufficient Cu supply in combination with avoidance of Cu toxicity, is based on a sophisticated transcriptional regulation. During Cu limitation, the Cu-sensing transcription factor Mac1 activates high-affinity Cu uptake mediated by the Ctr family members CtrA2 and CtrC (Park et al., 2014; Cai et al., 2017; Kusuya et al., 2017; Wiemann et al., 2017). Consequently, inactivation of Mac1 causes a growth defect under Cu limitation. On the other hand, the Cu excess-sensing transcription factor AceA activates Cu detoxification mediated mainly by cellular Cu export *via* the P-type ATPase CrpA (Wiemann et al., 2017; Cai et al., 2018). Consequently, inactivation of either AceA or CrpA increases the susceptibility of *A. fumigatus* to Cu. Both Mac1 and AceA have been shown to be important for *A. fumigatus* pathogenicity (Cai et al., 2017; Wiemann et al., 2017; Cai et al., 2018).

Mac1 was reported to also play a role in Fe regulation in *A. fumigatus* (Park et al., 2018), which could not be confirmed by us (Yap et al., 2020). In the latter study, we noticed that the nitrogen source used in the growth medium influences Cu resistance, i.e., Cu resistance was higher with glutamine (Gln) compared to nitrate. The aim of this study was thus to analyze the impact of nitrogen sources and ambient availability of amino acids (AAs), proteins, and Fe on Cu resistance.

MATERIALS AND METHODS

Fungal Strains and Growth Conditions

If not otherwise stated, the *A. fumigatus* strain used was A1160, termed wild type (wt) here, and derived mutant strains Δ*mac1* (lacking Mac1), ΔaceA (lacking Ace1), and Δ*crpA* (lacking CrpA), which have been described previously (Cai et al., 2017; Cai et al., 2018). Furthermore, *A. fumigatus* strains Afs35 (a Ku70 lacking a derivative of the clinical isolate D141) (Krappmann et al., 2006), the clinical isolate Af293 (Nierman et al., 2005), Afs77 (a Ku70 lacking a derivative of the clinical isolate ATCC46645), and the Afs77-derived Δ*cccA* (Gsaller et al., 2012) and Δ*sidA* (Schrettl et al., 2004) mutant strains were used. The strains were grown at 37°C either on solid complex media (CM) or on/in solid/liquid Aspergillus minimal media (AMM) according to Pontecorvo et al. (1953) with 0.03 mM $FeSO_4$ as Fe source (unless otherwise noted), 1% glucose as carbon source, and the nitrogen source described in the respective experiment. The Cu ($CuSO_4$) concentration used is described in the respective experiments. For limitation of Cu or Fe, addition of the respective metal was omitted. CM contained 1% glucose, 2 g/l peptone (Carl Roth GmbH + Co. KG, Karlsruhe, S.T.U, Germany), 1 g/l casamino acids (Sigma-Aldrich Chemical Co., St. Louis, MO, USA), 1 g/l yeast extract (Lab M Limited, Bury, Lancs, UK), and trace elements according to Pontecorvo et al. (1953) but without Cu and Fe. Amino acid (AA) supplements are described in the respective experiment; if not noted otherwise, AAs were used in the L-configuration and were not denominated "L." The nitrogen sources used were 20 mM ammonium (ammonium tartrate dibasic, $(NH_4)_2C_4H_4O_6$), 20 mM Gln, 20 mM nitrate (sodium nitrate, $NaNO_3$), 20 mM nitrite (sodium nitrite, $NaNO_2$), and 20 mM urea. For plate growth assays, 1×10^4 conidia were point-inoculated; AMM plates were incubated for 48 h at 37°C, and CM plates were incubated for 30 h at 37°C. For culturing in liquid medium, 100 ml AMM in 0.5-l Erlenmeyer flasks inoculated with 10^6/ml conidia was shaken at 200 rpm at 37°C for 24 h. Bovine serum albumin and bovine pancreatic RNase A were from Sigma-Aldrich Chemical Co., St. Louis, MO, USA.

Quantification of Cellular Cu and Fe Contents

The mycelia from liquid cultures were harvested by filtration, washed with distilled water, and freeze-dried to determine the dry weight of the biomass. For determination of the total cellular Fe content, 50 mg of freeze-dried mycelia was decomposed in closed polytetrafluorethylene vessels containing 2 ml of HNO_3 and 0.5 ml of hydrogen peroxide using a high-performance microwave digestion unit (MARS 6, CEM Microwave Technology, Buckingham, UK). Appropriate dilutions were made with distilled water, and the total contents in Cu and Fe were determined by graphite furnace atomic absorption spectrometry (Zeeman GF95Z M6 AAS, Thermo Fisher Scientific, Waltham, MA, USA) according to standard methods.

Northern Analyses

Total RNA was isolated according to the TRI Reagent (Sigma-Aldrich) method using peqGOLD PhaseTrap reaction tubes (PEQLAB, Erlangen, Germany). Formaldehyde-containing agarose gels were used to separate 10 µg of total RNA before blotting onto Hybond-N+ membranes (Amersham Biosciences, Amersham, UK) and hybridization with digoxigenin (Roche Diagnostics GmbH, Mannheim, Germany)-labeled probes. The digoxigenin-labeled hybridization probes used in this study were generated by PCR using primers 5′-ATGCGAACGAAC ATTGTCCC and 5′-CCAGCGGAAATGAGAAGATTCA for *crpA* (AfuA_3G12740), 5′-ATGGATCATATGAGCCAC and 5′-CTACCCGCAGCATTTG for *ctrC* (AfuA_2G03730), 5′-AAGCC

GAGAAAAAGGGGG and 5′-AACCCGATGAA GCCCAG for *mirB* (AfuA_3G03640), 5′-ATATGTTCCTCGTGCCGTTC and 5′-CCTCAGTGAACTCCATCTC for *tubA* (Afu1g10910), 5′-GGAGCAGCTCGATCGCCAT and 5′-AGTGTATGCCACCAT CGTTG for *atm1* (AFUA_6G12870), and 5′-CCCGTCTTCCAC CTGCTG and 5′-GCATCAACAGCGCTGACCTT for *atm1* (AFUA_4G04318).

RESULTS

Cu Resistance of *A. fumigatus* Is Influenced by the Nitrogen Source Used

We observed that the Cu resistance of *A. fumigatus* wt is higher with 20 mM Gln compared to 20 mM nitrate as nitrogen source (**Figure 1A**): *A. fumigatus* A1160/*Δku80*, which is termed wild type (wt) here, displayed similar radial growth on solid media in the presence of 0.1 and 0.01 mM Cu as well as under Cu limitation with Gln as nitrogen source, while its radial growth decreased with increasing Cu concentration with nitrate as nitrogen source. Notably, Cu limitation is reflected by the yellow color of conidia, as biosynthesis of the green conidial pigment is dependent on a Cu-requiring laccase (Tsai et al., 1999). These results suggested that either glutamine protects against Cu toxicity and/or that nitrate enhances Cu toxicity. To test the latter hypotheses, we analyzed the impact of different nitrogen sources on Cu resistance of *A. fumigatus* (**Figure 1B**). To increase the sensitivity of the growth assay, we used not only *A. fumigatus* wt but also mutant strains that have increased susceptibility to Cu-mediated toxicity due to lacking transcriptional activation of Cu detoxification (*ΔaceA*, lacking the transcription factor AceA) or cellular Cu export (Δ*crpA*, lacking the Cu exporter CrpA), respectively (Raffa et al., 2019). The *ΔaceA* and Δ*crpA* mutant strains were able to grow in the presence of 0.1 mM Cu when using the nitrogen source Gln or Gln in combination with nitrate or nitrite. In contrast, the *ΔaceA* and Δ*crpA* mutant strains were unable to grow in the presence of 0.1 mM Cu with nitrate, nitrite, ammonium, or urea as nitrogen source. Moreover, *ΔaceA* and Δ*crpA* displayed significantly decreased growth compared to wt in the presence of 0.01 mM Cu in the absence of Gln. Taken together, these data indicate that the presence of Gln protects against Cu toxicity. In contrast to the other nitrogen sources used, the growth of wt decreased with nitrate and nitrite in the presence of 0.1 mM Cu compared to 0.01 mM Cu, which indicates that nitrate and nitrite might decrease Cu resistance.

Supplementation With Different AAs Protects *A. fumigatus* Δ*crpA* Against Cu Toxicity to a Different Degree

As Gln is an AA and as some AAs are well known for providing the ligands for metal binding in proteins (Cao et al., 2017), we analyzed the impact of supplementation with different proteinogenic AAs in a concentration of 1 mM on Cu resistance of *A. fumigatus* (**Figure 2**). Therefore, *A. fumigatus* wt and Δ*crpA* strains were grown on AMM plates containing 0.1 mM Cu and ammonium as nitrogen source, which impedes the growth of Δ*crpA* (**Figure 1**). Only supplementation with 1 mM asparagine (Asn), aspartate (Asp), histidine (His), serine (Ser),

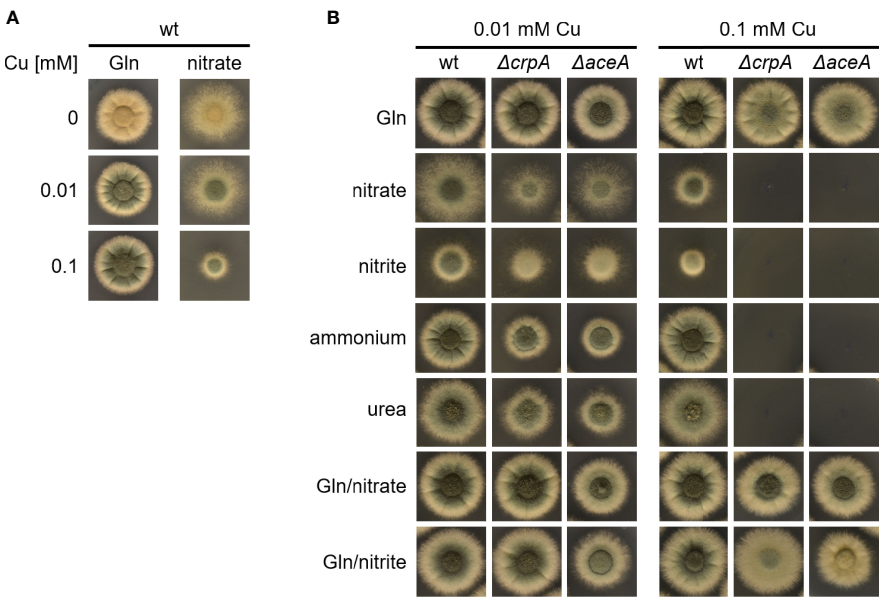

FIGURE 1 | Gln protects *A. fumigatus* against Cu toxicity. **(A)** *A. fumigatus* wt conidia were point-inoculated on solid AMM containing 0, 0.01, or 0.1 mM Cu with either Gln or nitrate as nitrogen source. **(B)** To analyze the effect of the nitrogen source on Cu resistance, *A. fumigatus* wt, Δ*crpA*, and Δ*aceA* conidia were point-inoculated on solid AMM containing either 0.01 or 0.1 mM Cu in combination with different nitrogen sources (in case of combination of two nitrogen sources, the same concentration of each was used).

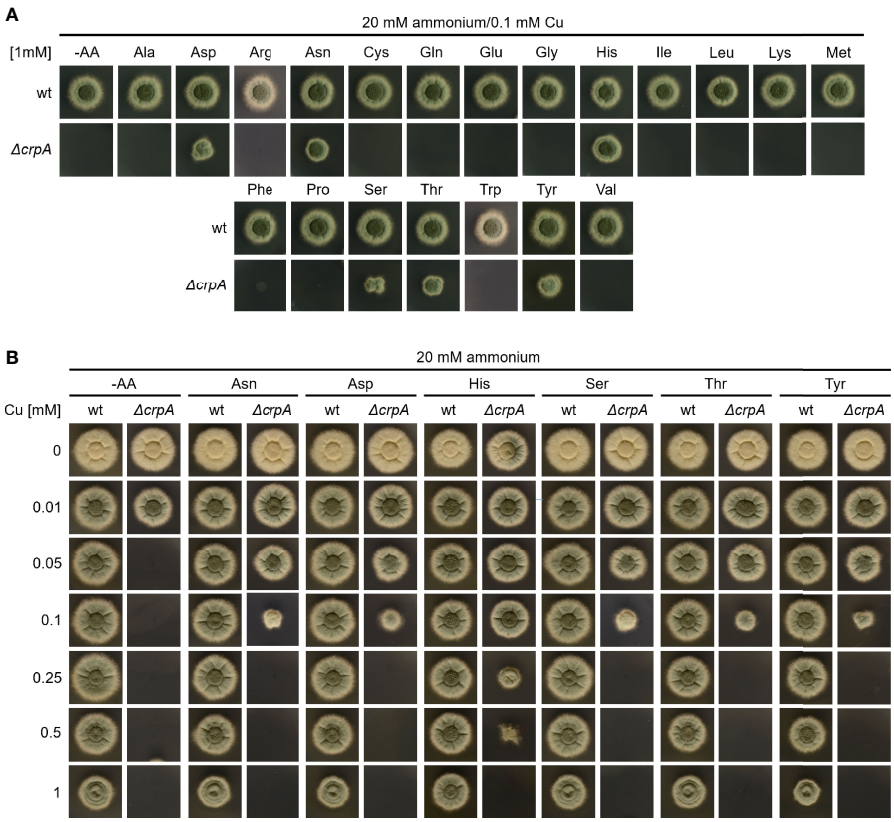

FIGURE 2 | Supplementation with Asn, Asp, Ser, Thr, Tyr, and particularly His protects *A. fumigatus* Δ*crpA* against Cu toxicity to a higher degree compared to other AAs. *A. fumigatus* wt and Δ*crpA* conidia were point-inoculated on solid AMM containing 20 mM ammonium as nitrogen source. **(A)** The growth medium contained 0.1 mM Cu and was supplemented with 1 mM of the different AAs indicated (arginine, Arg; cysteine, Cys; glutamate, Glu; glycine, Gly; isoleucine, Ile; leucine, Leu; lysine, Lys; methionine, Met; phenylalanine, Phe; proline, Pro; tryptophane, Trp; valine, Val); -AA was without AA supplementation. **(B)** The growth medium contained 1 mM of the indicated AA and the different Cu concentrations indicated.

threonine (Thr), or tyrosine (Tyr) rescued the growth of the Δ*crpA* mutant strain, indicating that these six AAs have a higher Cu-detoxifying capacity compared to the other tested AAs such as Gln (**Figure 2A**). In order to identify possible differences in the Cu detoxification activity of these six AAs, we analyzed the growth of *A. fumigatus* wt and Δ*crpA* strains on media containing ammonium as nitrogen source, 1 mM of the respective AA, and different Cu concentrations up to 1 mM (**Figure 2B**). Supplementation with Asn, Asp, Ser, Thr, and Tyr rescued the growth of the Δ*crpA* mutant strain up to 0.1 mM Cu and with His up to 0.5 mM Cu demonstrating that His has the strongest protecting activity against Cu. Notably, the growth of wt was significantly decreased in the presence of 1 mM Cu compared to low Cu concentrations and exclusively His supplementation improved the radial growth of wt at this Cu concentration (**Figure 2B**).

In a next step, we compare the Cu-detoxifying activity of Gln and His. Determination of the AA concentration that is required to permit the growth of Δ*crpA* in AMM with ammonium as nitrogen source and 0.1 mM Cu yielded 5 mM Gln and 0.2 mM His (**Figure 3A**), which underlines the difference of a low- and high-protecting AA. Moreover, determination of the Cu detoxification capacity of 20 mM Gln, the standard nitrogen source used in our laboratory, yielded 0.5 mM Cu (**Figure 3B**).

Taken together, His showed the highest Cu-detoxifying capacity with an about twofold molar excess, i.e., supplementation with 1 mM His allowed the growth of Δ*crpA* in the presence of a maximum of 0.5 mM Cu (**Figure 2B**) and 0.2 mM His permitted the growth of Δ*crpA* in the presence of 0.1 mM Cu, respectively (**Figure 3A**). Asn, Asp, Ser, Thr, and Tyr detoxified Cu in an approximately 10-fold molar excess, i.e., 1 mM supplementation with either of these AAs allowed the growth of Δ*crpA* in the presence of a maximum of 0.1 mM Cu (**Figure 2B**). Gln detoxified Cu in an approximately 40–50-fold molar excess, i.e., 5 mM Gln was required to allow the growth of Δ*crpA* in the presence of 0.1 mM Cu (**Figure 3A**) and 20 mM Gln allowed the growth of Δ*crpA* in the presence of a maximum of 0.5 mM Cu (**Figure 3B**).

Due to the Cu-detoxifying activity of AAs, we analyzed the Cu resistance of *A. fumigatus* wt and Δ*crpA* strains in complex medium (CM), which contains 0.2% peptone, 0.1% casamino acids, and 0.1% yeast extract. This medium allowed the growth of

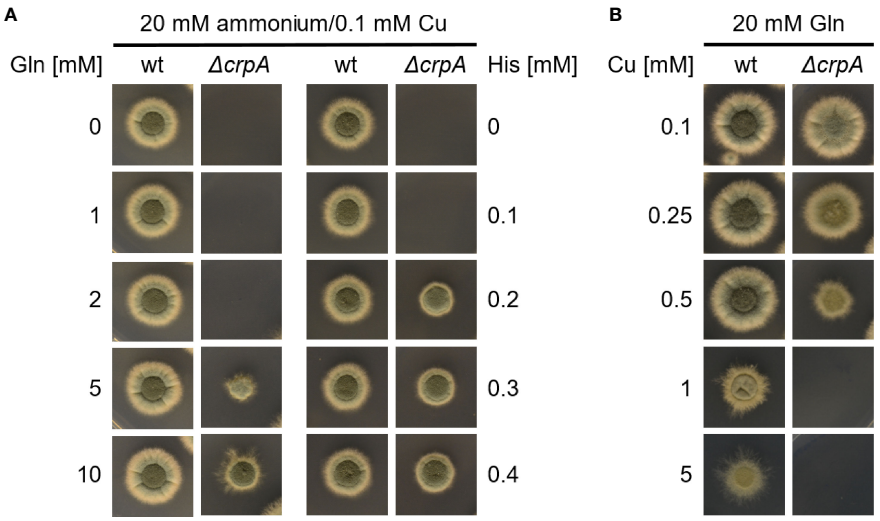

FIGURE 3 | Supplementation with His protects *A. fumigatus* Δ*crpA* against Cu toxicity to a higher degree compared to Gln. *A. fumigatus* wt and Δ*crpA* conidia were point-inoculated on solid AMM. **(A)** The growth medium contained 20 mM ammonium as nitrogen source, 0.1 mM Cu, and different concentrations of either Gln (left) or His (right). The plate assay without Gln (0 mM Gln) is the same as the one without His (0 mM His). **(B)** The growth medium contained 20 mM Gln as nitrogen source and different concentrations of Cu.

Δ*crpA* in the presence of a maximum of 0.5 mM Cu (**Figure 4**), which demonstrates its Cu-detoxifying activity. Each of the ingredients added to AMM with ammonium as nitrogen source improved the Cu resistance of Δ*crpA*, i.e., it allowed the growth of this mutant in the presence of up to 0.2 mM Cu (**Figure 4**). As these CM ingredients are not chemically defined components including AAs and peptides, we assayed in a next step the impact of a defined protein using bovine serum albumin (BSA). BSA supplementation to a final concentration of 0.1 mM also increased the Cu resistance of Δ*crpA* and allowed the growth of this mutant in the presence of up to 0.2 mM Cu (**Figure 4**). BSA consists of 583 AA residues, and consequently 0.1 mM BSA corresponds to 58.3 mM peptidic AAs. Therefore, at the level of AA molarity, BSA has a lower protecting activity compared to free AAs as 20 mM of the weakly protecting AA Gln allowed the growth of Δ*crpA* in the presence of up to 0.5 mM Cu (**Figure 3B**). Similar to BSA, supplementation with 0.47 mM RNase A, which consists of 124 AA residues and therefore corresponds to 0.1 mM BSA with respect to peptidic AA, allowed the growth of Δ*crpA* in the presence of up to 0.2 mM Cu, which underlines that the Cu resistance-promoting effect is a protein effect rather than being specific on the type of protein. Notably, the influence of proteins on Cu resistance might be influenced by proteolytic degradation of the proteins, but in the experiments conducted, proteolysis is expected to be low due to the presence of primary nitrogen (ammonium) and carbon (glucose) sources, which usually

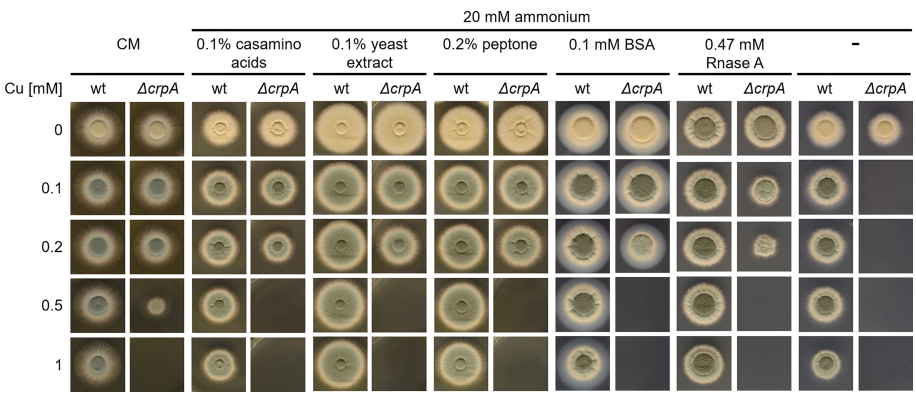

FIGURE 4 | The complex medium ingredients casamino acids, yeast extract, and peptone as well as proteins protect *A. fumigatus* Δ*crpA* against Cu toxicity. *A. fumigatus* wt and Δ*crpA* conidia were point-inoculated on solid CM or AMM with ammonium as nitrogen source and supplemented with 0.1% casamino acids, 0.1% yeast extract, 0.2% peptone, or 0.1 mM BSA and different Cu amounts. The CM plates were incubated for 30 h at 37°C and the AMM plates for 48 h at 37°C.

repress the expression of protease-encoding genes (Bergmann et al., 2009; Shemesh et al., 2017).

His Supplementation Protects Against Cu Toxicity by Inhibiting Cu Uptake

To investigate the mechanism of how His supplementation protects *A. fumigatus* Δ*crpA* against Cu toxicity, we compared the protecting activity of His (L-His) and its non-proteinogenic stereoisomer D-His. As shown in **Figure 5A**, supplementation with L- and D-configurations of His resulted in similar Cu resistance, which indicates that the mode of protection conferred by His supplementation does not involve metabolization of His. Therefore, we hypothesized that His protects against Cu toxicity by extracellular chelation of Cu. In line, His supplementation was found to hamper the growth of the *A. fumigatus* Δ*mac1* mutant strain in a concentration-dependent manner under Cu-limiting conditions as well as in the presence of 0.02 mM Cu (**Figure 5B**). These data indicate that the presence of His negatively affects Cu uptake in the absence of high-affinity Cu uptake as Mac1 is essential for the activation of high-affinity Cu uptake (Raffa et al., 2019). In agreement, the growth of wt that is capable of high-affinity Cu uptake was not affected by His supplementation (**Figure 5B**).

To further investigate the impact of AA supplementation on metal homeostasis, we analyzed the cellular contents in Cu and Fe (**Table 1**). Therefore, *A. fumigatus* wt and Δ*crpA* strains were grown in liquid AMM containing 0.005 mM Cu and 20 mM ammonium as nitrogen source without AAs or supplemented with either 5 mM Gln or 1 mM His. The biomass production of wt was similar in all three growth media. In agreement with the Cu susceptibility of Δ*crpA* and the different Cu-detoxifying capacities of His and Gln, biomass of Δ*crpA* was only 22% of that of the wt in AMM without AAs, increased to 74% with Gln supplementation, and reached the wt level with His supplementation (**Table 1**). The cellular Cu content of wt was similar in AMM without AAs and with Gln but was approximately halved in the presence of His. In agreement with defective Cu export, the cellular Cu content of Δ*crpA* was increased about five-fold in the absence of AAs. Supplementation with His and Gln decreased the cellular Cu content to about that of the wt grown under the same condition (**Table 1**). Taken together, these data indicate that supplementation with AAs such as His and Gln protects *A. fumigatus* against Cu toxicity by impeding its cellular uptake, most likely *via* complexation of this metal. Remarkably, the about five-fold increase in cellular Cu of Δ*crpA* was accompanied by an approximately 10-fold increased Fe content (**Table 1**), which indicates a link between Cu and Fe homeostasis.

The experiments discussed above demonstrate the protective effects of AAs against Cu toxicity mainly for the highly Cu-susceptible Δ*crpA* mutant strain. As shown in **Figure 6A**, His supplementation also increases the radial growth of different *A. fumigatus* strains including the genetic background strain of the Δ*crpA* mutant, A1160, termed wt here. To further investigate the role of His in protection against Cu toxicity, we analyzed the expression of Cu-detoxifying ABC transporter-encoding *crpA* and high-affinity Cu uptake permease *ctrC* by Northern blot analysis (**Figure 6B**). During Cu sufficiency, neither *crpA* nor *ctrC* was expressed. A short-term confrontation (45 min) of such mycelia with 0.2 mM Cu caused an induction of *crpA* reflecting Cu detoxification. In contrast, a short-term confrontation with His-complexed Cu (the same amount of Cu was preincubated with a 10-fold excess of His before addition to the mycelia) did not induce *crpA*. The expression of *ctrC* was detected in neither of these mycelia, which confirms repression of high-affinity Cu uptake in agreement with Cu sufficiency. These data indicate that

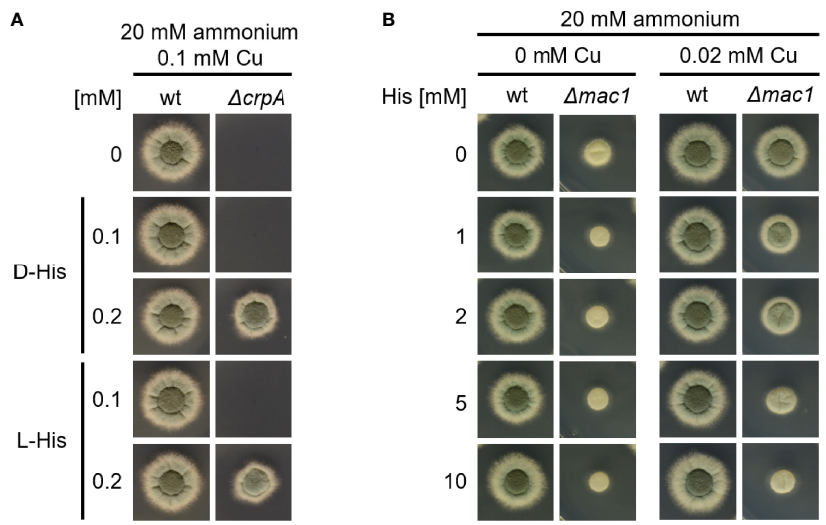

FIGURE 5 | L-His and D-His show a similar protection of *A. fumigatus ΔcrpA* against Cu toxicity **(A)**, and His supplementation impedes Cu uptake by *A. fumigatus Δ*mac1. **(B)** *A. fumigatus* wt and mutant conidia were point-inoculated on AMM plates with 20 mM ammonium as nitrogen source. **(A)** The growth medium contained 0.1 mM Cu and was supplemented with different concentrations of either L-His (left) or D-His (right). **(B)** The growth media contained different concentrations of Cu and His, respectively.

TABLE 1 | AA supplementation impacts biomass production and cellular contents in Cu and Fe of *ΔcrpA*.

Strain	Supplement	Biomass ± STD[g]	Cu ± STD[μg/g]	Fe ± STD[μg/g]	Fe/Cu
wt	**-AA**	0.451 ± 0.008	53.5 ± 0.46	58.2 ± 0.41	1.1
	+His	0.512 ± 0.006	27.5 ± 0.62	72.1 ± 0.32	2.6
	+Gln	0.425 ± 0.004	55.4 ± 0.56	63.4 ± 0.46	1.1
ΔcrpA	**-AA**	0.101 ± 0.005	257.4 ± 0.78	604.8 ± 0.51	2.3
	+His	0.521 ± 0.008	30.6 ± 0.67	81.2 ± 0.37	2.7
	+Gln	0.313 ± 0.005	70.0 ± 0.79	69.3 ± 0.43	1.0

A. fumigatus wt and ΔcrpA strains were grown in liquid AMM containing 0.005 mM Cu and 20 mM ammonium as nitrogen source without AAs (-AA) or supplemented either with 5 mM Gln (+Gln) or 1 mM His (+His). After cultivation, dry biomass and cellular contents in Cu and Fe were determined after freeze-drying of the harvested mycelia. The shown values are the mean ± standard deviation (STD) of three biological replicates.

complexation of Cu by His blocks Cu uptake in the absence of high-affinity Cu uptake. During Cu limitation, the expression of *crpA* was repressed and *ctrC* was induced (**Figure 6B**). A short-term confrontation with Cu caused the induction of *crpA* and a decrease in the *ctrC* transcript level. In comparison, a short-term confrontation with His-complexed Cu induced *crpA* to the same degree as non-complexed Cu but repressed *ctrC* significantly more strongly. The similar induction of *crpA* by His-complexed and non-complexed Cu indicates that His complexation does not block Cu uptake by high-affinity systems. Moreover, the stronger repression of *ctrC* by His-complexed Cu compared to non-complexed Cu might indicate an even higher bioavailability for high-affinity uptake systems of His-complexed Cu compared to Cu alone. In agreement with complexation of Cu by AA, we observed that AA form blue-colored complexes with Cu; **Figure 6C** shows exemplary His, Thr, Asn, and Gln. His displayed the most intensive color formation with Cu, which is consistent with the strongest protecting activity observed. Notably, there was no significant difference in color formation between Thr, Asn, and Gln, which display different protecting activities at a lower level (see above).

Fe Availability Impacts Cu Resistance and Vice Versa

Based on the concomitant increase in cellular Cu and Fe contents in *A. fumigatus ΔcrpA* (**Table 1**), we hypothesized that Fe is required to counteract Cu toxicity. Indeed, we found that the Cu resistance of *A. fumigatus ΔcrpA* increases with increasing Fe availability (**Figure 7A**); i.e., in the presence of 0.02 mM Cu, the radial growth of *ΔcrpA* was lowest during Fe limitation and increased with the degree of Fe supplementation. Furthermore, supplementation with ferricrocin-chelated Fe improved Cu resistance (**Figure 7A**). As Fe chelated by siderophores such as ferricrocin are taken up exclusively by siderophore-specific

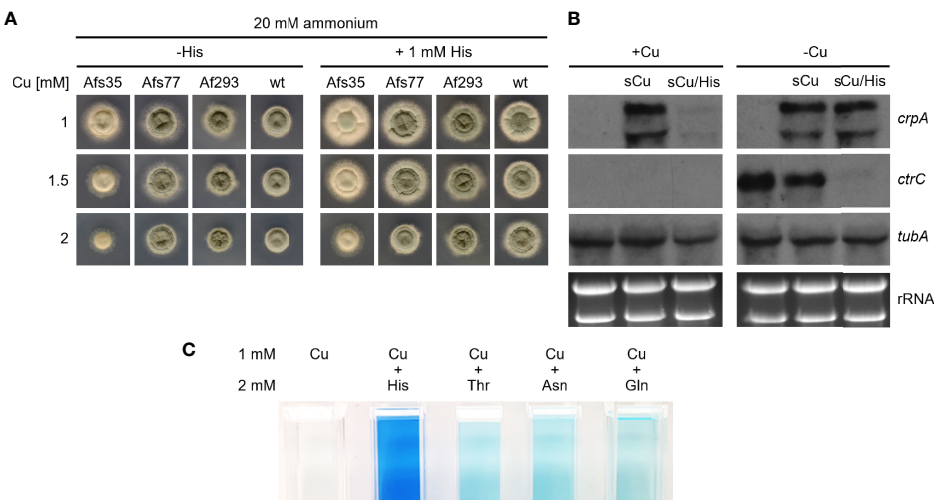

FIGURE 6 | His supplementation protects *A. fumigatus* wt by inhibition of His uptake. **(A)** *A. fumigatus* conidia were point-inoculated on AMM plates with 20 mM ammonium as nitrogen source containing different Cu concentrations without (-His) and with 1 mM His supplementation. The plates were incubated for 48 h at 37°C. **(B)** *A. fumigatus* wt was grown for 16 h at 37°C in AMM liquid cultures with ammonium as nitrogen source without (-Cu; Cu limitation) and with (+Cu, Cu sufficiency) 0.005 mM Cu, respectively. Subsequently, the mycelia were harvested or incubated for another 45 min after addition of Cu to a final concentration of 0.2 mM without (sCu) or with (sCu/His) concomitant addition of His to a final concentration of 2 mM. Notably, Cu and His have been mixed before the addition to allow Cu–His complex formation. After harvesting the mycelia, total RNA was isolated and subject to Northern analysis of the indicated genes. Ethidium bromide-stained rRNA and α-tubulin encoding *tubA* served as controls for loading and quality of RNA. As observed previously (Wiemann et al., 2017), *crpA* has two transcripts, which are slightly larger and smaller as the 26S rRNA. **(C)** His, Thr, Asn, and Gln form colored complexes with Cu. The photos show cuvettes with 1 mM Cu or 1 mM Cu mixed with 2 mM of the indicated AA.

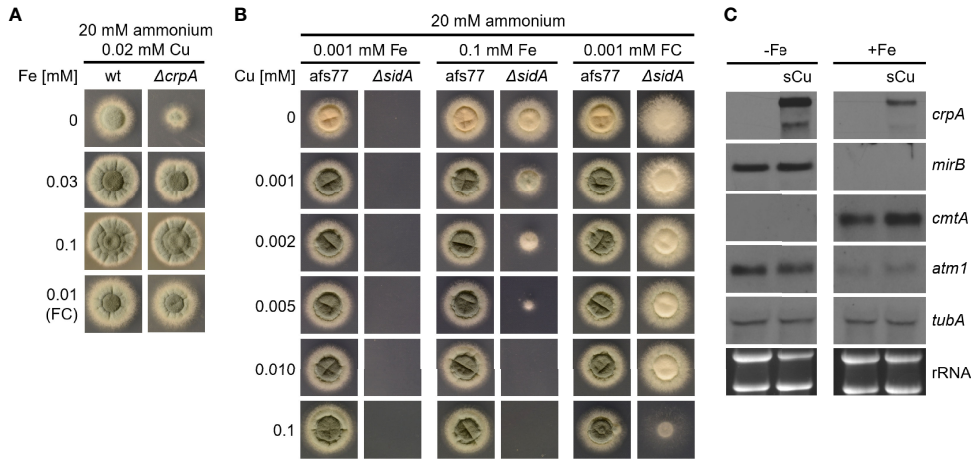

FIGURE 7 | Fe availability impacts Cu resistance. **(A)** *A. fumigatus* conidia were point-inoculated on AMM plates with 20 mM ammonium as nitrogen source and 0.02 mM Cu combined with different concentrations of Fe or ferricrocin (FC)-chelated Fe. **(B)** *A. fumigatus* conidia were point-inoculated on AMM plates with 20 mM ammonium as nitrogen source with different concentrations of Fe or FC-chelated Fe combined with different concentrations of Cu. Afs77 is the genetic background of the Δ*sidA* mutant strain (Schrettl et al., 2004). **(C)** *A. fumigatus* wt was grown for 16 h at 37°C in AMM liquid cultures with ammonium as nitrogen source and 0.005 mM Cu without (-Fe; Fe limitation) or with (+Fe, Fe sufficiency) 0.03 mM Fe, respectively. Subsequently, the mycelia were harvested or incubated for another 45 min after addition of Cu to a final concentration of 0.2 mM (sCu). After harvesting the mycelia, total RNA was isolated and subject to Northern analysis of the indicated genes. Siderophore transporter encoding *mirB* was used as control for cellular Fe starvation (Schrettl et al., 2010). Ethidium bromide-stained rRNA and α-tubulin encoding *tubA* served as controls for loading and quality of RNA.

transporters (Aguiar et al., 2021; Misslinger et al., 2021), these data exclude the possibility that the positive impact of Fe supplementation on Cu resistance of Δ*crpA* is the sole consequence of competition of Fe with Cu for uptake by low-affinity metal transporters. In line, a Δ*sidA* mutant, which lacks siderophore biosynthesis and consequently displays decreased Fe acquisition (Schrettl et al., 2004; Misslinger et al., 2021), as shown by lack of growth under low Fe availability, shows decreased Cu resistance when grown with either 0.1 mM Fe or 0.001 mM ferricrocin (**Figure 7B**). The ferricrocin experiment again excludes the possibility that the effects seen are based on competition of Cu and Fe for uptake. Moreover, a short-term confrontation with Cu was found to induce a higher *crpA* expression during Fe starvation compared to Fe sufficiency (**Figure 7C**), which supports higher Cu toxicity under Fe limitation. To further investigate the role of Fe in Cu resistance, we analyzed the expression of *cmtA* (also termed *crd2*) and *atm1*. *cmtA* encodes a putative metallothionein previously implicated in the Cu resistance of *A. fumigatus* (Cai et al., 2018); *atm1* encodes a mitochondrial ABC transporter that links mitochondrial and cytosolic Fe–sulfur cluster biosynthesis and that has recently been shown to play a role in Cu toxicity in *Cryptococcus neoformans* and *S. cerevisiae* (Garcia-Santamarina et al., 2017). The expression of *cmtA* was found to be repressed under Fe starvation compared to Fe sufficiency and showed a slight upregulation in response to a short-term confrontation with Cu during Fe sufficiency (**Figure 7C**). In contrast, *atm1* displayed a downregulation during Fe sufficiency compared to Fe starvation without a response to a short-term confrontation with Cu (**Figure 7C**).

To investigate if there is also an effect of Cu availability on Fe resistance of *A. fumigatus*, we employed the Δ*cccA* mutant that shows increased Fe toxicity due to the lack of a vacuolar transporter mediating vacuolar Fe deposition (Gsaller et al., 2012). As shown in **Figure 8**, Fe resistance of the Δ*cccA* mutant increased with increasing Cu availability (8 mM Fe). Under low Fe availability (0.03 mM Fe), the Δ*cccA* mutant lacked a growth defect and displayed wt-like Cu susceptibility. Taken together, these data demonstrate the importance of metal homeostasis, i.e., balanced cellular metal contents.

DISCUSSION

In this study, we observed that the ambient availability of AAs and proteins increase the Cu resistance of the Cu-susceptible *A. fumigatus* Δ*crpA* mutant. Different AAs and proteins showed different protective activities in the order His > Asn ~ Asp ~ Ser ~ Thr ~ Tyr > Gln and other proteinogenic AAs > protein such as BSA and RNase A (**Figures 1–4**). Moreover, His supplementation also increased the Cu resistance of different *A. fumigatus* wild-type strains (**Figure 6A**). To adapt to different metal availabilities, fungal species employ both high-affinity and low-affinity transporters. High-affinity transporters display metal specificity and are induced under shortage of the respective metal, while low-affinity transporters usually show a broader metal specificity and ensure supply under conditions of high metal availability. The high-affinity Cu transporters of *A. fumigatus* are CtrA2 and CtrC (Cai et al., 2017; Kusuya et al., 2017; Wiemann et al., 2017). Low-affinity Cu transport has not been characterized in *A. fumigatus* yet,

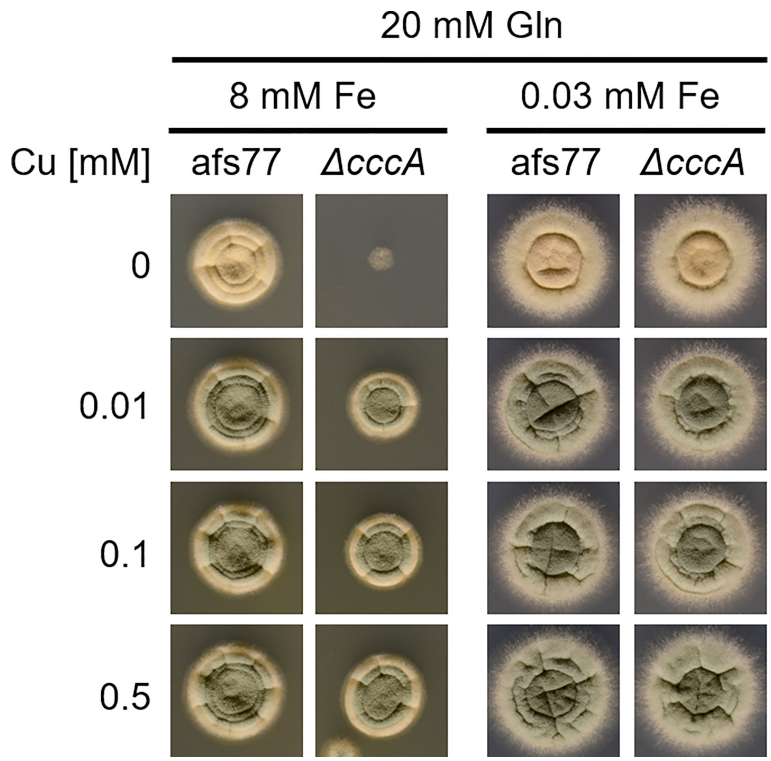

FIGURE 8 | Cu availability impacts Fe resistance. *A. fumigatus* conidia were point-inoculated on AMM plates with 20 mM Gln as nitrogen source containing different concentrations of Cu and Fe. Gln was used here as nitrogen source as this high Fe amount precipitates with ammonium as nitrogen source. Afs77 is the genetic background of the Δ*cccA* mutant strain (Gsaller et al., 2012).

but this mold possesses a homolog of *S. cerevisiae* Fet4, a low-affinity transporter for Cu, Fe, and zinc (Hassett et al., 2000). Several lines of evidence indicated that His and most likely other AAs, although to a lower degree, increase Cu resistance by extracellular Cu complexation, which impedes uptake by low-affinity but not high-affinity systems: (i) non-proteinogenic D-His and His displayed similar protection of Δ*crpA* against Cu toxicity, indicating that the mode of action does not involve metabolization of His (**Figure 5A**); (ii) His supplementation caused dose-dependent growth inhibition of the *A. fumigatus* Δ*mac1* mutant that lacks transcriptional activation of high-affinity Cu uptake but not of the wild-type strain that is capable of high-affinity Cu uptake (**Figure 5B**); (iii) His supplementation decreased the cellular Cu content of Δ*crpA* (**Table 1**); (iv) Cu-sufficient mycelia, which displayed downregulation of high-affinity Cu uptake, responded to short-term exposure to Cu, but not to His-complexed Cu, with transcriptional downregulation of *crpA* (**Figure 6B**); (v) Cu-starved mycelia, which displayed upregulation of high-affinity Cu uptake, responded to short-term exposure to Cu and His-complexed Cu with transcriptional upregulation of *crpA* (**Figure 6B**); (vi) His supplementation is highly efficient in protecting Δ*crpA* against Cu toxicity most likely because high-affinity Cu uptake is downregulated in this mutant due to the high intracellular Cu content that represses Mac1 (Cai et al., 2018); and (vii) Cu was found to form blue-colored complexes with AAs, whereby the most intense color formation was found with His, which also displayed the highest-protecting activity (**Figure 6C**). In agreement with the latter, AAs are known to be able to form different chelates with Cu(II), whereby the metal-to-ligand molar ratio is 1:2 in the most common complex in aqueous solution (Deschamps et al., 2005). Among all AAs, His was able to complex Cu with the highest affinity. Consistently, His supplementation protected the Δ*crpA* mutant against Cu in an about two-fold molar excess (**Figures 2B**, **3A**). Remarkably, in response to short-term Cu exposure of Cu-starved mycelia, His complexation increased the transcriptional downregulation of the high-affinity Cu transporter *ctrC* compared to uncomplexed Cu, which indicates that His complexation improves the efficacy of Cu uptake by high-affinity transporters in contrast to low-affinity uptake systems (**Figure 6B**). Possibly, His complexation increases the bioavailability of Cu by increasing its solubility. In the Δ*crpA*, mutant strain, an about 5-fold increase in the cellular Cu content was found to be accompanied by an about 10-fold increase in the cellular Fe content (**Table 1**). This indicated an important role of cellular metal balancing. In agreement, several lines of evidence supported a role of Fe in protection against Cu toxicity: (i) increased Fe availability improved the Cu resistance of Δ*crpA* (**Figure 7A**), (ii) impaired Fe acquisition due to lack of siderophore biosynthesis decreased Cu resistance (**Figure 7B**), and (iii) short-term confrontation with Cu induced a higher *crpA* expression during

Fe starvation compared to Fe sufficiency (**Figure 7C**). Vice versa, increased Cu availability was found to counteract Fe toxicity (**Figure 8**). These links between cellular Cu and Fe management might be explained by the fact that excess of a single metal might lead to mismetallation of proteins and/or that Fe and Cu are important for the detoxification of reactive oxygen species caused by excess of the respective other metal *via* Fenton/Fenton-like reaction, e.g., heme-Fe-containing catalases and peroxidases as well as Cu/Zn superoxide dismutase (Gerwien et al., 2018; Raffa et al., 2019; Brantl et al., 2021; Misslinger et al., 2021). Apparently, Fe does not decrease Cu toxicity *via* CrpA because Fe increased Cu resistance in both the absence (Δ*crpA*) and the presence of CrpA (Δ*sidA*) (**Figure 7B**). Recently, Fe–sulfur clusters have been shown to be targets for Cu toxicity in *C. neoformans* and *S. cerevisiae* and that the mitochondrial ABC transporter Atm1, which links mitochondrial and cytosolic Fe–sulfur biosynthesis, is transcriptionally upregulated in response to short-term exposure to Cu in *C. neoformans* but not *S. cerevisiae* (Garcia-Santamarina et al., 2017). We found that short-term exposure to Cu does not impact the expression of Atm1 at the transcript level in *A. fumigatus* (**Figure 7C**). Previously, genetic inactivation of the putative *A. fumigatus* metallothionein CmtA (also termed Crd2) was found to be dispensable for resistance to Cu as well as macrophage challenge (Wiemann et al., 2017; Cai et al., 2018). However, overexpression of CmtA in the absence of CrpA provided partial protection against Cu toxicity (Cai et al., 2018), indicating that CmtA plays a minor role in Cu resistance. Northern blot analysis demonstrated the repression of *cmtA* under Fe starvation compared to Fe sufficiency and a slight upregulation in response to short-term confrontation with Cu during Fe sufficiency (**Figure 7C**). These data might provide a hint for the role of Fe in Cu resistance. Nevertheless, it remains to be shown if CmtA is indeed a metallothionein. In line with the function as metallothionein, CmtA is a small protein rich in cysteine residues. However, previous studies indicated that both Cu availability and AceA do not impact *cmtA* expression; furthermore, the transcriptional Fe regulation is atypical for a metallothionein. Moreover, CmtA has been shown to physically interact with the monothiol glutaredoxin GrxD, which functions as a chaperon for distribution of Fe–sulfur clusters in the cytosol. Consequently, CmtA might have a role in Fe–sulfur cluster homeostasis.

The interaction of different metals in *A. fumigatus* has been reported previously. Due to the Cu dependence of reductive Fe assimilation (Askwith et al., 1994; Schrettl et al., 2004), impairment of Cu-independent siderophore-mediated Fe acquisition was found to increase the susceptibility of *A. fumigatus* to Cu starvation (Blatzer et al., 2011), and in line Cu starvation increases siderophore-mediated Fe acquisition (Yap et al., 2020). Moreover, Fe and zinc were found to be tightly linked: Fe starvation downregulates high-affinity zinc uptake and upregulates detoxification of zinc *via* vacuolar deposition in order to counteract zinc accumulation which displays higher toxicity during Fe starvation (Yasmin et al., 2009; Kurucz et al., 2018). In line, inactivation of the Fe regulator HapX was shown to impact zinc homeostasis (Schrettl et al., 2010) and Fe availability was reported to impact ZafA-mediated zinc regulation (Vicentefranqueira et al., 2019).

A crucial role of His in Cu handling has been previously noticed. For example, His auxotrophy combined with limited His supplementation was shown to decrease resistance to both starvation and excess of Cu in *A. fumigatus* (Dietl et al., 2016). Therefore, the avirulence caused by His auxotrophy (Dietl et al., 2016) might be a consequence not only of histidine shortage per se but also of metal mismanagement. Moreover, engineering of a *Saccharomyces cerevisiae* strain to display His oligopeptides at the surface increased Cu adsorption combined with increased Cu resistance (Kuroda et al., 2001). Moreover, it has been shown that His might decrease Cu toxicity also intracellularly under certain conditions in *S. cerevisiae* (Pearce and Sherman, 1999; Watanabe et al., 2014). AAs including Gln, Asn, Asp, Ser, and His were also found to play an important role in resistance to heavy metals including Cu in plants (Sharma and Dietz, 2006). Moreover, the human blood contains His-complexed Cu and the exchange of Cu(II) between His and albumin, which is able to bind Cu with high affinity and modulates cellular Cu availability (Deschamps et al., 2005; Sharma and Dietz, 2006).

In a process termed "nutritional immunity," the mammalian innate immune system exploits the essentiality and toxicity of nutrient metals by producing factors that limit the availability of metals such as Cu and Fe to starve pathogens or intoxicate the pathogen with metal excess (Monteith and Skaar, 2021). Therefore, the impact of the ambient availability of amino acids and proteins on Cu resistance of *A. fumigatus* as well as the links between Cu and Fe homeostasis most likely play a role in the host niche. In particular, the combination of Cu excess with restriction of Fe, which aggravate Cu toxicity as shown here, appears to be a highly sophisticated defense strategy. Indeed, this combinatorial strategy is employed in the phagolysosome to attack pathogens: the antimicrobial activity of Cu is employed *via* import by the ABC transporter ATP7A (Gerwien et al., 2018), and Fe is exported by the transporter Nramp1 to deplete the phagolysosome of Fe needed by pathogens for growth (Forbes and Gros, 2001) and at the same time to aggravate Cu toxicity, as indicated by the data provided.

DATA AVAILABILITY STATEMENT

The original contributions presented in the study are included in the article/supplementary material. Further inquiries can be directed to the corresponding author.

AUTHOR CONTRIBUTIONS

HH conceived and supervised the study. HH and RW secured the funding of the study. HH, AY, HT HL, and RW designed the experiments. AY and HT conducted the experiments. HH and AY analyzed the data. HH and AY wrote the manuscript draft.

All authors contributed to the article and approved the submitted version.

FUNDING

This work was supported by the Austrian Science Fund (FWF) doctoral program "host response in opportunistic infections (HOROS, W1253 to AY, RW, and HH). We are grateful to Ling Lu (Jiangsu Key Laboratory for Microbes and Functional Genomics, College of Life Sciences, Nanjing Normal University, Nanjing, China) for providing some of the fungal strains used in this work. The funders had no role in study design, interpretation, decision to publish, in the writing of the manuscript, and in the decision to submit the manuscript for publication.

REFERENCES

Aguiar, M., Orasch, T., Misslinger, M., Dietl, A. M., Gsaller, F., and Haas, H. (2021). The Siderophore Transporters *Sit1* and *Sit2* are Essential for Utilization of Ferrichrome-, Ferrioxamine-and Coprogen-Type Siderophores in *Aspergillus Fumigatus*. *J. Fungi* 7 (9), 768. doi: 10.3390/jof7090768

Anabosi, D., Meir, Z., Shadkchan, Y., Handelman, M., Abou-Kandil, A., Yap, A., et al. (2021). Transcriptional Response of *Aspergillus Fumigatus* to Copper and the Role of the Cu Chaperones. *Virulence* 12 (1), 2186–2200. doi: 10.1080/21505594.2021.1958057

Askwith, C., Eide, D., Van Ho, A., Bernard, P. S., Li, L., Davis-Kaplan, S., et al. (1994). The FET3 Gene of *S. Cerevisiae* Encodes a Multicopper Oxidase Required for Ferrous Iron Uptake. *Cell* 76 (2), 403–410. doi: 10.1016/0092-8674(94)90346-8

Bergmann, A., Hartmann, T., Cairns, T., Bignell, E. M., and Krappmann, S. (2009). A Regulator of *Aspergillus Fumigatus* Extracellular Proteolytic Activity is Dispensable for Virulence. *Infect. Immun.* 77 (9), 4041–4050. doi: 10.1128/IAI.00425-09

Besold, A. N., Culbertson, E. M., and Cullota, V. C. (2016). The Yin and Yang of Copper During Infection. *J. Biol. Inorg. Chem.* 21 (2), 137–144. doi: 10.1007/s00775-016-1335-1

Blatzer, M., Binder, U., and Haas, H. (2011). The Metalloreductase FreB is Involved in Adaptation of *Aspergillus Fumigatus* to Iron Starvation. *Fungal Genet. Biol.* 48 (11), 1027–1033. doi: 10.1016/j.fgb.2011.07.009

Brantl, V., Boysen, J. M., Yap, A., Golubtsov, E., Ruf, D., Heinekamp, T., et al. (2021). Peroxiredoxin Asp F3 is Essential for *Aspergillus Fumigatus* to Overcome Iron Limitation During Infection. *mBio*. 12 (4), 1–19. doi: 10.1128/mBio.00976-21

Cai, Z., Du, W., Zeng, Q., Long, N., Dai, C., and Lu, L. (2017). Cu-Sensing Transcription Factor Mac1 Coordinates With the Ctr Transporter Family to Regulate Cu Acquisition and Virulence in *Aspergillus Fumigatus*. *Fungal Genet. Biol.* 107, 31–43. doi: 10.1016/j.fgb.2017.08.003

Cai, Z., Du, W., Zhang, Z., Guan, L., Zeng, Q., Chai, Y., et al. (2018). The *Aspergillus Fumigatus* Transcription Factor AceA is Involved Not Only in Cu But Also in Zn Detoxification Through Regulating Transporters CrpA and ZrcA. 1–15. *Cell Microbiol.* 20 (10), e12864. doi: 10.1111/cmi.12864

Cao, X., Hu, X., Zhang, X., Gao, S., Ding, C., Feng, Y., et al. (2017). Identification of Metal Ion Binding Sites Based on Amino Acid Sequences. *PloS One* 12 (8), e0183756. doi: 10.1371/journal.pone.0183756

Deschamps, P., Kulkarni, P. P., Gautam-Basak, M., and Sarkar, B. (2005). The Saga of Copper(II)-L-Histidine. *Coord. Chem. Rev.* 249 (9-10), 895–909. doi: 10.1016/j.ccr.2004.09.013

Dietl, A. M., Amich, J., Leal, S., Beckmann, N., Binder, U., Beilhack, A., et al. (2016). Histidine Biosynthesis Plays a Crucial Role in Metal Homeostasis and Virulence of *Aspergillus Fumigatus*. *Virulence.* 7 (4), 465–476. doi: 10.1080/21505594.2016.1146848

Festa, R. A., and Thiela, D. J. (2011). Copper: An Essential Metal in Biology. *Curr Biol.* 21 (21), R877–883. doi: 10.1016/j.cub.2011.09.040

Forbes, J. R., and Gros, P. (2001). Divalent-Metal Transport by NRAMP Proteins at the Interface of Host-Pathogen Interactions. *Trends Microbiol.* 9 (8), 397–403. doi: 10.1016/s0966-842x(01)02098-4

Garcia-Santamarina, S., Uzarska, M. A., Festa, R. A., Lill, R., and Thiele, D. J. (2017). *Cryptococcus Neoformans* Iron-Sulfur Protein Biogenesis Machinery is a Novel Layer of Protection Against Cu Stress. *mBio.* 8 (5), e01742–e01177. doi: 10.1128/mBio.01742-17

Gerwien, F., Skrahina, V., Kasper, L., Hube, B., and Brunke, S. (2018). Metals in Fungal Virulence. *FEMS Microbiol. Rev.* 42 (1), fux050. doi: 10.1093/femsre/fux050

Gsaller, F., Eisendle, M., Lechner, B. E., Schrettl, M., Lindner, H., Müller, D., et al. (2012). The Interplay Between Vacuolar and Siderophore-Mediated Iron Storage in *Aspergillus Fumigatus*. *Metallomics*. 4 (12), 1262–1270. doi: 10.1039/c2mt20179h

Hassett, R., Dix, D. R., Eide, D. J., and Kosman, D. J. (2000). The Fe(II) Permease Fet4p Functions as a Low Affinity Copper Transporter and Supports Normal Copper Trafficking in *Saccharomyces Cerevisiae*. *Biochem. J.* 351 (2), 477–484. doi: 10.1042/0264-6021:3510477

Krappmann, S., Sasse, C., and Braus, G. H. (2006). Gene Targeting in *Aspergillus Fumigatus* by Homologous Recombination is Facilitated in a Nonhomologous End-Joining-Deficient Genetic Background. *Eukaryot Cell.* 5 (1), 212–215. doi: 10.1128/EC.5.1.212-215.2006

Kuroda, K., Shibasaki, S., Ueda, M., and Tanaka, A. (2001). Cell Surface-Engineered Yeast Displaying a Histidine Oligopeptide (Hexa-His) has Enhanced Adsorption of and Tolerance to Heavy Metal Ions. *Appl. Microbiol. Biotechnol.* 57 (5-6), 697–701. doi: 10.1007/s002530100813

Kurucz, V., Krüger, T., Antal, K., Dietl, A. M., Haas, H., Pócsi, I., et al. (2018). Additional Oxidative Stress Reroutes the Global Response of *Aspergillus Fumigatus* to Iron Depletion. *BMC Genomics* 19 (1), 1–19. doi: 10.1186/s12864-018-4730-x

Kusuya, Y., Hagiwara, D., Sakai, K., Yaguchi, T., Gonoi, T., and Takahashi, H. (2017). Transcription Factor *Afmac1* Controls Copper Import Machinery in *Aspergillus Fumigatus*. *Curr. Genet.* 63 (4), 777–789. doi: 10.1007/s00294-017-0681-z

Latgé, J. P., and Chamilos, G. (2019). *Aspergillus Fumigatus* and Aspergillosis in 2019. *Clin. Microbiol. Rev.* 33 (1), e00140–e00118. doi: 10.1128/CMR.00140-18

Misslinger, M., Hortschansky, P., Brakhage, A. A., and Haas, H. (2021). Fungal Iron Homeostasis With a Focus on *Aspergillus Fumigatus*. *Biochim. Biophys. Acta - Mol. Cell Res.* 1868 (1), 118885. doi: 10.1016/j.bbamcr.2020.118885

Monteith, A. J., and Skaar, E. P. (2021). The Impact of Metal Availability on Immune Function During Infection. *Trends Endocrinol. Metab.* 32 (11), 916–928. doi: 10.1016/j.tem.2021.08.004

Nierman, W. C., Pain, A., Anderson, M. J., Wortman, J. R., Kim, H. S., Arroyo, J., et al. (2005). Genomic Sequence of the Pathogenic and Allergenic Filamentous Fungus Aspergillus Fumigatus. *Nat.* 438 (7071), 1151–1156. doi: 10.1038/nature04332

Oberegger, H., Zadra, I., Schoeser, M., and Haas, H. (2000). Iron Starvation Leads to Increased Expression of Cu/Zn-Superoxide Dismutase in Aspergillus. *FEBS Lett.* 485 (2-3), 113–116. doi: 10.1016/S0014-5793(00)02206-7

Park, Y. S., Kang, S., Seo, H., and Yun, C. W. (2018). A Copper Transcription Factor, AfMac1, Regulates Both Iron and Copper Homeostasis in the Opportunistic Fungal Pathogen *Aspergillus Fumigatus*. *Biochem. J.* 475 (17), 2831–2845. doi: 10.1042/BCJ20180399

Park, Y. S., Lian, H., Chang, M., Kang, C. M., and Yun, C. W. (2014). Identification of High-Affinity Copper Transporters in Aspergillus Fumigatus. *Fungal Genet. Biol.* 73, 29–38. doi: 10.1016/j.fgb.2014.09.008

Pearce, D. A., and Sherman, F. (1999). Toxicity of Copper, Cobalt, and Nickel Salts is Dependent on Histidine Metabolism in the Yeast *Saccharomyces Cerevisiae*. *J. Bacteriol.* 181 (16), 4774–4779. doi: 10.1128/JB.181.16.4774-4779.1999

Pontecorvo, G., Roper, J. A., Hemmons, L. M., Macdonald, K. D., and Bufton, A. W. (1953). The Genetics of *Aspergillus Nidulans*. *Adv. Genet.* 5, 141–238. doi: 10.1016/s0065-2660(08)60408-3

Raffa, N., Osherov, N., and Keller, N. P. (2019). Copper Utilization, Regulation, and Acquisition by *Aspergillus Fumigatus*. *Int. J. Mol. Sci.* 20 (8), 1980-1993. doi: 10.3390/ijms20081980

Schrettl, M., Beckmann, N., Varga, J., Heinekamp, T., Jacobsen, I. D., Jöchl, C., et al. (2010). HapX-Mediated Adaption to Iron Starvation is Crucial for Virulence of *Aspergillus Fumigatus*. *PloS Pathog.* 6 (9), e1001124. doi: 10.1371/journal.ppat.1001124

Schrettl, M., Bignell, E., Kragl, C., Joechl, C., Rogers, T., Arst, H. N., et al. (2004). Siderophore Biosynthesis But Not Reductive Iron Assimilation is Essential for *Aspergillus Fumigatus* Virulence. *J. Exp. Med.* 200 (9), 1213–1219. doi: 10.1084/jem.20041242

Sharma, S. S., and Dietz, K. (2006). The Significance of Amino Acids and Amino Acid-Derived Molecules in Plant Responses and Adaptation to Heavy Metal Stress. *J. Exp. Bot.* 57 (4), 711–726. doi: 10.1093/jxb/erj073

Shemesh, E., Hanf, B., Hagag, S., Attias, S., Shadkchan, Y., Fichtman, B., et al. (2017). Phenotypic and Proteomic Analysis of the *Aspergillus Fumigatus* Δ*prtt*, Δ*xprg and* Δ*xprg/*Δ*prtt* Protease-Deficient Mutants. *Front. Microbiol.* 8. doi: 10.3389/fmicb.2017.02490

Tsai, H. F., Wheeler, M. H., Chang, Y. C., and Kwon-Chung, K. J. (1999). A Developmentally Regulated Gene Cluster Involved in Conidial Pigment Biosynthesis in *Aspergillus Fumigatus*. *J. Bacteriol.* 181 (20), 6469–6477. doi: 10.1128/JB.181.20.6469-6477.1999

Vicentefranqueira, R., Leal, F., Marín, L., Sánchez, C. I., and Calera, J. A. (2019). The Interplay Between Zinc and Iron Homeostasis in *Aspergillus Fumigatus* Under Zinc-Replete Conditions Relies on the Iron-Mediated Regulation of Alternative Transcription Units of *zafA* and the Basal Amount of the ZafA Zinc-Responsiveness Transcription Factor. *Environ. Microbiol.* 21 (8), 2787–2808. doi: 10.1111/1462-2920.14618

Watanabe, D., Kikushima, R., Aitoku, M., Nishimura, A., Ohtsu, I., Nasuno, R., et al. (2014). Exogenous Addition of Histidine Reduces Copper Availability in the Yeast *Saccharomyces Cerevisiae*. *Microb. Cell* 1 (7), 241–246. doi: 10.15698/mic2014.07.154

Wiemann, P., Perevitsky, A., Lim, F. Y., Shadkchan, Y., Knox, B. P., Landero Figueora, J. A., et al. (2017). Aspergillus Fumigatus Copper Export Machinery and Reactive Oxygen Intermediate Defense Counter Host Copper-Mediated Oxidative Antimicrobial Offense. *Cell Rep*. 19 (10), 1008–1021. doi: 10.1016/j.celrep.2017.04.019

Yap, A., Misslinger, M., and Haas, H. (2020). Absent Regulation of Iron Acquisition by the Copper Regulator Mac1 in *A . Fumigatus*. *Biochem. J.* 477 (16), 2967–2970. doi: 10.1042/BCJ20200286

Yasmin, S., Abt, B., Schrettl, M., Moussa, T. A., Werner, E. R., and Haas, H. (2009). The Interplay Between Iron and Zinc Metabolism in *Aspergillus Fumigatus*. *Fungal Genet. Biol.* 46 (9), 707–713. doi: 10.1016/j.fgb.2009.05.003

Conflict of Interest: The authors declare that the research was conducted in the absence of any commercial or financial relationships that could be construed as a potential conflict of interest.

Publisher's Note: All claims expressed in this article are solely those of the authors and do not necessarily represent those of their affiliated organizations, or those of the publisher, the editors and the reviewers. Any product that may be evaluated in this article, or claim that may be made by its manufacturer, is not guaranteed or endorsed by the publisher.

frontiers | Frontiers in Cellular and Infection Microbiology

ORIGINAL RESEARCH
published: 11 May 2022
doi: 10.3389/fcimb.2022.873536

The Regulatory Protein ChuP Connects Heme and Siderophore-Mediated Iron Acquisition Systems Required for *Chromobacterium violaceum* Virulence

Vinicius M. de Lima, Bianca B. Batista and José F. da Silva Neto *

Departamento de Biologia Celular e Molecular e Bioagentes Patogênicos, Faculdade de Medicina de Ribeirão Preto, Universidade de São Paulo, Ribeirão Preto, Brazil

OPEN ACCESS

Edited by:
Manuel L. Lemos, University of Santiago de Compostela, Spain

Reviewed by:
Angela Wilks, University of Maryland, Baltimore, United States
Lígia M. Saraiva, Universidade Nova de Lisboa, Portugal

***Correspondence:**
José F. da Silva Neto
jfsneto@usp.br

Specialty section:
This article was submitted to Bacteria and Host, a section of the journal Frontiers in Cellular and Infection Microbiology

Received: *10 February 2022*
Accepted: *30 March 2022*
Published: *11 May 2022*

Citation:
de Lima VM, Batista BB and da Silva Neto JF (2022) The Regulatory Protein ChuP Connects Heme and Siderophore-Mediated Iron Acquisition Systems Required for Chromobacterium violaceum Virulence. Front. Cell. Infect. Microbiol. 12:873536. doi: 10.3389/fcimb.2022.873536

Chromobacterium violaceum is an environmental Gram-negative beta-proteobacterium that causes systemic infections in humans. *C. violaceum* uses siderophore-based iron acquisition systems to overcome the host-imposed iron limitation, but its capacity to use other iron sources is unknown. In this work, we characterized ChuPRSTUV as a heme utilization system employed by *C. violaceum* to explore an important iron reservoir in mammalian hosts, free heme and hemoproteins. We demonstrate that the *chuPRSTUV* genes comprise a Fur-repressed operon that is expressed under iron limitation. The *chu* operon potentially encodes a small regulatory protein (ChuP), an outer membrane TonB-dependent receptor (ChuR), a heme degradation enzyme (ChuS), and an inner membrane ABC transporter (ChuTUV). Our nutrition growth experiments using *C. violaceum chu* deletion mutants revealed that, with the exception of *chuS*, all genes of the *chu* operon are required for heme and hemoglobin utilization in *C. violaceum*. The mutant strains without *chuP* displayed increased siderophore halos on CAS plate assays. Significantly, we demonstrate that ChuP connects heme and siderophore utilization by acting as a positive regulator of *chuR* and *vbuA*, which encode the TonB-dependent receptors for the uptake of heme (ChuR) and the siderophore viobactin (VbuA). Our data favor a model of ChuP as a heme-binding post-transcriptional regulator. Moreover, our virulence data in a mice model of acute infection demonstrate that *C. violaceum* uses both heme and siderophore for iron acquisition during infection, with a preference for siderophores over the Chu heme utilization system.

Keywords: iron homeostasis, heme uptake, heme transporter, bacterial physiology, bacterial virulence, siderophores, *Chromobacterium violaceum*

INTRODUCTION

Iron is an essential micronutrient required as a cofactor of proteins involved in different cellular processes (Braun and Hantke, 2011; Palmer and Skaar, 2016). The ability to vary from soluble ferrous (Fe^{2+}) to insoluble ferric (Fe^{3+}) states confers iron its catalytic properties but can result in high toxicity and low bioavailability (Braun and Hantke, 2011; Huang and Wilks, 2017). As a metal essential for both hosts and pathogens, iron is at the center of an evolutionary battle (Skaar, 2010; Hood and Skaar, 2012; Parrow et al., 2013; Sheldon et al., 2016). Hosts restrict iron availability using iron-sequestering proteins like transferrin, lactoferrin, haptoglobin, hemopexin, and calprotectin, a process known as nutritional immunity (Hood and Skaar, 2012; Cassat and Skaar, 2013; Ganz and Nemeth, 2015). Conversely, pathogens subvert the host-imposed iron limitation by employing strategies such as the production, release, and uptake of low-molecular-weight iron chelators (siderophores such as enterobactin) and high-affinity heme-binding proteins (hemophores such as HasA) (Wandersman and Delepelaire, 2012; Runyen-Janecky, 2013; Contreras et al., 2014; Sheldon et al., 2016).

Heme is a tetrapyrrole that coordinates iron at its center as Fe^{2+} (heme) or Fe^{3+} (hemin). It is a cofactor of proteins like cytochromes and catalases. Therefore, almost every organism requires heme, which is obtained by synthesis and/or uptake from exogenous sources (Runyen-Janecky, 2013; Choby and Skaar, 2016). The greatest iron reservoir in mammals is the heme bound into hemoglobin found inside the erythrocytes. Many bacteria use heme and hemoproteins (e.g., hemoglobin) from the host as an iron source, and the preference for heme or siderophore as the main iron acquisition strategy varies according to the bacterium and the infection status (Runyen-Janecky, 2013; Choby and Skaar, 2016; Sheldon et al., 2016; Zygiel et al., 2021). Heme uptake/utilization systems have been described in several bacterial pathogens, including *Pseudomonas aeruginosa* (Has, Phu, and Hxu), *Yersinia* spp (Hem and Hmu), *Escherichia coli* (Chu), and *Staphylococcus aureus* (Isd). In Gram-negative bacteria, the import of heme involves high-affinity TonB-dependent receptors (TBDRs) in the outer membrane (e.g., PhuR) and ABC-type transport systems in the periplasm and inner membrane (e.g., PhuTUV) (Eakanunkul et al., 2005; Noinaj et al., 2010; Fournier et al., 2011; Choby and Skaar, 2016; Huang and Wilks, 2017; Klebba et al., 2021). Once in the cytosol, heme is degraded by canonical or non-canonical heme oxygenases, releasing iron and other compounds (Contreras et al., 2014; Lamattina et al., 2016).

Genes encoding heme uptake systems are under complex regulation. They are regulated by Fur, a metalloregulator that uses Fe^{2+} as cofactor to repress the expression of iron uptake systems (da Silva Neto et al., 2009; Chandrangsu et al., 2017; Sarvan et al., 2018) and activated by heme-dependent regulatory systems, such as the extracytoplasmic function (ECF) sigma factor signaling cascade Has (Wandersman and Delepelaire, 2012; Huang and Wilks, 2017). Small proteins from the HemP/HmuP family have been described as required for heme utilization by regulating the expression of heme uptake genes. However, the proposed regulatory mechanisms are quite distinct. In *Bradyrhizobium japonicum* and *Burkholderia multivorans*, the HemP/HmuP proteins were described as direct transcriptional activators (Escamilla-Hernandez and O'Brian, 2012; Sato et al., 2017), while in *Ensifer meliloti* (formerly *Sinorhizobium meliloti*), HmuP appears to act as a post-transcriptional activator (Amarelle et al., 2010; Amarelle et al., 2019).

Chromobacterium violaceum is a Gram-negative beta-proteobacterium found in the water and soil of tropical and subtropical regions that causes opportunistic human infections with high mortality rates (Yang and Li, 2011; Kumar, 2012; Khalifa et al., 2015; Batista and da Silva Neto, 2017). An important virulence determinant in *C. violaceum* is the Cpi1/1a type III secretion system involved in hepatocyte invasion and innate immune system activation (Miki et al., 2010; Zhao et al., 2011; Maltez et al., 2015). Recently, we demonstrated that *C. violaceum* relies on the regulator Fur, two putative endogenous catecholate-type siderophores, and the siderophore-acquisition TBDRs CbuA and VbuA to overcome host-imposed iron limitation (Batista et al., 2019; Santos et al., 2020). However, *C. violaceum* mutants lacking siderophores had moderate attenuation in virulence in a mouse model of acute infection (Batista et al., 2019), suggesting that *C. violaceum* uses siderophore-independent mechanisms for iron acquisition during infection. In the current work, we demonstrate that an operon with six genes, here named *chuPRSTUV* (*chu* – *chromobacterium* heme utilization), encodes a Fur-regulated heme uptake system (ChuRTUV) that is required for heme and hemoglobin utilization in *C. violaceum*. We also show that the small heme-binding protein ChuP is required for heme and siderophore-mediated iron acquisition by acting as a post-transcriptional activator of the TBDR genes *chuR* and *vbuA*. Furthermore, using *in vivo* virulence assays in mice, we demonstrate that these heme and siderophore-mediated iron uptake systems work together to help *C. violaceum* overcome iron limitation in the host.

MATERIALS AND METHODS

Bacterial Strains, Plasmids, and Growth Conditions

The bacterial strains and plasmids used in this work are indicated in **Table 1**. *E. coli* strains were cultured in Luria-Bertani (LB) medium at 37°C. *C. violaceum* strains were cultured in LB medium or M9 minimal medium supplemented with 0.1% casein hydrolysate (M9CH) at 37°C (Batista et al., 2019). The cultures were supplemented with kanamycin (50 μg/mL), tetracycline (10 μg/mL), or ampicillin (100 μg/mL), when necessary. Iron deficiency was obtained by the addition of 2,2'-dipyridyl (DP) (Sigma) to the medium, while iron sufficiency was achieved by supplementation with $FeSO_4$ (Sigma), hemin (Hm) (Sigma), or hemoglobin (Hb) (Sigma).

Construction of *C. violaceum* Mutant and Complemented Strains

Null-mutant strains were generated by a previously established allelic exchange mutagenesis protocol (da Silva Neto et al., 2012; Batista et al., 2019; Santos et al., 2020). In-frame null-deletion

TABLE 1 | Bacterial strains and plasmids.

Strain or plasmid	Description[a]	Reference or source
Strains		
E. coli		
DH5α	*E. coli* strain for cloning purposes	(Hanahan, 1983)
S17-1	*E. coli* strain for plasmid mobilization	(Simon et al., 1983)
BL21(DE3)	*E. coli* strain for heterologous expression of proteins	Novagen
C. violaceum		
WT	*C. violaceum* ATCC 12472 wild-type strain with sequenced reference genome	(Brazilian National Genome Project Consortium, 2003)
WT[pMR20]	WT control strain harboring the empty pMR20 plasmid	This work
WT[p*chuP-lacZ*]	WT strain with the *chuP* (CV_RS19275)-*lacZ* fusion	This work
WT[p*chuR-lacZ*]	WT strain with the *chuR* (CV_RS19280)-*lacZ* fusion	This work
cbaF::pNPT	WT strain with insertion of pNPTS138 in the *cbaF* gene	(Batista et al., 2019)
vbaF::PNPT	WT strain with insertion of pNPTS138 in the *vbaF* gene	(Batista et al., 2019)
Δ*chuP*	WT strain with the CV_RS19275 gene deleted	This work
Δ*chuP*/*cbaF*::pNPT	Δ*chuP* strain with insertion of pNPTS138 in the *cbaF* gene	This work
Δ*chuP*/*vbaF*::pNPT	Δ*chuP* strain with insertion of pNPTS138 in the *vbaF* gene	This work
Δ*chuP*[*chuP*]	Δ*chuP* mutant complemented with WT copy of *chuP*	This work
Δ*chuP*[p*chuP-lacZ*]	Δ*chuP* strain with the *chuP* (CV_RS19275)-*lacZ* fusion	This work
Δ*chuP*[p*chuR-lacZ*]	Δ*chuP* strain with the *chuR* (CV_RS19280)-*lacZ* fusion	This work
Δ*chuR*	WT strain with the CV_RS19280 gene deleted	This work
Δ*chuR*[*chuR*]	Δ*chuR* mutant complemented with WT copy of *chuR*	This work
Δ*chuS*	WT strain with the CV_RS19285 gene deleted	This work
Δ*chuS*[*chuS*]	Δ*chuS* mutant complemented with WT copy of *chuS*	This work
Δ*chuTUV*	WT strain with the CV_RS19290-295-300 genes deleted	This work
Δ*chuTUV*[*chuTUV*]	Δ*chuTUV* mutant complemented with WT copy of *chuTUV*	This work
Δ*chuPRSTUV*	WT strain with the CV_RS19275-280-285-290-295-300 genes deleted	This work
Δ*chuPRSTUV* [*chuPRSTUV*]	Δ*chuPRSTUV* mutant complemented with WT copy of *chuPRSTUV*	This work
Δ*cbaCEBA*	WT strain with the *cbaCEBA* genes deleted	(Batista et al., 2019)
Δ*cbaCEBA*[*cbaCEBA*]	Δ*cbaCEBA* mutant complemented with WT copy of *cbaCEBA*	(Batista et al., 2019)
Δ*cbaCEBA*Δ*chuPRSTUV*	WT strain with combined mutations of *cbaCEBA* and *chuPRSTUV*	This work
Δ*cbaCEBA*Δ*chuPRSTUV*[pMR20]	Δ*cbaCEBA*Δ*chuPRSTUV* mutant harboring the empty pMR20 plasmid	This work
Δ*cbaCEBA*Δ*chuPRSTUV*[*chuPRSTV*]	Δ*cbaCEBA*Δ*chuPRSTUV* mutant complemented with WT copy of *chuPRSTUV*	This work
Δ*fur*	WT strain with the *fur* gene deleted	(Santos et al., 2020)
Δ*fur*[p*chuP-lacZ*]	Δ*fur* strain with the *chuP* (CV_RS19275)-*lacZ* fusion	This work
Plasmids		
pNPTS138	Suicide vector containing *oriT*, *sacB*; Kan^R	M.R.K. Alley
pMR20	Broad-host-range low-copy vector containing *oriT*, Tet^R	(Roberts et al., 1996)
pET15b	Expression of proteins with N-terminal His-tag; Amp^R	Novagen
pGEM-T easy	Cloning plasmid; Amp^R	Promega
pRK*lacZ*290	pRK2-derived vector with promoterless *lacZ* gene, Tet^R	(Gober and Shapiro, 1992)

[a]*Kan, kanamycin; Tet, tetracycline; Amp, ampicillin; R, resistance.*

mutants derived from the wild-type *C. violaceum* ATCC 12472 strain, with the exception of the Δ*cbaCEBA*Δ*chuPRSTUV* strain that was obtained using the Δ*cbaCEBA* mutant as background (Batista et al., 2019). The insertion mutants for the non-ribosomal peptide synthetase (NRPS) genes *cbaF* and *vbaF* were obtained by a protocol based on a single recombination event (Batista et al., 2019). For genetic complementation, the *chuP*, *chuR*, *chuS*, *chuTUV*, and *chuPRSTUV* genes were amplified by PCR, cloned into the low-copy-number plasmid pMR20, and transferred to the mutant strains by conjugation. The primers used for cloning, sequencing, and mutant confirmation are listed in **Supplementary Table 1**.

MIC Assay

To achieve iron-limited conditions in M9CH for *C. violaceum*, we determined the minimal inhibitory concentration (MIC) of DP in this medium, as previously performed in LB medium (Batista et al., 2019). Wild-type *C. violaceum* overnight cultures were diluted to an optical density at 600 nm (OD_{600}) of 0.01 in M9CH, without or with DP (100 μM, 112.5 μM, 125 μM, 132.5 μM, and 150 μM), and grown under agitation (250 rpm) at 37°C. The MIC of 132.5 μM DP for the WT strain was established based on the turbidity of the cultures after 24 h cultivation.

Growth Curves

Growth curves were determined in M9CH without or with Hm. Overnight cultures of *C. violaceum* strains were diluted in 5 mL of M9CH to an OD_{600} of 0.02. Then, a new dilution (1:2) was performed to achieve an OD_{600} 0.01 and the required concentrations of Hm in 200 μL final M9CH in 96-well plates. The plates were incubated at 37°C under moderate orbital agitation in SpectraMax i3 MiniMax Imaging Cytometer

(Molecular Devices). The measurements of OD_{600} were recorded every 15 minutes over 24 hours. The experiment was performed in three biological replicates.

Heme and Hemoglobin Nutrition Assay

The ability of *C. violaceum* to use Hm and Hb as iron sources was assessed using a nutrition assay (Balhesteros et al., 2017) with some modifications. *C. violaceum* overnight cultures in M9CH were diluted to an OD_{600} of 1.0 in M9CH. Then, 25 μL of each dilution were embedded in 25 mL of iron-depleted M9CH 0.8% agar (containing 50 μM, 100 μM, 125 μM or 150 μM of DP). Paper discs were added onto the plate surface, and 10 μL aliquots of 100 μM Hm, 20 mM NaOH, 150 μM Hb, and 100 mM NaCl were applied to individual discs. After incubation for 16 h at 37°C, we inspected for growth halos that developed around the discs. The growth area was quantified using the Image J software and normalized by subtracting the disc areas. The experiment was performed in three biological replicates.

Cell Viability in the Presence of Heme

The toxic concentrations of Hm for *C. violaceum* were assessed by cell viability. Overnight cultures were diluted to an OD_{600} of 0.01 in M9CH without or with Hm (30 μM, 600 μM, and 2000 μM), and grown under agitation (250 rpm) for 24 h at 37°C. Serial dilution in phosphate-buffered saline (PBS) was performed, and 10 μL were spotted onto M9CH plates. Hemin toxicity was determined based on the colony-forming units (CFU) displayed by the strains after incubation for 24 h at 37°C. These experiments were performed in three biological replicates.

Hemolysis Assay

The hemolytic activity was assessed in 5% (v/v) sheep-blood Mueller-Hinton agar plates. Five microliters of *C. violaceum* M9CH overnight cultures were spotted onto the plate. The hemolytic activity was detected by the lighter halos that developed due to erythrocyte lysis after incubation for 7 days at 37°C. The area of activity was quantified using the Image J software and normalized by subtracting the bacterial growth area. The experiment was performed in three biological replicates.

Siderophore Assay

Siderophores were detected by chrome azurol S (CAS) plate assay in modified peptone-sucrose agar (PSA-CAS) plates (Batista et al., 2019; Santos et al., 2020). Ten microliters of *C. violaceum* overnight cultures in M9CH were spotted onto the plate surface, and the siderophores were detected by the orange halos that developed after incubation for 24 hours at 37°C. The area of the halos was quantified using the Image J software and normalized by subtracting the bacterial growth area. The experiment was performed in three biological replicates.

Transcriptional *lacZ* Fusions and β-Galactosidase Assays

The upstream regions of genes of interest were amplified by PCR with specific primers (**Supplementary Table 1**) and cloned into the pGEM-T easy plasmid (Promega). After digestion with proper restriction enzymes (**Supplementary Table 1**), the inserts were subcloned into the pRKl*acZ*290 vector to generate transcriptional fusions to the *lacZ* gene. *C. violaceum* cultures harboring the reporter plasmids were grown until an OD_{600} of 0.6 – 0.8 in M9CH, and either untreated or treated with 100 μM Hm or 100 μM $FeSO_4$ for 2 h. For all expression assays, the M9CH medium was used as the iron-limited condition because we previously found that the expression of an iron-regulated gene was similarly high in M9CH or M9CH with DP (Santos et al., 2020). Bacterial cells were assayed for β-galactosidase activity as previously described (Santos et al., 2020). The experiment was performed in three biological replicates.

Co-Transcription by RT-PCR

The *C. violaceum* wild-type strain was grown in M9CH until an OD_{600} of 1.0 – 1.2. Total RNA was extracted using Trizol reagent (Invitrogen) and purified with Direct-zol™ RNA Miniprep Plus (Zymo Research). RT-PCR was performed with the SuperScript III One-Step RT-PCR System with Platinum Taq High Fidelity DNA Polymerase (Invitrogen). One microgram of each RNA sample and specific primers (**Supplementary Table 1**) that amplify regions from *chuP* to *chuR* (439 bp), *chuR* to *chuS* (373 bp), and *chuS* to *chuT* (662 bp) were used in the reactions. PCRs using conventional Taq DNA polymerase, and the same sets of primers, were performed with genomic DNA (positive control) and RNA (negative control) as templates.

Gene Expression by RT-qPCR

The *C. violaceum* wild type, Δ*chuP*, and Δ*chuP*[*chuP*] strains were grown in M9CH until midlog growth phase, and the cultures were either untreated or treated with 100 μM Hm or 100 μM $FeSO_4$ for 2 h. Total RNA was extracted and purified as described above. Two micrograms of total RNA from each sample were converted to cDNA using the High-Capacity cDNA Reverse Transcription kit (Thermo Fisher Scientific). Genomic DNA contamination (for RNA) and reverse transcription efficiency (for cDNA) were checked by conventional PCR with the primers for the *rpoH* gene (**Supplementary Table 1**). Quantitative PCR (qPCR) reactions were performed using the PowerUp™ SYBR™ Green Master Mix (Thermo Fisher Scientific), the specific primers (**Supplementary Table 1**), and 0.5 μL of cDNA. The relative expression was calculated by the $2^{-\Delta\Delta Ct}$ method (Livak and Schmittgen, 2001). Data from three biological replicates were normalized by an endogenous control (*rpoH* gene) and a reference condition (WT in M9CH 100 μM Hm). The treatment with Hm was used as a control based on the β-galactosidase assays that indicated an intermediate expression of the *chu* operon under this condition.

Expression and Purification of the Recombinant ChuP

The coding region of *chuP* was amplified by PCR (**Supplementary Table 1**) and cloned into the pET-15b plasmid (**Table 1**). After induction in *E. coli* BL21(DE3) with 1 mM Isopropyl β-D-1-thiogalactopyranoside (IPTG) for 2 h at 37°C, the His-ChuP protein was purified from the soluble extract by affinity chromatography in a Ni-NTA Superflow column (Qiagen). The

elution fractions were evaluated using 18% SDS-PAGE. The aliquots containing the purified His-ChuP were concentrated using a VivaSpin 6 column (Sartorius), and desalted by gel filtration in PD-10 column (GE Healthcare) in storage buffer (100 mM NaH_2PO_4, 600 mM NaCl, 20% glycerol, pH 8) (Puri and O'Brian, 2006). The concentration of the His-ChuP protein was determined by measurement of OD at 280 nm and using its extinction coefficient calculated by the Protparam Tool (ExPASy) (http://web.expasy.org/protparam).

Heme Binding Assay

The ability of the recombinant His-ChuP protein to interact with Hm was evaluated by spectrophotometry (Puri and O'Brian, 2006; Amarelle et al., 2016). The reactions were performed in interaction buffer (50 mM $Na_2H_2PO_4$, 300 mM NaCl, 10% glycerol, pH 8) without (reference cuvette) or with 10 μM of His-ChuP (sample cuvette). Aliquots of Hm (0 to 30 μM) were added to both cuvettes. After incubation for 5 minutes at 25°C in the dark, the absorbance between the wavelengths 300 and 600 nm was measured with 10 nm increments on a SpectraMax i3 MiniMax Imaging Cytometer. The binding of ChuP to Hm was determined by the change in absorbance at 413 nm fit to one-site binding model non-linear regression on Graph Pad Prism 7.

Electrophoretic Mobility Shift Assay (EMSA)

DNA sequences upstream of *chuP*, *chuR*, and CV_2599 were amplified by PCR using the primers listed in **Supplementary Table 1**. The DNA fragments were radiolabeled and used for interaction with His-ChuP following a previously described protocol (da Silva Neto et al., 2009; Previato-Mello et al., 2017), with the modification of adding the CV_2599 promoter fragment (negative control) in the same reaction.

Mouse Virulence Assays

Virulence assays were performed in a mouse intraperitoneal (i.p.) model of *C. violaceum* infection as previously established (Previato-Mello et al., 2017; Batista et al., 2019). Bacterial strains were diluted to an OD_{600} of 0.01 and cultured in 5 mL LB for 20 h at 37°C. A dose of 10^6 CFU in PBS was injected into 6-week-old female BALB/c mice, and the animals were monitored for 7 days post-infection. To assess the bacterial burden in the liver and spleen, mice were infected as above and euthanized 20 h or 96 h post-infection (h.p.i.). The organs were aseptically collected, homogenized in PBS, and the dilutions were plated for CFU counting. Mice were obtained and maintained at the Animal Facilities of Ribeirão Preto Medical School (FMRP-USP). The assays were performed according to the Ethical Principles in Animal Research adopted by the National Council for the Control of Animal Experimentation (CONCEA). The animal ethics protocol 146/2019 was approved by the Local Ethics Animal Committee (CEUA) of FMRP-USP.

Statistical Analysis

Data collected were employed for statistical analysis in GraphPad Prism version 7. For the column graphs, the normality test was performed using Shapiro-Wilk's test. Statistically significant p values and the tests that were performed are indicated in the figure legends.

RESULTS

The *chuPRSTUV* Operon Is Regulated by Fur According to the Iron Levels

In silico analysis of the *C. violaceum* ATCC 12472 genome sequence revealed a gene cluster with six genes (CV_RS19275-280-285-290-295-300) that resembles an operon encoding a putative heme utilization system. These genes, here named *chuPRSTUV*, are annotated as a HemP/HmuP family regulator (ChuP), a TonB-dependent receptor (ChuR), a hemin degrading factor (ChuS), and an ABC-transport system (ChuTUV) (**Figure 1A**). To evaluate if the *chuPRSTUV* genes are organized into an operon, we performed RT-PCR reactions using RNA from the WT strain grown in M9CH and a set of primers that amplify regions between *chuPR*, *chuRS*, and *chuST* genes (**Figures 1A, B**). After reverse transcription and amplification, bands with the expected sizes were detected for the three tested primer combinations, confirming that the *chuPRSTUV* genes are indeed co-transcribed (**Figure 1B**).

Our inspection of the promoter region of *chuP* revealed a putative Fur binding site sequence (ATGATAATGGTTATCATT) that resembles Fur boxes found in other bacteria (Sarvan et al., 2018). To investigate whether the *chu* operon is regulated by iron and Fur, we cloned the promoter region of *chuP* into a *lacZ* reporter plasmid. The WT and Δ*fur* strains harboring the p*chuP-lacZ* fusion were used to assess the *chuP* promoter activity by β-galactosidase assay in M9CH medium, which was previously reported as an iron-limited condition (Santos et al., 2020) and under iron sufficiency (M9CH supplemented with Hm or $FeSO_4$) (**Figure 1C**). The promoter activity was higher under iron-limited (M9CH) than iron-replete conditions in the WT strain. The reduction in activity was higher with $FeSO_4$ than with Hm supplementation. In the Δ*fur* mutant, the promoter was highly active regardless of iron levels. Moreover, the activity was twofold higher than that detected for the WT strain in M9CH, suggesting total promoter de-repression in the absence of Fur (**Figure 1C**). Altogether, these results demonstrate that the *chuPRSTUV* genes comprise a Fur-repressed operon that is expressed under iron limitation.

The *chuPRSTUV* Operon Encodes a Heme Uptake System (ChuRTUV) and a Regulatory Protein (ChuP) Required for Heme and Hemoglobin Utilization

To characterize the role of the *chuPRSTUV* operon in *C. violaceum*, we generated null-mutant strains deleted for single genes (Δ*chuP*, Δ*chuR*, and Δ*chuS*) or multiple genes (Δ*chuTUV* and Δ*chuPRSTUV*) of the *chu* operon, and their respective complemented strains. We also obtained a mutant strain lacking both the *chu* operon and the *cbaCEBA* genes (Δ*cbaCEBA*Δ*chuPRSTUV*). The CbaCEBA enzymes are involved in the synthesis of 2'3-DHB, the precursor of

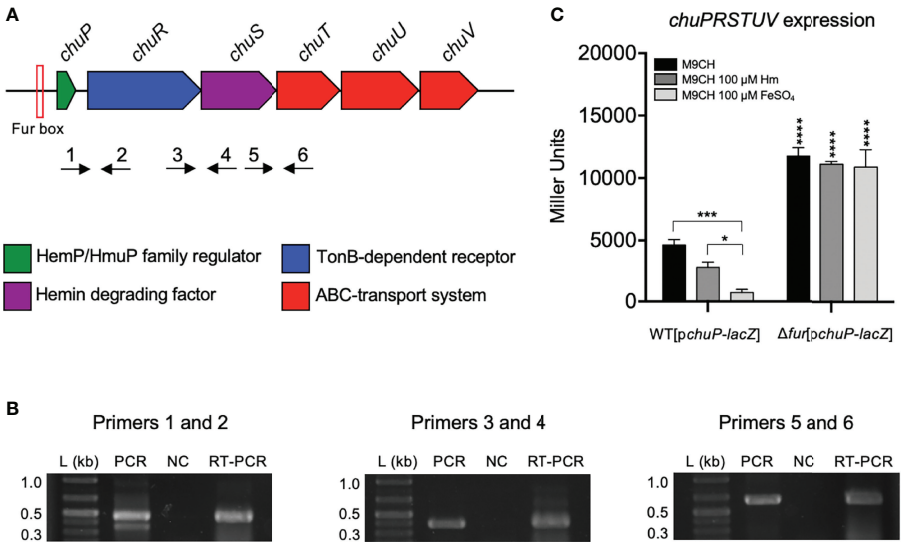

FIGURE 1 | The *chuPRSTUV* genes compose an operon regulated by the iron levels and Fur. **(A)** Genomic organization of the *chuPRSTUV* genes in *C. violaceum*. A predicted Fur box is indicated. Numbered arrows indicate the primers used in RT-PCR (not scaled). **(B)** Confirmation of co-transcription of the *chuPRSTUV* genes. The RT-PCR reactions amplified fragments of 439 bp (Primers 1 and 2), 373 bp (Primers 3 and 4), and 662 bp (Primers 5 and 6). Conventional PCR was performed using genomic DNA (PCR) and RNA (NC) as controls. L, 1 Kb plus DNA Ladder (Thermo Scientific). **(C)** Promoter activity of the *chu* operon in response to iron and Fur. β-galactosidase assays were performed from the WT and Δ*fur* strains harboring the *chuP-lacZ* fusion grown in M9CH medium and either untreated or treated with 100 µM Hm or 100 µM $FeSO_4$. Data are from three biological replicates. ****$p < 0.0001$; ***$p < 0.001$; *$p < 0.05$; when not indicated, not significant. Two-way ANOVA followed by Dunnett's multiple-comparison test.

catecholate-type siderophores in *C. violaceum* (Batista et al., 2019). All mutants showed regular fitness, as assessed by growth curves in M9CH and M9CH plus heme and by cell viability in LB (**Supplementary Figure 1**).

To test the involvement of the *C. violaceum chu* genes in heme and hemoglobin utilization, we developed a nutrition assay providing 100 µM Hm or 150 µM Hb as alternative iron sources in M9CH medium chelated for iron with different DP concentrations (**Supplementary Figure 2**). We chose 125 µM DP to compare all strains (**Figure 2**) because it was the best condition to visualize the growth halos in the WT strain (**Supplementary Figure 2**). Under these conditions (125 µM DP), the WT and the Δ*chuS* strains formed Hm and Hb-stimulated growth halos. All the other mutant strains of the *chuPRSTUV* operon lost the ability to grow when Hm and Hb were provided as iron sources (**Figure 2**). For the Δ*chuR* strain, a very weak growth stimulus could still be detected only in the presence of heme (**Figure 2B**). Genetic complementation of the mutant strains fully restored the growth in Hm and Hb under deficiency with 125 µM DP (**Figure 2**). The Δ*cbaCEBA* mutant that does not synthesize siderophores showed no growth halos at 125 µM DP (**Figure 2**), but its growth was clearly stimulated by Hm and Hb at 50 µM DP (**Supplementary Figure 2**). This is consistent with previous results indicating that the growth of a Δ*cbaCEBA* mutant is strongly impaired under DP-imposed iron limitation (Batista et al., 2019). Taken together, these results demonstrate that the *chuPRSTUV* operon encodes a heme uptake system (ChuRTUV) that is also involved in hemoglobin utilization. Moreover, the weak growth detected for the Δ*chuR* mutant with Hm but not with Hb suggests that *C. violaceum* has additional mechanisms in the outer membrane for heme uptake but relies specifically on ChuR for heme uptake from hemoglobin.

Considering that the Δ*chuS* strain showed no altered phenotype for Hm and Hb utilization (**Figure 2**), we evaluated its role on cell viability under heme excess (**Supplementary Figure 3**). However, growth defects were not observed for the WT, Δ*chuS*, and all mutant strains even at a high Hm concentration of 2 mM, indicating that the *chu* operon has no role during our heme excess conditions. Interestingly, deletion of the *chuPRSTUV* operon in the Δ*cbaCEBA* mutant strain improved the small colony size phenotype (**Supplementary Figure 3**), previously described for this strain (Batista et al., 2019). We also tested the hemolytic activity of the *chu* mutants on sheep-blood agar (**Supplementary Figure 4**). The strains Δ*chuR* (increased and intense halo) and Δ*cbaCEBA* (intense halo) showed altered hemolytic activity when compared to that of the WT and the other mutant strains. Although the meaning of these findings is unclear, we speculate that the increased hemolytic activity in these strains is a compensatory mechanism to deal with iron/heme scarcity.

The Δ*chuP* Mutant Has Increased Siderophore Halos Due to Viobactin

To verify whether the *chu* operon affects the production/release of siderophores in *C. violaceum*, we tested the *chu* mutants on

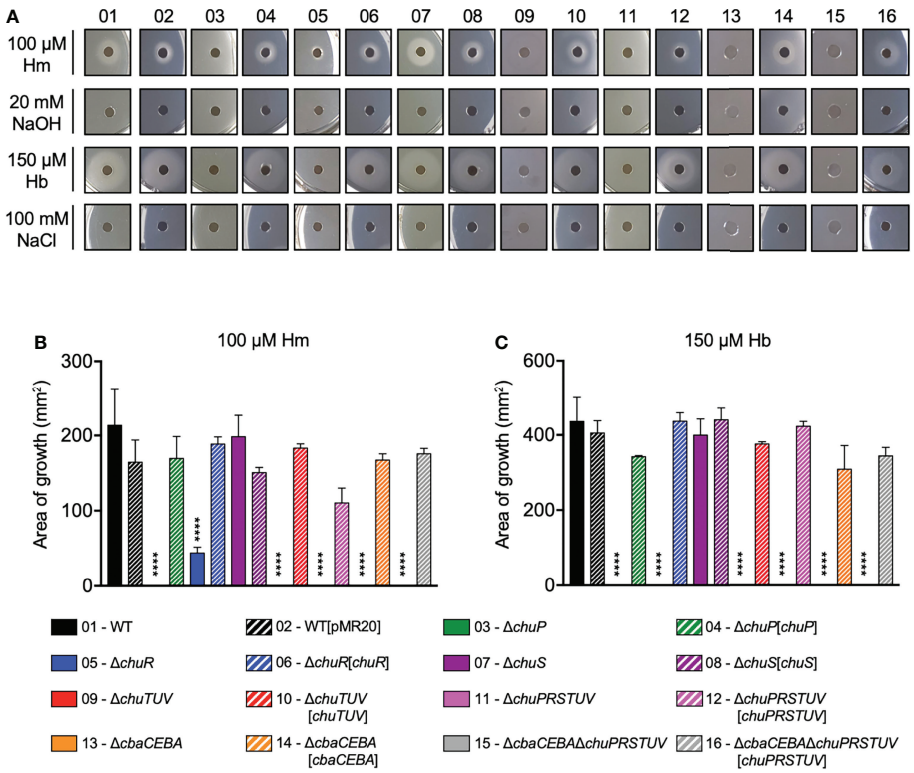

FIGURE 2 | The *chu* operon encodes a heme uptake system (ChuRTUV) and a regulatory protein (ChuP) required for heme and hemoglobin utilization. **(A)** Nutrition assay for Hm and Hb under DP-imposed iron deficiency. The indicated strains were embedded into M9CH medium supplemented with 125 µM DP. Aliquots of 100 µM Hm and 150 µM Hb were provided as iron sources, while 20 mM NaOH and 100 mM NaCl were used as negative controls. Growth halos around the discs indicate compound utilization. Representative images are shown. **(B, C)** Quantification of Hm and Hb-stimulated growth. The area of the growth halos stimulated by Hm **(B)** and Hb **(C)** was measured using Image J software by subtracting the area of the discs. Data are from three biological replicates. Mutant and complemented strains were compared to WT and WT[pMR20], respectively. ****$p < 0.0001$; when not indicated, not significant. One-way ANOVA followed by Tukey's multiple-comparison test.

PSA-CAS plates for siderophore detection as orange halos (**Figure 3**) as previously described (Batista et al., 2019). The Δ*chuP* and Δ*chuPRSTUV* mutants showed increased siderophore halos, while the Δ*chuR*, Δ*chuS*, and Δ*chuTUV* mutants had siderophore halos similar to that of the WT strain (**Figures 3A, B**). The Δ*cbaCEBA* strain showed no siderophore halo, as previously demonstrated (Batista et al., 2019), as well as the Δ*cbaCEBA*Δ*chuPRSTUV* strain (**Figures 3A, B**). After complementation, the siderophore halos were restored to WT levels in the Δ*chuP*[*chuP*] strain. For the strains Δ*chuPRSTUV* [*chuPRSTUV*] (almost absence of halo) and Δ*cbaCEBA* [*cbaCEBA*] (increased halo), the siderophore phenotypes reverted further on that observed in the WT strain (**Figures 3A, B**), perhaps owing to overexpression of the genes into the plasmid. These data indicate that the small regulatory protein ChuP controls the siderophore levels in *C. violaceum*.

C. violaceum produces the catecholate-type siderophores chromobactin and viobactin employing the NRPS enzymes CbaF and VbaF, respectively (Batista et al., 2019). We combined mutation in *chuP* with mutations in *cbaF* or *vbaF* to understand which siderophore contributes to the increased siderophore halos in Δ*chuP*. Individual deletion of *cbaF* or *vbaF* genes in the WT had no effect on siderophore halos (**Figures 3C, D**), as previously reported (Batista et al., 2019). When these genes were deleted in the Δ*chuP* mutant background, a decrease in siderophore halos was observed in both cases. However, the halos were similar to that of the WT strain only when *vbaF* was deleted (**Figures 3C, D**), demonstrating a prominent role of viobactin on the increased siderophore halos of Δ*chuP*. Altogether, these results suggest that ChuP controls the synthesis and/or uptake of the siderophore viobactin in *C. violaceum*.

ChuP Is a Heme-Binding Post-Transcriptional Regulator of *chuR* and *vbuA* Encoding TBDRs for Heme and the Siderophore Viobactin

Our data indicate that mutation of *chuP* in *C. violaceum* abolished heme utilization (**Figure 2**) and altered the levels of the siderophore viobactin (**Figure 3**). We employed different methodologies to elucidate how ChuP regulates these processes (**Figure 4**). First, we tested whether ChuP is a heme-binding

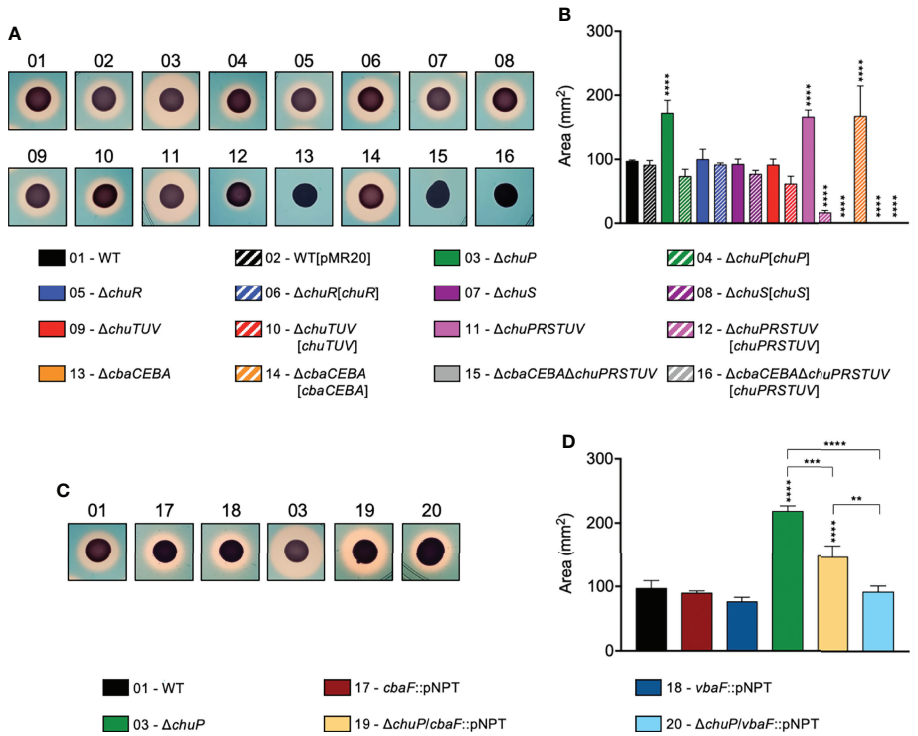

FIGURE 3 | Deletion of *chuP* impacts the siderophore levels in *C. violaceum*. **(A, B)** Role of the *chu* operon on the siderophore levels in *C. violaceum*. Mutant strains without *chuP* showed increased siderophore halos. **(C, D)** The effect of ChuP occurs on the siderophore viobactin. For all indicated strains, the siderophore detection was performed by CAS assays on PSA-CAS plates. *C. violaceum* cultures were spotted onto the plate surface, and the orange halos indicating secreted siderophores were photographed **(A, C)** and measured **(B, D)**, after incubation for 24 hours at 37°C, using Image J software. The area of the siderophore halos was calculated subtracting the area of bacterial growth. Data are from three biological replicates. Mutant and complemented strains **(B)** were compared to WT and WT [pMR20], respectively. Insertion mutants **(D)** were compared to the strains they derived from. $^{**}p < 0.01$; $^{***}p < 0.001$; $^{****}p < 0.0001$; when not indicated, not significant. Vertical asterisks indicate comparisons with the WT strain. One-way ANOVA followed by Tukey's multiple-comparison test.

protein. We purified the recombinant protein His-ChuP and performed a heme-binding assay (**Figure 4A**). After incubation with increasing Hm concentrations, a Soret peak at 413 nm was detected, indicating the formation of a ChuP-heme complex (**Figure 4A**). The differential absorption spectroscopy at 413 was used to fit a single binding model and determined that ChuP binds heme with a k_d = 18.36 ± 4.66 μM (**Figure 4A**, insert). Considering that HemP/HmuP proteins have been described as transcriptional activators (Escamilla-Hernandez and O'Brian, 2012; Sato et al., 2017), we tested whether the *C. violaceum* ChuP regulates and binds into the intergenic regions upstream of *chuP* (promoter of the *chu* operon) and *chuR* (**Figures 4B, C**). The WT and Δ*chuP* strains harboring these constructs (p*chuP-lacZ* or p*chuR-lacZ*) were assessed by β-galactosidase assay under different iron levels. The p*chuP-lacZ* promoter fusion was highly active under iron deficiency (M9CH) with a gradual decrease upon Hm and $FeSO_4$ supplementation (**Figure 4B**), as previously observed in the WT strain (**Figure 1C**). However, the same activity pattern was detected in the Δ*chuP* mutant strain, indicating that ChuP does not seem to regulate the promoter of the *chu* operon (**Figure 4B**). The p*chuR-lacZ* fusion had no promoter activity regardless of the strain or condition, indicating the absence of a promoter upstream of *chuR*. Therefore, this fusion is not useful to verify the effect of ChuP on *chuR* expression. Consistent with the β-galactosidase assays, our EMSA assays indicated that ChuP does not bind to the probes containing only the promoter of the *chu* operon or containing the entire region from *chuP* to *chuR* (**Figure 4C**). Altogether, these results demonstrate that ChuP does not regulate the promoter of the *chu* operon nor act as a DNA binding protein.

In *E. meliloti*, the HmuP protein activates the expression of the TBDR ShmR at a post-transcriptional level, probably by acting on a sequence HPRE (HmuP-responsive element). The HPRE sequences were predicted upstream of genes encoding heme TBDRs in many bacteria, including the *C. violaceum chuR* (sequence CCCGCAAGCCAGCCGACAGCCAGCCAGCG, -26 nt from the ATG start codon) (Amarelle et al., 2019). In addition to *chuR*, we found an HPRE sequence upstream of *vbuA* (sequence GCCAGCCAGACGACGCCGCCG, -49 nt from the ATG start codon), a TBDR gene located far from the *chu* operon (**Figures 4D, E**), raising the possibility that ChuP is a post-transcriptional regulator in *C. violaceum*. To verify this hypothesis, we performed RT-qPCR for *chuR*, *vbuA*, and *vbaF* genes with RNA harvested from the WT, Δ*chuP*, and Δ*chuP*

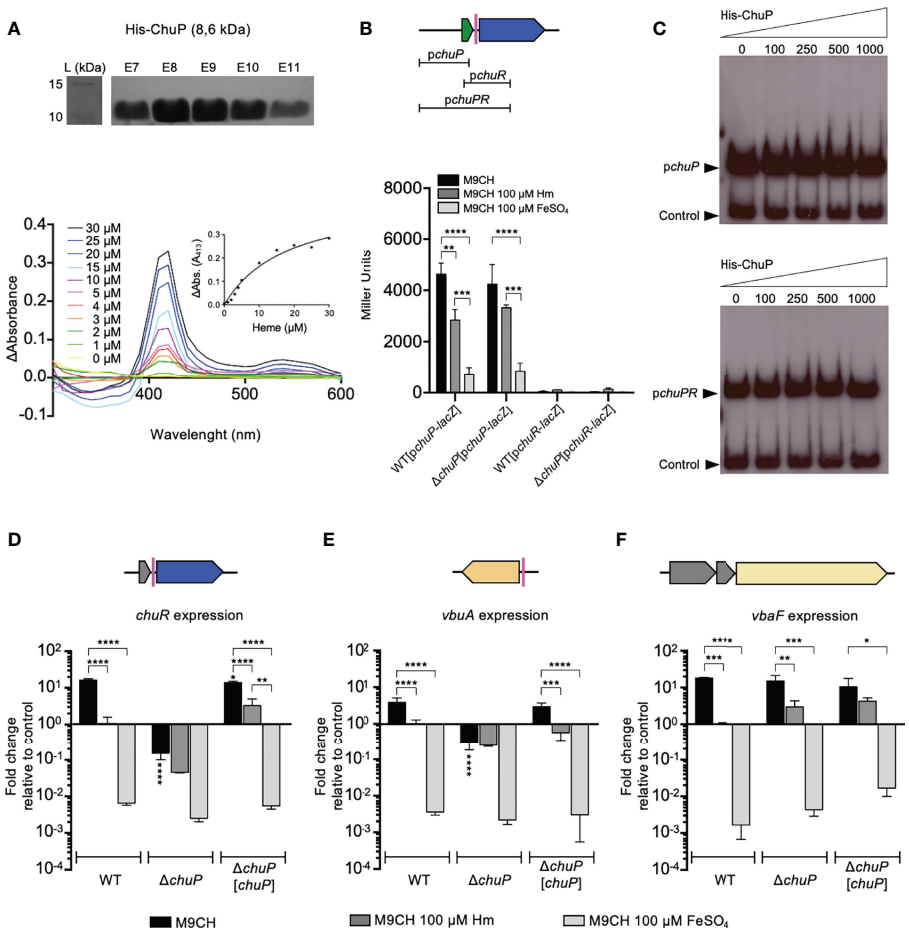

FIGURE 4 | ChuP is a heme-binding regulatory protein that controls *chuR* and *vbuA* expression at a post-transcriptional level. **(A)** ChuP binds heme. The His-ChuP protein was purified (top) and incubated (10 μM protein) with the indicated concentrations of Hm (bottom). The absorption spectra were measured from 300 nm to 600 nm on a SpectraMax i3 MiniMax Imaging Cytometer. The changes at 413 nm were used to calculate the ChuP-Hm affinity (insert). Data are shown as differential absorption spectra: the difference of values obtained from the sample cuvette (His-ChuP and Hm) against the reference cuvette (Hm). Data are from a single experiment of three independent replicates. L, protein ladder; E7 to E11, eluted fractions of purified ChuP. **(B)** ChuP does not regulate the promoter of the *chu* operon. The scheme (top) indicates the regions used for β-galactosidase or EMSA assays. β-galactosidase assays were performed from the WT and Δ*chuP* strains harboring *chuP-lacZ* and *chuR-lacZ* fusions grown in M9CH in the indicated conditions of iron availability. Data are from three biological replicates. **p < 0.01; ***p < 0.001; ****p < 0.0001. When not shown, n.s. (not significant). Two-way ANOVA followed by Dunnett's multiple-comparison test. **(C)** ChuP does not bind to DNA probes covering from *chuP* to *chuR*. The indicated concentrations of His-ChuP were used in EMSA assays with the *chu* indicated probes. In both cases, the promoter region of CV_2599 (control) was used as an in-reaction unspecific negative control. **(D-F)** *chuR* and *vbuA* but not *vbaF* have HPRE sequences and are regulated by ChuP. The predicted HPREs are indicated as colored bars in the gene maps. Expression was evaluated by RT-qPCR. cDNA was reverse transcribed from RNA obtained from the WT, Δ*chuP*, and Δ*chuP*[*chuP*] strains grown in M9CH, and either untreated or treated with 100 μM Hm or 100 μM $FeSO_4$. Expression of *chuR*, *vbuA*, and *vbaF* is shown as the fold change relative to the control condition (WT in M9CH 100 μM Hm). Data are from three biological replicates. ****p < 0.0001; ***p < 0.001; **p < 0.01; *p < 0.05; when not indicated, not significant. Vertical asterisks indicate comparisons with the WT strain at the same condition. One-way ANOVA followed by Tukey's multiple-comparison test.

[*chuP*] under different iron levels (**Figures 4D–F**). The expression of the three genes in the WT strain was high under iron-depleted and low under iron-sufficient conditions when compared to the control condition (WT grown in M9CH 100 μM Hm), as expected for genes related to iron acquisition (**Figures 4D–F**). Consistent with our phenotypic results and the presence of HPRE elements, the expression of *chuR* and *vbuA* was decreased in the Δ*chuP* strain regardless of the iron levels (**Figures 4D, E**), indicating that ChuP is a positive regulator required for the maximum expression of *chuR* and *vbuA* under iron limitation. Complementation of Δ*chuP* restored the expression of *chuR* and *vbuA* to the levels found in the WT strain (**Figures 4D, E**). No differences in *vbaF* expression were detected between the WT and Δ*chuP* strains in any of the tested conditions (**Figure 4F**), indicating that ChuP does not control the expression of VbaF, the NRPS for viobactin synthesis. Therefore, the decreased expression of *chuR* and *vbuA* in Δ*chuP* explains the inability of this mutant strain to use Hm and Hb (**Figure 2**) (via ChuR) and its increased siderophore halos (**Figure 3**) (inability to uptake viobactin *via* VbuA).

Indeed, a Δ*vbuA* mutant showed large siderophore halos (Batista et al., 2019) as those found in Δ*chuP*. Altogether, these results demonstrate that ChuP integrates the acquisition of heme and siderophore by acting as a heme-binding post-transcriptional regulator of the TBDR genes *chuR* and *vbuA*.

C. violaceum Employs Both Siderophores and Heme for Iron Acquisition During Infection

To assess the role of the heme utilization system ChuPRSTUV during *C. violaceum* infection, we performed mice virulence assays (**Figure 5**). The animals were i.p. injected with a dose of 10^6 bacterial cells and analyzed for survival during seven days post-infection (**Figures 5A, B**). The five null-mutant strains of the ChuPRSTUV system showed barely or no virulence attenuation compared to the *C. violaceum* WT strain (**Figure 5A**). Previously, we determined that abrogating siderophore production in *C. violaceum* by deletion of the *cbaCEBA* genes causes moderate attenuation in virulence (Batista et al., 2019). Therefore, we checked whether heme and siderophores cooperate for virulence. Indeed, the Δ*cbaCEBA* strain showed an intermediate virulence attenuation, as expected, while a more expressive virulence attenuation was observed for the Δ*cbaCEBA*Δ*chuPRSTUV* strain (**Figure 5A**). Complementation of the latter strain with the *chuPRSTUV* operon reverted its virulence attenuation phenotype to the pattern observed for the Δ*cbaCEBA* mutant (**Figure 5B**).

We evaluated the bacterial burden in the liver and spleen, two organs colonized during *C. violaceum* infection that are involved in host heme recycling. Interestingly, the Δ*cbaCEBA*Δ*chuPRSTUV* mutant displayed the same CFU counting as the WT strain at 20 hours post-infection in both organs (**Figures 5C, D**). However, the bacterial burden was reduced (in the liver) and eliminated (in the spleen) at 96 hours post-infection (**Figures 5C, D**). These results

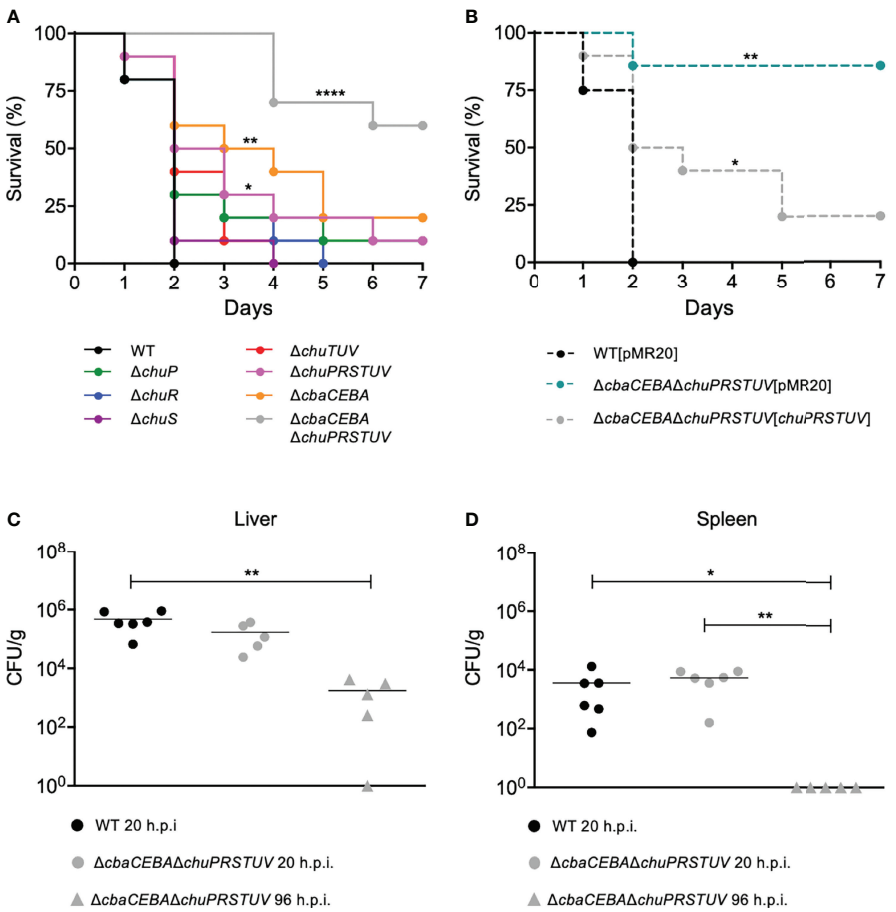

FIGURE 5 | *C violaceum* requires siderophores and heme but prefers siderophores in a mice model of acute infection. **(A, B)** Survival curves of infected BALB/c mice. Animals (n = 8 for WT[pMR20]; n = 7 for Δ*cbaCEBA*Δ*chuPSRTUV*[*chuPRSTUV*]; n = 10 for all other strains) were i.p. injected with 10^6 CFU of the indicated *C. violaceum* mutant **(A)** and complemented **(B)** strains. Animal survival was monitored daily for a week. *p < 0.05; **p < 0.01; ****p < 0.0001; when not shown, n.s. (not significant). Log-rank (Mantel-Cox) test. **(C, D)** Bacterial burden in organs. Animals were infected with 10^6 CFU of the indicated strains. After 20h or 96 h post-infection (h.p.i.), the liver **(C)** and the spleen **(D)** were collected, homogenized, serially diluted, and plated for CFU quantification. *p < 0.05; **p < 0.01; when not indicated, not significant. One-way ANOVA followed by Tukey's (liver) or Dunnett's (spleen) multiple-comparison tests.

indicate that the absence of siderophores and heme uptake does not impair initial colonization but impairs the bacterial maintenance in later infection stages. Altogether, these results indicate an interplay between the iron-acquisition strategies based on siderophore and heme during *C. violaceum* infection. In our acute infection model, the requirement of heme uptake for virulence becomes evident in the absence of siderophores.

DISCUSSION

In this work, we identified and characterized a heme and hemoglobin utilization system, here named ChuPRSTUV, which connects, *via* the regulatory protein ChuP, iron acquisition by heme and siderophore during *C. violaceum* infection (**Figure 6**). Our data indicated that the genes *chuPRSTUV* compose an operon repressed by Fur under iron sufficiency. During iron limitation (as found inside the host), high expression of the *chu* operon (for heme uptake by the transport system ChuR-ChuTUV) and the *vbaF* and *vbuA* genes (for synthesis and uptake of the siderophore viobactin) occurred (**Figures 6A, B**). Remarkably, we found that the maximum expression in iron scarcity of the TBDR genes *chuR and vbuA* depends on the small heme-binding protein ChuP. In our model, we propose that ChuP is a positive post-transcriptional regulator acting in the 5'-UTR of the *chuR and vbuA* transcripts (**Figure 6A**). Without ChuP, the expression of *chuR* and *vbuA* dropped, rendering the Δ*chuP* mutant strain its inability to use Hm and Hb *via* ChuR and its increased siderophore halos (deficiency to uptake viobactin *via* VbuA). Moreover, our

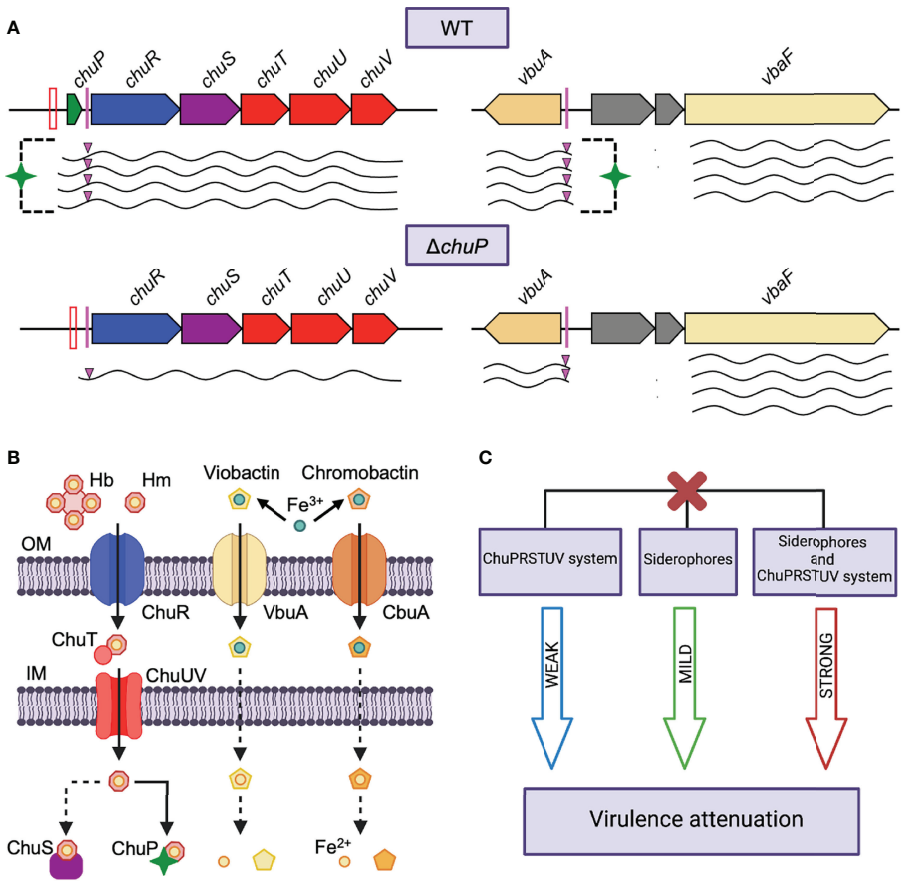

FIGURE 6 | Model of how *C. violaceum* connects iron acquisition by heme and siderophore during infection. **(A)** Regulatory function of ChuP over *chuR* and *vbuA*. **(B)** Iron acquisition systems in *C. violaceum* for the uptake of heme (this work) and the siderophores viobactin and chromobactin (Batista et al., 2019). **(C)** Interplay between the uptake of heme and siderophore in the *C. violaceum* virulence. We propose that ChuP links heme and siderophore utilization by acting as a positive regulator of *chuR* and *vbuA*, which encode TBDRs for the uptake of heme (ChuR) and the siderophore viobactin (VbuA). In addition to Fur derepression, the expression of *chuR* and *vbuA* depends on ChuP under iron deficiency, possibly by a post-transcriptional mechanism involving HPRE (HmuP-responsive elements) sequences found in the 5'-UTR of the *chuR* and *vbuA* transcripts. In the absence of ChuP, the abundance of *chuR* and *vbuA* transcripts decreases, causing a reduction in heme and viobactin utilization. Different levels of virulence attenuation occurred when the ChuPRSTUV system (weak), the siderophores (mild), or both (strong) were deleted, indicating that *C. violaceum* prefers siderophores over heme during infection but relies on heme in the absence of siderophores. Red bars, Fur boxes; Pink bars and triangles, predicted HPRE sequences; Green stars, ChuP protein; Waved lines, mRNAs; Red X, mutant strains; OM, Outer membrane; IM, Inner membrane; Dashed lines, unknown mechanisms.

virulence data in mice demonstrated that *C. violaceum* uses both heme and siderophore for iron acquisition during infection, with a preference for siderophores over the Chu heme uptake system (**Figure 6C**).

We demonstrated that the *chuPRSTUV* genes are co-transcribed from an iron-responsive and Fur-repressed promoter in *C. violaceum*, a gene cluster organization and expression pattern that fit with those found for heme uptake system in other bacteria, such as *B. multivorans*, *Yersinia* spp., and *P. aeruginosa* (Sato et al., 2017; Si et al., 2017; Schwiesow et al., 2018; Otero-Asman et al., 2019). Our nutrition assays indicated that, with the exception of *chuS*, all genes of the *chu* operon are required for heme and hemoglobin utilization in *C. violaceum*, suggesting that ChuRTUV, composed by the TBDR ChuR and the ABC transport system ChuTUV, is a heme uptake system. This mechanism of heme import across the cell envelope is found in many Gram-negative bacteria (Stojiljkovic and Hantke, 1992; Burkhard and Wilks, 2007; Balhesteros et al., 2017; Huang and Wilks, 2017). The mutant Δ*chuR* but not the mutant Δ*chuTUV* showed a small halo of heme utilization, and both mutants were unable to use hemoglobin, suggesting that *C. violaceum* maybe have another TBDR for heme uptake but relies specifically on ChuR to obtain heme from hemoglobin. Indeed, in *P. aeruginosa*, a bacterium with three heme uptake systems (Phu, Has, and Hxu), the same ABC-transport system (PhuTUV) transfers heme to the cytosol after uptake by the TBDRs PhuR and HasR (Ochsner et al., 2000; Smith and Wilks, 2015; Otero-Asman et al., 2019). ChuR appears to act as a direct heme uptake transporter given that we do not find genes encoding hemophores in *C. violaceum* and ChuR does not have an N-terminal extension typically found in hemophore-based heme uptake systems (Biville et al., 2004; Wandersman and Delepelaire, 2012; Huang and Wilks, 2017). Since the *C. violaceum* Δ*chuS* mutant showed no phenotype under heme limitation or excess, further biochemical studies are necessary to investigate whether ChuS is a heme chaperone or a non-canonical heme oxygenase involved in heme degradation, as described in other bacteria (Suits et al., 2005; Amarelle et al., 2016; Lee et al., 2017).

Recent studies have shown regulatory and functional connections between heme and siderophores (Otero-Asman et al., 2019; Batko et al., 2021; Glanville et al., 2021; Zygiel et al., 2021). The increased siderophore halos detected in Δ*chuP* and Δ*chuPRSTUV* mutant strains indicate that *chuP* is the gene of the *chu* operon that connects heme and siderophore utilization in *C. violaceum*. ChuP belongs to the HemP/HmuP protein family, whose members are found in many proteobacteria (Amarelle et al., 2019). However, only HmuP from *S. meliloti* and *B. japonicum* and HemP from *B. multivorans* have been characterized. They are small regulatory proteins required for heme utilization by acting as positive regulators of heme-acquisition TBDR genes (Amarelle et al., 2010; Escamilla-Hernandez and O'Brian, 2012; Sato et al., 2017; Amarelle et al., 2019). In *B. multivorans*, a *hmuP* mutant showed decreased siderophore halos, but the underlying mechanism remains unexplored (Sato et al., 2017). Our data indicate that ChuP links heme and siderophore utilization by acting as a positive regulator required for the expression of *chuR* and *vbuA*, genes encoding the TBDRs used by *C. violaceum* for the uptake of heme/hemoglobin (ChuR) and the siderophore viobactin (VbuA) (Batista et al., 2019). Our data favor a working model of ChuP as a heme-binding post-transcriptional regulator acting in the 5'-UTR of the *chuR and vbuA* transcripts (**Figure 6**). Supporting this model, we found that (i) ChuP of *C. violaceum* binds heme, as demonstrated for HmuP of *B. multivorans* (Sato et al., 2017); (ii) ChuP does not regulate the promoter of the *chu* operon (in front of *chuP*) and its effect on *chuR* does not occur at the transcriptional level since there is no promoter in front of *chuR* and ChuP does not bind to DNA probes covering the entire region from *chuP* to *chuR*; (iii) there is the presence, upstream of *chuR* and *vbuA*, of HPRE elements, which were described as conserved sequences probably acting on mRNA in the 5'-UTR of genes encoding heme-related TBDRs (Amarelle et al., 2019). Although HemP/HmuP proteins lack a typical DNA binding domain, they were described as direct DNA binding proteins in *B. japonicum* and *B. multivorans*, maybe by interacting with Irr and Fur (Escamilla-Hernandez and O'Brian, 2012; Sato et al., 2017). Our results suggest that ChuP in *C. violaceum* works similarly to HmuP in *E. meliloti*. However, it is necessary more work such as heme binding assays with detagged ChuP and mapping of the transcriptional start sites of *chuR* and *vbuA* to understand how ChuP binds heme and exerts its role as a post-transcriptional regulator on its target genes.

Several investigations have found that genes encoding heme uptake systems are upregulated *in vivo* (Cook et al., 2019; Rivera-Chávez and Mekalanos, 2019) and required for colonization and virulence of many bacterial pathogens (Skaar et al., 2004; Si et al., 2017; Abdelhamed et al., 2018; Cook et al., 2019; Rivera-Chávez and Mekalanos, 2019; Chatterjee et al., 2020). In many cases, bacteria explore multiple host iron sources, employing both heme and siderophore-based iron acquisition systems (Contreras et al., 2014; Huang and Wilks, 2017). Our prior work revealed that *C. violaceum* requires catecholate-type siderophores for virulence in mice (Batista et al., 2019). Our current findings based on the characterization of mutants without either siderophores, the *chu* operon, or both indicate that *C. violaceum* uses siderophores and heme but prioritizes siderophores over heme as an iron source during infection, at least in our mice model of acute systemic infection (**Figure 6C**). In agreement with our data, a study that characterized mutants of multiple iron uptake systems showed a clear predominance of siderophores over heme transport systems in *P. aeruginosa* infecting lung (Minandri et al., 2016). However, the preference for a particular iron source changes according to its availability or the infection context. For instance, *S. aureus* prefers heme but uses siderophores when heme is scarce (Skaar et al., 2004); *P. aeruginosa* prioritizes siderophore systems in acute infections but switches to heme in long-term chronic infections (Marvig et al., 2014; Nguyen et al., 2014); and *Vibrio cholerae* relies on heme released by cholera toxin-dependent damage in the intestine (Rivera-Chávez and Mekalanos, 2019). Currently, we are developing a mouse model of abscess for *C. violaceum* infection. It will be interesting to investigate in this model whether *C. violaceum* alters its preference for siderophores and heme in log-term infections.

DATA AVAILABILITY STATEMENT

The original contributions presented in the study are included in the article/**Supplementary Material**. Further inquiries can be directed to the corresponding author.

ETHICS STATEMENT

The animal study was reviewed and approved by Local Ethics Animal Committee (CEUA), Faculdade de Medicina de Ribeirão Preto, Universidade de São Paulo.

AUTHOR CONTRIBUTIONS

JFdSN and VL conceived and designed the study. VL and BB performed the experiments. VL and JFdSN performed data analysis and interpretation. VL and JFdSN wrote the paper. All authors contributed to the article and approved the submitted version.

FUNDING

This research was supported by grants from the São Paulo Research Foundation (FAPESP; grants 2018/01388-6 and 2020/00259-8) and Fundação de Apoio ao Ensino, Pesquisa e Assistência do Hospital das Clínicas da FMRP-USP (FAEPA). During this work VL (2018/17716-2) and BB (2018/19058-2) were supported by FAPESP fellowships.

SUPPLEMENTARY MATERIAL

The Supplementary Material for this article can be found online at: https://www.frontiersin.org/articles/10.3389/fcimb.2022.873536/full#supplementary-material

REFERENCES

Abdelhamed, H., Ibrahim, I., Baumgartner, W., Lawrence, M. L., and Karsi, A. (2018). The Virulence and Immune Protection of *Edwardsiella Ictaluri* HemR Mutants in Catfish. *Fish. Shellfish. Immunol.* 72, 153–160. doi: 10.1016/j.fsi.2017.10.041

Amarelle, V., Koziol, U., and Fabiano, E. (2019). Highly Conserved Nucleotide Motifs Present in the 5'UTR of the Heme-Receptor Gene *shmR* are Required for HmuP-Dependent Expression of *shmR* in *Ensifer Meliloti*. *Biometals* 32, 273–291. doi: 10.1007/s10534-019-00184-6

Amarelle, V., Koziol, U., Rosconi, F., Noya, F., O'Brian, M. R., and Fabiano, E. (2010). A New Small Regulatory Protein, HmuP, Modulates Haemin Acquisition in *Sinorhizobium Melioti*. *Microbiology* 156, 1873–1882. doi: 10.1099/mic.0.037713-0

Amarelle, V., Rosconi, F., Lázaro-Martinez, J. M., Buldain, G., Noya, F., O'Brian, M. R., et al. (2016). HmuS and HmuQ of *Ensifer/Sinorhizobium Meliloti* Degrade Heme *In Vitro* and Participate in Heme Metabolism *In Vivo*. *Biometals* 29, 333–347. doi: 10.1007/s10534-016-9919-3

Balhesteros, H., Shipelskiy, Y., Long, N. J., Majumdar, A., Katz, B. B., Santos, N. M., et al. (2017). TonB-Dependent Heme/Hemoglobin Utilization in *Caulobacter Crescentus* HutA. *J. Bacteriol.* 199, e00723-16. doi: 10.1128/JB.00723-16

Batista, J. H., and da Silva Neto, J. F. (2017). *Chromobacterium Violaceum* Pathogenicity: Updates and Insights From Genome Sequencing of Novel *Chromobacterium* Species. *Front. Micriobiol.* 8. doi: 10.3389/fmicb.2017.02213

Batista, B. B., Santos, R. E. R. S., Ricci-Azevedo, R., and da Silva Neto, J. F. (2019). Production and Uptake of Distinct Endogenous Cathecolate-Type Siderophores Are Required for Iron Acquisition and Virulence in *Chromobacterium Violaceum*. *Infect. Immun.* 87, e00577-19. doi: 10.1128/IAI.00577-19

Batko, I. Z., Flannagan, R. S., Guariglia-Oropeza, V., Sheldon, J. R., and Heinrichs, D. E. (2021). Heme-Ependent Siderophore Utilization Promotes Iron-Restricted Growth of the *Staphylococcus Aureus hemB* Small-Colony Variant. *J. Bacteriol.* 203, e0045821. doi: 10.1128/JB.00458-21

Biville, F., Cwerman, H., Létoffé, S., Rossi, M. S., Drouet, V., Ghigo, J. M., et al. (2004). Haemophore-Mediated Signaling in *Serratia Marcescens*: A New Mode of Regulation for an Extra Cytoplasmic Function (ECF) Sigma Factor Involved in Haem Acquisition. *Mol. Microbiol.* 53, 1267–1277. doi: 10.1111/j.1365-2958.2004.04207.x

Braun, V., and Hantke, K. (2011). Recent Insights Into Iron Import by Bacteria. *Curr. Opin. Chem. Biol.* 15, 328–334. doi: 10.1016/j.cbpa.2011.01.005

Brazilian National Genome Project Consortium (2003). The Complete Genome Sequence of *Chromobacterium Violaceum* Reveals Remarkable and Exploitable Bacterial Adaptability. *Proc. Natl. Acad. Sci. U. S. A.* 100, 11660–11665. doi: 10.1098/rspb.2013.1055

Burkhard, K. A., and Wilks, A. (2007). Characterization of the Outer Membrane Receptor ShuA From the Heme Uptake System of *Shigella Dysenteriae*. Substrate Specificity and Identification of the Heme Protein Ligands. *J. Biol. Chem.* 18, 15126–15136. doi: 10.1074/jbc.M611121200

Cassat, J. E., and Skaar, E. P. (2013). Iron in Infection and Immunity. *Cell Host Microbe* 13, 509–519. doi: 10.1016/j.chom.2013.04.010

Chandrangsu, P., Rensing, C., and Helmann, J. D. (2017). Metal Homeostasis and Resistance in Bacteria. *Nat. Rev. Microbiol.* 15, 338–350. doi: 10.1038/nrmicro.2017.15

Chatterjee, N., Cook, L. C. C., Lyles, K. V., Nguyen, H. A., Devlin, D. J., Thomas, L. S., et al. (2020). A Novel Heme Transporter From the Energy Coupling Factor Family Is Vital for Group A *Streptococcus* Colonization and Infections. *J. Bacteriol.* 202, e00205-20. doi: 10.1128/JB.00205-20

Choby, J. E., and Skaar, E. P. (2016). Heme Synthesis and Acquisition in Bacterial Pathogens. *J. Mol. Biol.* 428, 3408–3428. doi: 10.1016/j.jmb.2016.03.018

Contreras, H., Chim, N., Credali, A., and Goulding, C. W. (2014). Heme Uptake in Bacterial Pathogens. *Curr. Opin. Chem. Biol.* 19, 34–41. doi: 10.1016/j.cbpa.2013.12.014

Cook, L. C. C., Chatterjee, N., Li, Y., Andrade, J., Federle, M. J., and Eichenbaum, Z. (2019). Transcriptomic Analysis of *Streptococcus Pyogenes* Colonizing the Vaginal Mucosa Identifies *Hupy*, an MtsR-Regulated Adhesin Involved in Heme Utilization. *mBio* 10, e00848-19. doi: 10.1128/mBio.00848-19

da Silva Neto, J. F., Braz, V. S., Italiani, V. C. S., and Marques, M. V. (2009). Fur Controls Iron Homeostasis and Oxidative Stress Defense in the Oligotrophic Alpha-Proteobacterium *Caulobacter Crescentus*. *Nucleic Acids Res.* 37, 4812–4825. doi: 10.1093/nar/gkp509

da Silva Neto, J. F., Negretto, C. C., and Netto, L. E. S. (2012). Analysis of the Organic Hydroperoxide Response of *Chromobacterium Violaceum* Reveals That OhrR is a Cys-Based Redox Sensor Regulated by Thioredoxin. *PloS One* 7, e47090. doi: 10.1371/journal.pone.0047090

Eakanunkul, S., Lukat-Rodgers, G. S., Sumithran, S., Ghosh, A., Rodgers, K. R., Dawson, J. H., et al. (2005). Characterization of the Periplasmic Heme-Binding Protein ShuT From the Heme Uptake System of *Shigella Dysenteriae*. *Biochem* 44, 13179–13191. doi: 10.1021/bi050422r

Escamilla-Hernandez, R., and O' Brian, M. R. (2012). HmuP is a Coactivator of Irr-Dependent Expression of Heme Utilization Genes in *Bradyrhizobium Japonicum*. *J. Bacteriol.* 194, 3137–3143. doi: 10.1128/JB.00071-12

Fournier, C., Smith, A., and Delepelaire, P. (2011). Haem Release From Haemopexin by HxuA Allows *Haemophilus Influenzae* to Escape Host Nutritional Immunity. *Mol. Micribiol.* 80, 133–148. doi: 10.1111/j.1365-2958.2011.07562.x

Ganz, T., and Nemeth, E. (2015). Iron Homeostasis in Host Defence and Inflammation. *Nat. Rev. Immunol.* 15, 500–510. doi: 10.1038/nri3863

Glanville, D. G., Mullineaux-Sanders, C., Corcoran, C. J., Burger, B. T., Imam, S., Donohue, T. J., et al. (2021). A High-Throughput Method for Identifying Novel Genes That Influence Metabolic Pathways Reveals New Iron and Heme Regulation in *Pseudomonas Aeruginosa*. *mSystems* 6, e00933-20. doi: 10.1128/mSystems.00933-20

Gober, J. W., and Shapiro, L. (1992). A Developmentally Regulated *Caulobacter* Flagellar Promoter Is Activated by 3' Enhancer and IHF Binding Elements. *Mol. Biol. Cell.* 3, 913–926. doi: 10.1091/mbc.3.8.913

Hanahan, D. (1983). Studies of Transformation of *Escherichia Coli* With Plasmids. *J. Mol. Biol.* 166, 557–580. doi: 10.1016/S0022-2836(83)80284-8

Hood, M. I., and Skaar, E. P. (2012). Nutritional Immunity: Transition Metals at the Pathogen-Host Interface. *Nat. Rev. Micribiol.* 10, 525–537. doi: 10.1038/nrmicro2836

Huang, W., and Wilks, A. (2017). Extracellular Heme Uptake and the Challenge of Bacterial Cell Membranes. *Annu. Rev. Biochem.* 86, 799–823. doi: 10.1146/annurev-biochem-060815-014214

Khalifa, S. M. A., Khaldi, T. A., Alqahtani, M. M., and Ansari, A. M. A. (2015). Two Siblings With Fatal *Chromobacterium Violaceum* Sepsis Linked to Drinking Water. *BMJ Case Rep.* 2015, bcr2015210987. doi: 10.1136/bcr-2015-210987

Klebba, P. E., Newton, S. M. C., Six, D. A., Kumar, A., Yang, T., Nairn, B. L., et al. (2021). Iron Acquisition Systems of Gram-Negative Bacterial Pathogens Define TonB-Dependent Pathways to Novel Antibiotics. *Chem. Rev.* 121, 5193–5239. doi: 10.1021/acs.chemrev.0c01005

Kumar, M. R. (2012). *Chromobacterium Violaceum*: A Rare Bacterium Isolated From a Wound Over the Scalp. *Int. J. Appl. Basic. Med. Res.* 2, 70–72. doi: 10.4103/2229-516X.96814

Lamattina, J. W., Nix, D. B., and Lanzilotta, W. N. (2016). Radical New Paradigm for Heme Degradation in *Escherichia Coli* O157:H7. *Proc. Natl. Acad. Sci.* 113, 12138–12143. doi: 10.1073/pnas.1603209113

Lee, M. J. Y., Wang, Y., Jiang, Y., Li, X., Ma, J., Tan, H., et al. (2017). Function Coupling Mechanism of PhuS and HemO in Heme Degradation. *Sci. Rep.* 7, 1123. doi: 10.1038/s41598-017-11907-5

Livak, K. J., and Schmittgen, T. D. (2001). Analysis of Relative Gene Expression Data Using Real-Time Quantitative PCR and the 2(-Delta Delta C(T)) Method. *Methods* 25, 402–408. doi: 10.1006/meth.2001.1262

Maltez, V. I., Tubbs, A. L., Cook, K. D., Aachoui, Y., Falcone, E. L., Holland, S. M., et al. (2015). Inflammasomes Coordinate Pyroptosis and Natural Killer Cell Cytotoxicity to Clear Infection by a Ubiquitous Environmental Bacterium. *Immunity* 43, 987–997. doi: 10.1016/j.immuni.2015.10.010

Marvig, R. L., Damkiær, S., Khademi, S. M., Markussen, T. M., Molin, S., and Jelsbak, L. (2014). Within-Host Evolution of *Pseudomonas Aeruginosa* Reveals Adaptation Toward Iron Acquisition From Hemoglobin. *mBio* 5, e00966-14. doi: 10.1128/mBio.00966-14

Miki, T., Iguchi, M., Akiba, K., Hosono, M., Sobue, T., Danbara, H., et al. (2010). *Chromobacterium* Pathogenicity Island 1 Type III Secretion System is a Major Virulence Determinant for *Chromobacterium Violaceum*-Induced Cell Death in Hepatocytes. *Mol. Microbiol.* 77, 855–872. doi: 10.1111/j.1365-2958.2010.07248.x

Minandri, F., Imperi, F., Frangipani, E., Bonchi, C., Visaggio, D., Facchini, M., et al. (2016). Role of Iron Uptake Systems in *Pseudomonas Aeruginosa* Virulence and Airway Infection. *Infect. Immun.* 84, 2324–2335. doi: 10.1128/IAI.00098-16

Nguyen, A. T., O'Neill, M. J., Watts, A. M., Robson, C. L., Lamont, I. L., Wilks, A., et al. (2014). Adaptation of Iron Homeostasis Pathways by a *Pseudomonas Aeruginosa* Pyoverdine Mutant in the Cystic Fibrosis Lung. *J. Bacteriol.* 196, 2265–2276. doi: 10.1128/JB.01491-14

Noinaj, N., Guillier, M., Barnard, T. J., and Buchanan, S. K. (2010). TonB-Dependent Transporters: Regulation, Structure and Function. *Ann. Rev. Microbiol.* 64, 43–60. doi: 10.1146/annurev.micro.112408.134247

Ochsner, U. A., Johnson, Z., and Vasil, M. L. (2000). Genetics and Regulation of Two Distinct Haem-Uptake Systems, *Phu* and *has*, in. *Pseudomonas. Aeruginosa. Microbiol.* 146, 185–198. doi: 10.1099/00221287-146-1-185

Otero-Asman, J. R., García-García, A. I., Civantos, C., Quesada, J. M., and Llamas, M. A. (2019). *Pseudomonas Aeruginosa* Possesses Three Distinct Systems for Sensing and Using the Host Molecule Haem. *Environ. Microbiol.* 12, 4629–4647. doi: 10.1111/1462-2920.14773

Palmer, L. D., and Skaar, E. P. (2016). Transition Metals and Virulence in Bacteria. *Annu. Rev. Genet.* 50, 67–91. doi: 10.1146/annurev-genet-120215-035146

Parrow, N. L., Flemming, R. E., and Minnick, M. F. (2013). Sequestration and Scavenging of Iron in Infection. *Infect. Immun.* 81, 3503–3514. doi: 10.1128/IAI.00602-13

Previato-Mello, M., Meireles, D. A., Netto, L. E. S., and da Silva Neto, J. F. (2017). Global Transcriptional Response to Organic Hydroperoxide and the Role of OhrR in the Control of Virulence Traits in *Chromobacterium Violaceum*. *Infect. Immun.* 85, e00017-17. doi: 10.1128/IAI.00017-17

Puri, S., and O'Brian, M. R. (2006). The *hmuQ* and *hmuD* Genes From *Bradyrhizobium Japonicum* Encode Heme-Degrading Enzymes. *J. Bacteriol.* 188, 6476–6482. doi: 10.1128/JB.00737-06

Rivera-Chávez, F., and Mekalanos, J. J. (2019). Cholera Toxin Promotes Pathogen Acquisition of Host-Derived Nutrients. *Nature* 572, 244–248. doi: 10.1038/s41586-019-1453-3

Roberts, R. C., Toochinda, C., Acedissian, M., Baldini, R. L., Gomes, S. L., and Shapiro, L. (1996). Identification of a *Caulobacter Crescentus* Operon Encoding Hrca, Involved in Negatively Regulating Heat-Inducible Transcription, and the Chaperone Gene *grpE*. *J. Bacteriol.* 178, 1829–1841. doi: 10.1128/jb.178.7.1829-1841.1996

Runyen-Janecky, L. J. (2013). Role and Regulation of Heme Iron Acquisition in Gram-Negative Pathogens. *Front. Cell. Infect. Microbiol.* 3. doi: 10.3389/fcimb.2013.00055

Santos, R. E. R. S., Batista, B. B., and da Silva Neto, J. F. (2020). Ferric Uptake Regulator Fur Coordinates Siderophore Production and Defense Against Iron Toxicity and Oxidative Stress and Contributes to Virulence in Chromobacterium Violaceum. *Appl. Environm. Microbiol.* 86, e01620-20. doi: 10.1128/AEM.01620-20

Sarvan, S., Butcher, J., Stintzi, A., and Couture, J. F. (2018). Variation on a Theme: Investigating the Structural Repertoires Used by Ferric Uptake Regulator to Control Gene Expression. *Biometals* 31, 681–704. doi: 10.1007/s10534-018-0120-8

Sato, T., Nonoyama, S., Kimura, A., Nagata, Y., Ohtsubo, Y., and Tsuda, M. (2017). The Small Protein HemP Is a Transcriptional Activator of the Hemin Uptake Operon in *Burkholderia Multivorans* ATCC 17616. *App. Environm. Microbiol.* 83, e00479-17. doi: 10.1128/AEM.00479-17

Schwiesow, L., Metteret, E., Wei, Y., Miller, H. K., Herrera, N. G., Balderas, D., et al. (2018). Control of *Hmu* Heme Uptake Genes in *Yersinia Pseudotuberculosis* in Response to Iron Sources. *Front. Cell. Infect. Microbiol.* 8. doi: 10.3389/fcimb.2018.00047

Sheldon, J. R., Laakso, H. A., and Heinrichs, D. E. (2016). Iron Acquisition Strategies of Bacterial Pathogens. *Microbiol. Spectr.* 4, 2. doi: 10.1128/microbiolspec.VMBF-0010-2015

Simon, R., Priefer, U., and Pühler, A. (1983). A Broad Host Range Mobilization System for *In Vivo* Genetic Engineering: Transposon Mutagenesis in Gram-Negative Bacteria. *Nat. Biotechnol.* 1, 784–791. doi: 10.1038/nbt1183-784

Si, M., Wang, Y., Zhang, B., Zhao, C., Kang, Y., Bai, H., et al. (2017). The Type VI Secretion System Engages a Redox-Regulated Dual-Function Heme Transporter for Zinc Acquisition. *Cell Rep.* 20, 949–959. doi: 10.1016/j.celrep.2017.06.081

Skaar, E. P. (2010). The Battle for Iron Between Bacterial Pathogens and Their Vertebrate Hosts. *PloS Pathog.* 6, e1000949. doi: 10.1371/journal.ppat.1000949

Skaar, E. P., Humayun, M., Bae, T., Debord, K. L., and Schneewind, O. (2004). Iron-Source Preference of *Staphylococcus Aureus* Infections. *Science* 305, 1626–1628. doi: 10.1126/science.1099930

Smith, A. D., and Wilks, A. (2015). Differential Contributions of the Outer Membrane Receptors PhuR and HasR to Heme Acquisition in *Pseudomonas Aeruginosa*. *J. Biol. Chem.* 290, 7756–7766. doi: 10.1074/jbc.M114.633495

Stojiljkovic, I., and Hantke, K. (1992). Hemin Uptake System of *Yersinia Enterocolitica*: Similarities With Other TonB-Dependent Systems in Gram-Negative Bacteria. *EMBO J.* 11, 4359–4367. doi: 10.1002/j.1460-2075.1992.tb05535.x

Suits, M. D., Pal, G. P., Nakatsu, K., Matte, A., Cygler, M., and Jia, Z. (2005). Identification of an *Escherichia Coli* O157:H7 Heme Oxygenase With Tandem Functional Repeats. *Proc. Natl. Acad. Sci. U. S. A.* 102, 16955–16960. doi: 10.1073/pnas.0504289102

Wandersman, C., and Delepelaire, P. (2012). Haemophore Functions Revisited. *Mol. Microbiol.* 85, 618–631. doi: 10.1111/j.1365-2958.2012.08136.x

Yang, C. H., and Li, Y. H. (2011). *Chromobacterium Violaceum* Infection: A Clinical Review of an Important But Neglected Infection. *J. Clin. Med. Assoc.* 74, 435–441. doi: 10.1016/j.jcma.2011.08.013

Zhao, Y., Yang, J., Shi, J., Gong, Y. N., Lu, Q., Xu, H., et al. (2011). The NLRC4 Inflammasome Receptors for Bacterial Flagellin and Type III Secretion Apparatus. *Nature* 477, 596–600. doi: 10.1038/nature10510

Zygiel, E. M., Obisesan, A. O., Nelson, C. E., Oglesby, A. G., and Nolan, E. M. (2021). Heme Protects *Pseudomonas Aeruginosa* and *Staphylococcus Aureus* From Calprotectin-Induced Iron Starvation. *J. Biol. Chem.* 296, 100160. doi: 10.1074/jbc.RA120.015975

Conflict of Interest: The authors declare that the research was conducted in the absence of any commercial or financial relationships that could be construed as a potential conflict of interest.

Publisher's Note: All claims expressed in this article are solely those of the authors and do not necessarily represent those of their affiliated organizations, or those of the publisher, the editors and the reviewers. Any product that may be evaluated in this article, or claim that may be made by its manufacturer, is not guaranteed or endorsed by the publisher.

frontiers | Frontiers in Cellular and Infection Microbiology

REVIEW
published: 11 May 2022
doi: 10.3389/fcimb.2022.876667

The Iron Response of *Mycobacterium tuberculosis* and Its Implications for Tuberculosis Pathogenesis and Novel Therapeutics

G. Marcela Rodriguez, Nishant Sharma, Ashis Biswas and Nevadita Sharma*

The Public Health Research Institute, Department of Medicine, Rutgers University, New Jersey Medical School, Newark, NJ, United States

OPEN ACCESS

Edited by:
José F. da Silva Neto, University of São Paulo, Brazil

Reviewed by:
Celia Goulding, University of California, Irvine, United States
Miguel Balado, University of Santiago de Compostela, Spain

***Correspondence:**
G. Marcela Rodriguez
rodrigg2@njms.rutgers.edu

Specialty section:
This article was submitted to Bacteria and Host, a section of the journal Frontiers in Cellular and Infection Microbiology

Received: *15 February 2022*
Accepted: *25 March 2022*
Published: *11 May 2022*

Citation:
Rodriguez GM, Sharma N, Biswas A and Sharma N (2022) The Iron Response of Mycobacterium tuberculosis *and Its Implications for Tuberculosis Pathogenesis and Novel Therapeutics. Front. Cell. Infect. Microbiol. 12:876667. doi: 10.3389/fcimb.2022.876667*

Most pathogenic bacteria require iron for growth. However, this metal is not freely available in the mammalian host. Due to its poor solubility and propensity to catalyze the generation of reactive oxygen species, host iron is kept in solution bound to specialized iron binding proteins. Access to iron is an important factor in the outcome of bacterial infections; iron limitation frequently induces virulence and drives pathogenic interactions with host cells. Here, we review the response of *Mycobacterium tuberculosis* to changes in iron availability, the relevance of this response to TB pathogenesis, and its potential for the design of new therapeutic interventions.

Keywords: *M. tuberculosis*, iron-limitation, IdeR, ferritin, extracellular vesicles, iron-response

INTRODUCTION

Iron is an essential micronutrient for most living organisms. It undergoes reversible changes in its oxidation state, oscillating between the oxidized ferric (Fe^{3+}) and the reduced ferrous (Fe^{2+}) forms. Depending on the local ligand environment, iron-containing compounds exhibit a wide range of oxidation-reduction potentials making this metal a multipurpose biocatalyst and electro-carrier. Indeed, as mono-or binuclear species, in heme groups or iron-sulfur clusters [FeS], iron is incorporated into proteins that mediate vital cellular functions, including energy generation, metabolism, oxygen transport, gene regulation, oxidative stress defense, and DNA biosynthesis (Sanchez et al., 2017).

Before oxygenic photosynthesis, iron was abundant in its soluble, Fe^{2+} form and incorporated into a variety of enzyme cofactors. However, with the introduction of oxygen into the atmosphere, iron became poorly available and potentially toxic. In oxygenic environments, Fe^{+3} forms insoluble ferric hydroxides and promotes the generation of deleterious reactive oxygen species (ROS) thorough the Fenton reaction (Fenton, 1894; Imlay et al., 1988; Koppenol and Hider, 2019). The mammalian host keeps iron in solution bound to proteins such as transferrin (in plasma), lactoferrin (in secretory fluids), and ferritin (intracellularly). During the acute phase response to infection, iron-binding proteins are upregulated together with proteins that efflux iron from

intracellular microbial compartments (NRAMP1) or bind free heme (hemopexin) and hemoglobin (haptoglobin), further reducing iron available to invading microorganisms (Weinberg, 1999). This concerted effort mounted by the host to actively restrict iron availability constitutes the hallmark of nutritional immunity (Weinberg, 1984).

Tuberculosis (TB), caused by *Mycobacterium tuberculosis* (Mtb), is a leading cause of death from a single infectious agent. However, tools to effectively prevent and control TB remain scarce. BCG (Bacillus Calmette-Guerin), the only approved antitubercular vaccine protects against disseminated TB in infants, but is inefficient against adult pulmonary TB (Andersen and Doherty, 2005). Four different antibiotics taken for four months are needed to treat TB. This complex antibiotic regimen contributes to poor adherence and the rise of drug resistant Mtb strains. It is estimated that one-third of the world's population has been exposed to Mtb and might harbor bacteria that are not multiplying but remain viable causing chronic, latent TB infection (LTBI). LTBI is asymptomatic and not transmissible but nonetheless, highly problematic because it is difficult to diagnose and treat. Moreover, when immune control is compromised, LTBI can reactivate generating new acute TB cases (Lillebaek et al., 2002).

Mtb enters a new host *via* inhalation of fine aerosol droplets containing just a few bacilli. In the lung, Mtb creates an optimal niche for replication within alveolar macrophages. But it can also disseminate and replicate in multiple organs. Bacterial proliferation stimulates a pro-inflammatory response resulting in the recruitment of more macrophages and other immune cells, forming a granuloma. As adaptive immunity develops, the granuloma can restrict bacterial growth. However, cells in the granuloma can undergo necrosis, forming a necrotic core where Mtb is found extracellularly (Ramakrishnan, 2012). At these various stages of infection, Mtb experiences distinct iron conditions to which it must acclimate.

This review focuses on the intricate response of Mtb to changes in iron availability. Depending on accessibility to iron, this response ranges from increased iron acquisition, virulence, and growth to quiescence and long-term persistence (**Figure 1**). We highlight how the physiological response of Mtb to diverse iron conditions can influence TB pathogenesis and offer new opportunities for therapeutic intervention.

UPREGULATION OF IRON ACQUISITION AND CONTROL OF INTRACELLULAR IRON

Iron is highly abundant in the human host. But it is not readily accessible to infectious agents. It is always bound to iron-binding proteins or coordinated into the cofactor, heme. To overcome iron limitation, Mtb produces siderophores, namely the lipophilic, membrane-bound mycobactin, and the water-soluble, secreted carboxymycobactin (Hall and Ratledge, 1982; Barclay et al., 1985; Gobin et al., 1995; Lane et al., 1995). Additionally, in a siderophore-independent manner, Mtb can utilize heme as iron source (Jones and Neiderweis, 2011; Tullius et al., 2011; Mitra et al., 2019). Carboxymycobactin and mycobactin share a common core structure composed of a 2-hydroxyphenyl-oxazoline moiety, a β-hydroxy carbonyl motif and two N^{ε}- (hydroxy) lysin residues (Gobin et al., 1999). Mycobactin has a long alkyl chain substitution that makes this molecule highly hydrophobic and restricts it to the cell envelope (Ratledge et al., 1982). Mycobactin and carboxymycobactin have an extremely high affinity for Fe^{3+} and can withdraw it from insoluble hydroxides and iron-binding proteins (Gobin and Horwitz, 1996). Accordingly, Mtb requires siderophore synthesis to proliferate in macrophages and mice (De Voss et al., 2000; Reddy et al., 2013).

While carboxymycobactin is exported *via* the inner-membrane RND transporters MmpL4 and MmpL5 in association with the periplasmic adaptor proteins MmpS4 and MmpS5 (Wells et al., 2013), mycobactin is exported as a component of extracellular membrane vesicles (Prados-Rosales et al., 2014). Carboxymycobactin can transfer chelated Fe^{3+} to mycobactin on the cell surface by a process that requires the multifunctional protein HupB. HupB is primarily a nucleoid-associated protein that activates the transcription of siderophore synthesis genes (*mbt*). But surprisingly, HupB is also found on the cell surface, where it can bind carboxymycobactin. HupB has been postulated to serve as Fe^{3+}-carboxymycobactin receptor and direct transfer of iron from carboxymycobactin to mycobactin (Gobin and Horwitz, 1996; Choudhury et al., 2021). Iron bound to carboxymycobactin can also be imported into the cell independently of mycobactin, *via* the iron-regulated ABC transporter, IrtAB (Rodriguez and Smith, 2006; Rodriguez et al., 2008; Ryndak et al., 2010; Arnold et al., 2020). IrtAB is an inner membrane heterodimer and a unique transporter that couples Fe^{3+}-carboxymycobactin import and iron assimilation *via* the cytosolic amino-terminal domain of IrtA (Ryndak et al., 2010). This domain functions as a flavin reductase, reducing Fe^{3+} to Fe^{2+}, effectively dissociating Fe^{+2} from imported carboxymycobactin and from membrane associated mycobactin for subsequent incorporation into iron proteins (Ryndak et al., 2010; Arnold et al., 2020). Deletion of *irtAB* significantly impairs Mtb proliferation in macrophages and in mice (Rodriguez and Smith, 2006). The recent characterization of the three-dimensional structure of IrtAB is an important step towards developing therapeutics that target iron uptake in Mtb (Gold et al., 2001; Arnold et al., 2020).

Fe^{3+}-siderophore uptake also requires the type VII Esx-3 secretion system (Siegrist et al., 2009; Serafini et al., 2013). However, the precise function of the Esx-3 proteins in iron uptake remains unclear. The Esx-3 system is also necessary for Mtb virulence and therefore, an attractive drug target (Tufariello et al., 2016).

Once deferrated, carboxymycobactin is recycled and exported back. Failure to export carboxymycobactin is detrimental to Mtb *in vitro* and *in vivo*, supporting siderophore export proteins as promising anti-Mtb drug targets (Jones et al., 2014).

Carboxymycobactin and mycobactin are both potent iron chelators. However, carboxymycobactin molecules are susceptible to lipocalin, a protein induced under inflammatory conditions that

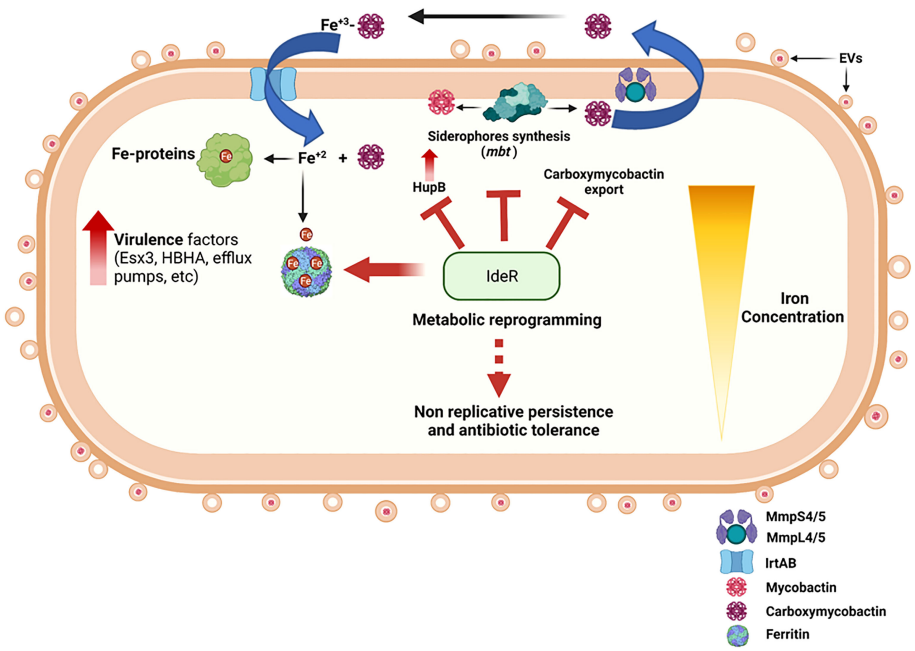

FIGURE 1 | Summary diagram of the Mtb response to iron availability. Iron limited Mtb upregulates expression of genes encoding siderophore synthesis (*mbt*), export (MmpL4/5-MmpS4/5), and import (IrtAB). Assimilated iron is incorporated into metalloproteins and stored in ferritins. Iron deficient Mtb also upregulates pathogenicity factors that facilitate immune evasion and proliferation, modifies its cell surface, and augments EVs secretion. Prolonged iron deprivation induces a strong iron sparing response and metabolic rewiring that enables long term persistence without replication and leads to phenotypic antibiotic resistance. These changes are fully reversible by restoring iron availability. Iron sufficient Mtb engages IdeR to control intracellular iron levels *via* repression of iron uptake and stimulation of iron storage, thus preventing iron dysregulation and oxidative stress that renders this pathogen highly vulnerable to host antimicrobial factors and antibiotic drugs. The figure was created with BioRender (BioRender.com.).

sequesters carboxymycobactin and thereby interferes with iron acquisition (Goetz et al., 2002). Accordingly, lipocalin deficient mice are highly susceptible to tuberculosis infection and exhibit increased bacterial burden, particularly in the alveolar epithelium (Saiga et al., 2008). In contrast, mycobactin packed into extracellular membrane vesicles might be less exposed to lipocalin and consequently more effective in delivering iron to Mtb in the context of inflammation. Thus, we postulate that the need to sequester iron in biochemically diverse host environments justifies the synthesis of two types of siderophores by Mtb.

To prevent toxicity derived from excess iron and maintain iron homeostasis, Mtb stores iron in bacterioferritin (BfrA) and ferritin (BfrB) (Gupta et al., 2009; Khare et al., 2011; Reddy et al., 2012). Ferritins characteristically exist as spherical macromolecular assemblies of 24 identical subunits. BfrB has a higher iron storage capacity than BfrA. BfrA can take up 4500 molecules of iron/protein whereas BfrB could take up to 6000 iron molecules/protein (Khare et al., 2017). The synthesis of BfrB is induced in high iron conditions whereas BfrA is synthesized in low and high iron medium. BfrB is the main storage compartment for excess iron. Mtb with deleted *bfrB* accumulates reactive iron, exhibits iron-dependent hypersensitivity to ROS and antibiotics, and survives poorly in the lungs of mice, particularly during the chronic phase of infection (Pandey and Rodriguez, 2012; Reddy et al., 2012). Notably, immunization of mice with a *bfrB* mutant of Mtb confers the same level of protection against virulent Mtb as compared to BCG vaccination (Subbian et al., 2014). BfrA on the other hand, is a heme-containing protein, that contributes to maintaining iron homeostasis during iron limitation (Khare et al., 2017). In addition, BfrA exhibits catalase and DNA protection activity; it associates with DNA and protects it from Fe^{2+}/H_2O_2 -induced oxidative damage (Mohanty et al., 2019). Although these findings highlight the potential of targeting mycobacterial ferritins to potentiate host and antibiotic-mediated killing of Mtb, direct inhibition of ferritins is challenging due to their compact molecular assembly and their homology to host ferritin. Alternatively, we postulate that targeting upregulation of ferritin in response to high iron conditions might lead to accumulation of oxygen radicals *via* Fenton chemistry and synergize with existing antitubercular antibiotics.

Mtb maintains cellular iron homeostasis by tightly regulating iron uptake, utilization, and storage. Siderophore synthesis is activated by the nuclei-associated protein HupB (Pandey et al., 2014) and repressed by the metal-dependent regulator IdeR (Dussurget et al., 1996; Pohl et al., 1999; Gold et al., 2001; Rodriguez et al., 2002). IdeR binds Fe^{2+} and DNA at a specific sequence present in the promoters of siderophore synthesis, export and import genes, as well as upstream of *hupB*, *bfrA*, and *bfrB* genes (Chou et al., 2004; Marcos-Torres et al., 2021). According to the location of the IdeR binding site (iron box), IdeR functions as a repressor or activator of gene transcription. Generally, iron uptake genes have a single iron box that overlaps

the promoter or transcriptional start site. Therefore, binding of IdeR to this sequence represses their transcription. In contrast, IdeR binding sites on *bfrA* and *bfrB* are located further upstream of the promoter region (Gold et al., 2001). IdeR activates *bfrB* transcription by antagonizing the histone-like protein Lsr2, which decorates the DNA region upstream of *bfrB* impeding its transcription. In complex with iron, IdeR binds to four tandem iron boxes located upstream of *bfrB*, likely displacing Lsr2 and aiding recruitment of RNA polymerase to the promoter (Kurthkoti et al., 2015). A strain unable to synthesize IdeR fails to establish infection in mice, indicating that controlling the response to iron is essential *in vivo* and validating IdeR as a promising drug target against Mtb (Pandey and Rodriguez, 2013). Despite the importance of IdeR as a drug target, only few virtual screenings for IdeR inhibitors have been reported so far (Rohilla et al., 2017; Kwofie et al., 2019). Transcriptional factors are notably difficult to target since protein-protein or protein-DNA interactions must be disrupted. However, since metal binding is needed for IdeR dimerization and DNA binding, blocking metal binding may be an effective way to inhibit IdeR function (Wisedchaisri et al., 2007). High throughput screenings for natural or synthetic IdeR inhibitors are needed to capitalize on Mtb's marked susceptibility to iron dysregulation.

UPREGULATION OF VIRULENCE-ASSOCIATED GENES

Iron limitation stimulates many bacterial pathogens to synthesize and release virulence factors that directly or indirectly increase iron bioavailability. For instance, enhanced production of hemolysins, cytotoxins, phospholipases, and proteases allows pathogens to release intracellular iron *via* cell lysis (Dorman et al., 1990; Tai et al., 1990; Karjalainen et al., 1991; Litwin and Calderwood, 1993; Garcia et al., 2003). More subtly, adhesins and motility proteins might provide access to new iron-supportive microenvironments. Other factors enable pathogens to highjack iron trafficking pathways of the host (Keenan and Allardyce, 2000).

Transcriptional profiling, gene deletion, and animal infection studies indicate that Mtb reacting to iron limitation simultaneously upregulates iron acquisition mechanisms and diverse virulence associated factors (Rodriguez et al., 2002) (Kurthkoti et al., 2017). For instance, iron limitation induces *pks10* (Sirakova et al., 2003) and *mmpL8* (Converse et al., 2003) encoding two proteins necessary for synthesis of the virulence associated cell envelope lipids dimycoserosyl phthiocerol (DIM) and sulfolipid-1 respectively. The phospholipase gene *plcA* and the cholesterol oxidase gene *choD*, which are required for virulence in macrophages are also induced by iron restriction (Raynaud et al., 2002; Brzostek et al., 2007). In addition, iron-deficient Mtb upregulates the mammalian cell entry protein-encoding gene mce3C (Yuan et al., 1998; Senaratne et al., 2008; Garces et al., 2010), the adhesin HbHA, and the genes encoding the virulence required ESX-1 secretion associated proteins, EspA and EspC (Garces et al., 2010). Furthermore, low iron signals induction of genes encoding regulatory proteins that control the expression of many genes and are functionally linked to Mtb survival *in vivo*, such as HspX, MprAB, SigF, and WhiB6 (Yuan et al., 1998; Zahrt and Deretic, 2001; Geiman et al., 2004; Chen et al., 2016).

Notably, Mtb evolved the ability to infect and survive in macrophages, cells that are central to host iron homeostasis. Macrophages are responsible for recycling iron from hemoglobin in senescent red blood cells (the largest iron pool in the host) and exporting it to satisfy systemic iron demand (Armstrong and Hart., 1975; Ganz, 2012). Mtb infecting macrophages inhibits phagosome-lysosome fusion while allowing phagosome interactions with early endosomes containing internalized transferrin, a reliable iron source accessible to Mtb *via* siderophores (Russell, 1996; Sturgill-Koszycki et al., 1996; Wagner et al., 2005; Clemens and Horwitz, 1996; Olakanmi et al., 2002). Therefore, it is not surprising that Mtb sensing iron deficiency upregulates phagosome maturation arresting factors such as the Esx-3 secretion apparatus and the protein kinase, PknG (Mehra et al., 2013; Cambier et al., 2014; Rodriguez et al., 2002).

During inflammation, macrophages are "instructed" by hepcidin, the principal regulator of systemic iron, to retain this metal intracellularly effectively restricting iron available to extracellular invaders (Drakesmith and Prentice, 2012). High macrophage iron stores are indeed associated with an increased risk of developing tuberculosis, while IFN-γ activated macrophages that downregulate iron uptake and reduce iron storage are less hospitable to Mtb and can eliminate it (Byrd and Horwitz, 1989). Suggestive of mycobacteria exploiting the macrophage for iron, infected macrophages show increased hepcidin secretion and accumulate intracellular iron (Abreu et al., 2020). Interestingly, Mtb infection can induce macrophage ferroptosis, a form of lytic cell-death resulting from iron dependent lipid peroxidation and membrane damage (Amaral et al., 2019). We think ferroptosis might be mechanistically linked to Mtb's efforts to increase iron available in the macrophage. Future studies are needed to validate this assumption. In the mature granuloma, Mtb promotes inflammation and cell necrosis that combined with the ability to utilize iron from heme and hemoglobin likely contribute to extracellular Mtb multiplication. A better understanding of the Mtb-macrophage interactions driven by iron limitation will likely uncover additional strategies used by Mtb to manipulate the macrophage and the immune system to secure essential iron.

CELL SURFACE MODIFICATION

Accumulated evidence from genetic and biochemical analyses indicates that iron restricted Mtb alters its cell envelope. Phenotypically, mycobacteria cultured in low iron medium exhibit increased aggregation, enhanced permeability and membrane fluidity associated with hypersensitivity to membrane perturbing agents and antibiotics (Pal et al., 2015). Iron-deprived mycobacteria reduce expression of MmpL3 (Pal et al., 2019), a lipid transporter responsible for translocating

trehalose monomycolate to the periplasm for the biosynthesis of trehalose dymicolates (TDM) and mycolyl arabinogalactan peptidoglycan, which are basic structural components of the mycobacterial cell envelope (Xu et al., 2017). In addition, iron-deprived mycobacteria exhibit decreased mycolic acid content suggestive of reduced outer membrane biogenesis (Bacon et al., 2007; Xu et al., 2017). Furthermore, a link between iron limitation and increased phospholipid catabolism was postulated based on lipidomic analysis and cell-wall lipid profiling that showed phospholipid reduction in iron deficient Mtb, a significant increase in triacylglycerols, and the presence of a novel wax ester in iron limited Mtb (Madigan et al., 2015). These observations and the significant number of uncharacterized iron regulated genes predicted to be involved in lipid metabolism support the concept that Mtb alters its cell envelope in response to iron limitation (Rodriguez et al., 2002; Kurthkoti et al., 2017). Controlled cell surface modification may facilitate iron uptake and expose biomolecules that enable novel interactions with host cells. Comprehensive studies that further characterize structural and functional changes in the cell envelope of iron limited Mtb might reveal new adaptations to the host environment. Additionally, knowledge about the molecular mechanisms used by Mtb to control cell envelope permeability with respect to iron can be harnessed to enhance antibiotic cell entry and effectiveness.

INCREASE RELEASE OF EXTRACELLULAR VESICLES

Iron limitation stimulates the release of mycobacterial extracellular vesicles (EVs) (Prados-Rosales et al., 2014). EVs are spherical, membrane-bound nanoparticles (60-300 nm in diameter) released by live cells to communicate with other cells in their environment. EVs carry bioactive molecules through the body, signaling distant tissues and triggering systemic responses. Pathogenic bacteria frequently secrete virulence factors concentrated and protected within EVs (Kuehn and Kesty, 2005). Mycobacteria produce EVs that originate at the plasma membrane and contain immunologically active lipids and proteins, including numerous TLR2 ligands (Prados-Rosales et al., 2011). Emerging evidence indicates that bacteria derived EVs might contribute to TB pathogenesis. EVs released by Mtb in culture or during macrophage infection influence cellular immune responses (Athman et al., 2015; Athman et al., 2017) and when injected into mice, mycobacterial EVs stimulate inflammation and interfere with the control of a subsequent Mtb infection (Prados-Rosales et al., 2011). EVs produced by iron limited Mtb may also aid in iron acquisition. They are loaded with mycobactin and can support the growth of iron deficient mycobacteria *in vitro*. As mycobactin can accept Fe^{+3} from carboxymycobactin, mycobactin packed in EVs is likely a mix of Fe^{+3}-mycobactin and apo-mycobactin capable of chelating environmental iron (Prados-Rosales et al., 2014).

We demonstrated that EV biogenesis in Mtb is dependent on the function of the dynamin-like proteins IniA and IniC. Accordingly, the *iniBAC* operon is induced during iron limitation (Gupta et al., 2020). Additionally, we propose that the cell envelope remodeling implemented by iron limited Mtb might be linked to increased EV production; conceivably, a more porous cell envelope could facilitate vesicle export. Further studies are needed to elucidate the relationship between cell envelope alteration and EV secretion in Mtb. Nonetheless, the current information indicates that EV-mediated secretion is yet, another pathogenicity associated function augmented in Mtb responding to iron restriction.

METABOLIC REPROGRAMMING

Without iron, Mtb downregulates anabolic functions and stops growth. Iron deficiency triggers intense metabolic adjustment broadly influenced by an effective iron-sparing response. This response is characterized by repression of dispensable iron containing proteins and prioritization of scarce iron for life sustaining activities. Specifically, the transcriptional profile of iron-deprived Mtb indicates the prioritization of [FeS] assembly over heme biosynthesis and the maintenance of iron proteins involved in electron transfer (Cyp138, FprB, RubA, and RubB) and NAD synthesis (NadA); and the [FeS]-containing regulators WhiB6 and WhiB7 (Kurthkoti et al., 2017). Metabolic and transcriptomic analyses of iron starved Mtb indicate reduced amino acid biosynthesis. Energy metabolism including the tricarboxylic acid (TCA) cycle and oxidative phosphorylation are also downregulated. This is expected given the number of [FeS]/hemeproteins involved in these pathways. Concomitantly, the expression of *atp* genes (encoding F_1F_0 ATP synthase) decreases, indicating reduced respiration associated ATP synthesis (Kurthkoti et al., 2017). We postulated that like *Lactobacillus* and *Borrelia*, two unique bacterial species that do not depend on iron and lack a functional TCA cycle and oxidative phosphorylation, iron starved Mtb might generate ATP *via* substrate phosphorylation. Also, *Lactobacillus sp* and *Borrelia sp* depend on pyruvate conversion to lactate to regenerate NAD+ required for continued glycolysis. Metabolic detection of lactate suggests that Fe-starved Mtb also performs homolactic fermentation. Additional studies are needed to identify metabolic adaptations that support iron starved Mtb and can be exploited as novel therapeutic targets to prevent chronic Mtb infection.

IRON-STARVED M. TUBERCULOSIS ENTERS A QUIESCENT STATE AND BECOMES TOLERANT TO ANTIBIOTICS

Characterization of Mtb cultures adapted to iron-starvation revealed a multi-phased response that included cell death, differential cultivability (DC), and non-replicative persistence (Kurthkoti et al., 2017). DC refers to the ability of bacterial cells to grow in liquid but not in a solid medium. This property is also observed in Mtb under intense stress and in bacteria present in

sputum samples from TB patients before treatment (Mukamolova et al., 2010). The DC phenotype is troubling because it potentially decreases the sensitivity of culture-based diagnostics and treatment efficacy assessments, which are still broadly used in low-resource settings.

Most Mtb cells adapt to complete iron deprivation by entering a non-replicative, persistent state fully reversible by iron (Kurthkoti et al., 2017). Iron starved Mtb ceases to replicate and becomes tolerant to several antibiotics, including the first-line TB drug isoniazid (INH), also used in latent TB reactivation preventive therapy (Kurthkoti et al., 2017). Although enhanced tolerance to antibiotics in non-growing cells can be simply explained by reduced abundance of the drug target, the response to lack of iron may specifically contribute to antibiotic tolerance. For instance, INH is a prodrug activated by catalase (KatG), a heme enzyme downregulated in response to iron-deprivation (Chouchane et al., 2000; Chouchane et al., 2003). Therefore, reduced INH activation may contribute to increased drug tolerance in iron starved Mtb. In addition, inhibition of the electron transport chain due to Fe-deficiency likely mediates enhanced tolerance to antibiotics such as aminoglycosides which require proton motive force for internalization into bacterial cell (Davis, 1987). Furthermore, the genes encoding recognized intrinsic antibiotic resistance-enhancers such as WhiB6 (Chen et al., 2016) and WhiB7 (Ramon-Garcia et al., 2013) and the fluoroquinolone efflux pump encoded by Rv2688c (Pasca et al., 2004) are also induced in response to iron deficiency, supporting an active role of the iron response in antibiotic tolerance (Kurthkoti et al., 2017).

Proteomic analysis of micro dissected lung granulomas obtained from individuals with extensive drug-resistant TB showed a high concentration of iron restricting host proteins in the necrotic center of advanced granulomas, which suggests the bacteria present in this microenvironment experience intense iron deprivation (Kurthkoti et al., 2017). Therefore, the capacity of Mtb to survive without iron in the face of a robust nutritional immunity might enable it to persist causing a chronic infection. This concept is compatible with reports of latent TB reactivation in individuals treated for anemia with iron supplements (Trousseau, 1872; Murray et al., 1978). Considering the data and the high prevalence of anemia worldwide, caution is recommended when implementing iron supplementation programs particularly in TB endemic areas.

CONCLUSIONS AND PERSPECTIVES

It has become clear in recent years that the Mtb response to iron limitation encompasses multiple aspects of bacterial cell biology and physiology that influence host-pathogen interactions and potentially shape the outcome of TB infection. Studies of this response have offered promising targets for intervention particularly IdeR and BfrB, whose inhibition leads to lethal iron intoxication and increased susceptibility to antibiotics. Inhibiting siderophore recycling is another promising way of killing Mtb. In contrast, targeting iron acquisition, unless done very early after infection, might trigger a persistent state characterized by antibiotic tolerance. Genetic evidence suggests that utilization of iron stored in ferritin enables long-term survival of Mtb without environmental iron (Kurthkoti et al., 2017). Therefore, targeting BfrB might also effectively preclude chronic TB infection. Implementing drug screenings using iron starved Mtb may lead to new compounds effective against Mtb surviving iron starvation in the host and causing latent TB, a form of TB that continues to affect over one billion people worldwide.

AUTHOR CONTRIBUTIONS

GMR, NeS, AB, and NiS wrote the manuscript. All authors contributed to the article and approved the submitted version.

FUNDING

AB is supported by NIH AI159055. GMR, NeS, and NiS are supported by AI162821.

REFERENCES

Abreu, R., Essler, L., Giri, P., and Quinn, F. (2020). Interferon-Gamma Promotes Iron Export in Human Macrophages to Limit Intracellular Bacterial Replication. *PLoS One* 15 (12), e0240949. doi: 10.1371/journal.pone.0240949

Amaral, E. P., Costa, D. L., Namasivayam, S., Riteau, N., Kamenyeva, O., Mittereder, L., et al. (2019). A Major Role for Ferroptosis in Mycobacterium Tuberculosis-Induced Cell Death and Tissue Necrosis. *J. Exp. Med.* 216 (3), 556–570. doi: 10.1084/jem.20181776

Andersen, P., and Doherty, T. M. (2005). The Success and Failure of BCG - Implications for a Novel Tuberculosis Vaccine. *Nat. Rev. Microbiol.* 3 (8), 656–662. doi: 10.1038/nrmicro1211

Armstrong, J. A., and Hart, P. D. A. (1975). Phagosome-Lysosome Fusion Interaction in Culture Macrophages Infected With Virulent Tubercle Bacteria. *J. Exp. Med.* 142, 1–16. doi: 10.1084/jem.142.1.1

Arnold, F. M., Weber, M. S., Gonda, I., Gallenito, M. J., Adenau, S., Egloff, P., et al. (2020). The ABC Exporter IrtAB Imports and Reduces Mycobacterial Siderophores. *Nature* 580 (7803), 413–417. doi: 10.1038/s41586-020-2136-9

Athman, J. J., Wang, Y., McDonald, D. J., Boom, W. H., Harding, C. V., and Wearsch, P.A. (2015). Bacterial Membrane Vesicles Mediate the Release of *Mycobacterium tuberculosis* Lipoglycans and Lipoproteins from Infected Macrophages. *J. Immunol.* 195 (3), 1044–1053. doi: 10.4049/jimmunol.1402894

Athman, J. J., Sande, O. J., Groft, S. G., Reba, S. M., Nagy, N., Wearsch, P. A., et al. (2017). *Mycobacterium tuberculosis* Membrane Vesicles Inhibit T Cell Activation. *J. Immunol.* 198 (5), 2028 2037. doi: 10.4049/jimmunol.1601199

Bacon, J., Dover, L. G., Hatch, K. A., Zhang, Y., Gomes, J. M., Kendall, S., et al. (2007). Lipid Composition and Transcriptional Response of *Mycobacterium tuberculosis* Grown Under Iron-Limitation in Continuous Culture: Identification of a Novel Wax Ester. *Microbiology* 153 (Pt 5), 1435–1444. doi: 10.1099/mic.0.2006/004317-0

Barclay, R., Ewing, D. F., and Ratledge, C. (1985). Isolation, Identification, and Structural Analysis of the *Mycobactins of Mycobacterium avium*, *Mycobacterium intracellulare*, *Mycobacterium scrofulaceum* and *Mycobacterium paratuberculosis*. *J. Bacteriol.* 164, 896–903.

Brzostek, A., Dziadek, B., Rumijowska-Galewicz, A., Pawelczyk, J., and Dziadek, J. (2007). Cholesterol Oxidase Is Required for Virulence of *Mycobacterium tuberculosis*. *FEMS Microbiol. Lett.* 275 (1), 106–112. doi: 10.1111/j.1574-6968.2007.00865.x

Byrd, T. F., and Horwitz, M. A. (1989). Interferon Gamma-Activated Human Monocytes Downregulate Transferrin Receptors and Inhibit the Intracellular Multiplication of *Legionella Pneumophila* by Limiting the Availability of Iron. *J. Clin. Invest.* 83 (5), 1457–1465. doi: 10.1172/JCI114038

Cambier, C. J., Falkow, S., and Ramakrishnan, L. (2014). Host Evasion and Exploitation Schemes of *Mycobacterium tuberculosis*. *Cell* 159 (7), 1497–1509. doi: 10.1016/j.cell.2014.11.024

Chen, Z., Hu, Y., Cumming, B. M., Lu, P., Feng, L., Deng, J., et al. (2016). Mycobacterial WhiB6 Differentially Regulates ESX-1 and the Dos Regulon to Modulate Granuloma Formation and Virulence in Zebrafish. *Cell. Rep.* 16 (9), 2512–2524. doi: 10.1016/j.celrep.2016.07.080

Choudhury, M., Koduru, T. N., Kumar, N., Salimi, S., Desai, K., Prabhu, N. P., et al. (2021). Iron Uptake and Transport by the Carboxymycobactin-*Mycobactin Siderophore* Machinery of *Mycobacterium tuberculosis* Is Dependent on the Iron-Regulated Protein HupB. *Biometals* 34 (3), 511–528. doi: 10.1007/s10534-021-00292-2

Chou, C. J., Wisedchaisri, G., Monfeli, R. R., Oram, D. M., Holmes, R. K., Hol, W. G., et al. (2004). Functional Studies of the *Mycobacterium tuberculosis* Iron-Dependent Regulator. *J. Biol. Chem.* 279 (51), 53554–53561. doi: 10.1074/jbc.M407385200

Chouchane, S., Lippai, I., and Magliozzo, R. S. (2000). Catalase-Peroxidase (Mycobacterium tuberculosis KatG) Catalysis and Isoniazid Activation. *Biochemistry* 39 (32), 9975–9983.

Chouchane, S., Girotto, S., Kapetanaki, S., Schelvis, J. P., Yu, S. , and Magliozzo, R. S. (2003). Analysis of Heme structural Heterogeneity in *Mycobacterium tuberculosis* Catalase-Peroxidase (KatG). *J. Biol. Chem.* 278 (10), 8154–8162. doi: 10.1074/jbc.M208256200

Clemens, D. L., and Horwitz, M. A. (1996). The *Mycobacterium tuberculosis* Phagosome Interacts With Early Endosomes and Is Accessible to Exogenously Administered Transferrin. *J. Exp. Med.* 184, 1349–1355.

Converse, S. E., Mougous, J. D., Leavell, M. D., Leary, J. A., Bertozzi, C. R., and Cox, J. S. (2003). MmpL8 Is Required for Sulfolipid-1 Biosynthesis and *Mycobacterium tuberculosis* Virulence. *Proc. Natl. Acad Sci. USA* 100 (10), 6121–6126. doi: 10.1073/pnas.1030024100

Davis, B. D. (1987). Mechanism of Bactericidal Action of Aminoglycosides. *Microbiol. Rev.* 51 (3), 341–350. doi: 10.1128/mr.51.3.341-350.1987

De Voss, J. J, Rutter, K., Schroeder, B. G., Su, H., Zhu, Y., and Barry, C. E.III (2000). The Salicylate-Derived Mycobactin Siderophores of *Mycobacterium tuberculosis* Are Essential for Growth in Macrophages. *Proc. Natl. Acad. Sci.* 97, 1252–1257. doi: 10.1073/pnas.97.3.1252

Dorman, C. J., Bhriain, N. N., and Higgins, C. F. (1990). DNA Supercoiling and Environmental Regulation of Virulence Gene Expression in \Fishigella Flexneri \fP. *Nature* 344, 789–792. doi: 10.1038/344789a0

Drakesmith, H., and Prentice, A. M. (2012). Hepcidin and the Iron-Infection Axis. *Science* 338 (6108), 768–772. doi: 10.1126/science.1224577

Dussurget, O., Rodriguez, G. M., and Smith, I. (1996). An ideR Mutant of Mycobacterium smegmatis Has a Derepressed Siderophore Production and an Altered Oxidative-Stress Response. *Mol. Microbiol.* 22, 535–544. doi: 10.1046/j.1365-2958.1996.1461511.x

Fenton, H. J. H. (1894). Oxidationof Tartaric Acid in Presence of Iron. *J. Chem.Soc.* 65 (65), 899–911. doi: 10.1039/CT8946500899

Ganz, T. (2012). Macrophage and Systemic Iron Homeostasis. *J. Innate Immun.* 4, 4446–4453. doi: 10.1159/000336423

Garcia, A. F., Chang, T. H., Benchimol, M., Klumpp, D. J., Lehker, M. W., and Alderete, J. F. (2003). Iron and Contact With Host Cells Induce Expression of Adhesins on Surface of Trichomonas Vaginalis. *Mol. Microbiol.* 47 (5), 1207–1224. doi: 10.1046/j.1365-2958.2003.03366.x

Garces, A., Atmakuri, K., Chase, M. R., Woodworth, J. S., Krastins, B., Rothchild, A. C., et al. (2010). EspA Acts as a Critical mediator of ESX1-Dependent Virulence in *Mycobacterium tuberculosis* by Affecting Bacterial Cell Wall Integrity. *PLoS Pathog.* 6 (6), e1000957. doi: 10.1371/journal.ppat.1000957

Geiman, D. E., Kaushal, D., Ko, C., Tyagi, S., Manabe, Y. C., Schroeder, B. G., et al. (2004). Attenuation of Late-Stage Disease in Mice Infected by the *Mycobacterium tuberculosis* Mutant Lacking the SigF Alternate Sigma Factor and Identification of SigF-Dependent Genes by Microarray Analysis. *Infect. Immun.* 72 (3), 1733–1745. doi: 10.1128/IAI.72.3.1733-1745.2004

Gobin, J., Moore, C. H., Reeve, J. R.Jr, Wong, D. K., Gibson, B. W., and Horwitz, M. A. (1995). Iron Acquisition by *Mycobacterium tuberculosis*: Isolation and Characterization of a Family of Iron-Binding Exochelins. *Proc. Natl. Acad. Sci. U. S. A.* 92, 5189–5193. doi: 10.1073/pnas.92.11.5189

Gobin, J., and Horwitz, M. (1996). Exochelins of *Mycobacterium tuberculosis* Remove Iron From Human Iron-Binding Proteins and Donate Iron to Mycobactins in the M. tuberculosis Cell Wall. *J. Exp. Med.* 183, 1527–1532. doi: 10.1084/jem.183.4.1527

Gobin, J. D., Wong, D. K., Gibson, B. W., and Horwitz, M. A. (1999). Characterization of Exochelins of the Exochelins of *Mycobacterium Bovis* Type Strain and BCG Substrains. *Infect. Immun.* 67, 2035–2039. doi: 10.1128/IAI.67.4.2035-2039.1999

Goetz, D. H., Holmes, M. A., Borregaard, N., Bluhm, M. E., Raymond, K. N., and Strong, R. K. (2002). The Neutrophil Lipocalin NGAL Is a Bacteriostatic Agent That Interferes With Siderophore-Mediated Iron Acquisition. *Mol. Cell* 10 (5), 1033–1043. doi: 10.1016/s1097-2765(02)00708-6

Gold, B., Rodriguez, G. M., Marras, M. P., Pentecost, M., and Smith, I. (2001). The *Mycobacterium Tuberculosis* IdeR Is a Dual Functional Regulator That Controls Transcription of Genes Involved in Iron Acquisition, Iron Storage and Survival in Macrophages. *Mol. Microbiol.* 42, 851–865. doi: 10.1046/j.1365-2958.2001.02684.x

Gupta, V., Gupta, R. K., Khare, G., Salunke, D. M., and Tyagi, A. K. (2009). Crystal Structure of BfrA From *Mycobacterium Tuberculosis:* Incorporation of Selenomethionine Results in Cleavage and Demetallation of Haem. *PloS One* 4 (11):e8028. doi: 10.1371/journal.pone.0008028

Gupta, S., Palacios, A., Khataokar, A., Weinrick, B., Lavin, J., Sampedro, L., et al. (2020). Dynamin-Like Proteins Are Essential for Vesicle Biogenesis in *Mycobacterium tuberculosis*. *BioRxiv* 2020.01.14.906362. doi: 10.1101/2020.01.14.906362

Hall, R. M., and Ratledge, C. (1982). A Simple Method for the Production of Mycobactin, the Lipid-Soluble Siderophore, From Mycobacteria. *FEMS Microbiol. Lett.* 15, 133–136. doi: 10.1016/0378-1097(82)90095-7

Imlay, J. A., Chin, S. M., and Linn, S. (1988). Toxic DNA Damage by Hydrogen Peroxide Through the Fenton Reaction *In Vivo* and *In Vitro*. *Science* 240, 640–642. doi: 10.1126/science.2834821

Jones, C. M., and Neiderweis, M. (2011). *Mycobacterium tuberculosis* Can Utilize Heme as an Iron Source. *J. Bacteriol.* 193, 1767–1770.

Jones, C. M., Wells, R. M., Madduri, A. V., Renfrow, M. B., Ratledge, C., Moody, D. B., et al. (2014). Self-Poisoning of *Mycobacterium tuberculosis* by Interrupting Siderophore Recycling. *Proc. Natl. Acad. Sci. USA* 111 (5), 1945–1950. doi: 10.1073/pnas.1311402111

Karjalainen, T. K., Evans, D. G., Evans, D. J., Graham, D. Y., and Lee, C. H. (1991). Iron Represses the Expression of CFA/1 Fimbriae of Enterotoxigenic E. Coli. *Microb. Pathog.* 11, 317–323. doi: 10.1016/0882-4010(91)90017-5

Keenan, J. I., and Allardyce, R. A. (2000). Iron Influences the Expression of *Helicobacter Pylori* Outer-Membrane Vesicle-Associated Virulence Factors. *Eur. J. Gastroenterol. Hepatol.* 12, 1267–1273. doi: 10.1097/00042737-200012120-00002

Khare, G., Gupta, V., Nangpal, P., Gupta, R. K., Sauter, N. K., and Tyagi, A. K. (2011). Ferritin Structure From *Mycobacterium tuberculosis*: Comparative Study With Homologues Identifies Extended C-Terminus Involved in Ferroxidase Activity. *PloS One* 6 (4). doi: 10.1371/journal.pone.0018570

Khare, R., Kumar, S., Shukla, T., Ranjan, A., and Trivedi, P. K. (2017). Differential Sulphur Assimilation Mechanism Regulates Response of Arabidopsis Thaliana Natural Variation Towards Arsenic Stress Under Limiting Sulphur Condition. *J. Hazard Mater* 337, 198–207. doi: 10.1016/j.jhazmat.2017.05.009

Koppenol, W. H., and Hider, R. H. (2019). Iron and Redox Cycling. Do's and Don'ts. *Free Radic. Biol. Med.* 133, 3–10. doi: 10.1016/j.freeradbiomed.2018.09.022

Kuehn, M. J., and Kesty, N. C. (2005). Bacterial Outer Mebrane Vesicles and the Host-Pathogen Interactions. *Genes Dev.* 19, 2645–2655. doi: 10.1101/gad.1299905

Kurthkoti, K., Tare, P., Paitchowdhury, R., Gowthami, V. N., Garcia, M. J., Colangeli, R., et al. (2015). The Mycobacterial Iron-Dependent Regulator IdeR Induces Ferritin (bfrB) by Alleviating Lsr2 Repression. *Mol. Microbiol.* 98 (5), 864–77. doi: 10.1111/mmi.13166

Kurthkoti, K., Amin, H., Marakalala, M. J., Ghanny, S., Subbian, S., Sakatos, A., et al. (2017). The Capacity of *Mycobacterium tuberculosis* To Survive Iron Starvation Might Enable It To Persist in Iron-Deprived Microenvironments of Human Granulomas. *MBio* 8 (4). doi: 10.1128/mBio.01092-17

Kwofie, S. K., Enninful, K. S., Yussif, J. A., Asante, L. A., Adjei, M., Kan-Dapaah, K., et al. (2019). Molecular Informatics Studies of the Iron-Dependent Regulator (Ider) Reveal Potential Novel Anti-Mycobacterium Ulcerans Natural Product-Derived Compounds. *Molecules* 24 (12). doi: 10.3390/molecules24122299

Lane, S. J., Marshall, P. S., Upton, R. J., Ratledge, C., and Ewing, E. (1995). Novel Extracellular Mycobactins, the Carboxymycobactins From *Mycobacterium avium*. *Tetrahedron Lett.* 36, 4129–4132. doi: 10.1016/0040-4039(95)00676-4

Lillebaek, T., Dirksen, A., Baess, I., Strunge, B., Thomsen, V. O., and Andersen, A. B. (2002). Molecular Evidence of Endogenous Reactivation of *Mycobacterium tuberculosis* After 33 Years of Latent Infection. *J. Infect. Dis.* 185 (3), 401–404. doi: 10.1086/338342

Litwin, C. M., and Calderwood, S. B. (1993). Role of Iron in Regulation of Virulence Genes. *Clin. Microbiol. Rev.* 6, 137–149. doi: 10.1128/CMR.6.2.137

Madigan, C. A., Martinot, A. J., Wei, J. R., Madduri, A., Cheng, T. Y., Young, D. C., et al. (2015). Lipidomic Analysis Links Mycobactin Synthase K to Iron Uptake and Virulence in *M. tuberculosis*. *PLoS Pathog.* 11 (3), e1004792. doi: 10.1371/journal.ppat.1004792

Marcos-Torres, F. J., Maurer, D., Juniar, L., and Griese, J. J. (2021). The Bacterial Iron Sensor IdeR Recognizes Its DNA Targets by Indirect Readout. *Nucleic Acids Res.* 49 (17), 10120–10135. doi: 10.1093/nar/gkab711

Mehra, A., Zahra, A., Thompson, V., Sirisaengtaksin, N., Wells, A., Porto, M., et al. (2013). *Mycobacterium tuberculosis* Type VII Secreted Effector EsxH Targets Host ESCRT to Impair Trafficking. *PLoS Pathog.* 9 (10), e1003734. doi: 1101371

Mitra, A., Ko, Y. H., Cingolani, G., and Niederweis, M. (2019). Heme and Hemoglobin Utilization by *Mycobacterium tuberculosis*. *Nat. Commun.* 10 (1), 4260. doi: 10.1038/s41467-019-12109-5

Mohanty, A., Subhadarshanee, B., Barman, P., Mahapatra, C., Aishwarya, B., and Behera, R. K. (2019). Iron Mineralizing Bacterioferritin A From *Mycobacterium tuberculosis* Exhibits Unique Catalase-Dps-Like Dual Activities. *Inorg. Chem.* 58 (8), 4741–4752. doi: 10.1021/acs.inorgchem.8b02758

Mukamolova, G. V., Turapov, O., Malkin, J., Woltmann, G., and Barer, M.R. (2010). Resuscitation-Promoting Factors Reveal an Occult Population of Tubercle Bacilli in Sputum. *Am. J. Respir. Crit. Care. Med.* 181 (2), 174–180. doi: 10.1164/rccm.200905-0661OC

Murray, M., Murray, A., Murray, M. B., and Murray, C. (1978). The Adverse Effect of Iron Repletion on the Course of Certain Infections. *Br. Med. J.* 2 (6145), 1113–1115. doi: 10.1136/bmj.2.6145.1113

Olakanmi, O., Schlesinger, L. S., Ahmed, A., and Britigan, B. E. (2002). Intraphagosomal *Mycobacterium tuberculosis* Acquires Iron From Both Extracellular Transferrin and Intracellular Iron Pools: Impact of Interferon-Gamma and Hemochromatosis. *J. Biol. Chem.* 277(51):49727–34. doi: 10.1074/jbc.M209768200

Pal, R., Hameed, S., and Fatima, Z. (2015). Iron Deprivation Affects Drug Susceptibilities of Mycobacteria Targeting Membrane Integrity. J. Pathog. 2015, 938523. doi: 10.1155/2015/938523

Pal, R., Hameed, S., and Fatima, Z. (2019). Altered Drug Efflux Under Iron Deprivation Unveils Abrogated MmpL3 Driven Mycolic Acid Transport and Fluidity in Mycobacteria. *Biometals* 32 (1), 49–63. doi: 10.1007/s10534-018-0157-8

Pandey, R., and Rodriguez, G. M. (2012). A Ferritin Mutant of *Mycobacterium tuberculosis* Is Highly Suceptible to Killing by Antibiotics and Is Unable to Establish a Chronic Infection in Mice. *Infect. Immun.* 80 (10), 3650–3659. doi: 10.1128/IAI.00229-12

Pandey, R., and Rodriguez, G. M. (2013). IdeR Is Required for Iron Homeostasis and Virulence in *Mycobacterium tuberculosis*. *Mol. Microbiol.* 91 (1), 98–109. doi: 10.1111/mmi.12441

Pandey, S. D., Choudhury, M., Yousuf, S., Wheeler, P. R., Gordon, S. V., Ranjan, A., et al. (2014). Iron-Regulated Protein HupB of *Mycobacterium tuberculosis* Positively Regulates Siderophore Biosynthesis and Is Essential for Growth in Macrophages. *J. Bacteriol.* 196 (10), 1853–1865. doi: 10.1128/JB.01483-13

Pasca, M. R., Guglierame, P., Arcesi, F., Bellinzoni, M., De Rossi, E., and Riccardi, G. (2004). Rv2686c-Rv2687c-Rv2688c, An ABC Fluoroquinolone Efflux Pump in *Mycobacterium tuberculosis*. *Antimicrob. Agents Chemother* 48 (8), 3175–3178. doi:–10.1128/AAC.48.8.3175-3178.2004

Pohl, E., Holmes, R. K., and Hol, W. G. J. (1999). Crystal Structure of the Iron-Dependent Regulator (IdeR) From *Mycobacterium Tuberculosis* Shows Both Metal Binding Sites Fully Occupied. *J. Mol. Biol.* 285, 1145–1156. doi: 10.1006/jmbi.1998.2339

Prados-Rosales, R. , Weinrick, B., Piqué, D., Jacobs, W. R. Jr, Casadevall, A., and Rodriguez, G. M. (2014). Role for *Mycobacterium tuberculosis* Membrane Vesicles in Iron Acquistion. *J. Bacteriol.* 196 (6), 1250–1256. doi: 10.1128/JB.01090-13

Prados-Rosales, R., Baena, A., Martinez, L. R., Luque-Garcia, J., Kalscheuer, R., Veeraraghavan, U., et al (2011). Mycobacteria Release Active Membrane Vesicles that Modulate Immune Responses in a TLR2-Dependent Manner in Mice. *J. Clin. Invest.* 121 (4), 1471–1483. doi: 10.1172/JCI44261

Ramakrishnan, L. (2012). Revisiting the Role of the Granuloma in Tuberculosis. *Nat. Rev. Immunol.* 12 (5), 352–366. doi: 10.1038/nri3211

Ramon-Garcia, S., Ng, C., Jensen, P. R., Dosanjh, M., Burian, J., Morris, R. P., et al. (2013). WhiB7, An Fe-S-Dependent Transcription Factor That Activates Species-Specific Repertoires of Drug Resistance Determinants in Actinobacteria. *J. Biol. Chem.* 288 (48), 34514–34528. doi: 10.1074/jbc.M113.516385

Ratledge, C., Patel, P. V., and Mundy, J. (1982). Iron Transport in *Mycobacterium Smegmatis*: The Location of Mycobactin by Electron Microscopy. *J. Gen. Microbiol.* 128, 1559–1565. doi: 10.1099/00221287-128-7-1559

Raynaud, C., Guilhot, C., Rauzier, J., Bordat, Y., Pelicic, V., Manganelli, R., et al. (2002). Phospholipases C Are Involved in the Virulence of *Mycobacterium tuberculosis*. *Mol. Microbiol.* 45 (1), 203–217. doi: 10.1046/j.1365-2958.2002.03009.x

Reddy, P. V., Puri, R. V., Khera, A., and Tyagi, A. K. (2012). Iron Storage Proteins Are Essential for the Survival and Pathogenesis of *Mycobacterium tuberculosis* in THP-1 Macrophages and the Guinea Pig Model of Infection. *J. Bacteriol* 194 (3), 567–575. doi: 10.1128/JB.05553-11

Reddy, P. V., Puri, R. V., Chauhan, P., Kar, R., Rohilla, A., Khera, A., et al. (2013). Disruption of Mycobactin biosynthesis Leads to Attenuation of *Mycobacterium tuberculosis* for Growth and Virulence. *J. Infect. Dis.* doi: 10.1093/infdis/jit250

Rodriguez, G. M., Gardner, R. A., Kaur, N., and Phanstiel, O. (2008). Utilization of Fe+3-Acinetoferrin Analogues as an Iron Source by *Mycobacterium Tuberculosis*. *Biometals* 21, 93–103. doi: 10.1007/s10534-007-9096-5

Rodriguez, G. M., Voskuil, M. I., Gold, B., Schoolnik, G. K., and Smith, I. (2002). *Ider*, An Essential Gene in *Mycobacterium Tuberculosis*: Role of IdeR in Iron-Dependent Gene Expression, Iron Metabolism, and Oxidative Stress Response. *Infect. Immun.* 70 (7), 3371–3381. doi: 10.1128/IAI.70.7.3371-3381.2002

Rodriguez, G. M., and Smith, I. (2006). Identification of an ABC Transporter Required for Iron Acquisition and Virulence in *Mycobacterium tuberculosis*. *J. Bacteriol.* 188 (2), 424–430. doi: 10.1128/JB.188.2.424-430.2006

Rohilla, A., Khare, G., and Tyagi, A. K. (2017). Virtual Screening, Pharmacophore Development and Structure Based Similarity Search to Identify Inhibitors Against IdeR, A Transcription Factor of Mycobacterium Tuberculosis. *Sci. Rep.* 7 (1), 4653. doi: 10.1038/s41598-017-04748-9

Russell, D. G., Dant, J, and Sturgill-Koszycki, S. (1996). Mycobacterium avium and *Mycobacterium tuberculosis* Containing Vacules Are Dynamic, Fusion Competent Vesicles that Are Accesible to Glycosphingolipids From the Host Cell Plasmalemma. *J. Immunol.* 156, 4764–4773

Ryndak, M., Wang, S., I, S., and Rodriguez, G. M. (2010). The *Mycobacterium Tuberculosis* High-Affinity Iron Importer, IrtA, Contains an FAD-Binding Domain. *J. Bacteriol.* 192 (3), 861–869. doi: 10.1128/JB.00223-09

Saiga, H., Nishimura, J., Kuwata, H., Okuyama, M., Matsumoto, S., Sato, S., et al. (2008). Lipocalin 2-Dependent Inhibition of Mycobacterial Growth in Alveolar Epithelium. *J. Immunol.* 181 (12), 8521–8527. doi: 10.4049/jimmunol.181.12.8521

Sanchez, M., Sabio, L., Galvez, N., Capdevila, M., and Dominguez-Vera, J. M. (2017). Iron Chemistry at the Service of Life. *IUBMB Life* 69 (6), 382–388. doi: 10.1002/iub.1602

Senaratne, R. H., Sidders, B., Sequeira, P., Saunders, G., Dunphy, K., Marjanovic, O., et al. (2008). *Mycobacterium tuberculosis* Strains Disrupted in mce3 and

mce4 Operons Are Attenuated in Mice. *J. Med. Microbiol.* 57 (Pt 2), 164–170. doi: 10.1099/jmm.0.47454-0

Serafini, A., Pisu, D., Palu, G., Rodriguez, G. M., and Manganelli, R. (2013). The Esx-3 Secretion System Is Necessary for Iron and Zinc Homeostasis in *Mycobacterium tuberculosis*. *PloS One* 8 (10), e78351. doi: 10.1371/journal.pone.0078351

Siegrist, M. S., Unnikrishnan, M., McConnell, M. J., Borowsky, M., Cheng, T. Y., Siddiqi, N., et al. (2009). Mycobacterial Esx-3 Is Required for Mycobactin-Mediated Iron Acquisition. *Proc. Natl. Acad. Sci. U.S.A.* 106 (44), 18792–18797. doi: 10.1073/pnas.0900589106

Sirakova, T. D., Dubey, V. S., Cynamon, M. H., and Kolattukudy, P. E. (2003). Attenuation of *Mycobacterium tuberculosis* by Disruption of a Mas-Like Gene or a Chalcone Synthase-Like Gene, Which Causes Deficiency in Dimycocerosyl Phthiocerol Synthesis. *J. Bacteriol.* 185 (10), 2999–3008. doi: 10.1128/JB.185.10.2999-3008.2003

Sturgill-Koszycki, S., Schaible, U. E., and Russell, D. G. (1996). Mycobacterium-Containing Phagosomes Are Accessible to Early Endosomes and Reflect a Transitional State in Normal Phagosome Biogenesis. *EMBO J.* 15 (24), 6960–6968.

Subbian, S., Pandey, R., Soteropoulus, P., and Rodriguez, G. M. (2014). Vaccination With an Attenuated Ferritin Mutant Protects Mice Against Virulent *Mycobacterium Tuberculosis*. *J. Immunol. Res. 2014*. doi: 10.1155/2015/385402

Tai, S. P. S., Krafft, A. E., Nootheti, P., and Holmes, R. K. (1990). Coordinate Regulation of Siderophore and Diphtheria Toxin Production by Iron in *Corynebacterium Diphtheriae*. *Microb. Pathog.* 9, 267–273. doi: 10.1016/0882-4010(90)90015-I

Trousseau, A. (1872). *Lectures on Clinical Medicine* (London: New Sydenam society), 96.

Tufariello, J. M., Chapman, J. R., Kerantzas, C. A., Wong, K. W., Vilcheze, C., Jones, C. M., et al. (2016). Separable Roles for *Mycobacterium Tuberculosis* ESX-3 Effectors in Iron Acquisition and Virulence. *Proc. Natl. Acad. Sci. USA* 113 (3), E348–E357. doi: 10.1073/pnas.1523321113

Tullius, M. V., Harmston, C. A., Owens, C. P., Chim, N., Morse, R. P., McMath, L. M., et al. (2011). Discovery and Characterization of a Unique Mycobacterial Heme Acquisition System. *Proc. Natl. Acad. Sci. U.S.A.* 108 (12), 5051–5056. doi: 10.1073/pnas.1009516108

Wagner, D., Maser, J., Lai, B., Cai, Z., Barry, C. E. 3rd, Honer Zu Bentrup, K., et al. (2005). Elemental Analysis of *Mycobacterium avium*-, *Mycobacterium tuberculosis*-, and *Mycobacterium smegmatis*-Containing Phagosomes Indicates Pathogen-Induced Microenvironments Within the Host Cell's Endosomal System. *J. Immunol.* 174 (3), 1491–1500. doi: 10.4049/jimmunol.174.3.1491

Weinberg, E. D. (1984). Iron Withholding: A Defense Against Infection and Neoplasia. *Physiol. Rev.* 64, 65–102. doi: 10.1152/physrev.1984.64.1.65

Weinberg, E. D. (1999). Iron Loading and Disease Surveillance. *Emerg. Infect. Dis.* 5, 346–352. doi: 10.3201/eid0503.990305

Wells, R. M., Jones, C. M., Xi, Z., Speer, A., Danilchanka, O., Doornbos, K. S., et al. (2013). Discovery of a Siderophore Export System essential for Virulence of *Mycobacterium tuberculosis*. *PLoS Pathog.* 9 (1), e1003120. doi: 10.1371/journal.ppat.1003120

Yuan, Y., Crane, D. D., Simpson, R. M., Zhu, Y. Q., Hickey, M. J., Sherman, D. R., et al. (1998). The 16-kDa Alpha-Crystallin (Acr) Protein of *Mycobacterium tuberculosis* Is Required for Growth in Macrophages. *Proc. Natl. Acad. Sci. USA* 95 (16), 9578–9583. doi: 10.1073/pnas.95.16.9578

Wisedchaisri, G., Chou, C. J., Wu, M., Roach, C., Rice, A. E., Holmes, R. K., et al. (2007). Crystal Structures, Metal Activation, and DNA-Binding Properties of Two-Domain IdeR From *Mycobacterium tuberculosis*. *Biochemistry* 46 (2), 436–447. doi: 10.1021/bi0609826

Xu, Z., Meshcheryakov, V. A., Poce, G., and Chng, S. S. (2017). MmpL3 is the Flippase for Mycolic Acids in Mycobacteria. *Proc. Natl. Acad. Sci. U.S.A.* 114 (30), 7993–7998. doi: 10.1073/pnas.1700062114

Zahrt, T. C., and Deretic, V. (2001). *Mycobacterium tuberculosis* Signal Transduction System Required for Persistent Infections. *Proc. Natl. Acad. Sci. U.S.A.* 98 (22), 12706–12711. doi: 10.1073/pnas.221272198

Conflict of Interest: The authors declare that the research was conducted in the absence of any commercial or financial relationships that could be construed as a potential conflict of interest.

Publisher's Note: All claims expressed in this article are solely those of the authors and do not necessarily represent those of their affiliated organizations, or those of the publisher, the editors and the reviewers. Any product that may be evaluated in this article, or claim that may be made by its manufacturer, is not guaranteed or endorsed by the publisher.

frontiers | Frontiers in Cellular and Infection Microbiology

ORIGINAL RESEARCH
published: 18 May 2022
doi: 10.3389/fcimb.2022.875543

Airway Epithelial Cells Differentially Adapt Their Iron Metabolism to Infection With *Klebsiella pneumoniae* and *Escherichia coli In Vitro*

Philipp Grubwieser[1], *Alexander Hoffmann*[1,2], *Richard Hilbe*[1], *Markus Seifert*[1], *Thomas Sonnweber*[1], *Nina Böck*[3], *Igor Theurl*[1], *Günter Weiss*[1,2] *and Manfred Nairz*[1]*

[1] Department of Internal Medicine II, Infectious Diseases, Immunology, Rheumatology, Medical University of Innsbruck, Innsbruck, Austria, [2] Christian Doppler Laboratory for Iron Metabolism and Anemia Research, Medical University of Innsbruck, Innsbruck, Austria, [3] Biocenter, Institute of Bioinformatics, Medical University of Innsbruck, Innsbruck, Austria

OPEN ACCESS

Edited by:
José F. da Silva Neto,
University of São Paulo, Brazil

Reviewed by:
Diego Luis Costa,
University of São Paulo, Brazil
Esther G. Meyron-Holtz,
Technion Israel Institute of Technology, Israel
Andrew Armitage,
University of Oxford, United Kingdom
Megan Teh,
University of Oxford, United Kingdom
in collaboration with reviewer AA

***Correspondence:**
Manfred Nairz
Manfred.nairz@gmail.com

Specialty section:
This article was submitted to Bacteria and Host, a section of the journal Frontiers in Cellular and Infection Microbiology

Received: 15 February 2022
Accepted: 22 April 2022
Published: 18 May 2022

Citation:
Grubwieser P, Hoffmann A, Hilbe R, Seifert M, Sonnweber T, Böck N, Theurl I, Weiss G and Nairz M (2022) Airway Epithelial Cells Differentially Adapt Their Iron Metabolism to Infection With Klebsiella pneumoniae and Escherichia coli In Vitro. Front. Cell. Infect. Microbiol. 12:875543. doi: 10.3389/fcimb.2022.875543

Background: Pneumonia is often elicited by bacteria and can be associated with a severe clinical course, respiratory failure and the need for mechanical ventilation. In the alveolus, type-2-alveolar-epithelial-cells (AECII) contribute to innate immune functions. We hypothesized that AECII actively adapt cellular iron homeostasis to restrict this essential nutrient from invading pathogens – a defense strategy termed 'nutritional immunity', hitherto mainly demonstrated for myeloid cells.

Methods: We established an *in-vitro* infection model using the human AECII-like cell line A549. We infected cells with *Klebsiella pneumoniae* (*K. pneumoniae*) and *Escherichia coli* (*E. coli*), two gram-negative bacteria with different modes of infection and frequent causes of hospital-acquired pneumonia. We followed the entry and intracellular growth of these gram-negative bacteria and analyzed differential gene expression and protein levels of key inflammatory and iron metabolism molecules.

Results: Both, *K. pneumoniae* and *E. coli* are able to invade A549 cells, whereas only *K. pneumoniae* is capable of proliferating intracellularly. After peak bacterial burden, the number of intracellular pathogens declines, suggesting that epithelial cells initiate antimicrobial immune effector pathways to combat bacterial proliferation. The extracellular pathogen *E. coli* induces an iron retention phenotype in A549 cells, mainly characterized by the downregulation of the pivotal iron exporter ferroportin, the upregulation of the iron importer transferrin-receptor-1 and corresponding induction of the iron storage protein ferritin. In contrast, cells infected with the facultative intracellular bacterium *K. pneumoniae* exhibit an iron export phenotype indicated by ferroportin upregulation. This differential regulation of iron homeostasis and the pathogen-specific inflammatory reaction is likely mediated by oxidative stress.

Conclusion: AECII-derived A549 cells show pathogen-specific innate immune functions and adapt their iron handling in response to infection. The differential regulation of iron

transporters depends on the preferential intra- or extracellular localization of the pathogen and likely aims at limiting bacterial iron availability.

Keywords: nutritional immunity, iron, ferroportin, airway epithelium, nosocomial pneumonia, *E. coli*, *K. pneumoniae*

INTRODUCTION

Infections of the lower respiratory tract, including bacterial pneumonia, remain a major public health problem and a leading cause of death worldwide (Mizgerd, 2008; GBD Collaborators, L. R. I., 2018) . A large variety of microorganisms, including bacteria, viruses and fungi, can invade the distal airways and alveoli, causing a pronounced acute inflammatory response in the lung parenchyma and thus the clinical syndrome of pneumonia (Torres et al., 2021). Based on its etiology, pneumonia is broadly categorized into community-acquired pneumonia (CAP) and hospital-acquired pneumonia (HAP). The latter form is the second most common cause of hospital-acquired infection (Haque et al., 2018). Ventilation-associated pneumonia (VAP), a subset of HAP, affects 10-25% of all patients on mechanical ventilation and is the most common cause of nosocomial infection and death in the ICU (Torres et al., 2017; Torres et al., 2021).

In each entity, the most prevalent causative microorganisms differ. CAP is commonly caused by *Streptococcus pneumoniae*, *Haemophilus influenzae* or respiratory viruses. In contrast, HAP is predominantly elicited by *Staphylococcus aureus* or by different gram-negative bacilli such as *Klebsiella pneumoniae, Pseudomonas aeruginosa* and *Escherichia coli* (Jean et al., 2020).

The clinical outcome of pneumonia is tightly linked to the virulence of the invading pathogen and the inflammatory response in the lung. The latter requires a balancing act between clearance of the causative agent and minimizing tissue damage resulting from the host response (Quinton et al., 2018). Several host defense systems work in tandem to achieve this, with the innate immune system playing a crucial role in detecting and inhibiting initial bacterial proliferation, thus containing the infection (Bals and Hiemstra, 2004; Weitnauer et al., 2016). As the first line of defense against invading pathogens, epithelial cells are increasingly recognized to directly contribute to innate immune functions. Specifically in the alveolus, type-II alveolar epithelial cells (AECII) have been shown to play critical roles in host defense: pathogen detection, intercellular communication and production of bactericidal compounds (Bals and Hiemstra, 2004; Chuquimia et al., 2013). Several *in vitro* and *in vivo* studies conducted in mice have revealed, that AECII internalize bacterial pathogens, including *K. pneumoniae* (de Astorza et al., 2004; Chuquimia et al., 2012; Hsu et al., 2015).

One decisive factor in host-pathogen interactions is the combat for nutrients essential for both opponents. The sequestration of these nutrients such as the trace metal iron from pathogens is regarded as an efficient host defense strategy, a concept known as *nutritional immunity* (Núñez et al., 2018; Nairz and Weiss, 2020). Iron is essential to almost all forms of life, contingent on its ability to act as a universal redox catalyst and involvement as a co-factor in an abundance of biochemical processes critical to life (Núñez et al., 2018). Proliferation capacity of bacteria is affected by the amount of iron in their environment (Griffiths, 1991). In the intestine, increased dietary iron may even drive the selection of microorganisms to commensalism, emphasizing this trace metals multifaceted role in host pathogen interactions (Sanchez et al., 2018). In the case of infection, the host has evolved several mechanisms to take advantage of bacterial iron demand by adapting the spatio-temporal regulation of its iron metabolism. Dependent on the extra- or intracellular localization of a pathogen, the host response withholds iron from the pathogen's compartment, thus limiting bacterial proliferation (Nairz et al., 2010; Haschka et al., 2021a). In parallel, bacteria have developed diverse mechanisms to counteract *nutritional immunity* and acquire iron to sustain survival and proliferation, once confined in the microenvironment of the host. Exemplary of this co-evolutionary arms race are high-affinity iron-binding molecules known as siderophores (eg. *enterobactin*), secreted predominantly by gram-negative bacterial species to scavenge iron from their host (Behnsen and Raffatellu, 2016; Kramer et al., 2020). In turn, several host cells, including the airway epithelium, produce the immune mediator lipocalin-2 (Neutrophil-gelatinase associated lipocalin, NGAL), which binds iron-loaded *enterobactin*, rendering it inaccessible for bacterial uptake. Some *Enterobacteriaecae* (e.g. *K. pneumoniae)* are able to evade this immune strategy by producing alternative siderophores that NGAL cannot bind, such as yersiniabactin and salmochelin. In the case of *K. pneumoniae*, the expression of yersiniabactin is a virulence factor promoting respiratory tract infections through evasion of NGAL (Bachman et al., 2011). Systemically, iron overload is associated with an increased risk for infections with multiple bacterial pathogens, including *E. coli* (Parrow et al., 2013).

In the lung, sequestration of iron and other trace metals affects immune cell function and alters the response to infection, rendering tight regulation of iron bioavailability in the respiratory system vital to the host (Healy et al., 2021). In airway epithelia, typical iron transport proteins have been identified, including the cellular iron influx transporter transferrin-receptor-1 (TFR1) (Heilig et al., 2006), the cellular iron exporter ferroportin (FPN) (Yang et al., 2005), and the iron

Abbreviations: µg, microgram; µM, micromolar; µm, micrometer; ACTB, actin beta; AECII, type-2 alveolar epithelial cells; CFU, colony forming units; *E. coli*, Escherichia coli; Fig., figure; FPN, ferroportin; FT, ferritin; FTH, ferritin heavy chain; FTL, ferritin light chain; h, hour; HAMP, hepcidin antimicrobial peptide; HO1, heme oxygenase-1; IL-1B, interleukin 1 beta; IL-6, interleukin 6; IL-8, interleukin 8; *K. pneu., Klebsiella pneumonia;* LPS, lipopolysaccharide; min, minute; KEAP1, Kelch-like ECH-associated protein 1; NAC, N-acetyl-cysteine; NGAL, Neutrophil gelatinase-associated lipocalin 2;NRF2, NF-E2-related factor 2; OD_{600}, optical density (600nm); Qpcr, quantitative real-time polymerase chain reaction; ROS, reactive oxygen species; STAT3, signal transducer and activator of transcription – 3; TFR1, transferrin-receptor-1; TLR4, toll-like receptor 4.

storage protein ferritin (FT) (Ghio et al., 1998). The ability to differentially regulate cellular iron metabolism in response to infection with intra- or extracellular proliferating bacteria greatly benefits host defense, and has thus far mostly been ascribed to myeloid cells (Soares and Weiss, 2015).

In times of increasing antibiotic resistance, alternative strategies to combat bacterial infections are in need. Thus, the concept of *nutritional immunity* remains a highly relevant and evolving field. This study aimed to examine the reaction of AECII-derived A549 cells to infection with *K. pneumoniae* and *E. coli*, both of which can cause HAP, one of the most severe and difficult-to-treat forms of respiratory tract infections. We adapted an *in vitro* model to investigate the differential regulation of iron homeostasis and inflammatory reaction induced by these gram-negative pathogens.

MATERIAL AND METHODS

Cell and Bacterial Culture

We used the human cell line A549 (DMSZ, ACC 107), which closely recapitulates the AECII phenotype as our model system (Nardone and Andrews, 1979; Foster et al., 1998). Cells were propagated in DMEM (PAN-Biotech) containing 10% FBS (PAN-Biotech) and 1% Penicillin/Streptomycin (Lonza). For infection experiments, cells were washed with PBS and seeded into 6-well plates (Greiner bio-one) or 10cm dishes (Falcon) in an antibiotic-free medium containing 1% FBS.

Bacteria (*E. coli* ATCC 25922 and *K. pneumoniae* ATCC 43816) were grown from overnight cultures under sterile conditions in LB Broth (Sigma-Aldrich) to late logarithmic phase [optical density 600nm (OD600) 0.45-0.6]. Bacterial counts were determined before each experiment using a cell counter and analyzer (CASY, 45µm capillary, OLS OMNI Life Science).

For growth assays, bacteria were diluted to OD_{600} of 0.005 in cell culture medium in 96-well plates (Greiner bio-one), and directly afterwards incubated in an automated microplate reader (Spark, TECAN) at 37°C, 5% CO2 under constant double orbital shaking. OD_{600} was measured every 5min for a total of 10h.

For heat-inactivation, bacteria were incubated at 70°C for 20min and afterwards plated on LB plates to confirm absence of viable bacteria.

Fluorescence Microscopy

Bacteria were made electro-competent using glycerol/mannitol density step centrifugation, as described in an established protocol (Warren, 2011). The plasmid pBC20 with a gene encoding for the fluorescent protein Ypet (517/530nm) downstream of the constitutively active *PybaJ* promoter was electroporated into *E. coli* and *K. pneumoniae*. To visualize possible cell invasion of bacteria, A549 cells were seeded onto sterilized coverslips inside 6-well plates and infected with fluorescent bacteria at a multiplicity of infection (MOI) of 10 for 2h. Subsequently, cells on coverslips were washed thrice with PBS (Lonza) and fixed with 4% paraformaldehyde solution for 20min. Samples were permeabilized with 0.2% Triton X-100 (Roth) for 30min. Alexa-flour-594-labeled phalloidin (Invitrogen, A12381) was used to stain the actin cytoskeleton, and 4′,6-diamidino-2-phenylindole (DAPI, BioLegend, 422801) was used to stain nuclei for 30 min at room temperature. Samples were mounted with Faramount Mounting Medium (Dako, S3025) onto slides. Imaging was performed immediately after sample preparation using a VS120-S6 fluorescence microscope (Olympus). Images were captured with a 40-x objective using 387/440nm (DAPI), 485/525nm (Ypet), and 560/607nm (phalloidin) lasers and filters.

Gentamicin Protection Assay

We applied a gentamicin-protection assay (Elsinghorst, 1994) to establish the entry and presence of viable (colony-forming) intracellular bacteria over a period of up to 24h with the following adaptions: cells were infected with either *E. coli* or *K. pneumoniae* at a MOI of 10. After a 2h incubation phase, cells were washed thrice with PBS containing gentamicin (Life Technologies, 50µg/ml) and incubated in fresh medium containing 1% FCS and gentamicin (25µg/ml) during the intracellular infection phase. Gentamicin treatment during the intracellular infection phase facilitates the killing of extracellular bacteria, but does not affect pathogens that have entered cells, as gentamicin has no intracellular bactericidal activity (Elsinghorst, 1994). In parallel, we subjected uninfected control cells to identical steps of washing and incubation with gentamicin. At indicated time points (0h = directly after incubation phase), cells were washed thrice again in PBS and lysed in 0.5% sodium deoxycholic acid (Sigma-Aldrich). Cell lysates were plated immediately on LB plates, and colony-forming units (CFUs) were quantified after overnight incubation. A timeline of experimental procedures is depicted in **Supplementary Figure 1**.

Where indicated, cells were stimulated 3h before the incubation phase and during the intracellular infection phase with 25µM iron (III) nitrate nonahydrate (Sigma-Aldrich). Where appropriate, cells were treated with 5mM N-acetyl-cysteine (NAC) 20min before infection, during incubation phase and intracellular infection phase. When iron-loaded cells were infected, bacteria were iron starved in an iron-free medium (IMDM, Lonza) while growing to the late logarithmic phase.

Quantitative Real-Time PCR

The quantitative real-time PCR was carried out as described elsewhere (Hoffmann et al., 2021). In brief, total RNA isolation was prepared using acid guanidinium thiocyanate-phenol-chloroform extraction with peqGOLD Tri-Fast™ (Peqlab). For reverse transcription 2 µg RNA, random hexamer primers (200 ng/µl) (Roche), dNTPs (10 mM) (GE Healthcare LifeSciences) 20 U RNasin (Promega) and 200 U M-MLV reverse transcriptase (Invitrogen) in first-strand buffer (Invitrogen) were used. Ssofast Probes Supermix and Ssofast EvaGreen Supermix (Bio-Rad Laboratories GmbH) were used according to the manufacturer's instructions. Real-time PCR reactions were performed on QuantStudio 3 and 5 real-time PCR systems (Thermo Fisher Scientific). Gene expression was normalized

using the ΔΔct method using *Tubulin* (*TUB*) and *ornithine decarboxylase antizyme 1* (*OAZ1)* as reference transcripts.

The following TaqMan PCR primers and probes were used (all 5'→3'; primer forward; primer reverse; probe):

TUB: TCCTTCAACACCTTCTTCAGTGAGACG; GGTGC CAGTGCGAACTTCATCA; ATGTGCCCCGGGCAGTGTTT GTAGACTTG

OAZ1: GGATCCTCAATAGCCACTGC; TACAGCAGTGG AGGGAGACC; TGGATGGTGGCGCTGGGTTTATC

FPN: TGACCAGGGCGGGAGA; GAGGTCAGGTAGTCG GCCAA; CACAACCGCCAGAGAGGATGCTGTG

TFR1: TCCCAGCAGTTTCTTTCTGTTTT; CTCAATCAG TTCCTTATAGGTGTCCA; CGAGGACACAGATTATCCTTA TTTGGGTACCACC

HAMP: AGACGGGACAACTTGCAG, TCCCACACTTTG ATCGATGAC, ACACCCACTTCCCCATCTGCATT

IL-1B: CTG CTC TGG GAT TCT CTT CAG; ATC TGT TTA GGG CCA TCA GC

IL-6: AGCCCACCGGGAACGAAAGAGA; AAGGCAGCA GGCAACACCAGG; AACTCCTTCTCCACAAGCGCCTTC

IL-8: AGCCTTCCTGATTTCTGCAG; GTCCACTCTCAAT CACTCTCA

HO1: TCAGGCAGAGGGTGATAGAAG; TTGGTGTCATG GGTCAGC; TGGATGTTGAGCAGGAACGCAGT

FTH: CTCCTACGTTTACCTGTCCATG; TTTCTCAGCAT GTTCCCTCTC

FTL: AACCATGAGCTCCCAGATTC; CGGTCGAAATAG AAGCCCAG

KEAP1: AACAGAGACGTGGACTTTCG; GTGTCTGTATC TGGGTCGTAAC

Western Blot

Protein extraction and Western blotting were performed as described previously (Hoffmann et al., 2021). The following antibodies were used: a rabbit FPN antibody [1:2000; Eurogentec, custom made (Petzer et al., 2020)], a mouse TFR1 antibody (1:1000; Sigma Cat# SAB4300398), a rabbit FT antibody (1:500; Sigma), a rabbit NGAL antibody (1:1000 Abcam, ab63929), a rabbit NRF2 antibody (1:1000, Abcam, ab31163), and a rabbit actin antibody (1:500; Sigma Cat# A2066). Appropriate HRP-conjugated secondary antibodies (1:2000, anti-rabbit; Dako Cat# P0399 1:4000, anti-mouse; Dako Cat# P0447) were used. For quantification, densitometry data were acquired on a ChemiDoc Touch Imaging System (Bio-Rad) and analyzed with Image Lab 5.2.1. (Bio-Rad Laboratories GmbH).

ROS Assay

For evaluation of ROS in A549 cells during the 2h incubation phase, A549 cells were seeded into 12-well-plates in antibiotic-free medium. Cells were infected with either *E. coli* or *K. pneumoniae* at MOI of 10 and stained with 2.5μM CellROX Deep Red Reagent (Thermo Fisher Scientific). Immediately afterwards, infected cells were incubated at 37°C in an automated multimode microplate reader (Spark, TECAN) and 670nm fluorescence was read at 16 different localizations in each well every 5min for a total of 2h

Statistical Analysis

Statistical analysis was carried out using GraphPad Prism version 9.1 for Windows and Mac (GraphPad Software). Data are presented as mean with 95% CI or SEM as dispersion characteristic. Significant differences between groups were determined using ANOVA with *post-hoc* analysis. Multiple comparisons were adjusted using Tukey's or Holm-Šídák's methods. For non-normal distributed data, as evaluated by Kolmogorov-Smirnov- or Shapiro-Wilk-test, Kruskal-Wallis test with Dunn's multiple comparisons test was performed. $p < 0.05$ was used as the significance threshold.

RESULTS

E. coli and *K. pneumoniae* Infect Alveolar Epithelial Cells

We infected A549 cells with either of the two pathogens under the same conditions. Applying fluorescence microscopy using transformed bacteria that constitutively express Ypet fluorescent protein, we aimed to shed light on the cellular localization of the pathogens upon *in vitro* infection. As depicted in **Figure 1A**, imaging revealed bacteria predominantly in the extracellular space in the case of *E. coli* infection. In contrast, large numbers of *K. pneumoniae* were found intracellularly. Additional, lower magnification microscopy images are provided in **Supplementary Figure 2**.

Using an adapted gentamicin protection assay, we saw that both bacterial pathogens, *E. coli* and *K. pneumoniae* are capable of invading A549 cells, with significantly more *K. pneumoniae* entering cells directly after the incubation phase (**Figure 1B** and **Supplementary Figure 1**). After invasion, only *K. pneumoniae* was capable of intracellular proliferation, with a maximum of viable intracellular bacteria being recovered after 3h of intracellular infection. After this peak bacterial load, numbers of recovered *K. pneumoniae* decreased, suggesting that epithelial cells initiate antimicrobial immune pathways to effectively combat intracellular bacterial proliferation and decrease bacterial numbers. *E. coli*, regarded as a typical extracellular pathogen (Kaper et al., 2004), was unable to sustain intracellular proliferation in our experiments, indicated by an invariable and low bacterial load at all time intervals.

To examine the impact of elevated intracellular iron levels on bacterial growth capacity, we stimulated A549 cells with 25μM iron (III)-nitrate prior to infection and further during intracellular infection phase. **Figure 1C** demonstrates that cells loaded with iron exhibited higher bacterial burden, when infected with *K. pneumoniae*. In contrast, the extracellular pathogen *E. coli* showed no increase in intracellular proliferation. This indicates, that while higher intracellular iron concentration in epithelial cells promote the growth of *K. pneumoniae*, capable of intracellular proliferation, it

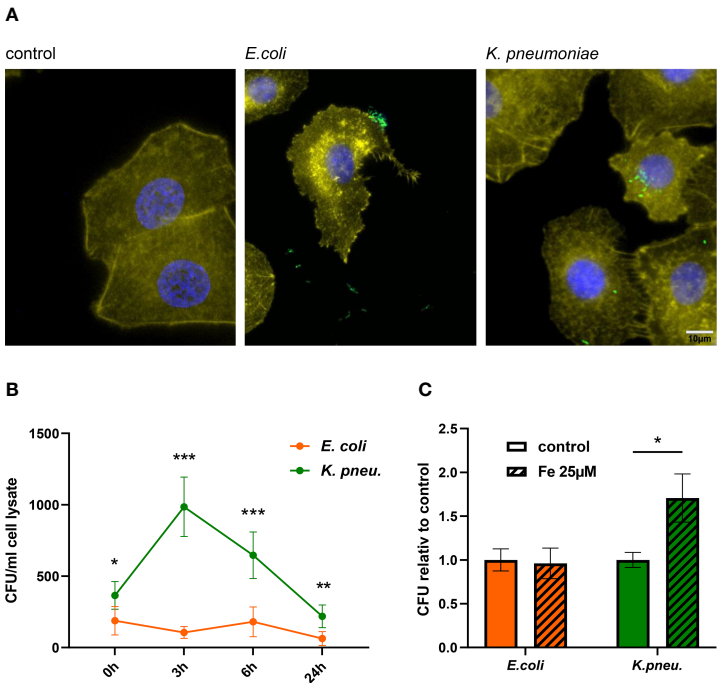

FIGURE 1 | Immune fluorescence imaging reveals the predominant localization of bacteria: *E. coli* in the extracellular space and *K. pneumoniae* in the intracellular space of A549 cells **(A)**. Representative images, showing Ypet expressing bacteria (green) infecting A549 cells (DAPI= blue, phalloidin= yellow) at 400x magnification with a 10µm scale bar. Time course of bacterial load (recovered intracellular CFU) in A549 cells **(B)**. A549 cells were infected with *E. coli* or *K. pneumoniae* for 2h at MOI of 10 and were lysed directly after incubation phase (0h time point) or at noted time intervals of intracellular infection. Lysates were plated onto LB-agar plates for CFU quantification. Data are shown as mean CFU/ml lysate ± 95% CI of three separate experiments.Intracellular bacterial load increases in *K. pneumoniae* infected, iron-loaded cells **(C)**.A549 cells were stimulated with 25µM iron (III) nitrate nonahydrate 3h before infection. Cells were infected with either *E. coli* or *K. pneumoniae* at MOI of 10 for 2h in fresh iron-adequate medium. Subsequently, cells were washed thoroughly and further incubated in gentamicin-containing medium ± 25µM iron(III) nitrate nonahydrate for 6h, until cells were lysed, and intracellular bacteria plated for CFU quantification. Data from three separate experiments are shown as mean ± SEM, normalized to the corresponding control condition. * denotes p<0.05, ** denotes p<0.01, *** denotes p<0.001 for *post-hoc* statistical testing. CFU, colony-forming-units; *K. pneu.*, *K. pneumonia.*

does not enable the growth of extracellular pathogens like *E. coli*. In contrast to this, both pathogens similarly benefit from elevated iron concentration in an extracellular growth assay (**Supplementary Figure 3**).

Taken together, our experiments revealed that both, *E. coli* and *K. pneumoniae* can infect and invade AECII-derived A549 cells. Solely *K. pneumoniae* is capable of proliferating intracellularly, with increased growth capacity in iron-loaded cells.

Alveolar Epithelial Cells Differentially Adapt Their Iron Metabolism to *E. coli* and *K. pneumoniae* Infection

Next, we evaluated the differential gene and protein expression of key players of iron metabolism in A549 cells in response to infection with either pathogen. Three hours after the incubation phase, the only known ferrous iron exporter *FPN* showed decreased mRNA expression in cells infected with either pathogen (**Figure 2A**). Strikingly, after 6h of intracellular infection, *FPN* mRNA showed a differential regulation pattern in infected cells. While *E. coli* infected cells depicted persistent negative regulation, cells infected with *K. pneumoniae* revealed increased *FPN* mRNA levels (**Figure 2B**). At both time points, FPN protein levels (**Figure 2E** shows representative blot, **Supplementary Figures 4A**, **B** show densitometry of all blots) resembled this dynamic and pathogen-specific regulation pattern.

Notably, *TFR1* mRNA expression was increased solely in *E. coli* infected cells at both time points (**Figures 2C, D**) and TFR1 and FT protein levels were also drastically increased in cells challenged with the extracellular pathogen (**Figure 2E** and **Supplementary Figure 4**). In contrast to this, A549 cells infected with *K. pneumoniae* showed no upregulation of TFR1 and FT levels. This suggests that upon detection of intracellular bacterial proliferation, cellular iron sequestration is limited.

To summarize, the extracellular pathogen *E. coli* induces an iron retention phenotype, mainly characterized by the downregulation of the pivotal iron exporter FPN, the upregulation of the iron importer TFR1 and corresponding induction of the storage protein FT. Contrarily, cells infected with the intracellularly proliferating bacterium *K. pneumoniae*

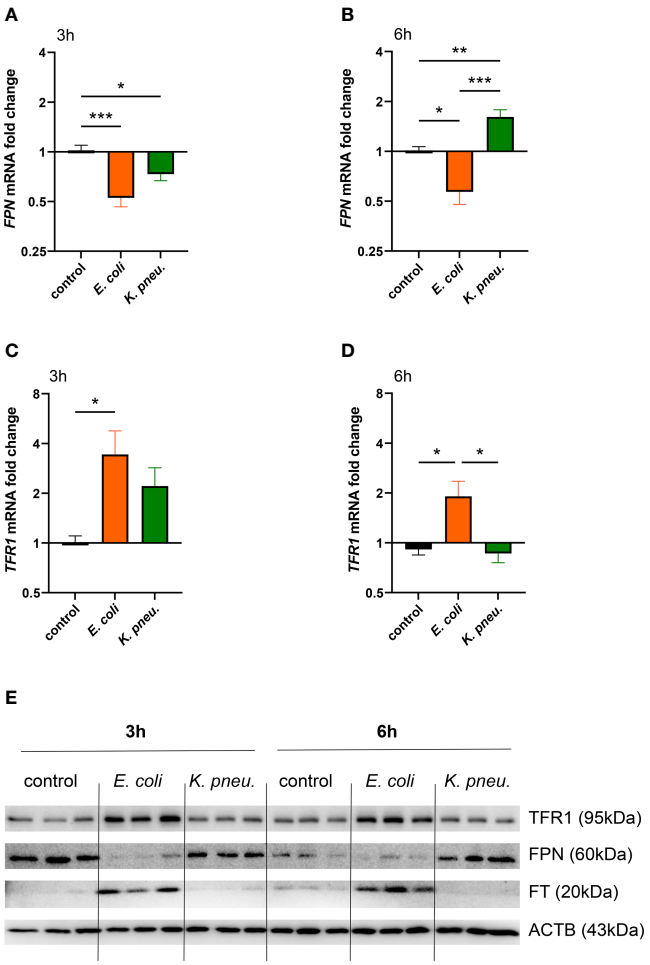

FIGURE 2 | Differential expression of *FPN* **(A, B)** and *TFR1* **(C, D)** mRNA in infected A549 cells. A549 cells were infected for 2h with *E. coli* or *K. pneumoniae* at MOI of 10, subsequently washed thoroughly and harvested after 3h **(A–C)** or 6h **(B–D)** of intracellular infection. Data are shown as mean ± SEM of 3 separate experiments.Western blot of iron transport proteins in infected A549 cells **(E)**. A549 cells were infected for 2h with *E. coli* or *K. pneumoniae* at MOI of 10, subsequently washed thoroughly and harvested after 3h **(A, C)** or 6h **(B, D)** of intracellular infection. Representative image of three separate experiments.* denotes p<0.05, ** denotes p<0.01, *** denotes p<0.001 for *post-hoc* statistical testing. *K. pneu., K, pneumoniae*; TFR1, transferrin-receptor-1; FPN, ferroportin; FT, ferritin; ACTB, β-actin.

lacked induction of iron retention proteins and exhibited an increased iron export phenotype indicated by FPN upregulation.

Pathogen-Specific Inflammatory Reaction of A549 Cells

Next, we characterized the inflammatory reaction of AECII-derived A549 cells infected with either of the two pathogens. In our experiments, only cells infected with *E. coli* showed strong induction in *HAMP* mRNA, already after 3h of intracellular infection (**Figure 3A**). Conversely, these cells also depicted higher mRNA expression levels of pro-inflammatory cytokines *IL1B*, *IL-6* and *IL-8* at 6h of intracellular phase (**Figures 3B–D**).

Likewise, NGAL showed a differential regulation pattern in our infection model (**Figure 3E**). Moderate NGAL induction on the protein level was revealed in *E. coli* infected cells, most prominently at the 6h time point. In contrast, a steep increase of this siderophores-scavenger was induced in cells infected with *K. pneumoniae*.

Our experiments thus demonstrated pathogen-specific inflammatory reactions in infected epithelial cells. In *E. coli* infected cells, the expression of key iron regulator *HAMP*, as well as inflammatory cytokines were strongly induced. In contrast, the innate immune effector NGAL showed striking induction in *K. pneumoniae* infected cells, possibly related to the intracellular proliferation of this pathogen.

Pathogen-Specific Reactions of A549 Cells Are Mediated by Oxidative Stress

Subsequently, we investigated possible mechanisms underlying pathogen-specific gene expression. To this end, we examined oxidative stress generation in A549 cells during the initial 2h incubation phase (**Figure 4A**). Our experiments showed

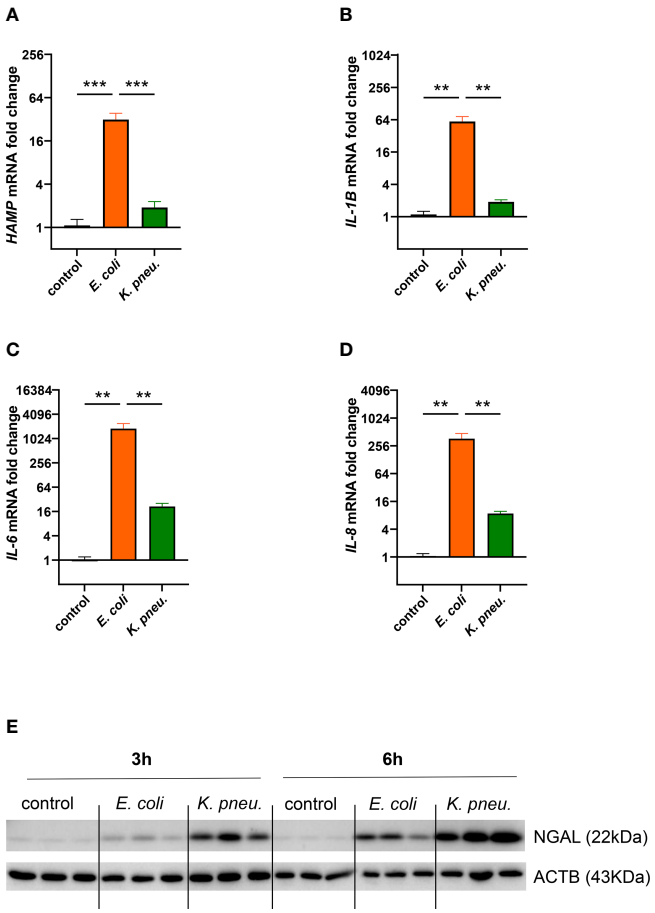

FIGURE 3 | Differential mRNA expression of *HAMP* **(A)** and pro-inflammatory cytokines *IL-1B* **(B)** *IL-6* **(C)**, and *IL-8* **(D)** in infected A549 cells.A549 cells were infected for 2h with *E. coli* or *K. pneumoniae* at MOI of 10, subsequently washed thoroughly and harvested after 3h **(A)** or 6h **(B–D)** of intracellular infection. Data from three separate experiments are shown as mean ± SEM.Western blotting of NGAL in infected AECII **(E)**. A549 cells were infected for 2h with *E. coli* or *K. pneumoniae* at MOI of 10, subsequently washed thoroughly and harvested after 3h (left) or 6h (right) of intracellular infection. Representative image of three separate experiments. ** denotes p<0.01, *** denotes p<0.001 for *post-hoc* statistical testing. *K. pneu., K. pneumoniae*; HAMP, hepcidin antimicrobial peptide; NGAL, neutrophil gelatinase-associated lipocalin 2; ACTB, β-actin.

significantly higher levels of reactive oxygen species (ROS) in cells infected with *K. pneumoniae*, compared to both, *E. coli* infected cells as well as uninfected controls. Elevated ROS levels, as found in *K. pneumoniae* infected cells, modulate cellular signaling and could thus at least partly explain the pathogen-specific reaction in iron homeostasis and inflammatory response (Spooner and Yilmaz, 2011). Correspondingly, Western blots of nuclear extracts revealed higher levels of the oxidative-stress-response transcription factor NF-E2-related factor 2 (NRF2) in cells infected with *K. pneumoniae* as compared to *E. coli* infected cells and uninfected controls (**Figures 4B, C**).

Furthermore, we analyzed differential gene expression of NRF2 pathway-related- as well as target-genes involved in iron metabolism. Appropriately, *Kelch-like ECH-associated protein 1* (*KEAP1*) mRNA expression was increased in *K. pneumoniae* infected A549 cells (**Figure 4E**). *Heme oxygenase-1* (*HO1*), a phase II detoxifying enzyme and NRF2 target gene, showed significant mRNA upregulation in cells infected with *K. pneumoniae* (**Figure 4D**). Another target gene is the iron storage protein FT (Cairo et al., 1995). After analyzing both, *ferritin heavy-* (*FTH*) and *light-* (*FTL*) chain transcripts, we found a significant increase of only *FTL* mRNA levels in *K. pneumoniae* infected cells (**Figures 4F, G**). In addition, treatment with the ROS-scavenger NAC revealed a negative effect on the expression of NRF2- related genes in *K. pneumoniae* infected cells (**Supplementary Figure 5**).

DISCUSSION

AECII are amongst the first cell types to encounter respiratory pathogens. Unlike alveolar macrophages, AECII are not typically considered to be ′professional′ immune cells, but still express various pattern-recognition receptors (PRRs) (Bals and

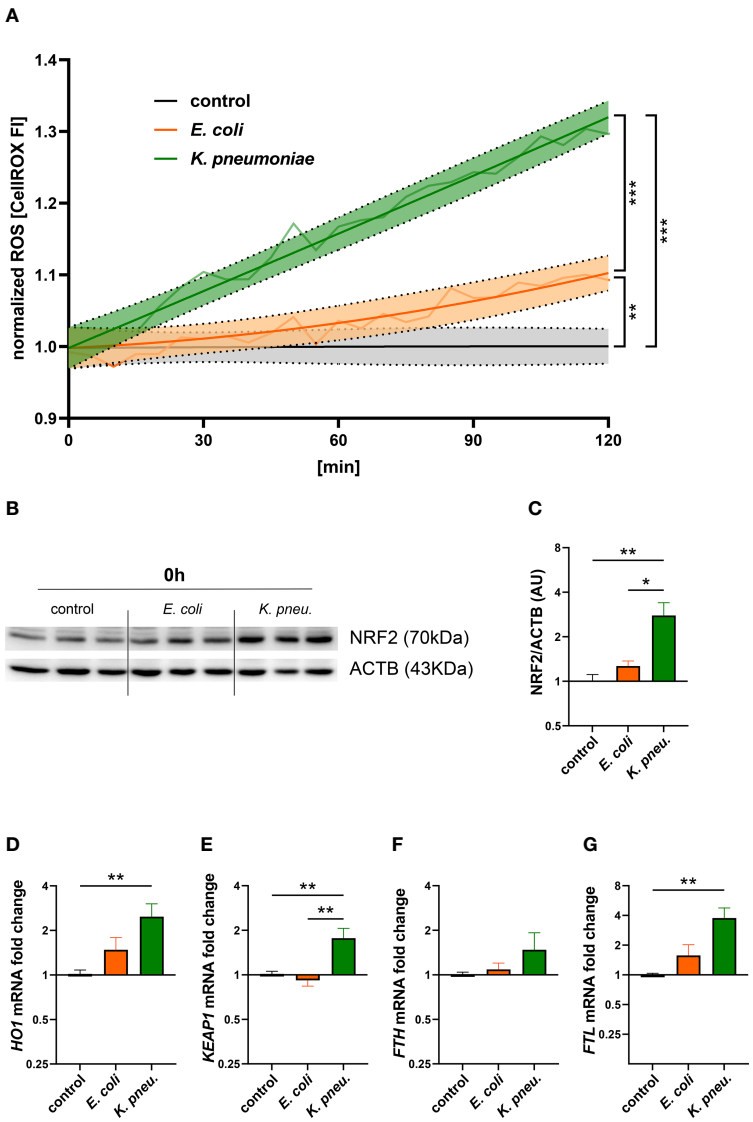

FIGURE 4 | Time-course of ROS formation during the 2h incubation phase in A549 cells infected with either *E. coli* or *K. pneumoniae* **(A)**. The means of fluorescence intensity of three independent experiments are shown as a light colored line. Dark colored lines display a non-linear regression line-fit with 95% CI as error bands. Results were normalized to uninfected controls. Statistical testing was performed for the 120min time point. Western blot **(B)** of NRF2 and corresponding densitometry of two separate experiments **(C)** in infected A549 cells. A549 cells were infected for 2h with *E. coli* or *K. pneumoniae* at MOI of 10, subsequently washed thoroughly and directly harvested. Data are shown as mean ± SEM of 2 separate experiments. Differential mRNA expression of NRF2-targeted genes *HO1* **(D)**, *KEAP1* **(E)**, *FTH* **(F)**, and *FTL* **(G)** in infected A549 cells. A549 cells were infected for 2h with *E. coli* or *K. pneumoniae* at MOI of 10, subsequently washed thoroughly and harvested after 6h of intracellular infection. Data are shown as mean ± SEM of three separate experiments. * denotes p<0.05, ** denotes p<0.01, *** denotes p<0.001 for *post-hoc* statistical testing. ROS, reactive oxygen species; *K. pneu., K. pneumoniae*; NRF2, NF-E2-related factor 2; ACTB, β-actin; HO1, Heme oxygenase-1; KEAP1, Kelch-like ECH-associated protein 1; FTH, ferritin heavy chain; FTL, ferritin light chain.

Hiemstra, 2004). In this study, we provide first *in-vitro* evidence that epithelial cells are able to mount a pathogen-specific nutritional immune response. Specifically, A549 cells infected with *K. pneumoniae* which resides intracellularly (de Astorza et al., 2004; Hsu et al., 2015) induce the expression of the iron exporter FPN. In contrast, A549 cells display an iron-retention phenotype when exposed to *E. coli*, a prototypical extracellular bacterium. This ability to differentially regulate cellular iron metabolism in response to infection with intra- or extracellular bacteria has hitherto only been ascribed to myeloid cells. A proposed model of this pathogen-specific reaction of AECII to invading bacteria is depicted in **Figure 5**.

We found higher bacterial loads in iron-loaded cells infected with *K. pneumoniae*, emphasizing this metal's crucial role in infection. Supporting these findings, higher available iron in the pathogen's compartment is associated with increased bacterial

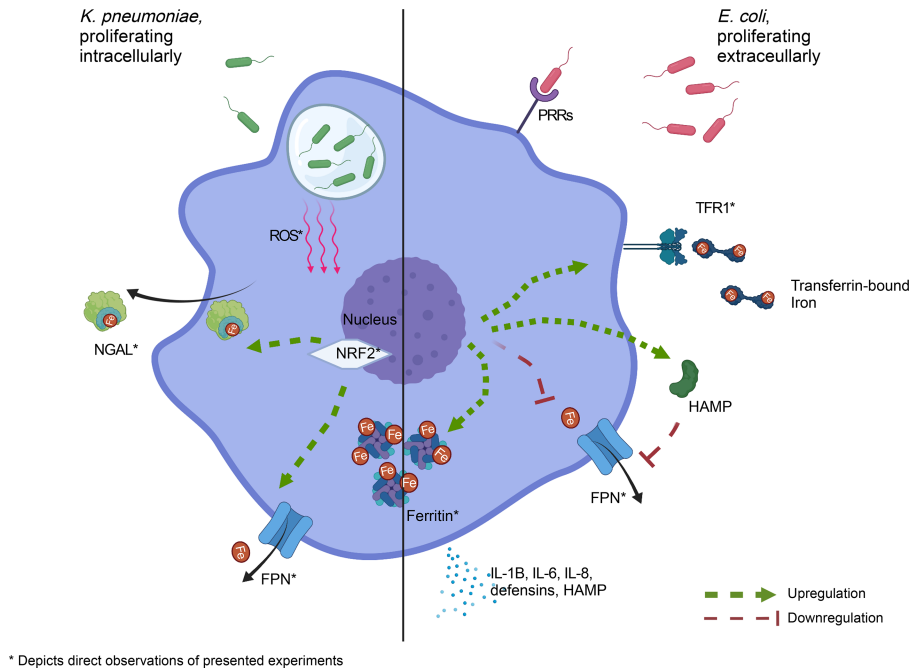

FIGURE 5 | Pathogen-specific adaption of cellular iron homeostasis in AECII. Left panel: *K. pneumoniae*, capable of proliferating intracellularly, elicits an iron-export phenotype, likely mediated by oxidative stress. Right panel: *E. coli*, which proliferates predominantly in the extracellular space, induces an iron retention phenotype in infected AECII. * denotes direct experimental observations AECII, type-2 alveolar epithelial cell; ROS, reactive oxygen species; NGAL, neutrophil gelatinase-associated lipocalin 2; PRR, pattern recognition receptor; TFR1, transferrin receptor-1; FPN, ferroportin; NRF2, NF-E2-related factor 2; Created with BioRender.com.

growth in various models (Pan et al., 2010; Schmidt et al., 2018; Haschka et al., 2021b; Hoffmann et al., 2021). Thus, it is pivotal for the host to deprive iron of an invading pathogen during the spatio-temporal dynamics of the host-pathogen interaction. Specifically, the balance between iron uptake, export and storage needs to be adapted to the niche of the invading pathogen. This raises the question of how the pathogen is sensed and how this information is subsequently translated into altered cellular iron handling.

Typically, downstream signaling of PRRs such as toll-like-receptors (TLRs) is responsible for early innate immune responses to bacteria and bacterial components (Knapp et al., 2008). Specifically, TLR-4 mediated detection of bacterial lipopolysaccharide (LPS) showed to be responsible for inflammatory cytokine induction in airway epithelial cells, an effect that could be diminished by TLR4-blockade (Grandel et al., 2009; John et al., 2010). In the case of iron homeostasis, the expression of the only known ferrous iron exporter FPN is transcriptionally repressed by TLR signaling (Ludwiczek et al., 2003). This mechanism is likely mediating the transcriptional response in infected A549 cells, as we found decreased *FPN* mRNA expression in infected cells with both pathogens in the early phase of infection. Strikingly, we found *FPN* mRNA levels increased in cells infected with intracellularly proliferating *K. pneumoniae* at the later time interval, possibly decreasing iron availability to the pathogen. This positive *FPN* regulation pattern seems to be dependent on the metabolism and/or proliferation of a viable intracellular pathogen, as revealed by experiments with heat-killed bacteria: The challenge of cells with heat-killed bacteria led to a negative *FPN* regulation pattern at early and late time points, possibly because of the high abundance of pathogen-associated molecules, derived from either bacterium (**Supplementary Figure 6**). In myeloid cells infected with intracellularly proliferating *Salmonella*, a very similar dynamic regulation of FPN expression has been observed (Nairz et al., 2007). In contrast, cells infected with the predominantly extracellular pathogen *E. coli* revealed an iron-retention-phenotype, depicted by TFR1 and FT upregulation. This finding is parallel to several cell types reacting to extracellular bacteria with iron sequestration, to withhold this essential nutrient from invading pathogens (Healy et al., 2021).

At the interface of iron and immunity, the hepcidin antimicrobial peptide (HAMP) acts as a key regulator of systemic (endocrine) and localized (paracrine) iron metabolism (Theurl et al., 2008). HAMP binds the iron exporter FPN, leading to its internalization and degradation, thus increasing intracellular iron sequestration (Nemeth et al., 2004). AECII also express HAMP, suggested to have a paracrine function in the lung (Chen et al., 2014; Zhang et al., 2019). Upon systemic infection, inflammatory cytokines like IL-6 lead to increased *HAMP* transcription *via* signal transducer and activator of transcription (STAT)-3 in hepatocytes (Wrighting and Andrews, 2006). Intriguingly, *HAMP* induction has also been reported by LPS treatment independent of IL-6 in various cell types, including alveolar macrophages (Nguyen et al., 2006; Lee

et al., 2017). In the local environment of infection, direct sensing of bacterial components could thus affect cellular iron transport. Our experiments showed that both, inflammatory cytokines as well as *HAMP* expression were significantly increased in *E. coli* infected A549 cells, but HAMP could not be detected in supernatants of infected cells *via* ELISA (data not shown).

Our data thus suggests that the iron sequestration phenotype depicted by *E. coli* infected cells is accomplished *via* intracellular signaling following pathogen sensing, a response very similar to the response observed in alveolar macrophages (Nguyen et al., 2006).

It is of note, that adaption of iron metabolism in a state of inflammation not only affects the microenvironment of infection but may also disrupt systemic iron allocation. Increased iron retention, caused by chronic state of inflammation in infections, proliferative or autoimmune disorders may render iron inaccessible for erythropoiesis, leading to anemia of chronic disease (Weiss and Goodnough, 2005; Valente de Souza et al., 2021).

Interestingly, upon infection, various bactericidal mechanisms have been described in AECII. One such antimicrobial immune effector molecule produced by AECII in response to bacterial infection is NGAL (Saiga et al., 2008; Ruaro et al., 2021). NGAL takes part in inhibiting bacterial iron acquisition by binding bacterial siderophores and plays a significant role in the lung's innate immune defense against *Enterobacteriacae* (Chan et al., 2009; Wu et al., 2010). Our experiments revealed a differential regulation pattern of this immune molecule in A549 cells, with only moderate induction in *E. coli* infected cells, compared to striking induction in *K. pneumoniae* infected cells. Moderate induction could be explained by autocrine effects of inflammatory cytokines, like IL-1beta, as sole bacterial LPS stimulation does not translate into increased NGAL expression (Cowland et al., 2003). In contrast, high NGAL induction in the lung has been reported with other intracellular bacteria (Guglani et al., 2012). As another factor possibly at play, *K. pneumoniae* is capable of NGAL evasion by producing alternative siderophores, which the immune molecule cannot bind, possibly translating into a bacterial survival advantage (Bachman et al., 2012). At last, NGAL overexpression is also linked to oxidative stress, as elevated cellular levels of ROS lead to NGAL induction in myeloid cells (Fritsche et al., 2012). Furthermore, NGAL itself exerts antioxidant effects, thus ameliorating ROS-mediated toxicity (Roudkenar et al., 2011). Accordingly, we found elevated ROS levels in *K. pneumoniae* infected A549 cells. This finding is in line with intracellular pathogens being associated with ROS-generation in host cells, and with reports of *K. pneumoniae* infected airway epithelial cells suffering from increased oxidative stress (Shin et al., 2010; Spooner and Yilmaz, 2011; Leone et al., 2016). Of note, NGAL can export iron out of macrophages by employing a mammalian siderophore and thereby limiting access of iron for bacteria residing within macrophages (Nairz et al., 2009). However, this may be of benefit for some bacteria, such as *Streptococcus pneumoniae*, were NGAL expression was associated with an impaired infection control (Warszawska et al., 2013).

Pathogen-specific reactions regarding the inflammatory response and iron homeostasis could at least partly be explained by differences in elicited cellular ROS. After detecting oxidative stress, the transcription factor NRF2 initiates a whole cassette of cytoprotective genes including iron transporters and has also been linked to host defense against bacteria (Battino et al., 2018). NRF2 controls its own degradation through an auto-regulatory negative feedback loop. Its activation leads to increased expression of *KEAP1*, the primary inhibitor of NRF2 (Lee et al., 2007). Consequently, our experiments revealed higher protein levels of NRF2 as well as target gene induction (*FPN*, *FTL*, *HO1*, *KEAP1*) in *K. pneumoniae* infected cells. In line with these findings, NRF2 target genes showed a trend towards reduced expression in *K. pneumoniae* infected cells, when treated with the ROS-scavenger NAC. Of note, cellular protein concentrations of the NRF2-target FT are primarily regulated post-transcriptionally (Torti and Torti, 2002), explaining the discrepancy between mRNA regulation and total cellular protein abundance. In macrophages infected with intracellular bacteria, the pivotal upregulation of FPN was shown to be NRF2 dependent (Nairz et al., 2013). Underlining this relationship, a mouse pneumonia model showed NRF2 null animals infected with *Streptococcus pneumoniae* suffered from increased mortality rates (Gomez et al., 2016).

To conclude, we could demonstrate pathogen-specific inflammatory and innate functions in AECII-derived A549 cells, which are in line with the concept of *nutritional immunity*. Multi-drug resistant bacteria, including carbapenem-resistant *K. pneumoniae* and extended-spectrum beta-lactamase-producing *E. coli*, are continually emerging and are a critical priority global health concern (Pitout et al., 2015). An improved understanding of innate and adaptive immune functions, including *nutritional immunity*, might provide new treatment options for patients infected with these multi-drug resistant bacteria.

DATA AVAILABILITY STATEMENT

The raw data supporting the conclusions of this article will be made available by the authors, without undue reservation.

AUTHOR CONTRIBUTIONS

MN, GW, and IT planned and designed the project. PG, AH, RH, and MS performed experiments. PG did the visualization of the data and performed the statistical analysis. PG and MN prepared and created the initial draft. AH, IT, GW, TS, NB, and RH were included in the critical review and writing of the manuscript. MN, IT, and GW were responsible for supervision and funding acquisition. All authors contributed to the article and approved the submitted version.

FUNDING

This project was enabled and supported by grants of the Austrian Science Fund (FWF, DOC 82 doc.fund; doctoral program MCBD).

ACKNOWLEDGMENTS

The authors want to thank Beatrice Claudi and Prof. Dr. Dirk Bumann (Biozentrum, University of Basel) for providing the bacterial pBC20-Ypet plasmid. Financial support by the Christian Doppler Society (Laboratory of Iron Metabolism and Anemia Research) and the "Verein zur Förderung von Forschung und Weiterbildung in Infektiologie und Immunologie an der Medizinischen Universität Innsbruck" is gratefully acknowledged.

SUPPLEMENTARY MATERIAL

The Supplementary Material for this article can be found online at: https://www.frontiersin.org/articles/10.3389/fcimb.2022.875543/full#supplementary-material

Supplementary Figure 1 | Timeline of the experimental setup. After a 2h incubation phase with either model pathogen, cells were washed and incubated in a gentamicin-containing medium for the intracellular infection phase. Cells were harvested at different time points for analysis, as depicted.

Supplementary Figure 2 | Additional immune fluorescence images reveal the predominant localization of bacteria at lower magnification: *E. coli* in the extracellular space **(A)** and *K. pneumoniae* in the intracellular space **(B)** of A549 cells. Images show Ypet expressing bacteria (green) infecting A549 cells (DAPI= blue, phalloidin= yellow) at 200x magnification with a 50µm scale bar.

Supplementary Figure 3 | Growth assay of *E. coli* **(A)** or *K. pneumoniae* **(B)**. Bacteria in logarithmic growth phase were diluted to an OD_{600} 0.005 in cell culture medium or medium supplemented with 25µM iron (III) nitrate nonahydrate. OD_{600} was continually measured over 600 minutes, means ± 95% CI (n=5) are shown.

Supplementary Figure 4 | Densitometry of Western blots of key iron metabolism proteins FPN **(A, B)**, TFR1 **(C, D)**, FT **(E, F)** and NGAL **(G, H)** in infected A549 cells. A549 cells were infected for 2h with *E. coli* or *K. pneumoniae* at MOI of 10, subsequently washed thoroughly and harvested after 3h (left) or 6h (right) of intracellular infection. Data from three separate experiments are shown as mean ± SEM. * denotes p<0.05, ** denotes p<0.01, *** denotes p<0.001 for *post-hoc* statistical testing. *K. pneu.*, *K. pneumoniae*; FPN, ferroportin; TFR1, transferrin-receptor-1; FT, ferritin; NGAL, neutrophil gelatinase-associated lipocalin 2.

Supplementary Figure 5 | Differential mRNA expression of NRF2-associated genes *FPN* **(A)**, *HO1* **(B)**, *FTH* **(C)**, *FTL* **(D)**. and *KEAP1* **(E)** in infected A549 cells, treated with ROS-scavenger NAC. A549 cells were infected for 2h with *E. coli* or *K. pneumoniae* at MOI of 10, subsequently washed thoroughly and harvested after 6h of intracellular infection. Cells were treated with 5mM NAC 20 min before infection, and during intracellular infection. Data (n=3) shown as mean ± SEM, normalized to corresponding solvent controls ROS, reactive oxygen species; NAC, N-acetyl-cysteine; *K. pneu.*, *K. pneumoniae*; NRF2, NF-E2-related factor 2; *FPN*, ferroportin; HO1, Heme oxygenase-1; FTH, ferritin heavy chain; FTL, ferritin light chain; KEAP1, Kelch-like ECH-associated protein 1.

Supplementary Figure 6 | Differential mRNA expression of *FPN* in cells treated with heat-killed bacteria. A549 cells were treated with heat-killed (HK) *E. coli* or *K. pneumoniae* at MOI of 100 for 2h, subsequently washed thoroughly and harvested after 3h **(A)** and 6h **(B)**. Data (n=3) shown as mean ± SEM, normalized to untreated controls. HK, heat-killed; *K. pneu.*, *K. pneumoniae*; *FPN*, ferroportin.

REFERENCES

Bachman, M. A., Lenio, S., Schmidt, L., Oyler, J. E., and Weiser, J. N. (2012). Interaction of Lipocalin 2, Transferrin, and Siderophores Determines the Replicative Niche of Klebsiella Pneumoniae During Pneumonia. *mBio* 3 (6), e00224–e00211. doi: 10.1128/mBio.00224-11

Bachman, M. A., Oyler, J. E., Burns, S. H., Caza, M., Lépine, F., Dozois, C. M., et al. (2011). Klebsiella Pneumoniae Yersiniabactin Promotes Respiratory Tract Infection Through Evasion of Lipocalin 2. *Infection Immun.* 79 (8), 3309–3316. doi: 10.1128/IAI.05114-11

Bals, R., and Hiemstra, P. S. (2004). Innate Immunity in the Lung: How Epithelial Cells Fight Against Respiratory Pathogens. *Eur. Respir. J.* 23 (2), 327–333. doi: 10.1183/09031936.03.00098803

Battino, M., Giampieri, F., Pistollato, F., Sureda, A., de Oliveira, M. R., Pittalà, V., et al. (2018). Nrf2 as Regulator of Innate Immunity: A Molecular Swiss Army Knife! *Biotechnol. Adv.* 36 (2), 358–370. doi: 10.1016/j.biotechadv.2017.12.012

Behnsen, J., and Raffatellu, M. (2016). Siderophores: More Than Stealing Iron. *mBio* 7 (6). doi: 10.1128/mBio.01906-16

Cairo, G., Tacchini, L., Pogliaghi, G., Anzon, E., Tomasi, A., and Bernelli-Zazzera, A. (1995). Induction of Ferritin Synthesis by Oxidative Stress. Transcriptional and Post-Transcriptional Regulation by Expansion of the "Free" Iron Pool. *J. Biol. Chem.* 270 (2), 700–703. doi: 10.1074/jbc.270.2.700

Chan, Y. R., Liu, J. S., Pociask, D. A., Zheng, M., Mietzner, T. A., Berger, T., et al. (2009). Lipocalin 2 Is Required for Pulmonary Host Defense Against Klebsiella Infection. *J. Immunol.* 182 (8), 4947–4956. doi: 10.4049/jimmunol.0803282

Chen, Q., Wang, L., Ma, Y., Wu, X., Jin, L., and Yu, F. (2014). Increased Hepcidin Expression in Non-Small Cell Lung Cancer Tissue and Serum Is Associated With Clinical Stage. *Thorac. Cancer* 5 (1), 14–24. doi: 10.1111/1759-7714.12046

Chuquimia, O. D., Petursdottir, D. H., Periolo, N., Fernández, C., and Flynn, J. L. (2013). Alveolar Epithelial Cells Are Critical in Protection of the Respiratory Tract by Secretion of Factors Able To Modulate the Activity of Pulmonary Macrophages and Directly Control Bacterial Growth. *Infect. Immun.* 81 (1), 381–389. doi: 10.1128/IAI.00950-12

Chuquimia, O. D., Petursdottir, D. H., Rahman, M. J., Hartl, K., Singh, M., and Fernández, C. (2012). The Role of Alveolar Epithelial Cells in Initiating and Shaping Pulmonary Immune Responses: Communication Between Innate and Adaptive Immune Systems. *PLoS One* 7 (2), e32125. doi: 10.1371/journal.pone.0032125

Cowland, J. B., Sørensen, O. E., Sehested, M., and Borregaard, N. (2003). Neutrophil Gelatinase-Associated Lipocalin Is Up-Regulated in Human Epithelial Cells by IL-1β, But Not by TNF-α. *J. Immunol.* 171 (12), 6630–6639. doi: 10.4049/jimmunol.171.12.6630

de Astorza, B., Cortés, G., Crespí, C., Saus, C., Rojo, J. M., and Albertí, S. (2004). C3 Promotes Clearance of Klebsiella Pneumoniae by A549 Epithelial Cells. *Infect. Immun.* 72 (3), 1767–1774. doi: 10.1128/IAI.72.3.1767-1774.2004

Elsinghorst, E. A. (1994). "Measurement of Invasion by Gentamicin Resistance", in *Methods in Enzymology* (New York, NY: Elsevier, USA), 405–420.

Foster, K. A., Oster, C. G., Mayer, M. M., Avery, M. L., and Audus, K. L. (1998). Characterization of the A549 Cell Line as a Type II Pulmonary Epithelial Cell Model for Drug Metabolism. *Exp. Cell Res.* 243 (2), 359–366. doi: 10.1006/excr.1998.4172

Fritsche, G., Nairz, M., Libby, S. J., Fang, F. C., and Weiss, G. (2012). Slc11a1 (Nramp1) Impairs Growth of Salmonella Enterica Serovar Typhimurium in Macrophages *via* Stimulation of Lipocalin-2 Expression. *J. Leukocyte Biol.* 92 (2), 353–359. doi: 10.1189/jlb.1111554

GBD Collaborators, L.R.I (2018). Estimates of the Global, Regional, and National Morbidity, Mortality, and Aetiologies of Lower Respiratory Infections in 195 Countries 1990-2016: A Systematic Analysis for the Global Burden of Disease Study 2016. *Lancet Infect. Dis.* 18 (11), 1191–1210. doi: 10.1016/s1473-3099(18)30310-4

Ghio, A. J., Carter, J. D., Samet, J. M., Reed, W., Quay, J., Dailey, L. A., et al. (1998). Metal-Dependent Expression of Ferritin and Lactoferrin by Respiratory Epithelial Cells. *Am. J. Physiol. Lung Cell. Mol. Physiol.* 274 (5), L728–L736. doi: 10.1152/ajplung.1998.274.5.L728

Gomez, J. C., Dang, H., Martin, J. R., and Doerschuk, C. M. (2016). Nrf2 Modulates Host Defense During Streptococcus Pneumoniae Pneumonia in Mice. *J. Immunol.* 197 (7), 2864–2879. doi: 10.4049/jimmunol.1600043

Grandel, U., Heygster, D., Sibelius, U., Fink, L., Sigel, S., Seeger, W., et al. (2009). Amplification of Lipopolysaccharide-Induced Cytokine Synthesis in Non–Small Cell Lung Cancer/Neutrophil Cocultures. *Mol. Cancer Res.* 7 (10), 1729–1735. doi: 10.1158/1541-7786.Mcr-09-0048

Griffiths, E. (1991). Iron and Bacterial Virulence — A Brief Overview. *Biol. Metals* 4 (1), 7–13. doi: 10.1007/BF01135551

Guglani, L., Gopal, R., Rangel-Moreno, J., Junecko, B. F., Lin, Y., Berger, T., et al. (2012). Lipocalin 2 Regulates Inflammation During Pulmonary Mycobacterial Infections. *PLoS One* 7 (11), e50052. doi: 10.1371/journal.pone.0050052

Haque, M., Sartelli, M., McKimm, J., and Abu Bakar, M. (2018). Health Care-Associated Infections - An Overview. *Infect. Drug Resist.* 11, 2321–2333. doi: 10.2147/idr.S177247

Haschka, D., Hoffmann, A., and Weiss, G. (2021a). Iron in Immune Cell Function and Host Defense. *Semin. Cell Dev. Biol.* 115, 27–36. doi: 10.1016/j.semcdb.2020.12.005

Haschka, D., Tymoszuk, P., Petzer, V., Hilbe, R., Heeke, S., Dichtl, S., et al. (2021b). Ferritin H Deficiency Deteriorates Cellular Iron Handling and Worsens Salmonella Typhimurium Infection by Triggering Hyperinflammation. *JCI Insight* 6 (13). doi: 10.1172/jci.insight.141760

Healy, C., Munoz-Wolf, N., Strydom, J., Faherty, L., Williams, N. C., Kenny, S., et al. (2021). Nutritional Immunity: The Impact of Metals on Lung Immune Cells and the Airway Microbiome During Chronic Respiratory Disease. *Respir. Res.* 22 (1), 133. doi: 10.1186/s12931-021-01722-y

Heilig, E. A., Thompson, K. J., Molina, R. M., Ivanov, A. R., Brain, J. D., and Wessling-Resnick, M. (2006). Manganese and Iron Transport Across Pulmonary Epithelium. *Am. J. Physiol.-Lung Cell. Mol. Physiol.* 290 (6), L1247–L1259. doi: 10.1152/ajplung.00450.2005

Hoffmann, A., Haschka, D., Valente de Souza, L., Tymoszuk, P., Seifert, M., von Raffay, L., et al. (2021). Baseline Iron Status and Presence of Anaemia Determine the Course of Systemic Salmonella Infection Following Oral Iron Supplementation in Mice. *EBioMedicine* 71, 103568. doi: 10.1016/j.ebiom.2021.103568

Hsu, C.-R., Pan, Y.-J., Liu, J.-Y., Chen, C.-T., Lin, T.-L., Wang, J.-T., et al. (2015). Klebsiella Pneumoniae Translocates Across the Intestinal Epithelium *via* Rho GTPase- and Phosphatidylinositol 3-Kinase/Akt-Dependent Cell Invasion. *Infect. Immun.* 83 (2), 769–779. doi: 10.1128/IAI.02345-14

Jean, S. S., Chang, Y. C., Lin, W. C., Lee, W. S., Hsueh, P. R., and Hsu, C. W. (2020). Epidemiology, Treatment, and Prevention of Nosocomial Bacterial Pneumonia. *J. Clin. Med.* 9 (1), 275. doi: 10.3390/jcm9010275

John, G., Yildirim, A. O., Rubin, B. K., Gruenert, D. C., and Henke, M. O. (2010). TLR-4-Mediated Innate Immunity Is Reduced in Cystic Fibrosis Airway Cells. *Am. J. Respir. Cell Mol. Biol.* 42 (4), 424–431. doi: 10.1165/rcmb.2008-0408OC

Kaper, J. B., Nataro, J. P., and Mobley, H. L. T. (2004). Pathogenic Escherichia Coli. *Nat. Rev. Microbiol.* 2 (2), 123–140. doi: 10.1038/nrmicro818

Knapp, S., von Aulock, S., Leendertse, M., Haslinger, I., Draing, C., Golenbock, D. T., et al. (2008). Lipoteichoic Acid-Induced Lung Inflammation Depends on TLR2 and the Concerted Action of TLR4 and the Platelet-Activating Factor Receptor. *J. Immunol.* 180 (5), 3478–3484. doi: 10.4049/jimmunol.180.5.3478

Kramer, J., Özkaya, Ö., and Kümmerli, R. (2020). Bacterial Siderophores in Community and Host Interactions. *Nat. Rev. Microbiol.* 18 (3), 152–163. doi: 10.1038/s41579-019-0284-4

Lee, O.-H., Jain, A. K., Papusha, V., and Jaiswal, A. K. (2007). An Auto-Regulatory Loop Between Stress Sensors INrf2 and Nrf2 Controls Their Cellular Abundance. *J. Biol. Chem.* 282 (50), 36412–36420. doi: 10.1074/jbc.M706517200

Lee, Y.-S., Kim, Y.-H., Jung, Y. S., Kim, K.-S., Kim, D.-K., Na, S.-Y., et al. (2017). Hepatocyte Toll-Like Receptor 4 Mediates Lipopolysaccharide-Induced Hepcidin Expression. *Exp. Mol. Med.* 49 (12), e408–e408. doi: 10.1038/emm.2017.207

Leone, L., Mazzetta, F., Martinelli, D., Valente, S., Alimandi, M., Raffa, S., et al. (2016). Klebsiella Pneumoniae Is Able to Trigger Epithelial-Mesenchymal Transition Process in Cultured Airway Epithelial Cells. *PLoS One* 11 (1), e0146365. doi: 10.1371/journal.pone.0146365

Ludwiczek, S., Aigner, E., Theurl, I., and Weiss, G. (2003). Cytokine-Mediated Regulation of Iron Transport in Human Monocytic Cells. *Blood* 101 (10), 4148–4154. doi: 10.1182/blood-2002-08-2459

Mizgerd, J. P. (2008). Acute Lower Respiratory Tract Infection. *N. Engl. J. Med.* 358 (7), 716–27. doi: 10.1056/NEJMra074111

Nairz, M., Schleicher, U., Schroll, A., Sonnweber, T., Theurl, I., Ludwiczek, S., et al. (2013). Nitric Oxide-Mediated Regulation of Ferroportin-1 Controls Macrophage Iron Homeostasis and Immune Function in Salmonella Infection. *J. Exp. Med.* 210 (5), 855–873. doi: 10.1084/jem.20121946

Nairz, M., Schroll, A., Sonnweber, T., and Weiss, G. (2010). The Struggle for Iron – a Metal at the Host–Pathogen Interface. *Cell. Microbiol.* 12 (12), 1691–1702. doi: 10.1111/j.1462-5822.2010.01529.x

Nairz, M., Theurl, I., Ludwiczek, S., Theurl, M., Mair, S. M., Fritsche, G., et al. (2007). The Co-Ordinated Regulation of Iron Homeostasis in Murine Macrophages Limits the Availability of Iron for Intracellular Salmonella Typhimurium. *Cell Microbiol.* 9 (9), 2126–2140. doi: 10.1111/j.1462-5822.2007.00942.x

Nairz, M., Theurl, I., Schroll, A., Theurl, M., Fritsche, G., Lindner, E., et al. (2009). Absence of Functional Hfe Protects Mice From Invasive Salmonella Enterica Serovar Typhimurium Infection *via* Induction of Lipocalin-2. *Blood* 114 (17), 3642–3651. doi: 10.1182/blood-2009-05-223354

Nairz, M., and Weiss, G. (2020). Iron in Infection and Immunity. *Mol. Aspects Med.* 75, 100864. doi: 10.1016/j.mam.2020.100864

Nardone, L. L., and Andrews, S. B. (1979). Cell Line A549 as a Model of the Type II Pneumocyte: Phospholipid Biosynthesis From Native and Organometallic Precursors. *Biochim. Biophys. Acta (BBA) - Lipids Lipid Metab.* 573 (2), 276–295. doi: 10.1016/0005-2760(79)90061-4

Nemeth, E., Tuttle, M. S., Powelson, J., Vaughn, M. B., Donovan, A., Ward, D. M., et al. (2004). Hepcidin Regulates Cellular Iron Efflux by Binding to Ferroportin and Inducing Its Internalization. *Science* 306 (5704), 2090–2093. doi: 10.1126/science.1104742

Nguyen, N.-B., Callaghan, K. D., Ghio, A. J., Haile, D. J., and Yang, F. (2006). Hepcidin Expression and Iron Transport in Alveolar Macrophages. *Am. J. Physiol.-Lung Cell. Mol. Physiol.* 291 (3), L417–L425. doi: 10.1152/ajplung.00484.2005

Núñez, G., Sakamoto, K., and Soares, M. P. (2018). Innate Nutritional Immunity. *J. Immunol.* 201 (1), 11. doi: 10.4049/jimmunol.1800325

Pan, X., Tamilselvam, B., Hansen, E. J., and Daefler, S. (2010). Modulation of Iron Homeostasis in Macrophages by Bacterial Intracellular Pathogens. *BMC Microbiol.* 10 (1), 64. doi: 10.1186/1471-2180-10-64

Parrow, N. L., Fleming, R. E., Minnick, M. F., and Maurelli, A. T. (2013). Sequestration and Scavenging of Iron in Infection. *Infect. Immun.* 81 (10), 3503–3514. doi: 10.1128/IAI.00602-13

Petzer, V., Tymoszuk, P., Asshoff, M., Carvalho, J., Papworth, J., Deantonio, C., et al. (2020). A Fully Human Anti-BMP6 Antibody Reduces the Need for Erythropoietin in Rodent Models of the Anemia of Chronic Disease. *Blood* 136 (9), 1080–1090. doi: 10.1182/blood.2019004653

Pitout, J. D., Nordmann, P., and Poirel, L. (2015). Carbapenemase-Producing Klebsiella Pneumoniae, a Key Pathogen Set for Global Nosocomial Dominance. *Antimicrob. Agents Chemother.* 59 (10), 5873–5884. doi: 10.1128/AAC.01019-15

Quinton, L. J., Walkey, A. J., and Mizgerd, J. P. (2018). Integrative Physiology of Pneumonia. *Physiol. Rev.* 98 (3), 1417–1464. doi: 10.1152/physrev.00032.2017

Roudkenar, M. H., Halabian, R., Bahmani, P., Roushandeh, A. M., Kuwahara, Y., and Fukumoto, M. (2011). Neutrophil Gelatinase-Associated Lipocalin: A New Antioxidant That Exerts Its Cytoprotective Effect Independent on Heme Oxygenase-1. *Free Radic. Res.* 45 (7), 810–819. doi: 10.3109/10715762.2011.581279

Ruaro, B., Salton, F., Braga, L., Wade, B., Confalonieri, P., Volpe, M. C., et al. (2021). The History and Mystery of Alveolar Epithelial Type II Cells: Focus on Their Physiologic and Pathologic Role in Lung. *Int. J. Mol. Sci.* 22 (5), 2566 doi: 10.3390/ijms22052566

Saiga, H., Nishimura, J., Kuwata, H., Okuyama, M., Matsumoto, S., Sato, S., et al. (2008). Lipocalin 2-Dependent Inhibition of Mycobacterial Growth in Alveolar Epithelium. *J. Immunol.* 181 (12), 8521–8527. doi: 10.4049/jimmunol.181.12.8521

Sanchez, K. K., Chen, G. Y., Schieber, A. M. P., Redford, S. E., Shokhirev, M. N., Leblanc, M., et al. (2018). Cooperative Metabolic Adaptations in the Host Can Favor Asymptomatic Infection and Select for Attenuated Virulence in an Enteric Pathogen. *Cell* 175 (1), 146–158.e115. doi: 10.1016/j.cell.2018.07.016

Schmidt, I. H. E., Gildhorn, C., Böning, M. A. L., Kulow, V. A., Steinmetz, I., and Bast, A. (2018). Burkholderia Pseudomallei Modulates Host Iron Homeostasis

to Facilitate Iron Availability and Intracellular Survival. *PloS Negl. Trop. Dis.* 12 (1), e0006096. doi: 10.1371/journal.pntd.0006096

Shin, D. M., Jeon, B. Y., Lee, H. M., Jin, H. S., Yuk, J. M., Song, C. H., et al. (2010). Mycobacterium Tuberculosis Eis Regulates Autophagy, Inflammation, and Cell Death Through Redox-Dependent Signaling. *PLoS Pathog.* 6 (12), e1001230. doi: 10.1371/journal.ppat.1001230

Soares, M. P., and Weiss, G. (2015). The Iron Age of Host–Microbe Interactions. *EMBO Rep.* 16 (11), 1482–1500. doi: 10.15252/embr.201540558

Spooner, R., and Yilmaz, O. (2011). The Role of Reactive-Oxygen-Species in Microbial Persistence and Inflammation. *Int. J. Mol. Sci.* 12 (1), 334–352. doi: 10.3390/ijms12010334

Theurl, I., Theurl, M., Seifert, M., Mair, S., Nairz, M., Rumpold, H., et al. (2008). Autocrine Formation of Hepcidin Induces Iron Retention in Human Monocytes. *Blood* 111 (4), 2392–2399. doi: 10.1182/blood-2007-05-090019

Torres, A., Cilloniz, C., Niederman, M. S., Menéndez, R., Chalmers, J. D., Wunderink, R. G., et al. (2021). Pneumonia. *Nat. Rev. Dis. Primers* 7 (1), 1–28. doi: 10.1038/s41572-021-00259-0

Torres, A., Niederman, M. S., Chastre, J., Ewig, S., Fernandez-Vandellos, P., Hanberger, H., et al. (2017). International ERS/ESICM/ESCMID/ALAT Guidelines for the Management of Hospital-Acquired Pneumonia and Ventilator-Associated Pneumonia: Guidelines for the Management of Hospital-Acquired Pneumonia (HAP)/ventilator-Associated Pneumonia (VAP) of the European Respiratory Society (ERS), European Society of Intensive Care Medicine (ESICM), European Society of Clinical Microbiology and Infectious Diseases (ESCMID) and Asociación Latinoamericana Del Tórax (ALAT). *Eur. Respir. J.* 50 (3), 1700582. doi: 10.1183/13993003.00582-2017

Torti, F. M., and Torti, S. V. (2002). Regulation of Ferritin Genes and Protein. *Blood* 99 (10), 3505–3516. doi: 10.1182/blood.V99.10.3505

Valente de Souza, L., Hoffmann, A., and Weiss, G. (2021). Impact of Bacterial Infections on Erythropoiesis. *Expert Rev. Anti-Infect. Ther.* 19 (5), 619–633. doi: 10.1080/14787210.2021.1841636

Warren, D. J. (2011). Preparation of Highly Efficient Electrocompetent Escherichia Coli Using Glycerol/Mannitol Density Step Centrifugation. *Anal. Biochem.* 413 (2), 206–207. doi: 10.1016/j.ab.2011.02.036

Warszawska, J. M., Gawish, R., Sharif, O., Sigel, S., Doninger, B., Lakovits, K., et al. (2013). Lipocalin 2 Deactivates Macrophages and Worsens Pneumococcal Pneumonia Outcomes. *J. Clin. Invest.* 123 (8), 3363–3372. doi: 10.1172/jci67911

Weiss, G., and Goodnough, L. T. (2005). Anemia of Chronic Disease. *N. Engl. J. Med.* 352 (10), 1011–1023. doi: 10.1056/NEJMra041809

Weitnauer, M., Mijošek, V., and Dalpke, A. H. (2016). Control of Local Immunity by Airway Epithelial Cells. *Mucosal Immunol.* 9 (2), 287–298. doi: 10.1038/mi.2015.126

Wrighting, D. M., and Andrews, N. C. (2006). Interleukin-6 Induces Hepcidin Expression Through STAT3. *Blood* 108 (9), 3204–3209. doi: 10.1182/blood-2006-06-027631

Wu, H., Santoni-Rugiu, E., Ralfkiaer, E., Porse, B. T., Moser, C., Høiby, N., et al. (2010). Lipocalin 2 Is Protective Against E. Coli Pneumonia. *Respir. Res.* 11 (1), 96. doi: 10.1186/1465-9921-11-96

Yang, F., Haile, D. J., Wang, X., Dailey, L. A., Stonehuerner, J. G., and Ghio, A. J. (2005). Apical Location of Ferroportin 1 in Airway Epithelia and Its Role in Iron Detoxification in the Lung. *Am. J. Physiol.-Lung Cell. Mol. Physiol.* 289 (1), L14–L23. doi: 10.1152/ajplung.00456.2004

Zhang, V., Nemeth, E., and Kim, A. (2019). Iron in Lung Pathology. *Pharm (Basel)* 12 (1), 30. doi: 10.3390/ph12010030

Conflict of Interest: The authors declare that the research was conducted in the absence of any commercial or financial relationships that could be construed as a potential conflict of interest.

Publisher's Note: All claims expressed in this article are solely those of the authors and do not necessarily represent those of their affiliated organizations, or those of the publisher, the editors and the reviewers. Any product that may be evaluated in this article, or claim that may be made by its manufacturer, is not guaranteed or endorsed by the publisher.

frontiers | Frontiers in Cellular and Infection Microbiology

ORIGINAL RESEARCH
published: 03 June 2022
doi: 10.3389/fcimb.2022.903070

Iron Deprivation Modulates the Exoproteome in *Paracoccidioides brasiliensis*

Aparecido Ferreira de Souza[1†], Laurine Lacerda Pigosso[1†], Lana O'Hara Souza Silva[1], Italo Dany Cavalcante Galo[1], Juliano Domiraci Paccez[1], Kleber Santiago Freitas e Silva[1], Milton Adriano Pelli de Oliveira[2], Maristela Pereira[1] and Célia Maria de Almeida Soares[1]*

[1] Laboratório de Biologia Molecular, Instituto de Ciências Biológicas, ICB II, Campus II, Universidade Federal de Goiás, Goiânia, Brazil, [2] Instituto de Patologia Tropical e Saúde Pública, Universidade Federal de Goiás, Goiânia, Brazil

Fungi of the *Paracoccidioides* genus are the etiological agents of the systemic mycosis paracoccidioidomycosis and, when in the host, they find a challenging environment that is scarce in nutrients and micronutrients, such as Fe, which is indispensable for the survival of the pathogen. Previous studies have shown that fungi of this genus, in response to Fe deprivation, are able to synthesize and capture siderophores (Fe^{3+} chelators), use Fe-containing host proteins as a source of the metal, and use a non-canonical reductive pathway for Fe^{3+} assimilation. Despite all of these findings, there are still gaps that need to be filled in the pathogen response to metal deprivation. To contribute to the knowledge related to this subject, we obtained the exoproteome of *Paracoccidioides brasiliensis* (*Pb*18) undergoing Fe deprivation and by nanoUPLC-MS^E. One hundred forty-one proteins were identified, and out of these, 64 proteins were predicted to be secreted. We also identified the regulation of several virulence factors. Among the results, we highlight Cyb5 as a secreted molecule of *Paracoccidioides* in the exoproteome obtained during Fe deprivation. Cyb5 is described as necessary for the Fe deprivation response of *Saccharomyces cerevisiae* and *Aspergillus fumigatus.* Experimental data and molecular modeling indicated that Cyb5 can bind to Fe ions *in vitro*, suggesting that it can be relevant in the arsenal of molecules related to iron homeostasis in *P. brasiliensis*.

Keywords: secretome, cytochrome b5 (CYB5), microbial adaptation, Fe, nutritional immunity

OPEN ACCESS

Edited by:
Charley Staats, Federal University of Rio Grande do Sul, Brazil

Reviewed by:
Ane Wichine Acosta Garcia, Federal University of Health Sciences of Porto Alegre, Brazil
Rosana Puccia, Federal University of São Paulo, Brazil

***Correspondence:**
Célia Maria de Almeida Soares
cmasoares@gmail.com

†These authors share first authorship

Specialty section:
This article was submitted to Bacteria and Host, a section of the journal Frontiers in Cellular and Infection Microbiology

Received: *23 March 2022*
Accepted: *06 May 2022*
Published: *03 June 2022*

Citation:
Souza AF, Pigosso LL, Silva LOS, Galo IDC, Paccez JD, e Silva KSF, de Oliveira MAP, Pereira M and Soares CMA (2022) Iron Deprivation Modulates the Exoproteome in Paracoccidioides brasiliensis. Front. Cell. Infect. Microbiol. 12:903070. doi: 10.3389/fcimb.2022.903070

INTRODUCTION

Sophisticated arsenals, elaborate tactics, and constant strategic changes: what could be the description of a war scenario also characterizes the host–pathogen interaction event (Asehnoune et al., 2016; Gonzalez and Hernandez, 2016). Among the myriad of aspects studied in the pathogen–host interaction, nutritional immunity occupies a prominent place because it consists of the innate ability of hosts to control the bioavailability of essential nutrients and micronutrients, affecting the survival of pathogens (Wang and Cheraryil, 2009; Soares and Weiss, 2015; Núñez et al., 2018).

Pathogen survivability relies on the competition between pathogen and host for micronutrients such as iron (Fe), triggered by nutritional immunity. Biologically, the micronutrient Fe is predominantly found as ferrous (Fe^{2+}) and ferric ions (Fe^{3+}). The flexibility between these

oxidation states allows the metal to be used in several vital cellular processes such as energy metabolism, gene expression, and protein stability (Nairz et al., 2010; Dlouhy and Outten, 2013). However, it should be noted that the same flexibility of Fe oxidation states also gives a toxic potential; therefore, strict control of metal metabolism is indispensable. To this end, both pathogens and hosts employ mechanisms to maintain adequate amounts of Fe to meet their metabolic demands and counteract their toxicity, which characterizes Fe homeostasis (Tandara and Salamunic, 2012).

An increasing number of works in the literature have gradually contributed to the understanding of mechanisms that pathogenic bacteria and fungi employ for the uptake of Fe in the host (Schaible and Kaufmann, 2004; Wang and Cheraryil, 2009; Caza and Kronstad, 2013; Choi et al., 2015). Regarding pathogenic fungi, the mechanisms they use to obtain iron in the context of infection can be summarized in the following: 1) absorption of siderophores or heme/hemoglobin mediated by receptors, which characterizes non-reductive assimilation pathways of Fe, in addition to 2) a reductive Fe assimilation pathway allowed by enzymatic complexes that promote oxidation of the metal and its uptake (Bailão et al., 2012; Caza and Kronstad, 2013; Bairwa et al., 2017; Roy and Kornitzer, 2019). Some fungi employ more specific strategies, such as *Histoplasma capsulatum*, which secretes gamma-glutamyl transpeptidase (GGT) that acts in capturing Fe by generating a dipeptide with a high reducing power by cleaving glutathione (Zarnowski and Woods, 2005; Zarnowski et al., 2008). It is also known that cytochrome b5 (Cyb5) regulates the Fe metabolism of some fungi, such as *Saccharomyces cerevisiae* (Dap1) and *Aspergillus fumigatus*, in a process linked to ergosterol biosynthesis (Craven et al., 2007; Misslinger et al., 2017).

Fungi of the *Paracoccidioides* genus are the etiologic agents of paracoccidioidomycosis (PCM), an endemic systemic mycosis in Latin America whose accurate diagnosis and short-term therapeutic approach are still challenges (Shikanai-Yasuda et al., 2017). Previous studies have shown that the response of *Paracoccidioides* to Fe depletion is an important virulence attribute for the pathogen (Silva et al., 2020). Once under metal depletion, *Paracoccidioides* spp. undergoes intense adaptation of its metabolism (Parente et al., 2011). The mechanisms that the fungus uses to obtain Fe when in the host have been targets of study. *Paracoccidioides* spp. is able to synthesize and use siderophores, capturing them *via* receptors. Those fungi present orthologous genes encoding the enzymes necessary for the biosynthesis of hydroxamates, and plasma membrane proteins related to the transport of these molecules, all induced in iron deprivation (Silva-Bailão et al., 2014). *Paracoccidioides* spp. is able to use siderophores as an iron source, increasing the fungus ability to survive inside macrophages, an iron-poor environment (Silva-Bailão et al., 2014). The addition of the xenosiderophore ferrioxamine B (FOB) to *Paracoccidioides brasiliensis* culture medium results in repression of the SidA products, the first enzyme of the siderophore biosynthesis pathway (Silva et al., 2020), suggesting that *P. brasiliensis* blocks siderophore biosynthesis and can explore those molecules in the environment to scavenge iron. Silenced mutants of the *sidA* gene were obtained by antisense RNA technology, which displayed decreased siderophore biosynthesis in iron deprivation and reduced virulence to an invertebrate model. Studies have also indicated that the fungus could use both a non-classical reductive iron assimilation (RIA), comprising ferric reductases and Fe/Zn permeases, under iron-limited conditions (Bailão et al., 2015). We have demonstrated that *Paracoccidioides* spp. is able to reduce iron, and the reductase activity is linked to ferric iron uptake in *P. brasiliensis*. After reduction, the data suggest that Fe^{2+} is probably internalized through an Fe/Zn permease (Zrt). This suggestion is because *Paracoccidioides* spp. genomes do not present a ferric reductase *ftr1* homolog and the *zrt1* and *zrt2* transcripts are upregulated during iron deprivation. Of particular relevance is the fungus ability to use hemoglobin as the preferential host iron source for *Paracoccidioides* spp. To acquire hemoglobin, the fungus presents hemolytic activity and the ability to internalize the entire molecule instead of promoting the iron release extracellularly. A Glycosylphosphatidylinositol (GPL)-anchored hemoglobin receptor, Rbt5, has been described as a virulence factor (Bailão et al., 2014).

Despite the robust contribution of those studies performed by our group, there is still a need to expand the knowledge about how fungi of this genus respond to Fe depletion. Some studies that addressed *Paracoccidioides* exoproteome are available in scientific literature; however, the changes that Fe depletion induces in the exoproteome of these fungi have not been investigated yet (Vallejo et al., 2012; Weber et al., 2012; Chaves et al., 2015; Rodrigues et al., 2018). The present work addresses the changes triggered by Fe deprivation in the exoproteome of *P. brasiliensis* and lists and explores new proteins involved in that context.

MATERIALS AND METHODS

Ethics Statement

Animal experiments were approved by the Ethics Committee on the use of Animal Experimentation (Federal University of Goiás, CEUA-UFG) under protocol number 018/20 following the guidelines of the Brazilian National Council for Control of Animal Experimentation.

Strain Used and Culture Media

The *P. brasiliensis Pb*18 isolate (ATCC 32069–*Pb*18) was used in the present study. The yeast form of the fungus was maintained by cultivating it in semisolid Fava Netto medium supplemented with glucose 4% (w/v) at a temperature of 36°C (Fava Netto, 1961). To obtain *P. brasiliensis* exoproteomes under Fe depletion, cells cultured for 3 days in semisolid Fava Netto medium were inoculated in 250 ml of liquid Fava Netto medium supplemented with 4% glucose (w/v) and maintained for 72 h under constant agitation (120 rpm) at a temperature of 36°C. Then, fungal cells were washed 2 times (800 g, 5 min, 4°C) with PBS. Cell viability was verified by the trypan blue method,

and 10^6 viable cells/ml were transferred to 250 ml of chemically defined Chemically defined minimal medium modified, without Fe (Restrepo and Jiménez, 1980). The cells were kept for 48 h under constant agitation (120 rpm) at a temperature of 36°C. For the condition of Fe depletion (treatment), 50 μM of the Fe chelator bathophenanthrolinedisulfonic acid (BPS; Sigma-Aldrich, St. Louis, MO, USA) was added, since in a previously published work, cultivation in minimal medium (MMcM) of *P. brasiliensis* exposed to this chelator molarity for 48 h did not affect fungus viability (Parente et al., 2011). For the control condition, 10 μM of Fe $(NH_4)_2(SO_4)_2$ was added to the medium. All media and solutions were prepared with ultrapure water for Fe depletion experiments. All glassware used for the preparation of media and solutions was previously treated with 5N HCl for 1 h and washed extensively with ultrapure water afterward, as a strategy to minimize contamination by metals, including Fe.

Obtaining the Exoproteome of *P. brasiliensis*

To obtain *P. brasiliensis* exoproteome under Fe depletion, the strategy described by Weber et al. (2012) was followed with some modifications. The culture supernatants were collected (800 g, 15 min, 4°C), and to minimize the contamination by possible fungal cells in suspension, the supernatants were filtered through membranes of 0.22-μm pores. Subsequently, the filtered supernatants were concentrated 250 times through 10-kDa exclusion-level membranes (Amicon Ultra centrifugal filter, Millipore, Bedford, MA, USA) and washed 3 times with 50 mM NH_4HCO_3 buffer, pH 8.5. The entire process of concentration and handling of the samples was carried out at low temperatures (≤4°C) to minimize the activity of proteases. The samples obtained were stored at -20°C until they were used. To verify the possibility of cell lysis, we performed diagnostic PCR for the detection of genomic DNA in culture supernatants, as described by Weber et al. (2012).

Sample Preparation for NanoUPLC-MS^E

Exoproteomes obtained were quantified using the Bradford method (Bradford, 1976). Afterward, 150 μg of proteins from each biological replica (three of each condition) were individually prepared to be subjected to high-resolution liquid chromatography, on a nanoscale, coupled to mass spectrometry with independent data acquisition (nanoUPLC-MS^E), as previously described (Murad et al., 2011). Initially, 10 μl of 50 mM NH_4HCO_3, pH 8.5, was added to the samples. Then, as a surfactant, 75 μl of a 0.2% (w/v) RapiGEST^{TM} solution (Waters, USA) was added, and the mixture was incubated at 80°C for 15 min. After this incubation period, 2.5 μl of 100 mM Dithiothreitol (DTT), a disulfide bridge-reducing agent, was added and a new incubation, at 60°C, for 30 min was performed. At the end of the incubation period, when the samples reached room temperature, we added 2.5 μl of 300 mM iodoacetamide, an alkylating agent, and the mixture remained at rest for 30 min at room temperature, protected from light. Then, the samples were submitted to tryptic digestion. For that, 30 μl of a 0.05-μg/μl trypsin solution (Promega, USA) was added and incubation at 37°C for 16 h was performed. Subsequently, for precipitation of the surfactant, 30 μl of 5% trifluoroacetic acid (v/v) was added and incubation at 37°C was carried out for another 90 min. Then, the samples were centrifuged at 13,000 g for 30 min, at 4°C, and the supernatants were transferred to new tubes. The centrifugation process was repeated until there was no more formation of precipitate. The samples were concentrated in a vacuum. The peptides obtained from each sample were resuspended in 80 μl of a solution containing 20 mM ammonium formiate at pH 10 and 200 fmol of Rabbit Phosphorylase B (PHB; Waters Corporation, Manchester, UK) (MassPREPTM protein). PHB was used as an internal standard for the quantification of the obtained peptides.

High-Performance Liquid Chromatography at Nanoscale Coupled to Mass Spectrometry

The samples that underwent the tryptic digestion treatment described in the previous session were subjected to high-resolution liquid chromatography, on nanoscale, using the ACQUITY UPLC® M-Class system (Waters Corporation, USA). Peptide fractionation was performed in a reverse-phase pre-column XBridge® Peptide 5 μm BEH130 C18 300 μm × 50 mm (Waters, USA), a system that was maintained in a flow of 0.5 μl/min with an initial condition of acetonitrile (ACN) of 3% (v/v), representing the first dimension. The peptides were subjected to 5 fractionations (F1-F5) through different linear gradients of ACN concentrations (F1, 11.4%; F2, 14.7%; F3, 17.4%; F4-20, 7%; and F5, 50%). To perform the second dimension, each fraction was eluted in a Trap trapping column, 2D Symmetry® 5 μm BEH100 C18, 180 μm × 20 mm (Waters, USA) and passed through an analytical column separation Peptide CSH^{TM} BEH130 C18 1.7 μm, 100 μm × 100 mm (Waters, USA), in a flow of 0.4 μl/min at 40°C. The human [Glu1]-Fibronopeptide B protein (GFP; Sigma-Aldrich, USA) was used for mass calibration, which was measured every 30 s and in a constant flow of 0.5 μl/min. GFP was used at a concentration of 200 fmol. The peptides were identified and quantified by a Synapt G1 MSTM mass spectrometer (Waters, USA) equipped with a NanoElectronSpray source and two mass analyzers [a first quadrupole and the second flight time (TOF) operating in V mode], operating in MSE mode, which switches between low energy (6V) and high energy (40V) in each acquisition mode every 0.4 s. Adding the biological replicates, each condition went through 8 experimental replicates.

Spectra Processing and Proteomic Analysis

After nanoUPLC-MSE, data processing was performed using ProteinLynx Global Server version 3.0.2 (PLGS) software (Waters, Manchester, UK), which allowed the determination of the exact mass retention time (EMRT) of the peptides and their molecular weight through the mass/charge ratio (m/z). For the identification of peptides, the spectra obtained (together with reverse sequences) were compared with sequences from the database of *P. brasiliensis* (https://www.uniprot.org/uniprot/?

query=paracoccidioides+brasiliensis+strain+pb18&sort=score). Protein identification criteria included the following: (i) detection of at least two ions per fragment of peptides, (ii) five by protein fragments, (iii) determination of at least one peptide per protein, (iv) detection rate of false positive at most 4%, (v) cysteine carbamidomethylation, (vi) methionine oxidation, (vii) serine, threonine and tyrosine phosphorylation, (viii) and a trypsin lost cleavage site was allowed. Microsoft Office Excel (Microsoft®, USA) was used for the management of tables and the generation of graphs. In the subsequent analyses, proteins present in at least two of the three experimental replicates of each biological replicate were included. Proteins present in at least two of the three biological replicates were subjected to differential expression analysis. For this purpose, initially, the proteins that presented the lowest variance coefficient and that were detected in all replicates were used for intensity normalization. Afterward, the Expression Algorithm (Expression^E), which is part of the PLGS software (Geromanos et al., 2009), was used for the analysis of differential expression. Proteins were considered regulated with differences (fold change) ± 2.0 between the quantification in the extract obtained in the depletion of Fe × presence of Fe. Homology search for hypothetical proteins were obtained through the online tool BLASTp (Basic Local Alignment Search Tool–https://blast.ncbi.nlm.nih.gov/Blast.cgi?PAGE=Proteins). Information on molecular function, biological processes, and subcellular location of the identified proteins was obtained from the *Paracoccidioides* database (available at http://paracoccidioides.com/). The protein sequences were subjected to additional *in silico* analysis to check for the presence of signal peptide using the online tool SignalP 4.1 Server (available at http://www.cbs.dtu.dk/services/SignalP-4.1/). For the prediction of proteins secreted by non-classical pathways, the online tool SecretomeP 2.0 (available at http://www.cbs.dtu.dk/services/SecretomeP/) was used.

RNA Extraction and Quantitative Real-Time PCR (RT-qPCR)

After incubation for 6 and 24 h in MMcM supplemented with 50 μM of BPS or 10 μM of $Fe(NH_4)_2(SO_4)_2$, the yeast cells were collected and total RNA extraction was accomplished using TRIzol (TRI Reagent, Sigma-Aldrich, St. Louis, MO, USA) and mechanical cell rupture (Mini-Beadbeater–Biospec Products Inc., Bartlesville, OK, USA). SuperScript III First-Strand Synthesis SuperMix (Invitrogen, Life Technologies) was used to obtain the cDNAs that were submitted to RT-qPCR in the QuantStudio™ 5 real-time PCR System (Applied Biosystems Inc.) using SYBR Green PCR Master Mix (Applied Biosystems, Foster City, CA). The reaction was performed in triplicate for each cDNA. Normalization used the gene encoding the *L34* protein (PADG_04085). The standard curve method for relative quantification was used for calculating the relative expression levels of transcripts of interest. Standard curve was obtained using an aliquot from each cDNA sample. Statistical analysis was based on the Student's t-test, and p values ≤0.05 were considered statistically significant. Primers used in RT-qPCR are shown in **Table S1**.

Recombinant Cyb5 Expression in *Escherichia coli*, Protein Purification, and Polyclonal Antibodies

Total RNA was extracted from fungal yeast cells using the TRIzol reagent (TRI Reagent®, Sigma-Aldrich, St. Louis, MO, USA) and mechanical cell rupture (MiniBeadbeater—BioSpec Products), as described by the manufacturer's protocol. From the extracted RNA, cDNA was synthetized following the manufacturer recommendation of the SuperScript® Reverse Transcriptase Kit (Invitrogen™, Waltham, MA, USA). The cDNA was used to amplify the *cyb5* gene (PADG_03559) using the polymerase High Fidelity (Invitrogen™, Waltham, MA, USA). The cDNA product obtained by RT-PCR was cloned into the expression vector pET-32a. Bacterial cells, strain *Escherichia coli* C43, harboring the recombinant plasmid were grown in Luria–Bertani (LB) medium supplemented with 100 μg/ml ampicillin (w/v) under agitation at 37°C until the optical density (OD) reached an absorbance of 0.6 at a wavelength of 600 nm. The reagent isopropyl-β-D-thiogalactopyranoside (IPTG) was added to the growing culture to a final concentration of 0.1 mM. Bacterial cells were harvested by centrifugation at 10,000 × g for 10 min after 16 h of incubation at 15°C and resuspended in phosphate buffered saline (PBS) 1×. The recombinant Cyb5 protein fused to Trx-His-Tag was used to produce polyclonal antibodies in 4 BALB/c male mice aged 6–8 weeks. The fusion protein was removed from Sodium Dodecyl Sulfate Polyacrylamide Gel Electrophoresis gels and injected into mice along with Freund's adjuvant three times at intervals of 15 days. Serum containing polyclonal antibodies was collected and stored at −20°C. The protein was produced in inclusion bodies and was solubilized using 50 μl of a 20% (w/v) N-lauroylsarcosine sodium salt (Sigma Aldrich, Missouri, KS, USA) solution for 5 ml of bacterial extracts and sonicated (5 times, 10 min). SDS-PAGE analysis showed the protein in the soluble fraction, and then the protein was purified by a nickel resin chromatography system (Qiagen Inc., Germantown, MD, USA).

Western Blotting

Proteins in SDS-PAGE were transferred to the nitrocellulose membrane that was then incubated with polyclonal anti-*Pb*18Cyb5 at 1:250 dilution for 2 h at room temperature. After washing, the membranes were incubated with peroxidase-coupled mouse anti-IgG secondary antibody (1:1,000 dilution). The reaction was revealed by chemiluminescence with the ECL Western Blotting Analysis System (GE Healthcare). Negative control was obtained with pre-immune mouse serum (1:250 dilution). Reaction was developed in a chemiluminescent imager (Amersham Imager 600, GE Healthcare).

Dot-Blot Analysis

Nitrocellulose membrane containing 30 μg of $FeSO_4$ and BPS exoproteome extracts was incubated with anti-*Pb*18Cyb5 polyclonal antibodies (diluted 1:500) or pre-immune sera (diluted 1:1,000). Antibody anti-mouse IgG coupled to peroxidase (diluted 1:1,000) from ECL Western Blotting Analysis System (GE Healthcare) was used as secondary

antibody. Reaction was developed in a chemiluminescent imager (Amersham Imager 600, GE Healthcare).

Immunofluorescence Assays

For immunofluorescence, 10^6 yeast cells/ml were fixed in ice-cold pure methanol for 3 h at 20°C. Subsequently, cells were incubated for 30 min at room temperature in the dark in blocking buffer containing 3% (w/v) bovine serum albumin (BSA-Sigma) and 0.2% (v/v) Tween 20 in PBS, followed by incubation with the primary anti-*Pb*18Cyb5 polyclonal antibodies at 1:250 dilution, for 1 h. Subsequently, it was added with fluorescein isothiocyanate-labeled mouse secondary antibody-FITC (Sigma) at 1:750 dilution for 1 h. Cells were washed three times with PBS. Images were taken in bright field and at 450–490 nm for visualization of FITC fluorophore using the Axio Scope A1 fluorescence microscope. Digital images were acquired using AxionVision software (Carl Zeiss AG, Germany).

3D Structure Prediction *via* Molecular Modeling

The three-dimensional structure of Cyb5 heme-binding protein was predicted by the I-TASSER (Iterative Threading Assembly Refinement) server (Zhang, 2008; Yang et al., 2015). The structural modeling relies on templates of homologous proteins available on the PDB (protein data bank) database (Berman, 2000). The I-TASSER server uses Monte Carlo simulations to cluster homologous fragments together (Swendsen and Wang, 1986). The determination of the best protein conformation starts *via* prediction of the target secondary structure by PSSpred (Protein Secondary Structure Prediction) and the identification of similar templates by LOMETS (Local Meta-Threading-Server) (Wu and Zhang, 2007). The distribution of templates into clusters allows the classification of such sequences according to topology and stability through SPICKER (Zhang and Skolnick, 2004) in order to predict structures that are more likely to be similar to the native condition of the protein target. Eventually, the best ranked structures are submitted to molecular dynamics, and the biological function is predicted by COACH (Yang et al., 2013). The quality of the final structure was assessed through MolProbity (Williams et al., 2018).

Prediction of Iron-Binding Sites in Cytochrome b5

The prediction of the iron-binding sites in the Cyb5 structure was performed by the fragment transformation method (FTM). This approach compares the structure of the target with experimentally determined metal iron-binding proteins available in the PDB. The server MIB (metal ion binding) compares iron-binding site templates and takes into consideration residues within at least 3.5 Å from the iron center. FTM (Lu et al., 2006) performs structural alignments of fragments from the target protein and the iron-binding template. A score is attributed to the amino acids in the target protein based on similarity and according to a BLOSUM substitution matrix (Henikoff and Henikoff, 1992) and the root mean square deviation (RMSD) of the alignments. Amino acids with a score higher than the cutoff value (1.0 and 95% accuracy) are prone to bind to iron.

Spectrophotometric Analysis of the Interaction Between Recombinant Cytochrome b5 and Inorganic Iron

The binding capacity of Cyb5 to iron was investigated experimentally. Spectrophotometric analyses were performed as described (Oliveira et al., 2020). Briefly, the purified Cyb5 protein treated or not previously with reducing solution (sodium hydrosulfite at 100 μM, 1 h at room temperature; Sigma-Aldrich, USA, Ref. No. 71699) was subjected to incubation in ferrous sulfate at 100 μM (Sigma-Aldrich) for 1 h at room temperature. Then, samples and controls were deposited in a 96-well plate and subjected to absorbance analysis on a SpectraMax® Paradigm® Multi-Mode Detection Platform (Molecular Devices, Austria). The scan was performed between the wavelengths of 230–700 nm.

RESULTS

Exoproteome Analysis of *P. brasiliensis* Submitted to Fe Deprivation

To verify the possible changes that Fe deprivation can promote in *P. brasiliensis* exoproteome, the fungus was grown in depletion or presence of the metal. Culture supernatants containing the proteins secreted by the fungus were collected and, after tryptic digestion, subjected to nanoUPLC-MS^E. As an indirect way of verifying the presence of cytoplasmic contaminants (cell lysis), we checked by diagnostic PCR the presence of genomic DNA in the culture supernatants (Weber et al., 2012). According to **Supplementary Figure S1**, there was no amplification of genomic DNA from samples of culture supernatants. Thus, we carried out the analysis. In agreement with **Figure 1** and **Supplementary Table S2**, a total of 141 proteins were identified, of which, considering the fold change of 2.0, 93 (66%) were positively regulated (**Supplementary Table S3**). Prediction was made for protein secretion by a classical pathway (signal peptide dependent), secretion by non-classical pathways, or evidence of secretion in the *Paracoccidioides* literature (Vallejo et al., 2012; Weber et al., 2012; Chaves et al., 2015; Rodrigues et al., 2018; Moreira et al., 2020). As shown in **Figure 1**, 64 proteins (45.4%) were predicted to be secreted. Information on molecular function, classic biological processes, and classic subcellular location of the identified proteins is available in **Supplementary Tables S2, S3**.

Among the positively regulated proteins, a virulence factor of *P. brasiliensis* previously described was identified as serine proteinase (PADG_07422), in addition to adhesins such as enolase (PADG_04059), dihydrolipoil dehydrogenase (PADG_06494), and translation elongation factor Tu (PADG_01949) (Borges et al., 2005; Donofrio et al., 2009; Nogueira et al., 2010; Parente et al., 2010; Marcos et al., 2012; Marcos et al., 2016; Landgraf et al., 2017; Pigosso et al., 2017). Regarding the fungus response to Fe depletion, a gamma-

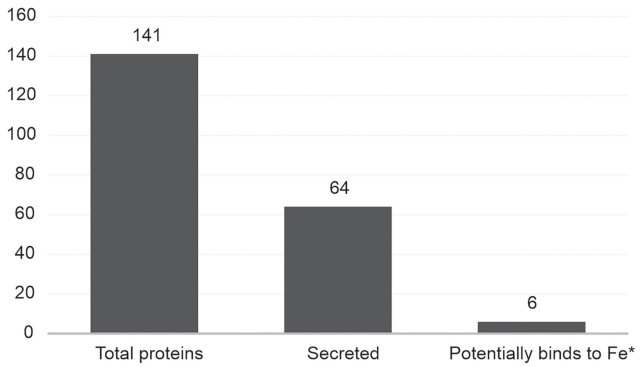

*

Accession	Description
PADG_03569	Cytochrome b5
PADG_03852	LiPid Depleted family member
PADG_05321	Mitochondrial nuclease
PADG_08270	UBX domain-containing protein
PADG_08391	Plama membrane ATPase
PAGD_08466	Homogentisate 1,2-dioxygenase

FIGURE 1 | Summary of proteomic findings. *P. brasiliensis* yeast cells were subjected to Fe deprivation for 48 h, and fungal secreted proteins were identified by nanoUPCL-MS^E. A total of 141 proteins were identified. To increase the analysis stringency, the identified proteins were submitted to analysis of secretion prediction by online tools and data available in the literature, which resulted in the number of 64 proteins. Of those 64 proteins, 6 have potential ability to bind to iron.

glutamyl transpeptidase was identified (PADG_01479) 2.4 times more expressed. There were proteins identified only in the condition of depletion of Fe: homogentisate 1,2-dioxigenase (PADG_08466), plasma membrane ATPase (PADG_08391), UBX domain-containing protein (PADG_08270), mitochondrial nuclease (PADG_05321), LiPid-depleted family member (PADG_03852), previously predicted as Fe ligands (Tristão et al., 2015), and surprisingly, Cyb5 (PADG_03559), positively regulated 20.4 times.

Iron Deprivation Promotes Upregulation of Transcripts of *Paracoccidioides Cyb5* and *Ggt2* Genes

In order to validate the results obtained in proteomics, we performed the analysis of *cyb5* (PADG_03559) and *ggt2* (PADG_01479) gene transcripts, since the resulting proteins were identified as upregulated in the imposed Fe deprivation condition. For that, we used RT-qPCR, and, according to **Figure 2**, it is possible to verify that positive regulation of the products of these genes occurs. These data corroborate the proteomic findings. Additionally, it is possible to notice that there is higher gene expression at the 6-h point, which can be associated with the flow of gene information and the consequent accumulation of Cyb5 and Ggt2 proteins at the 48-h time point used for proteomics.

Cytochrome b5 Is Secreted in Response to Iron Deprivation

The fact that the Cyb5 protein was upregulated more than 20 times in the *P. brasiliensis* exoproteome led us to further investigate the secretion dynamics of this protein. Therefore, recombinant Cyb5 was produced (**Supplementary Figure S2A**)

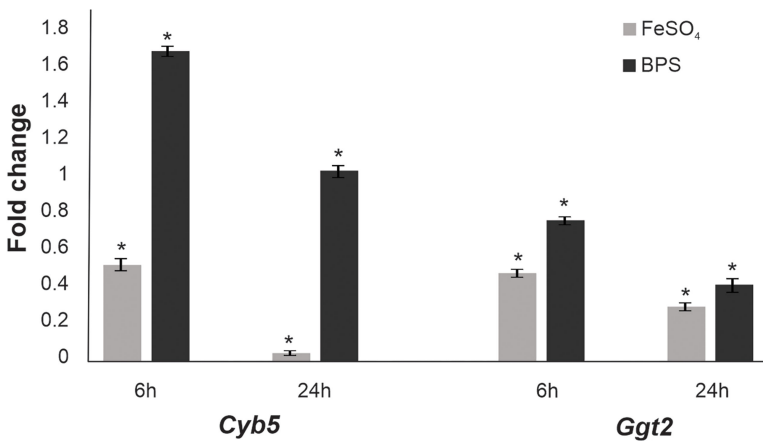

FIGURE 2 | Expression quantification of selected genes in *Paracoccidioides brasiliensis* by RT-qPCR. Quantitative RT-PCR data showing the transcript levels of cytochrome b5 (*Cyb5*) and gamma-glutamyl transpeptidase (*Ggt2*) in the presence and absence of iron at 6 and 24 h. The data were normalized using the gene encoding the 60S ribosomal protein L34 as the endogenous control and are presented as relative expression to the control. Data are expressed as the mean ± standard deviation of the triplicates of independent experiments. Student's t-test was used for statistical comparisons. Error bars represent the standard deviation of three biological replicates, and * represents $p \leq 0.05$.

and injected into mice to obtain polyclonal serum that specifically recognized the recombinant protein (**Supplementary Figure S2B**). Then, we verified whether the polyclonal serum obtained was able to recognize the Cyb5 protein in *P. brasiliensis* exoproteome. Therefore, we performed dot-blot analysis and verified that Cyb5 is recognized in the exoproteome of *P. brasiliensis*, with higher amount in the exoproteome obtained from iron deprivation condition, corroborating the proteomic findings (**Figure 3A**). Afterward, by indirect immunofluorescence assays, it was possible to verify that in non-permeabilized cells of *P. brasiliensis*, Cyb5 was present on the surface and presented a higher fluorescence in cells exposed to Fe deprivation, as shown in **Figure 3B**. All these findings confirm proteomics results and place Cyb5 as a molecule potentially involved in the response of *P. brasiliensis* to Fe deprivation.

*Pb*Cyb5 Is an Fe-Binding Protein

The fact that Cyb5 is a relatively small heme-containing protein and the high regulation shown in cells submitted to Fe deprivation placed this protein as a possible mediator of the fungal response to Fe deprivation. We then investigated the ability of recombinant Cyb5 to bind Fe by spectroscopic analysis; the results identified the possible event at least *in vitro* (**Figure 4A**). To refine our findings, we performed molecular modeling analyses of the Cyb5 and iron interaction. The protein from the PDB that has the closest structural similarity to Cyb5 from *P. brasiliensis* with the highest TM score (0.712) was the human Cyb5 under the PDB accession number 2I96. We identified two potential iron-binding sites in the Cyb5 protein with scores higher than 1.0 (**Figure 4B**). The amino acid residue His15 scored 1.773 and Glu56 scored 1.225. The two-colored regions in **Figure 4** represent the structural alignment performed between the target protein Cyb5 and the iron-binding site templates. The interaction distance between His residue and iron is 2.1 Å (**Figure 4C**) and between Glu is 3.4 Å (**Figure 4D**). The higher score achieved for the His residue is related to a smaller distance between this amino acid and the iron ion. It is important to highlight that the interaction sites of Cyb5 with Fe occur in regions different from where the heme group binds, which suggests that the interaction of Cyb5 with Fe does not depend on the heme group. In addition, other residues bind to iron with a lower score but above the threshold, showing that several residues contribute to the free energy of binding to the metal ion. Glutamic acid 11 (Glu11) and aspartic acid 20 (Asp20) bind to iron in the distance of 3.1 and 3.6 Å, respectively (**Figure 4C**), and isoleucine 115 (Ile115) binds to iron in the distance of 3.6 Å (**Figure 4D**).

DISCUSSION

Previous studies have demonstrated the importance of the response of *Paracoccidioides* spp. to depletion of Fe for the

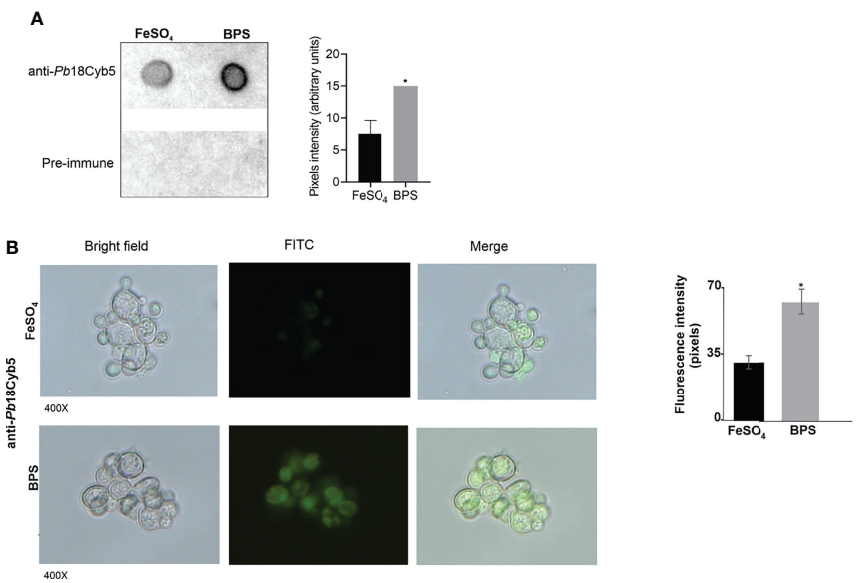

FIGURE 3 | Analyzing the expression dynamics of *Paracoccidioides* Cyb5 in iron deprivation. **(A)** Dot-blot analysis. Nitrocellulose membranes containing exoproteomes ($FeSO_4$ and BPS) were incubated with anti-*Pb*18Cyb5 (1:500) polyclonal antibodies or pre-immune sera (1:1,000). Pixel intensity was measured by densitometric analysis of immunoblotting dots using ImageJ software. Statistics analysis was performed through Student's t-test. * Represents $p \leq 0.05$.**(B)** Fluorescence microscopy of *P. brasiliensis* (*Pb*18) cells cultured in the presence or absence of iron for 24 h and subsequently incubated with primary antibody anti-Cyb5 and later with the secondary antibody anti-mouse IgG labeled with fluorescein isothiocyanate (FITC; Sigma). The data for fluorescence intensity evaluation were obtained through the AxioVision Software (Carl Zeiss). The values of fluorescence intensity (in pixels) and the standard error of each analysis were used to plot the graph. Data are expressed as mean ± standard error (represented using error bars); * represents $p \leq 0.05$. One hundred cells of each condition were evaluated. All representative images in panel **B** were magnified ×400.

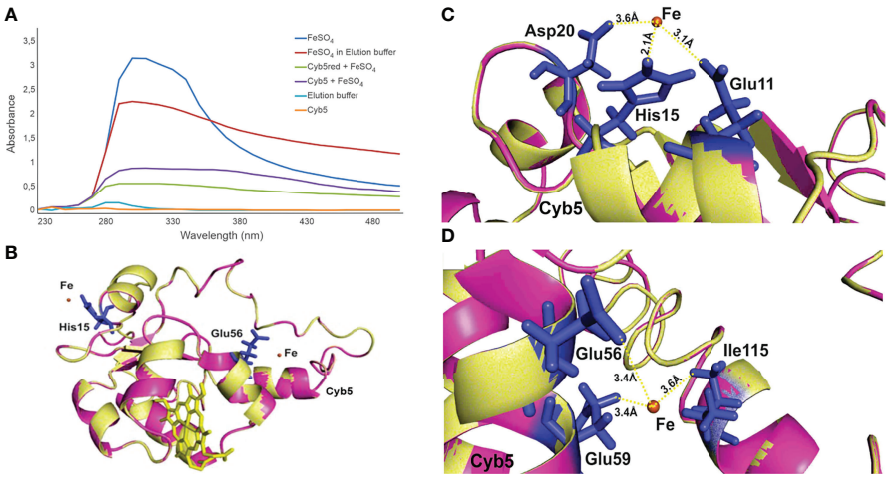

FIGURE 4 | Cyb5 of *Paracoccidioides brasiliensis* is an Fe-binding protein. **(A)** Absorbance spectra of the purified recombinant Cyb5 protein in a lower oxidation state (green—sample previously treated with a reducing agent) and higher oxidation (purple). Controls: ferrous sulfate solution (dark blue), ferrous sulfate prepared in elution buffer (red), elution buffer (light blue), and purified recombinant Cb5 (orange). **(B)** The structural alignment of Cyb5 with iron-binding motifs resulted in two sites of iron binding for this protein with significant scores. Residues interacting with the iron ion are shown as sticks and labeled as His for histidine and Glu for glutamate. These are the amino acid residues less distant from the iron centers. Iron is shown as a brown sphere. **(C)** The structural alignment showed that His15 binds to iron in the distance of 2.1 Å, reaching a score above the threshold. The same residue may interact with iron more than once. Glutamic acid 11 (Glu11) and aspartic acid 20 (Asp20) bind to iron in the distance of 3.1 and 3.6 Å, respectively. **(D)** The structural alignment showed that the residues Glu56 and Glu59 bind to iron within the distance of 3.4 **(A)** Isoleucine 115 (Ile115) binds to iron with a lower score but still above the threshold. Bonds to the iron are shown as dotted yellow lines, with bond distances indicated next to the lines.

pathogenicity of fungi of this genus, since their exposure to conditions that mimic those found in the host induces the expression of genes related to high-affinity and -specificity mechanisms for Fe uptake (Bailão et al., 2006; Bailão et al., 2007; Parente et al., 2011; Bailão et al., 2014; Kuznets et al., 2014; Bailão et al., 2015). Large-scale proteomic analyses have contributed positively in recent years to the understanding of the biology of *Paracoccidioides* spp. Studies with a similar approach enlisted virulence factors and metabolic profiles in response to several stressful conditions, including Fe depletion (Parente et al., 2011). Despite the biological relevance of the fungal secretory response to stressful conditions, as far as we know, there are no published studies that have evaluated the effect of Fe depletion on the exoproteome of pathogenic fungi. The only work available in the literature with a similar approach is that of Sorgo et al. (2013), who performed an analysis of the cell wall proteome of *Candida albicans* after exposure of the fungus to Fe depletion, whose results pointed to the positive regulation of proteins related to high-affinity mechanisms for capturing the metal, such as Als3, Rbt5, and Pga7 (Sorgo et al., 2013). The scarcity of studies using this approach points to the relevance of the present study, which can be extended beyond the genus *Paracoccidioides*.

Of the 64 proteins identified in the present work, 36 were also identified in the work performed by Vallejo et al. (2012), who studied the protein content of extracellular vesicles of *Paracoccidioides*, structures whose biology and impact on host–pathogen interaction have been elucidated in recent years (Vallejo et al., 2012; da Silva et al., 2016; Peres da Silva et al., 2019; Baltazar et al., 2021). Finding proteins from these structures in our work confirms that our sample enrichment strategy was effective. It was observed that Fe depletion promoted the positive regulation of virulence factors already described for *Paracoccidioides* spp. (Gonzalez and Hernandez, 2016). Among the virulence factors identified, it is worth mentioning serine proteinase (PADG_07422), a virulence factor described for *Paracoccidioides* spp. (Parente et al., 2010). In an intranasal murine infection model, this enzyme was secreted in the lung tissue and therefore listed as a potential participant in the pathogenesis process (Pigosso et al., 2017). Of relevance, the protein is also a surface molecule, promoting the fungus interaction with macrophages (Tomazett et al., 2019). It should be noted that in a previous study, serine proteinase showed positive regulation at the transcriptional level when the fungus was treated with human plasma, which hypothetically occurred due to the depletion of Fe experienced by the fungus under suh condition (Bailão et al., 2007). This hypothesis was built based on the information that *Bacillus subtilis* employs a serine proteinase for the proteolysis of transferrin, a protein that transports Fe in mammals. The Fe released in the process allows the uptake of the metal mediated by bacterial siderophores (Park et al., 2006). The positive regulation of serine proteinase after Fe depletion in the present study corroborates this hypothesis.

In the present work, it was also possible to verify the positive regulation of *Paracoccidioides* spp. adhesins previously described. Enolase (PADG_04059) was 2.2 times more expressed in the Fe depletion condition. This enzyme classically known as a participant in glycolysis was also described on the cell surface of *P. brasiliensis* (Oliveira et al., 2012). Enolase has adhesin properties, since it is able to bind to the cell matrix components such as fibronectin and plasminogen

and promotes the adhesion of the fungus to A549 epithelial cells and murine macrophages (Donofrio et al., 2009; Nogueira et al., 2010; Oliveira et al., 2012). The enzyme dihydrolipoyl dehydrogenase (PADG_06494) was described in a relatively recent work as an exoantigen of *P. brasiliensis*. The stimulation of macrophages with the recombinant protein increased their phagocytic and microbicidal activity, which positioned this protein as possibly related to the interaction of the fungus with the host (Landgraf et al., 2017). Another positively regulated adhesin identified in the present study was the Tu translation elongation factor (PADG_01949), described as a fibronectin and plasminogen ligand and participant in the interaction of *P. brasiliensis* with pneumocytes (Marcos et al., 2016). It should be noted that despite previous works that evaluated the exoproteome of *Paracoccidioides* spp., this is the first time that this protein has been identified in this subproteome, which reiterates iron depletion as a modulating condition of the fungus exoproteome. It is worth mentioning the protein homogentisate 1,2-dioxigenase (PADG_08466), which was identified only in the condition of Fe depletion. Previous work points out that this protein is also a plasminogen ligand putatively involved in the process of adhesion, invasion, and spread of the fungus during infection (Chaves et al., 2015).

Glutathione-dependent ferric reductase activity has been reported by a previous study in culture supernatants of *Blastomyces dermatitidis*, *Sporothrix schenckii*, *Histoplasma capsulatum*, and *P. brasiliensis* (Zarnowski and Woods, 2005). Later work demonstrated that in *H. capsulatum*, this activity is dependent on a gamma-glutamyl transpeptidase (Zarnowski et al., 2008). The enzyme has been shown to act on glutathione to generate the dipeptide cysteinylglycine, which has a strong reducing power in a pH-dependent process (Zarnowski et al., 2008). *P. brasiliensis* presents two GGTs: PADG_07986 (Ggt1) and PADG_01479 (in this work called Ggt2). Homology studies and transcriptional analyses have identified Ggt1 as the secreted enzyme active in the reduction of Fe^{3+} (Silva et al., 2011; Bailão et al., 2012; Bailão et al., 2015). Previous studies identified Ggt2 in the exoproteome of *P. brasiliensis* and *P. lutzii* (Vallejo et al., 2012; Weber et al., 2012). In the present work, we identified the positive regulation of gamma-glutamyl transpeptidase (PADG_01479) Ggt2 in the *P. brasiliensis* exoproteome subjected to metal depletion, corroborating the literature and providing new information about the enzyme.

A very relevant finding in the present work was the upregulation of *Pb*Cyb5, secreted in response to Fe deprivation. Cyb5 and related enzymes are involved in multiple cellular processes, including sterol biosynthesis, maintenance of cell membranes, and azole resistance (Misslinger et al., 2017; Zhang et al., 2021). Cyb5 is also related to the regulation of Fe homeostasis in *S. cerevisiae* (Dap1) and *A. fumigatus* (CybE) (Craven et al., 2007; Misslinger et al., 2017). The data obtained in these works seem to conflict with the ones we obtained because, instead of upregulation, the authors verified another regulation process. It should be noted that these studies focused on the intracellular level, and therefore, comparing them with exoproteome results is not an obvious task.

To the best of our knowledge, this is the first time that Cyb5 has been described in a fungal exoproteome in response to Fe deprivation. Cyb5 is able to bind inorganic iron, as shown in **Figure 4A**. By bioinformatics analyses, we verified that this protein presents a similarity to the canonical iron-binding site of transferrin, where a His residue is linked to iron in an alpha-helix domain (Baker and Baker, 2012). Histidine residues are also present as an iron-binding site in cysteine dioxygenase, which is active in cysteine thiol oxidation (Simmons et al., 2006) and as iron-detoxifying membrane transporter from pathogens (Sharma et al., 2021). Glutamate (Glu) has been identified in certain iron-binding motifs (Sharma et al., 2021), such as in membrane transporters and in iron-binding adhesins that regulate biofilm formation in bacteria (Jiang et al., 2020). The higher score achieved for the His residue is related to a smaller distance between this amino acid and the iron ion. In membrane transporters, the distance between His and Glu to the iron ion is in the range of 2.0 Å (Jiang et al., 2020), and in iron transport proteins, the His residue is also 2.0 Å from the metal ion (Abdizadeh et al., 2017).

The findings of this work demonstrate that the *Paracoccidioides* exoproteome is dynamic and that it is modulated in response to stressful conditions, such as Fe deprivation. Upregulation of several virulence factors may be linked to the predictive adaptation hypothesis, since Fe deprivation is a condition imposed by the host in association with a myriad of other stressors (Brunke and Hube, 2014). Additionally, we identified Cyb5 as a new molecule of *Paracoccidioides* spp. related to the fungal response to Fe deprivation. The current world scenario presents fungi with increasing resistance to antifungal agents and the absence of new compounds approved to treat mycoses. Studying the host–pathogen interaction interface is key to bioprospecting new antifungal targets. Since Fe uptake is an essential attribute for the infective success of pathogens, listing new molecules that act in the process is a promising strategy to list new targets for antifungal compounds. It is now necessary to investigate which are the interaction partners of Cyb5 and whether Cyb5 is sufficient to promote the availability of Fe to the fungus.

DATA AVAILABILITY STATEMENT

The datasets presented in this study can be found in online repositories. The names of the repository/repositories and accession number(s) can be found below: http://www.peptideatlas.org/, PASS01753.

ETHICS STATEMENT

The animal study was reviewed and approved by the Comissão de ética no uso de animais (CEUA) Universidade Federal de Goiás.

AUTHOR CONTRIBUTIONS

CS, AS, LP, and LS conceived and designed the experiments. AS, LP, LS, IG, JP, MO, and KS performed the experiments. KS and

MP performed the molecular dynamics analyses. CS and MP contributed reagents and materials. CS, AS, LP, LS and KS wrote the article. All authors have read and agreed to the published version of the article.

FUNDING

Funding was provided by Fundação de Amparo à Pesquisa do Estado de Goiás, Institute Nacional of Thecnology of Host Pathogen Interaction (INCT-IPH), and Conselho Nacional de Desenvolvimento Científico e Tecnológico (CNPq) process number 302085/2019-0.

SUPPLEMENTARY MATERIAL

The Supplementary Material for this article can be found online at: https://www.frontiersin.org/articles/10.3389/fcimb.2022.903070/full#supplementary-material

REFERENCES

Abdizadeh, H., Atilgan, A. R., Atilgan, C., and Dedeoglu, B. (2017). Computational Approaches for Deciphering the Equilibrium and Kinetic Properties of Iron Transport Proteins. *Metallomics* 9, 1513–1533. doi: 10.1039/C7MT00216E

Asehnoune, K., Villadangos, J., and Hotchkiss, R. S. (2016). Understanding Host–Pathogen Interaction. *Intensive Care Med.* 42, 2084–2086. doi: 10.1007/s00134-016-4544-8

Bailão, E. F. L. C., Lima, P., de, S., Silva-Bailão, M. G., Bailão, A. M., da Fernandes, G R., et al. (2015). *Paracoccidioides* Spp. Ferrous and Ferric Iron Assimilation Pathways. *Front. Microbiol.* 6. doi: 10.3389/fmicb.2015.00821

Bailão, E. F. L. C., Parente, A. F. A., Parente, J. A., Silva-Bailão, M. G., de Castro, K.P, Kmetzsch, L., et al. (2012). Metal Acquisition and Homeostasis in Fungi. *Curr. Fungal Infect. Rep.* 6, 257–266. doi: 10.1007/s12281-012-0108-8

Bailão, E. F. L. C., Parente, J. A., Pigosso, L. L., de Castro, K. P., Fonseca, F. L., Silva-Bailão, M. G., et al. (2014). Hemoglobin Uptake by Paracoccidioides Spp. Is Receptor-Mediated. *PLoS Neglected Trop. Dis.* 8, 1–20. doi: 10.1371/journal.pntd.0002856

Bailão, A. M., Schrank, A., Borges, C. L., Dutra, V., Molinari-Madlum, E. E. W. I., Felipe, M. S. S., et al. (2006). Differential Gene Expression by Paracoccidioides Brasiliensis in Host Interaction Conditions: Representational Difference Analysis Identifies Candidate Genes Associated With Fungal Pathogenesis. *Microbes Infect.* 8, 2686–2697. doi: 10.1016/j.micinf.2006.07.019

Bailão, A. M., Shrank, A., Borges, C. L., Parente, J. A., Dutra, V., Felipe, M. S. S., et al. (2007). The Transcriptional Profile of Paracoccidioides Brasiliensis Yeast Cells is Influenced by Human Plasma. *FEMS Immunol. Med. Microbiol.* 51, 43–57. doi: 10.1111/j.1574-695X.2007.00277.x

Bairwa, G., Hee Jung, W., and Kronstad, J. W. (2017). Iron Acquisition in Fungal Pathogens of Humans. *Metallomics* 9, 215–227. doi: 10.1039/C6MT00301J

Baker, H. M., and Baker, E. N. (2012). A Structural Perspective on Lactoferrin Function 1 This Article is Part of a Special Issue Entitled Lactoferrin and has Undergone the Journal's Usual Peer Review Process. *Biochem. Cell Biol.* 90, 320–328. doi: 10.1139/o11-071

Baltazar, L. M., Ribeiro, G. F., Freitas, G. J., Queiroz-Junior, C. M., Fagundes, C. T., Chaves-Olórtegui, C., et al. (2021). Protective Response in Experimental Paracoccidioidomycosis Elicited by Extracellular Vesicles Containing Antigens of Paracoccidioides Brasiliensis. *Cells* 10, 1–14. doi: 10.3390/cells10071813

Berman, H. M. (2000). The Protein Data Bank. *Nucleic Acids Res.* 28, 235–242. doi: 10.1093/nar/28.1.235

Borges, C. L., Pereira, M., Felipe, M. S. S., de Faria, F. P., Gomez, F. J., Deepe, G. S., et al. (2005). The Antigenic and Catalytically Active Formamidase of *Paracoccidioides Brasiliensis*: Protein Characterization, cDNA and Gene Cloning, Heterologous Expression and Functional Analysis of the Recombinant Protein. *Microbes infect. / Institut. Pasteur* 7, 66–77. doi: 10.1016/j.micinf.2004.09.011

Bradford, M. M. (1976). A Rapid and Sensitive Method for the Quantitation of Microgram Quantities of Protein Utilizing the Principle of Protein-Dye Binding. *Analytical Biochem.* 72, 248–254. doi: 10.1016/0003-2697(76)90527-3

Brunke, S., and Hube, B. (2014). Adaptive Prediction As a Strategy in Microbial Infections. *PLoS Pathog.* 10, 1–4. doi: 10.1371/journal.ppat.1004356

Caza, M., and Kronstad, J. W. (2013). Shared and Distinct Mechanisms of Iron Acquisition by Bacterial and Fungal Pathogens of Humans. *Front. Celullar Infect. Microbiol.* 3. doi: 10.3389/fcimb.2013.00080

Chaves, E. A. C., Weber, S. S., Báo, S. N., Pereira, L. A., Bailão, A. B., Borges, C. L., et al. (2015). Analysis of *Paracoccidioides* Secreted Proteins Reveals Fructose 1,6-Bisphosphate Aldolase as a Plasminogen-Binding Protein. *BMC Microbiol.* 15, 1–14. doi: 10.1186/s12866-015-0393-9

Choi, J., Jung, W. H., and Kronstad, J. W. (2015). The cAMP/Protein Kinase A Signaling Pathway in Pathogenic Basidiomycete Fungi: Connections With Iron Homeostasis. *J. Microbiol.* 53, 579–587. doi: 10.1007/s12275-015-5247-5

Craven, R. J., Mallory, J. C., and Hand, R. A. (2007). Regulation of Iron Homeostasis Mediated by the Heme-Binding Protein Dap1 (Damage Resistance Protein 1) *via* the P450 Protein Erg11/Cyp51. *J. Biol. Chem.* 282, 36543–36551. doi: 10.1074/jbc.M706770200

da Silva, T. A., Roque-Barreira, M. C., Casadevall, A., and Almeida, F. (2016). Extracellular Vesicles From Paracoccidioides Brasiliensis Induced M1 Polarization *In Vitro*. *Sci. Rep.* 6, 1–10. doi: 10.1038/srep35867

Dlouhy, A. C., and Outten, C. E. (2013). The Iron Methallome in Eukaryotic Organisms. *Metal Ions Life Sci.* 12, 241–278. doi: 10.1007/978-94-007-5561-1

Donofrio, F. C., Carolina, A., Calil, A., Miranda, E. T., Marisa, A., Almeida, F., et al. (2009). Enolase From Paracoccidioides Brasiliensis: Isolation and Identification as a Fibronectin-Binding Protein. *J. Med. Microbiol.* 58, 706–713. doi: 10.1099/jmm.0.003830-0

Fava Netto, C. (1961). Contribuição Para O Estudo Imunológico Da Blastomicose De Lutz (Blastomicose Sul-Americana). *Rev. Inst Adolfo Lutz* 21, 99–194. doi: 10.53393/rial.1961.v21.33404

Geromanos, S. J., Vissers, J. P. C., Silva, J. C., Dorschel, C. A., Li, G. Z., Gorenstein, M. V., et al. (2009). The Detection, Correlation, and Comparison of Peptide Precursor and Product Ions From Data Independent LC-MS With Data Dependant LC-Ms/MS. *Proteomics* 9, 1683–1695. doi: 10.1002/pmic.200800562

Gonzalez, A., and Hernandez, O. (2016). New Insights Into a Complex Fungal Pathogen: The Case of *Paracoccidioides* Spp. *Yeast* 33, 113–128. doi: 10.1002/yea

Henikoff, S., and Henikoff, J. G. (1992). Amino Acid Substitution Matrices From Protein Blocks. *Proc. Natl. Acad. Sci.* 89, 10915–10919. doi: 10.1073/pnas.89.22.10915

Jiang, W., Ubhayasekera, W., Breed, M. C., Norsworthy, A. N., Serr, N., Mobley, H. L. T., et al. (2020). MrpH, A New Class of Metal-Binding Adhesin, Requires Zinc to Mediate Biofilm Formation. *PLoS Pathog.* 16, e1008707. doi: 10.1371/journal.ppat.1008707

Kuznets, G., Vigonsky, E., Weissman, Z., Lalli, D., Gildor, T., Kauffman, S. J., et al. (2014). A Relay Network of Extracellular Heme-Binding Proteins Drives *C. Albicans* Iron Acquisition From Hemoglobin. *PLoS Pathog.* 9, 1–14. doi: 10.1371/journal.ppat.1004407

Landgraf, T. N., Costa, M. V., Oliveira, A. F., and Ribeiro, W. C. (2017). Involvement of Dihydrolipoyl Dehydrogenase in the Phagocytosis and Killing of Paracoccidioides Brasiliensis by Macrophages. *Front. Microbiol.* 8. doi: 10.3389/fmicb.2017.01803

Lu, C.-H., Lin, Y.-S., Chen, Y.-C., Yu, C.-S., Chang, S.-Y., and Hwang, J.-K. (2006). The Fragment Transformation Method to Detect the Protein Structural Motifs. *Proteins: Structure Function Bioinf.* 63, 636–643. doi: 10.1002/prot.20904

Marcos, M. C., de Fátima da Silva, J., Cesar de Oliveira, H., Aparecida Moraes da Silva, R., Soares Mendes-Giannini, M. J., Fusco-Almeida, A. M., et al. (2012). Surface-expressed Enolase Contributes to the Adhesion of *Paracoccidioides brasiliensis* to Host Cells. *FEMS Yeast Res.* 12, 557-570. doi: 10.1111/j.1567-1364.2012.00806.x

Marcos, C. M., de Oliveira, H. C., da Silva, J., de, F., Assato, P. A., Yamazaki, D. S., et al. (2016). Identification and Characterisation of Elongation Factor Tu, a Novel Protein Involved in *Paracoccidioides brasiliensis*-Host Interaction. *FEMS Yeast Res.* 16, 1–14. doi: 10.1093/femsyr/fow079

Misslinger, M., Gsaller, F., Hortschansky, P., Müller, C., Bracher, F., Bromley, M. J., et al. (2017). The Cytochrome B5 CybE is Regulated by Iron Availability and is Crucial for Azole Resistance in A. Fumigatus. *Metallomics* 9, 1655–1665. doi: 10.1039/c7mt00110j

Moreira, A. L.E., Oliveira, M. A.P., Silva, L. O.S., Inácio, M. M., Bailão, A. M., Parente-Rocha, J. A., et al. (2020). Immunoproteomic Approach of Extracellular Antigens From Paracoccidioides Species Reveals Exclusive B-Cell Epitopes. *Front. Microbiol.* 10, 1–17. doi: doi: 10.3389/fmicb.2019.02968.

Murad, A. M., Souza, G. H. M. F., Garcia, J. S., and Rech, E. L. (2011). Detection and Expression Analysis of Recombinant Proteins in Plant-Derived Complex Mixtures Using nanoUPLC-MS^{E}. *J. Separation Sci.* 34, 2618–2630. doi: 10.1002/jssc.201100238

Nairz, M., Schroll, A., Sonnweber, T., and Weiss, G. (2010). The Struggle for Iron – a Metal at the Host – Pathogen Interface. *Cell. Microbiol.* 12, 1691–1702. doi: 10.1111/j.1462-5822.2010.01529.x

Nogueira, S. V., Fonseca, F. L., Rodrigues, M. L., Mundodi, V., Abi-Chacra, E. A., Winters, M. S., et al. (2010). *Paracoccidioides Brasiliensis* Enolase Is a Surface Protein That Binds Plasminogen and Mediates Interaction of Yeast Forms With Host Cells. *Infect. Immun.* 78, 4040–4050. doi: 10.1128/IAI.00221-10

Núñez, G., Sakamoto, K., and Soares, M. P. (2018). Innate Nutritional Immunity. *J. Immunol.* 201, 11–18. doi: 10.4049/jimmunol.1800325

Marcos, C. M., Silva, J. de F. da, Oliveira, H. C. de, Silva, R. A. M. da, Mendes-Giannini, M. J. S., and Fusco-Almeida, A. M. (2012). Surface-Expressed Enolase Contributes to the Adhesion of *Paracoccidioides Brasiliensis* to Host Cells. *FEMS Yeast Res.* 12, 557–570. doi:–doi: 10.1111/j.1567-1364.2012.00806.x

Oliveira, L. N., Gonçales, R. A., Silva, M. G., Lima, R. M., Tomazett, M. V., de Curcio, J.S, et al. (2020). Characterization of a Heme-Protein Responsive to Hypoxia in *Paracoccidioides Brasiliensis*. *Fungal Genet. Biol.* 144, 1–11. doi: 10.1016/j.fgb.2020.103446

Parente, A. F. A., Bailão, A. M., Borges, C. L., Parente, J. A., Magalhães, A. D., Ricart, C. A. O., et al. (2011). Proteomic Analysis Reveals That Iron Availability Alters the Metabolic Status of the Pathogenic Fungus Paracoccidioides Brasiliensis. *PLoS One* 6:1–14. doi: 10.1371/journal.pone.0022810

Parente, J. A., Salem-izacc, S. M., Santana, J. M., Pereira, M., Borges, C. L., Bailão, A. M., et al. (2010). A Secreted Serine Protease of Paracoccidioides Brasiliensis and its Interactions With Fungal Proteins. *BMC Microbiol.* 10, 1–10. doi: 10.1186/1471-2180-10-292

Park, R. Y., Sun, H. Y., Choi, M. H., Bai, Y. H., Chung, Y. Y., and Shin, S. H. (2006). Proteases of a Bacillus Subtilis Clinical Isolate Facilitate Swarming and Siderophore-Mediated Iron Uptake *via* Proteolytic Cleavage of Transferrin. *Biol. Pharm. Bull.* 29, 850–853. doi: 10.1248/bpb.29.850

Peres da Silva, R., Longo, L., da Cunha, J.P.C., Sobreira, T. J. P., Rodrigues, M. L., Faoro, H., et al. (2019). Comparison of the RNA Content of Extracellular Vesicles Derived From Paracoccidioides Brasiliensis and Paracoccidioides Lutzii. *Cells* 8, 765. doi: 10.3390/cells8070765

Pigosso, L. L., Baeza, L. C., Tomazett, M. V., Faleiro, M. B. R., Moura, V. M. B., Bailão, A. M., et al. (2017). Paracoccidioides Brasiliensis Presents Metabolic Reprogramming and Secretes a Serine Proteinase During Murine Infection. *Virulence* 8, 1417–1434. doi: 10.1080/21505594.2017.1355660

Restrepo, A., and Jiménez, B. E. (1980). Growth of *Paracoccidioides Brasiliensis* Yeast Phase in a Chemically Defined Culture Medium. *J. Clin. Microbiol.* 12, 279–281. doi: 10.1128/JCM.12.2.279-281.1980

Rodrigues, A., Oliveira, D., Nojosa, L., Soares, D. A., Parente-rocha, J. A., and Baeza, L. C. (2018). Characterization of Extracellular Proteins in Members of the Paracoccidioides Complex. *Fungal Biol.* 122, 738–751. doi: 10.1016/j.funbio.2018.04.001

Roy, U., and Kornitzer, D. (2019). Heme-Iron Acquisition in Fungi. *Curr. Opin. Microbiol.* 52, 77–83. doi: 10.1016/j.mib.2019.05.006

Schaible, U. E., and Kaufmann, S. H. E. (2004). Iron and Microbial Infection. *Nat. Rev.* 2, 946–954. doi: 10.1038/nrmicro1046

Sharma, P., Tóth, V., Hyland, E. M., and Law, C. J. (2021). Characterization of the Substrate Binding Site of an Iron Detoxifying Membrane Transporter From Plasmodium Falciparum. *Malaria J.* 20, 295. doi: 10.1186/s12936-021-03827-7

Shikanai-Yasuda, M. A., Mendes, R. P., Colombo, A. L., Queiroz-telles, F., Satie, A., Kono, G., et al. (2017). Brazilian Guidelines for the Clinical Management of Paracoccidioidomycosis. *Rev. Soc. Bras. Med. Trop.* 50 (5), 715–740. doi: 10.1590/0037-8682-0230-2017

Silva, M. G., Schrank, A., Bailão, E. F.L.C.C., Bailão, A. M., Borges, C. L., Staats, C. C., et al. (2011). The Homeostasis of Iron, Copper, and Zinc in Paracoccidioides Brasiliensis, Cryptococcus Neoformans Var. Grubii, and Cryptococcus Gattii: A Comparative Analysis. *Front. Microbiol.* 2, 1–19. doi: doi: 10.3389/fmicb.2011.00049.

Silva-Bailão, M. G., Bailão, E. F. L. C., Lechner, B. E., Gauthier, G. M., Lindner, H., Bailão, A. M., et al. (2014). Hydroxamate Production as a High Affinity Iron Acquisition Mechanism in Paracoccidioides Spp. *PLoS One* 9, 1–14. doi: 10.1371/journal.pone.0105805

Silva, M. G., de Curcio, J. S., Silva-Bailão, M. G., Lima, R. M., Tomazett, M. V., de Souza, A. F., et al. (2020). Molecular Characterization of Siderophore Biosynthesis in Paracoccidioides Brasiliensis. *IMA Fungus* 11, 11. doi: 10.1186/s43008-020-00035-x

Simmons, C. R., Liu, Q., Huang, Q., Hao, Q., Begley, T. P., Karplus, P. A., et al. (2006). Crystal Structure of Mammalian Cysteine Dioxygenase. *J. Biol. Chem.* 281, 18723–18733. doi: 10.1074/jbc.M601555200

Soares, M. P., and Weiss, G. (2015). The Iron Age of Host – Microbe Interactions. *EMBO Rep.* 16, 1482–1500. doi: 10.15252/embr.201540558

Sorgo, A. G., Brul, S., de Koster, C. G., de Koning, L. J., and Klis, F. M. (2013). Iron Restriction-Induced Adaptations in the Wall Proteome of Candida Albicans. *Microbiol. (United Kingdom)* 159, 1673–1682. doi: 10.1099/mic.0.065599-0

Swendsen, R. H., and Wang, J.-S. (1986). Replica Monte Carlo Simulation of Spin-Glasses. *Phys. Rev. Lett.* 57, 2607–2609. doi: 10.1103/PhysRevLett.57.2607

Tandara, L., and Salamunic, I. (2012). Iron Metabolism: Current Facts and Future Directions. *Biochem. Med. (Zagreb)* 22, 311–328. doi: 10.11613/BM.2012.034

Tomazett, M. V., Baeza, L. C., Paccez, J. D., Parente-Rocha, J. A., Ribeiro-Dias, F., and Maria de Almeida Soares, C. (2019). Identification and Characterization of Paracoccidioides Lutzii Proteins Interacting With Macrophages. *Microbes Infect.* 21 (8-9), 401–411. doi: 10.1016/j.micinf.2019.03.002

Tristão, G. B., Assunção, L. P., dos Santos, L. P. A., Borges, C. L., Silva-Bailão, M. G., de Almeida Soares, C. M., et al. (2015). Predicting Copper-, Iron-, and Zinc-Binding Proteins in Pathogenic Species of the Paracoccidioides Genus. *Front. Microbiol.* 6. doi: 10.3389/fmicb.2014.00761

Vallejo, M. C., Nakayasu, E., Matsuo, A., Sobreira, T., Longo, L., Ganiko, L., et al. (2012). Vesicle and Vesicle-Free Extracelullar Proteome of Paracoccidioides Brasiliensis: Comparative Analysis With Other Pathogenic Fungi. *J. Proteomics* 11, 1676–1685. doi: 10.1124/dmd.107.016501.CYP3A4-Mediated

Wang, L., and Cheraryil, B. J. (2009). Ironing Out the Wrinkles in Host Defense: Interections Beween Iron Homeostasis and Innate Immunity. *J. Innate Immun.* 1, 455–464. doi: 10.1159/000210016

Weber, S. S., Parente, A. F. A., Borges, C. L., Parente, J. A., Bailão, A. M., and de Soares, C.M. A. (2012). Analysis of the Secretomes of Paracoccidioides Mycelia and Yeast Cells. *PLoS One* 7, 1–19. doi: 10.1371/journal.pone.0052470

Williams, C. J., Headd, J. J., Moriarty, N. W., Prisant, M. G., Videau, L. L., Deis, L. N., et al. (2018). MolProbity: More and Better Reference Data for Improved All-Atom Structure Validation. *Protein Sci.* 27, 293–315. doi: 10.1002/pro.3330

Wu, S., and Zhang, Y. (2007). LOMETS: A Local Meta-Threading-Server for Protein Structure Prediction. *Nucleic Acids Res.* 35, 3375–3382. doi: 10.1093/nar/gkm251

Yang, J., Roy, A., and Zhang, Y. (2013). Protein–ligand Binding Site Recognition Using Complementary Binding-Specific Substructure Comparison and Sequence Profile Alignment. *Bioinformatics* 29, 2588–2595. doi: 10.1093/bioinformatics/btt447

Yang, J., Yan, R., Roy, A., Xu, D., Poisson, J., and Zhang, Y. (2015). The I-TASSER Suite: Protein Structure and Function Prediction. *Nat. Methods* 12, 7–8. doi: 10.1038/nmeth.3213

Zarnowski, R., Cooper, K. G., Brunold, L. S., Calaycay, J., and Woods, J. P. (2008). *Histoplasma Capsulatum* Secreted γ-Glutamyltransferase Reduces Iron by Generating an Efficient Ferric Reductant. *Mol. Microbiol.* 70, 352–368. doi: 10.1111/j.1365-2958.2008.06410.x.Histoplasma

Zarnowski, R., and Woods, J. P. (2005). Glutathione-Dependent Extracellular Ferric Reductase Activities in Dimorphic Zoopathogenic Fungi. *Microbiol. (N Y)* 151, 2233–2240. doi: 10.1099/mic.0.27918-0.Glutathione-dependent

Zhang, Y. (2008). I-TASSER Server for Protein 3D Structure Prediction. *BMC Bioinf.* 9, 40. doi: 10.1186/1471-2105-9-40

Zhang, C., Ren, Y., Gao, L., Gu, H., and Lua, L. (2021). Electron Donor Cytochrome B5 Is Required for Hyphal Tip Accumulation of Sterol-Rich Plasma Membrane Domains and Membrane Fluidity in Aspergillus Fumigatus. *Appl. Environ. Microbiol.* 87, 1–16. doi: 10.1128/AEM.02571-20

Zhang, Y., and Skolnick, J. (2004). SPICKER: A Clustering Approach to Identify Near-Native Protein Folds. *J. Comput. Chem.* 25, 865–871. doi: 10.1002/jcc.20011

Conflict of Interest: The authors declare that the research was conducted in the absence of any commercial or financial relationships that could be construed as a potential conflict of interest.

Publisher's Note: All claims expressed in this article are solely those of the authors and do not necessarily represent those of their affiliated organizations, or those of the publisher, the editors and the reviewers. Any product that may be evaluated in this article, or claim that may be made by its manufacturer, is not guaranteed or endorsed by the publisher.

frontiers | Frontiers in Cellular and Infection Microbiology

ORIGINAL RESEARCH
published: 14 June 2022
doi: 10.3389/fcimb.2022.867963

HupZ, a Unique Heme-Binding Protein, Enhances Group A Streptococcus Fitness During Mucosal Colonization

Kristin V. Lyles[1], *Lamar S. Thomas*[2], *Corbett Ouellette*[1], *Laura C. C. Cook*[2] *and Zehava Eichenbaum*[1]*

[1] Department of Biology, Georgia State University, Atlanta, GA, United States, [2] Binghamton Biofilm Research Center, Department of Biology, Binghamton University, Binghamton, NY, United States

Group A Streptococcus (GAS) is a major pathogen that causes simple and invasive infections. GAS requires iron for metabolic processes and pathogenesis, and heme is its preferred iron source. We previously described the iron-regulated *hupZ* in GAS, showing that a recombinant HupZ-His_6 protein binds and degrades heme. The His_6 tag was later implicated in heme iron coordination by HupZ-His_6. Hence, we tested several recombinant HupZ proteins, including a tag-free protein, for heme binding and degradation *in vitro*. We established that HupZ binds heme but without coordinating the heme iron. Heme-HupZ readily accepted exogenous imidazole as its axial heme ligand, prompting degradation. Furthermore, HupZ bound a fragment of heme c (whose iron is coordinated by the cytochrome histidine residue) and exhibited limited degradation. GAS, however, did not grow on a heme c fragment as an iron source. Heterologous HupZ expression in *Lactococcus lactis* increased heme b iron use. A GAS *hupZ* mutant showed reduced growth when using hemoglobin as an iron source, increased sensitivity to heme toxicity, and decreased fitness in a murine model for vaginal colonization. Together, the data demonstrate that HupZ contributes to heme metabolism and host survival, likely as a heme chaperone. HupZ is structurally similar to the recently described heme c-degrading enzyme, Pden_1323, suggesting that the GAS HupZ might be divergent to play a new role in heme metabolism.

Keywords: Group A Streptococcus, HupZ, heme, heme utilization, heme toxicity, iron, mice colonization

OPEN ACCESS

Edited by:
Mauricio H. Pontes, The Pennsylvania State University, United States

Reviewed by:
Steven Omid Mansoorabadi, Auburn University, United States
William Lanzilotta, University of Georgia, United States

***Correspondence:**
Zehava Eichenbaum
zeichen@gsu.edu

Specialty section:
This article was submitted to Bacteria and Host, a section of the journal Frontiers in Cellular and Infection Microbiology

Received: *01 February 2022*
Accepted: *09 May 2022*
Published: *14 June 2022*

Citation:
Lyles KV, Thomas LS, Ouellette C, Cook LCC and Eichenbaum Z (2022) HupZ, a Unique Heme-Binding Protein, Enhances Group A Streptococcus Fitness During Mucosal Colonization. Front. Cell. Infect. Microbiol. 12:867963. doi: 10.3389/fcimb.2022.867963

INTRODUCTION

Group A Streptococcus (GAS, or *Streptococcus pyogenes)* is an obligate human pathogen that primarily infects the skin and the upper respiratory system. GAS can also produce invasive, systemic diseases, including Streptococcal toxic shock syndrome and necrotizing fasciitis, both with high mortality rates (Walker et al., 2014). In some cases, superficial GAS infections can cause harmful immune responses leading to post-streptococcal sequelae like glomerulonephritis and rheumatic heart disease (Watkins et al., 2017). There was a marked increase in invasive GAS infections in the

United States and Europe in the 1980s with the emergence of more virulent strains, particularly the M1T1 strain (Barnett et al., 2018). The rise in invasive infections is of particular concern since there is no vaccine, and GAS is becoming increasingly resistant to tetracycline and macrolides (Davies et al., 2015; CDC, 2019).

There is very little free iron in the human body; much of the metal is sequestered by proteins that facilitate transport and storage and reduce iron-mediated toxicity (Marchetti et al., 2020). Most iron in the body is bound to a porphyrin ring, called heme, and two-thirds of the body heme is found in hemoglobin (i.e., heme b). There are other types of heme in the body; for example, heme c is bound to cytochrome c and differs from heme b in that it is covalently bound to a proteinaceous region. For clarity, in this manuscript, we will use "heme" to refer to heme b.

Iron-requiring pathogens, such as GAS, have evolved mechanisms to obtain heme iron from the host. GAS hemolysins lyse erythrocytes and other cell types, releasing heme and hemoproteins, such as hemoglobin and cytochromes. The *sia* and *hupYZ* operons allow GAS to acquire heme from various hemoproteins and transport it into the cell (Bates et al., 2003; Sun et al., 2010; Chatterjee et al., 2020). The metalloregulator, MtsR, controls both the *sia* and *hupYZ* operons, permitting elevated expression in low-iron conditions (Bates et al., 2005). This regulon is also upregulated during vaginal colonization of GAS in mice (Cook et al., 2019). How heme is degraded by GAS is not known, but the putative cytoplasmic protein HupZ was implicated in the process (Sachla et al., 2016).

Many organisms use heme oxygenases to degrade heme and release the iron. The first heme oxygenase (HO-1) was identified in mammals (Tenhunen et al., 1969). Subsequently, homologs were identified in several bacterial species, such as HmuO of *Corynebacterium diptheriae*, HemO of *Neisseria menigitidis*, and HemO/PigA of *Pseudomonas aeruginosa* (Schmitt, 1997; Zhu et al., 2000; Ratliff et al., 2001). These enzymes degrade heme through the canonical or HO-1-like pathway, which consists of three oxygenation steps resulting in equal amounts of α-biliverdin, ferrous iron, and carbon monoxide (CO) (Wilks and Heinzl, 2014; Wilks and Ikeda-Saito, 2014; Lyles and Eichenbaum, 2018). The first noncanonical heme oxygenases, IsdG, and its homolog IsdI were identified in *Staphylococcus aureus* (Skaar et al., 2004). The IsdG/I reaction yields a mixture of β- and δ-staphylobilin and releases formaldehyde instead of CO. Some pathogenic bacteria utilize proteins from the flavin mononucleotide (FMN)-binding subfamily for heme-binding or degradation, such as HugZ from *Helicobacter pylori* (which produces δ-biliverdin) and ChuZ from *Campylobacter jejuni* (Hu et al., 2011; Zhang et al., 2011). Pden_1323, from *Paracoccus denitrificans*, is a member of this family, and while it lacks the conserved axial heme ligand from HugZ and ChuZ, it can degrade fragments of heme c (Li et al., 2021).

GAS HupZ shares structural similarity to the HugZ family (Sachla et al., 2016). HupZ purified with a His_6-tag binds and degraded heme *in vivo*, releasing CO, free iron, and an unidentified chromophore. Further investigation of the recombinant protein using EPR and resonance Raman spectroscopy indicated that a histidine residue coordinated the heme iron, yet site mutation of the only histidine residue in HupZ did not affect the spectra (Traore et al., 2021). These observations suggested that the His_6-tag facilitated the heme-binding and degradation exhibited by the HupZ-His_6 protein. Here, we investigate heme-binding and degradation by HupZ expressed without a His_6 tag and use mutagenesis, heterologous expression, and a mice model to probe the protein's function *in vivo*. The data confirm that HupZ plays a role in heme use and tolerance in GAS and suggest that HupZ is a member of an emerging group of heme-binding proteins in bacteria.

MATERIALS AND METHODS

Strains, Media, and Chemicals

E. coli were grown at 37°C aerobically (225 rpm) in Luria-Bertani (LB) broth or agar, supplemented with appropriate antibiotics. GAS was grown statically in Todd Hewitt yeast broth (THYB, 5 ml of media in 15-ml screw-top tubes, Thermo Scientific #33965) or agar (THYA) at 37°C. *L. lactis* was grown statically in GM17 at 30°C (10 ml of media in 15-ml screw-top tubes). Plasmid extractions were performed using the Promega Wizard Miniprep kit (PR-A7510) or the Qiagen Midiprep kit (12123). Genomic DNA was harvested with Invitrogen PureLink (K1820-01). Unless otherwise specified, chemicals were purchased from Sigma.

Plasmid Construction

A list of strains and plasmids can be found in **Table 1**, and primer sequences are shown in **Table 2**. Plasmid engineering was confirmed with restriction digest and PCR analyses.

A *hupZ::cm*^{R} (chloramphenicol acetyltransferase) allele with flanking regions of chromosome homology was assembled in pUC19 using NEBuilder HiFi Assembly Kit (#E5520) generating plasmid pKV111. The chromosomal *hupZ* upstream region was cloned from GAS strain NZ131 using primers ZE844 and ZE845. The downstream arm using ZE842 and ZE843 and the *cm*^{R} gene was amplified from pDC123 using primers ZE840 and ZE841. The *hupZ::cm*^{R} allele was amplified from pKV111 with ZE876 and ZE787 primers, adding flanking *Eco*RI sites to move the fragment into the temperature-sensitive vector pJRS700, generating pKV117.

The shuttle vector, pKV138, expressing *hupZ* under GAS *recA* promoter, was generated for complementation. The *hupZ* gene was amplified from NZ131 gDNA and ligated into pLC007. The empty vector control (pKV141) was generated by cutting pLC007 with *Hind*III and self-ligating.

The vector pKV105, expressing *hupZ* under nisin regulation, was used for heterologous expression in *Lactococcus lactis*. The gene was cloned from NZ131 strain using primers ZE685 and ZE686. The insert and pNZ8008 were digested, ligated, and electroporated into MC4100 *E. coli*. Competent MG1363 *L. lactis* that already contained pXL14, which codes the nisin

TABLE 1 | Strains and plasmids.

Strains	Relevant properties	Source/reference
M49Rescue	NZ131 wild-type rescue strain	This study
M49Lyles	NZ131 containing *hupZ::cm*^{R} mutation	This study
M49Lyles + pKV127	NZ131 containing *hupZ::cm*^{R} mutation and pKV127	This study
pDC123	Source of Cm^R allele	(Chaffin and Rubens, 1998)
pET/His$_6$/MBP/TEV	N-terminal His$_6$ followed by MBP, P_{T7}, Kan^R	Addgene plasmid #29656
pET MBP TEV	N-terminal MBP, P_{T7}, Amp^R	Addgene plasmid #48311
pJRS700	pVE6037 derivative, Kan^R, TM^S	(Bates et al., 2005)
pKV102	Expresses HupZ-Strep from P_{T7}	Vector Builder
pKV105	pNZ8008 derivative expresses *hupZ*, P^{nisA}, CM^R	This study
pKV111	pUC19 derivative containing *hupZ::cm*^{R} allele, Amp^R	This study
pKV113	pKV111 derivative with a site mutation to add *Eco*RI site downstream of *hupZ::cm*^{R} allele	This study
pKV117	pJRS700 derivative containing *hupZ::cm*^{R} allele, Kan^R, TM^S	This Study
pKV135	pET MBP TEV derivative that expresses MBP-HupZ from P_{T7}	This Study
pKV138	pLC007 derivative expressing *hupZ*, Spec^R, P_{RecA}	This study
pKV141	pLC007 derivative *hupY* deleted, Spec^R, P_{RecA}	This study
pLC007	Expresses *hupY*, Spec^R, P_{RecA}	(Cook et al., 2019)
pNZ8008	pSH71 replicon with promoterless *gusA* gene, P_{nisA}, Cm^r	(de Ruyter et al., 1996)
pNZ9530	pAMb1 replicon expressing *nisR* and *nisK*, Ery$_R$, P_{RepA}	(Kleerebezem et al., 1997)
pRK793	p15A replicon expressing SuperTev, P_{tac}, Kan^R, CM^R	(Tropea et al., 2009)
pUC19	pET101 derivative expresses HupX-His$_6$, Amp^R, P_{T7}	Invitrogen
pZZ2	pET101 derivative expresses HupZ-His$_6$, Amp^R, P_{T7}	(Sachla et al., 2016)

response regulator, were electroporated with either pKV105 or pNZ8008 (as a negative control).

Plasmid pKV102 expressing HupZ with a C-terminal Strep-tag was purchased from Vector Builder. The HupZ sequence was placed in a pET bacterial protein expression vector that contains a T7 promoter and pBR322 origin of replication.

Maltose binding protein (MBP) fusion (pKV130 or pKV135) was generated with ligation-independent cloning into pET/His$_6$/MBP/TEV (Addgene plasmid #29656 or pET/MBP/TEV (Addgene plasmid #48311) expression vector as previously described (Porter and Christianson, 2019). Briefly, *hupZ* was cloned from NZ131 with primers ZE978 and ZE979 that added the following upstream, 5'TACTTCCAATCCAATGCA3', and downstream, 5'TTATCCACTTCAATGTTATTA3', sequences to the insert. The purified PCR products were incubated with T4 DNA polymerase (Invitrogen 1800-5017), bovine serum albumin (BSA), dithiothreitol (DTT), dCTP, and T4 polymerase buffer. The vector pET/His$_6$/MBP/TEV or pET/MBP/TEV was linearized with *Ssp*I restriction enzyme and then incubated with T4 DNA polymerase, BSA, DTT, dGTP, and T4 polymerase buffer. The reactions were cleaned using ethanol precipitation and resuspended in 12 µl of diH_2O. One microliter of the vector was incubated with 4 µl of insert for 30 min at room temperature. One microliter of 25 mM EDTA was added to the solution and allowed to sit for an additional 15 min and then transformed into *E. coli*.

The GAS Δ*hupZ::cm*^{R} mutant was generated using insertion inactivation to knock out *hupZ* in the GAS M49 strain NZ131. Competent NZ131 was transformed with the temperature-sensitive pKV117 (harboring the *hupZ::cm*^{R} allele and flanking chromosomal region) and plated on THYA with kanamycin (the vector marker) at 30°C. Colonies were then passed three times in THYB with kanamycin at 37°C and were plated with either chloramphenicol or no antibiotic at 30°C. The resulting GAS

TABLE 2 | Primers.

Prime	Target	Comment	Sequence
ZE685-S	pNZ8008		5'CCCTTGAATTCCACTAGCGTTGCTTTACTG
ZE686-A	pNZ8008		5'GCGCGAAGCTTGGTCCTAAATACTGTTACAG
ZE728-S	*hupZ*		5'CACTCAAAATGATAACACAAGAAATGAAAGAT
ZE729-A	*hupZ*		5'GAGAAGCTTTTAAAATAAGGGTCCTAAATACT
ZE838-S	pUC19		5'GCTGAGATACGCGTAATCATGGTCA
ZE839-A	pUC19		5'ATGGGACAAGCTCGAATTCACTGGC
ZE840-S	pDC123	CM^R	5'TAGCAATGGTTGCTAACATAGCATTACGG
ZE841-A	pDC123	CM^R	5'CCAGATTGTACCTAGCGCTCTCATAT
ZE842-S	5' region of *hupZ*		5'GAGCGCTAGGTACAATCTGGTGCTAAT
ZE843-A	5' region of h*upZ*		5'ATGATTACGCGTATCTCAGCTATCTTAG
ZE844-S	3' region of *hupZ*		5'TGAATTCGAGCTTGTCCCATATTGC
ZE845-A	3' region of *hupZ*		5'CTATGTTAGCAACCATTGCTAATTGG
ZE876-S	pKV111	Adds *Eco*RI to *hupZ::cm*^{R}	5'CATAGAATTCATGTGCTGAAGGCGAT
ZE876-A	pKV111	Adds *Eco*RI to *hupZ::cm*^{R}	5'CATAGAATTCGTTGTGTGGAATTGTGAGC
ZE978-S	*hupZ*	Adds LIC sequence	5'TACTTCCAATCCAATGCAATGATAACACAAGAAATG
ZE979-A	*hupZ*	Adds LIC sequence	5'TTATCCACTTCCAATGTTATTATTAGTTACTTTCACTGTT

clones harboring an integrated pKV117 were confirmed by PCR. Daily, individual colonies were propagated at 37°C and screened through replica plating to ensure the loss of the vector marker and the maintenance (knockout mutant) or loss of the cm^R gene (wild-type rescue). The replacing of *hupZ* with *hupZ::cm*^{R} allele in M49Lyles or the regeneration of the wild-type *hupZ* allele in M49Rescue was confirmed with PCR.

Protein Expression

The pKV135 (expressing MBP-HupZ) plasmid was transformed into Invitrogen Chemically Competent BL21(DE3) cells before each expression. All others were grown overnight from a glycerol stock and then diluted in fresh LB media. Cultures were grown at 37°C with 225 rpm until they reached an OD_{600} of 1, induced with 1 mM isopropyl β-D-1-tiogalactopyranosie (IPTG), and incubated overnight at 20°C with 180 rpm. The following day, cells were harvested by centrifugation. HupZ-His_6- or MBP-HupZ-expressing cells were resuspended in 20 mM Tris (pH 8.0), 100 mM NaCl, and 0.1% Triton X-100. HupZ-Strep cells were resuspended in 20 mM Tris/HCl and 500 mM NaCl. One cOmpleteEDTA-free Protease inhibitor tablet (Roche #1183670001) per 500 ml of grown culture was added before sonification. The cellular debris was pelleted by centrifugation at 20,000 × *g* for 30 min at 4°C, and the lysate was filtered using a 0.22 μM filter unit. Protein was purified on an AKTA FPLC using Cytiva HisTrap HP, MBPTrap HP, or StrepTrap HP Sepharose columns.

Protein purification and size were confirmed using sodium dodecyl sulfate-polyacrylamide gel electrophoresis (SDS-PAGE, **Figure 1A**). Protein concentration was determined by the ThermoScientific Lowry Protein Assay Kit (23240). The buffer used for reconstitutions and degradations consisted of 20 mM sodium phosphate and 500 mM NaCl (pH 7.4). Arginine (30 mM) and 0.1% glycerol were added to the buffer for HupZ-Strep protein to promote solubility.

TEV Protease Cleavage of His-MBP-HupZ

Purified TEV protease (expressed from pRK793) was generously provided by Dr. Nicholas Noinaj of Purdue University (Tropea et al., 2009). Purified His-MBP-HupZ was incubated with TEV protease at 100 μg/1 μg, respectively, in 200-μl aliquots overnight statically. Cut protein circulated for 1 h at 4°C with resin from three NEBExpress Ni Spin Column rotating head to head in a clean gravity column to remove free His-MBP. Flow-through was collected and subsequently processed *via* an AKTA-FPLC system using Cytiva MBPTrap HP columns to further remove His-MBP. Collected flow-through of tag-free HupZ was concentrated using Amicon® Ultra-15 Centrifugal Filter Unitfilters. Purity was assessed by SDS-PAGE (**Figure 1B**) and quantified by Lowry.

Mice Mucosal Colonization

Female outbred CD1 (Charles River) mice aged 6 to 8 weeks were used for all experiments. Experiments were performed as previously described (Patras and Doran, 2016; Cook et al., 2018). A day prior to inoculation (day −1), mice were given an intraperitoneal injection of 0.5 mg of β-estradiol valerate (Alfa Aesar) suspended in 100 μl of filter-sterilized sesame oil (Acros Organics MS) to synchronize estrus. On day 0, WT and *ΔhupZ::cm*^{R} mutant strains were grown to an OD_{600} = 0.4 and mixed 1:1. Mice were vaginally inoculated with the mixed culture in 10 μl of PBS containing 10^7 CFU. On days 1, 2, 3, and 5, the vaginal lumen was washed with 50 μl of sterile PBS, using a pipette to gently circulate the fluid approximately 6–8 times. The lavage fluid was then collected and placed on ice for no more than 30 min. Vaginal lavage was serially diluted in PBS and plated on CHROMagar StrepB (WT) or CHROMagar StrepB with chloramphenicol (Δ*hupZ*) plates to obtain CFU counts (Cook et al., 2018). Murine colonization studies were reviewed and approved by Binghamton University Laboratory Animal Resources (LAR) and by the Binghamton Institutional Animal Care and Use Committee (IACUC) under protocols 803-18 and 857-21.

RESULTS

Recombinant HupZ Proteins Expressed Without a His_6 Tag Binds Heme b

We previously showed that a recombinant HupZ protein containing a C-terminal fusion to His_6 tag (HupZ-His_6) binds and degrades heme *in vitro* (Sachla et al., 2016). HupZ-His_6 crystalized as a homodimer with a split β-barrel conformation, a fold also seen in FMN-binding heme-degrading proteins described in several bacterial species (Sachla et al., 2016; Lyles and Eichenbaum, 2018). Additional investigations revealed that this recombinant HupZ protein interacts with heme *in vitro* by its His_6 tag, leading to a higher-order oligomeric structure, heme stacking, and degradation (Traore et al., 2021). These findings cast doubts about the function and the role of HupZ in heme metabolism. To reexamine heme-binding by HupZ, we constructed a new recombinant C-terminal fusion replacing the His_6 with a Step-tag (HupZ-Strep) to facilitate purification. We expressed and purified the recombinant HupZ-Strep (**Figure 1A**), but the purified protein was not stable and precipitated out of the solution. We added 1% glycerol and 30 mM arginine to the buffer to increase stability for later heme titration experiments (Vagenende et al., 2009; Kudou et al., 2011). Titration of HupZ-Strep with externally added heme revealed the formation of a growing UV-VIS absorption peak at 404 nm that is indicative of heme-binding (**Figure 1B**). However, the heme bound form of HupZ-Strep exhibited a shift in absorption maxima compared to the holo HupZ-His_6, which has a 414-nm Soret peak (**Figure 1C**). Additionally, unlike HupZ-His_6, the absorption spectrum of HupZ-Strep did not include the α and β bands between 500 and 600 nm, implying HupZ-Strep binds heme without an axial heme ligand that coordinates the iron (Giovannetti, 2012).

The crystal structure of HupZ-His_6 indicates that the protein's C-terminus is close to where the HupZ dimers form a quaternary β-barrel (Sachla et al., 2016). To avoid the possibility that a C-terminal addition may interfere with the function and stability of HupZ, we constructed N-terminal fusions to two

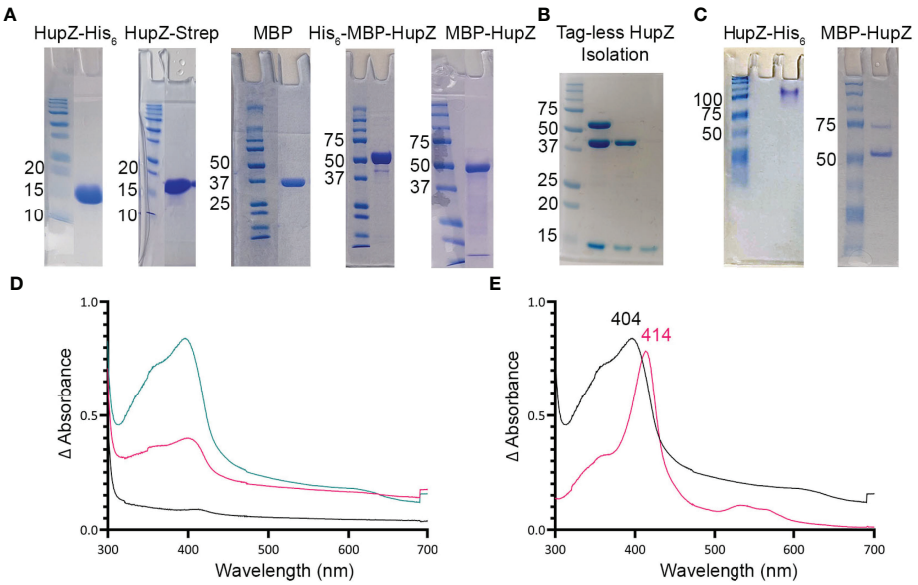

FIGURE 1 | HupZ-Strep binds heme b but without iron coordination. **(A)** SDS-PAGE showing 10 mM of recombinant proteins next to molecular markers. HupZ-His_6 (18.5 kD) and HupZ-Strep (18.7 kD) were run on 13% acrylamide gel. MBP (40.2 kD) and MBP-HupZ (56.5 kD) were run on 10% acrylamide gels. **(B)** SDS-PAGE (12.5%) showing the cleavage and purification of tag-less HupZ (15 kD). Lane 2 shows partial cleavage, lane 3 shows complete cleavage, and lane 4 is isolated HupZ. **(C)** Native PAGE showing 10 mM of purified proteins next to molecular markers. HupZ-His_6 (left) or MBP-HupZ (right). **(D)** UV–VIS absorption spectrum of 10 μM HupZ-Strep incubated for 1 h with 5 (pink) or 10 (teal) μM heme. The blank contains reaction buffer with 1% glycerol, 30 mM Arg, and a corresponding amount of heme. **(E)** UV–VIS absorption spectrum of heme bound to HupZ-Strep (black) or HupZ-His6 (pink). Protein samples (10 mM) were incubated with heme for 24 h, free heme was removed by a PD-10 column, and the UV-VIS spectrum was recorded.

different MBP-containing vectors (His-MBP-HupZ and MBP-HupZ) and purified the proteins (**Figure 1A**). We generated a tag-less HupZ by cleaving His-MBP-HupZ with TEV protease (**Figure 1B**), leaving a serine residue after cleavage. We assayed heme binding by incubating 10 μM of tag-less HupZ with increasing heme concentration (**Figure 2A**). To confirm heme binding, the protein was allowed to set with 2× concentration of heme overnight and then passed through a PD-10 desalting column to remove any upbound heme (**Figure 2B**). Overall, tag-less HupZ exhibited a heme-binding spectrum similar to HupZ-Strep and different from HupZ-His_6 (**Figures 1D, E**). Tag-less HupZ's Soret was broad and peaked at 385 nm. The 500- through 600-nm range lacked the α and β bands that indicated coordination of the central heme-iron.

Tag-less HupZ was not highly stable and prone to precipitate. Due to the solubility problems, further testing used a fusion to MBP (MBP-HupZ), which often aids in protein solubility. Unlike HupZ-Strep and tag-less HupZ, MBP-HupZ is soluble. Heme

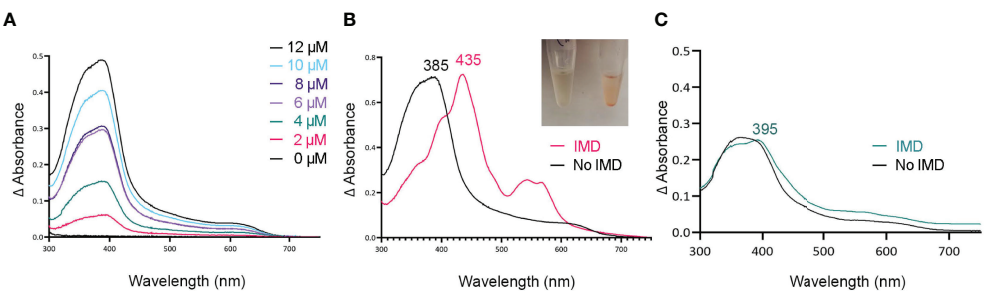

FIGURE 2 | Tag-less HupZ requires the imidazole group to coordinate heme b iron. UV-VIS absorption spectra of 10 μM tag-less HupZ **(A)** incubated for 1 h with a range of heme concentrations. The blank contained the reaction buffer and equivalent concentration of heme. Tag-less HupZ was incubated with 20 μM heme for 24 h, free heme was removed with PD-10 column (**B**, black). Then 1.6 mM imidazole (IMD, pink) was added to the cuvette. This addition causes the solution in the test tubes to change to pink (Insert). Lastly **(C)**, the spectra for 10 μM of heme was taken in the standard reaction buffer (black) and with the addition of 1.6 mM IMD (teal). The blank contained only the reaction buffer.

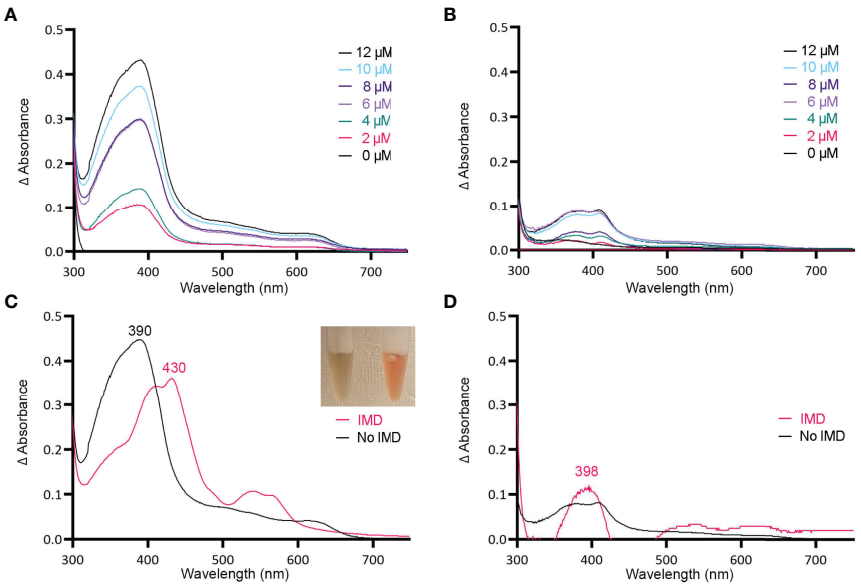

FIGURE 3 | MBP-HupZ binds heme b and uses exogenous histidine for iron coordination. UV-VIS absorption spectra of 10 μM MBP-HupZ **(A)** or MBP **(B)** incubated for 1 h with a range of heme concentrations. The blank contained the reaction buffer and equivalent concentration of heme. MBP-HupZ was incubated with 20 μM heme for 24 h, free heme was removed, and the UV-VIS spectrum was determined before (**C**, black) or after the addition of 1.6 mM imidazole (IMD, pink). MBP (10 μM) was incubated with 20 μM heme for 24 h, free heme was removed, and the UV-VIS spectrum was determined before (**D**, black) or after the addition of IMD (pink).

titration and reconstitution experiments demonstrated that the holo MBP-HupZ's UV-VIS spectrum (**Figures 3A, C**) is similar to heme binding by tag-less HupZ. We also assess the heme-binding of a purified MBP protein as a negative control. MBP bound only a negligible amount of heme, exhibiting a vastly different absorption spectrum during heme titrations and reconstitutions (**Figures 3B, D**). MBP-HupZ also migrated as a monomer on native PAGE, indicating that it does not assemble into a high oligomeric state *in vitro* like HupZ-His_6 (**Figure 1C**) (Traore et al., 2021). Therefore, all three recombinant HupZ proteins bind heme, albeit without an axial heme ligand. These findings suggest that heme-binding is native to the HupZ protein and independent of the tag, the location of the fusion, or the multimeric state.

Tag-Less and MBP-HupZ Use an Exogenous Histidine for Iron Coordination Of Heme b

Histidine is a common residue in short peptides that bind heme and often functions as the heme axial ligand in hemoproteins (Wissbrock et al., 2019). The imidazole moiety of histidine interacts with iron and other transition metals during binding. Since holo tag-less and MBP-HupZ did not exhibit iron coordination, we tested if exogenous imidazole could serve this function *in vitro* (**Figures 2B** and **3C**). In both recombinant proteins, the addition of 1.6 mM imidazole caused a shift in the Soret peak, the generation of α and β bands, and the protein solution turned red (**Figures 2B** inset and **3C** inset). As a control, we also measured the UV-VIS spectrum of MBP after incubation with heme, which exhibited minor spectral changes and still lacked α and β bands (**Figure 3D**). The UV-VIS spectra of free heme did not change with the addition of imidazole (**Figure 2C**). These observations suggest that exogenous imidazole can coordinate the iron in holo tag-less and MBP-HupZ but not in MBP or free heme. Together, this indicates that HupZ binds heme without an axial heme ligand but can readily interact with an exogenous imidazole group to coordinate the iron.

MBP-HupZ Degrades Heme b in the Presence of an Exogenous Imidazole

HupZ-His_6 degrades heme *in vitro*, releasing CO, free iron, and a chromophore (Sachla et al., 2016). Since externally added imidazole can coordinate the heme iron in holo-MBP-HupZ, we tested if MBP-HupZ can also break down the heme under these conditions. Holo-MBP-HupZ was incubated with 1.6 mM imidazole, ferredoxin (as a reducing agent), NADPH, an NADPH regeneration system (glucose-6-phosphate and glucose-6-phosphate dehydrogenase), and catalase (to control for non-enzymatic degradation of heme by hydrogen peroxide) and allowed to run for 6 h (**Figure 4A**). As indicated by the arrows, the Soret and the α and β bands decreased steadily during incubation, indicating heme degradation (**Figure 4B**). Still, the MBP-HupZ reaction did not result in an absorption peak at 600–700 mm, indicating the formation of biliverdin or similar molecules. *In vitro* heme degradation by some heme oxygenases (e.g., HemO and HemO/PigA) can result in ferric-biliverdin, which has no absorption properties (Zhu et al., 2000; Ratliff et al., 2001). To liberate the iron, we treated the MBP-

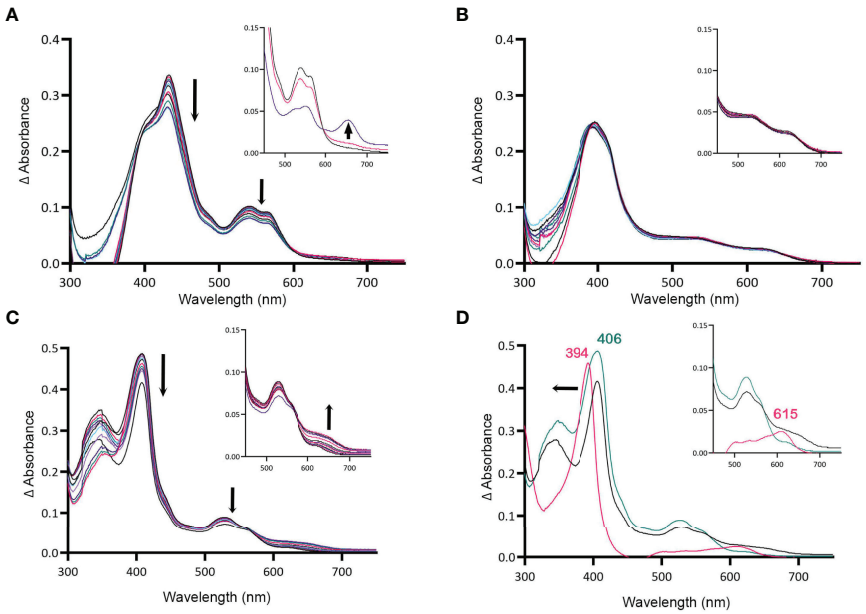

FIGURE 4 | MBP-HupZ degrades heme with the exogenous imidazole group. UV-VIS absorption spectra of 10 μM heme b bound to MBP-HupZ with 1.6 mM imidazole **(A)** or without **(B)** incubated with 10 μM ferredoxin, NADPH, an NADPH regeneration system, and catalase. After acidification of the MBP-HupZ reaction with imidazole, a peak at 660 nm formed (**A,** inset, purple). The blank contained 10 μM ferredoxin, NADPH, an NADPH regeneration system, and catalase, with or without 1.6 mM imidazole. MBP-HupZ (10 μM) in solution with 10 μM MP11, 10 μM ferredoxin, NADPH, an NADPH regeneration system, and catalase **(C)**. **(D)** The zero minute of the MP11 (teal) and the 6-h time point (black). After acidification of the reaction (pink), the Soret shifted from 406 to 394 nm, and a peak formed at 626 nm (**D**, inset, pink). The blank contained 10 μM ferredoxin, an NADPH regeneration system, and catalase, with or without 1.6 mM imidazole.

HupZ reaction with acid. As with HemO, the reaction acidification caused the reduction of the α and β bands and formed a chromophore, although at 660 nm and not 680 nm as with HemO. Hence, holo MBP-HupZ can degrade heme only when an externally provided imidazole group is present to coordinate the iron. No significant spectral changes were observed in the absence of imidazole (**Figure 4B**), indicating that holo-MBP-HupZ did not degrade the heme.

HupZ Showed Weak Degradation of Heme c (MP11)

All of the heme-degrading proteins described to date catalyze the breakdown of heme b. The one exception is Pden_1323, from *Paracoccus denitrificans*, who also belongs to the HugZ family. Pden_1323 lacks the C-terminal loop that contains the axial heme ligand (His245 in HugZ) but degrades heme c bound to a cytochrome fragment (MP11) (Li et al., 2021). In cytochrome c, the heme iron is coordinated by a histidine in proteaceous region attached to heme c and that histidine is retained in MP11 (Kranz et al., 2009). Since MBP-HupZ can degrade heme if the iron is coordinated by exogenous imidazole, we also tested if it could degrade heme c provided by MP11. MBP-HupZ bound MP11 with a 406-nm Soret and had α and β bands (**Figure 4D**). MBP-HupZ bound to MP11 was then tested for degradation with ferredoxin, NADPH, and NADPH regeneration system (in the presence of catalase). The reaction resulted in a progressive, though limited, decrease in the Soret and the α and β bands (**Figure 4C**). Like with heme b, the HupZ reaction did not produce an absorption peak between 600 and 700 mm. However, subsequent acidification of the solution led to forming a 615-nm chromophore (**Figure 4D**). Together, the data show that using ferredoxin, HupZ only moderately degrades heme b and heme c *in vitro*. It is possible that the fusion with MBP may hinder the degradation or *in vitro* conditions are not optimal.

Heme c Does Not Appear to Serve as an Iron Source for GAS

To test if the observed heme c *in vitro* degradation by HupZ is biologically relevant, we constructed a Δ*hupZ* mutant in GAS by insertion inactivation and assessed the ability of both the wild-type rescue and Δ*hupZ* strains to use a fragment of heme c (MP11) as an iron source (**Figure 5**). Inactivation of *hupZ* had a small positive impact on growth in the regular laboratory THYB (**Figure 5A**). Adding the iron chelator dipyridyl to THYB (THYB-DP) restricted growth in both strains to less than 20% and supplementing the medium with a range of 5–20 μM of MP11 could not significantly restore growth in either strain of bacteria, as indicated by a 1-way ANOVA across treatment types within each strain. There was also no significant difference between wild-type and Δ*hupZ* strains when comparing identical treatment conditions using a Student's *t*-test (**Figure 5**). A 2-way ANOVA covering aggregated data points for wild-type percentage growth to aggregated Δ*hupZ* percentage growth indicated that there was a significant mean difference in the wild type compared to the mutant in the iron-depleted media (17.5% to 14.2%, respectively). Indicating that while GAS does

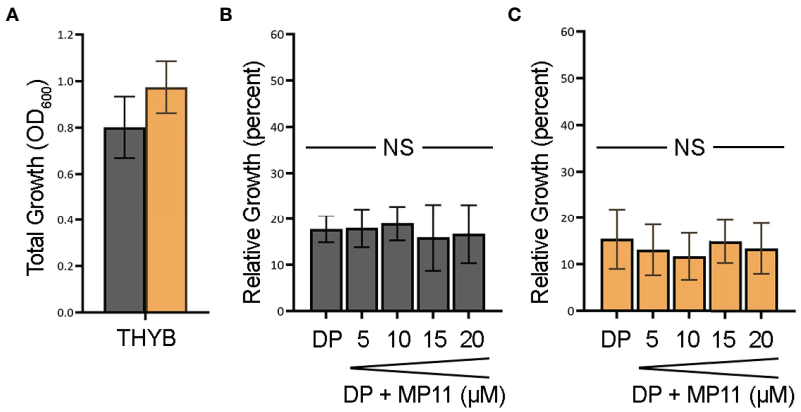

FIGURE 5 | GAS cannot use MP11 as an iron source. Overnight growth of GAS wild-type rescue (gray) and Δ*hupZ* (orange) strains in THYB **(A)**. Relative growth of GAS wild-type rescue THYB-DP with a range of MP-11 compared to THYB growth **(B)**. Relative growth Δ*hupZ* under the same conditions **(C)**. No significance was determined using the Student's *t*-test. NS, not significant.

not utilize MP11 as an iron source, HupZ may provide relief from heme c toxicity.

HupZ Contributes to Heme b Metabolism *In Vivo*

To further evaluate the role of HupZ in heme use *in vivo*, we examined the mutant and the wild-type rescue strain for heme use and sensitivity. Unlike with MP11, supplementation of THYB-DP with hemoglobin at a range of 2.5 to 20 μM restored GAS growth in THYB-DP, indicating that both strains can use hemoglobin as an iron source (**Figures 6A, B**). The hemoglobin dose–response was delayed in the Δ*hupZ* strain compared to the wild-type rescue strain. For complementation, we expressed *hupZ* in trans from GAS *recA* promoter. Comparing the complemented and control (empty vector) strains revealed a small but statistically significant difference between the strains when grown on hemoglobin iron (**Figures 6C, D**). First, data show that losing *hupZ* reduces GAS' ability to use heme iron.

The moderate phenotype of the *hupZ* mutant suggests redundancy in mechanisms to gain iron by GAS. Hence, we also tested the influence of *hupZ* expression on hemoglobin iron use by a heterologous host. HupZ was expressed from the P_{nis} promoter in

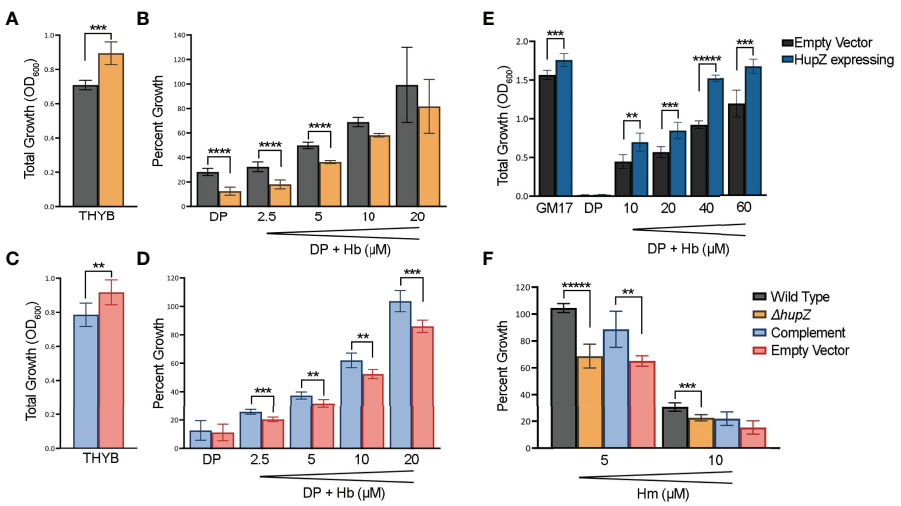

FIGURE 6 | HupZ contributes to bacterial growth on heme b-iron and aids GAS in heme b tolerance. Overnight growth of GAS wild-type rescue (gray) and Δ*hupZ* (orange) strains in THYB **(A)**. Relative growth of GAS wild-type rescue and Δ*hupZ* strains in THYB-DP with a range of hemoglobin (Hb) compared to THYB growth **(B)**. Overnight growth of complement (light blue) and empty vector (pink) in THYB **(C)**. Relative growth of GAS Δ*hupZ* strain with HupZ expressing (light blue, complement) or empty vector (pink) in THYB-DP with a range of HB **(D)**. Overnight growth of *L. lactis* in GM17 **(E)**, GM17-DP, or GM17-DP and a range of Hb, with either an empty (black) or HupZ expressing vector (dark blue). Relative growth of GAS wild-type rescue, complement, and empty vector strains in THYB with either 5 or 10 μM heme (Hm) compared to normal THYB growth **(F)**. The data represent three independent experiments and were analyzed using the Student's *t*-test, where ** indicates a P-value > 0.001, *** > 0.0001, **** > 0.00001, and ***** > 0.000001.

L. lactis (**Figure 6E**). Lactococcal growth in GM17 was inhibited with 10 mM DP. Adding hemoglobin to the iron-restricted medium restored growth, indicating that *L. lactis* can use hemoglobin as an iron source. *L. lactis* expressing *hupZ* responds to a lower hemoglobin concentration and reaches a higher maximal density than the *L. lactis* harboring an empty vector. Second, HupZ promotes the use of heme iron in both GAS and *L. lactis*.

We tested the sensitivity of the GAS mutant and the wild-type rescue strains to free heme (**Figure 6F**). The addition of 5 mM heme to THYB restricted the growth of the *hupZ* mutant while it had no impact on the rescue strain. The addition of 10 μM heme inhibited the growth of both strains, but the wild-type rescue strain grew better than the *hupZ* mutant. Third, *hupZ* helps GAS manage heme toxicity at a low heme concentration.

Loss of *hupZ* Decreases the Fitness of GAS in a Mucosal Colonization Competition

Colonization of the host mucosa constitutes an important first step in GAS pathogenesis *in vivo* (Walker et al., 2014; Zhu et al., 2020). We used a murine colonization model to determine whether *hupZ* plays a role in the ability of GAS to colonize the vaginal mucosa. When wild-type rescue and Δ*hupZ* mutant cells were mixed at a 1:1 ratio and inoculated intravaginally into mice, they were initially able to colonize in approximately equal ratios (**Figure 7**). Following the initial vaginal lavage on day 1, the mutants were no longer able to compete with the WT cells, and the ratio of recovered WT:Δ*hupZ* mutant cells increased dramatically. The data indicate that *hupZ* is important in allowing GAS to maintain host surface colonization.

DISCUSSION

Heme acquisition and iron release are vital for GAS infections, as they supply the pathogen with growth-essential iron in the host environment. GAS lacks genes that share sequence homology to canonical heme oxygenases, and hence how this pathogen processes heme to release the iron is an enigma. We hypothesized that HupZ, a small and presumably cytoplasmic protein, is involved in heme metabolism because it is regulated by MtsR and is co-expressed with the heme receptor, *hupY*. The crystal structure of HupZ-His_6 is similar to the heme-degrading enzyme HugZ, particularly on the split barrel fold of the C-terminal domain (Sachla et al., 2016). HupZ, however, lacks the N-terminal domain. Moreover, *in vitro* analysis revealed that a recombinant HupZ-His_6 binds and degrades heme *in vitro*. Holo-HupZ-His_6 exhibits a UV-VIS spectrum with a prominent Soret and α and β bands in the 500–600 nm range indicative of heme bound with an axial heme ligand (Sachla et al., 2016). Resonance Raman spectroscopy indicated that the axial heme ligand in HupZ-His_6 was a histidine residue, but replacing the only native HupZ histidine residue with alanine did not affect the spectrum (Traore et al., 2021). These observations suggest that one of the six histidine residues in the purification tag interacts in the heme-binding capacity of the recombinant HupZ-His_6 protein.

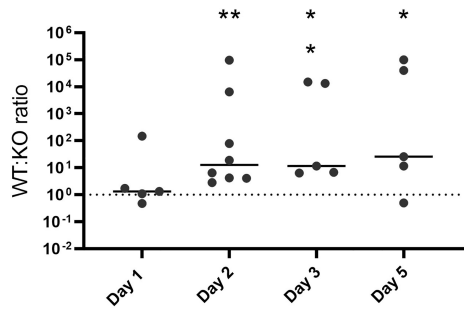

FIGURE 7 | HupZ aids GAS fitness in mucosal colonization model. Mixtures (1:1) of WT and Δ*hupZ* mutant cells were inoculated intravaginally into mice on day 0. Vaginal lavage samples taken at days 1, 2, 3, and 5 post-inoculation were plated to determine the competitive index of WT:Δ*hupZ* mutant cells recovered. By day 2 and through to day 5, significantly fewer Δ*hupZ* mutant cells were recovered compared to WT. The data represent two independent experiments and were analyzed using the Kruskal–Wallis test of ratios, where * indicates a *p*-value > 0.01 and ** > 0.001.

In this study, we examined HupZ's function using biochemical and genetic approaches. Using new recombinant HupZ proteins with a carboxy-terminal fusion to a Strep-tag (HupZ-Strep), a tag-less HupZ, or an amino-terminal fusion to MBP (MBP-HupZ), we demonstrated that HupZ binds heme independently of the tag nature or location (**Figures 1**–**3**). Interestingly, without the His_6 tag, MBP-HupZ does not appear to assemble into the high oligomeric state exhibited by the HupZ-His_6 variant, (**Figure 1C**). This state is thought to promote heme degradation by HupZ-His_6 (Traore et al., 2021). More work, however, is needed to determine the oligomeric state of native HupZ. While the spectrum indicates that HupZ lacks a native axial heme ligand, tag-less and MBP-HupZ exhibited iron coordination provided by free imidazole (**Figures 2** and **3**) or heme c (**Figure 4**).

As we see with HupZ, the protein framework can provide sufficient interactions for binding within a relatively heme-specific binding pocket. Historically, it was presumed that the bond(s) between the heme iron and the amino acid(s) coordinating the iron is the major force holding the heme into the protein. However, experiments on globin and cytochrome mutants in which the proximal histidine was changed to glycine and the side chain was replaced by an imidazole showed that the protein could still incorporate heme even without a coordinate/covalent bond attachment (Schneider et al., 2007). Additionally, mutation of the HugZ axial heme ligand, His245, to alanine, glutamine, or asparagine, could all degrade heme, indicating that the side chain of the residues was not required for enzymatic degradation and may serve a role in the recognition and binding specificity of heme (Hu et al., 2011). Indeed, when the axial heme ligand (His209) of the heme shuttle protein, PhuS, of *P. aeruginosa* is mutated, the *in vitro* protein can coordinate the iron with neighboring His210 or His212 instead (Tripathi et al., 2013).

MBP-HupZ with heme-iron coordinated in the presence of a reducing partner exhibited a weak decrease in the Soret and the α and β band (**Figure 4**). Heme degradation enzymes require reduction partners that provide the electrons necessary for

degradation. Cytochrome P450 reductase is the native reducing partner of the mammalian HO-1. The native partners of most bacterial heme-degrading enzymes are not known. The only exceptions are the ferredoxin reductase FPR in *P. aeruginosa* and the reductases IruO and NtrA in *S. aureus*, which facilitate the reaction of HemO/PigA and IsdG/I, respectively (Wang et al., 2007; Hannauer et al., 2015). Heme degradation with native reducing partners results in forming a linear porphyrin (e.g., biliverdin) and free iron. The HupZ degradation reaction, using ferredoxin as a reducing partner, results in a product that does not have spectral properties. The formation of a chromophore that absorbed at 660 nm after acidification (**Figure 4D**, inset) suggests that the HupZ reaction stopped after the formation of ferric-biliverdin (or a similar molecule), which is missing a spectroscopic signature. Similar observations were made with the heme-degrading enzyme PigA/HemO of *P. aeruginosa*, and HemO of *N. meningitidis*, as well as the oxidoreductive cleavage of verdohemochrome IX-α (Saito and Itano, 1982; Zhu et al., 2000; Ratliff et al., 2001).

MBP-HupZ-bound MP11 spectra contained α and β bands consistent with coordination of the heme iron and limited degradation to a 615-nm chromophore over 6 h (released by acidification, **Figure 4D**). Hence, HupZ weakly degrades heme c *in vitro*. HupZ's dependency on exogenous imidazole and heme c degradation are reminiscent of Pden_1323, the only heme c-degrading enzyme to be described. Still, Pden_1323 fully oxygenates MP11 in 5 min while HupZ facilitates only partial (~0.2–0.4) turnover in 6 h. The weak degradation activity could result from the absence of the native reducing partner or the MBP fusion, or it is not physiologically relevant. To assess the physiological relevance, we tested the ability of WT NZ131 and a Δ*hupZ* strain to use the heme c fragment, MP11, as an iron source but did not see notable growth (**Figure 5**). Pden_1323 and HupZ create a new subgroup in the FMN-binding class of heme-binding or -degrading enzymes. While sharing overall homology with the HugZ protein family, they both lack the C-terminal loop that typically contains the axial heme ligand and the N-terminal α/β domain. This omission creates a larger opening where the heme-binding pocket is believed to be based, allowing Pden_1323 and HupZ to accommodate the larger heme c ligand. Interestingly, HugZ N-terminus is not required for heme degradation; in fact, a C-terminal domain truncated mutant of HugZ demonstrated an increased rate of degradation compared to full-length HugZ (Hu et al., 2011).

In vivo, the loss of *hupZ* results in a decrease in heme b iron use by GAS at low concentrations (**Figure 6B**). The increase in growth on hemoglobin iron exhibited by *L. lactis* expressing *hupZ* provides additional support and *hupZ* contribution to heme b metabolism (**Figure 6E**). Together, these observations are consistent with a function as a heme chaperone.

Transcriptome analysis of GAS during murine vaginal carriage showed that the *hupYZ* operon is significantly upregulated, exhibiting a 27- and 37-fold increase in expression of *hupY* and *hupZ*, respectively, compared with bacteria grown in a chemically defined medium (Cook et al., 2019). We tested the *hupZ* mutant in a murine mucosal colonization competition (**Figure 7**). While the ratio of wild-type rescue to mutant was equal on the first day, by the second day, there were significantly fewer *hupZ* mutant cells recovered than wild-type rescue, a trend that continued through to the 5 days. In all, this indicates that *hupZ* promotes bacterial fitness in the host.

Lastly, polyhistidine tags are one of the most widely used for protein purification. Often the tags are removed after purification by inserting a protease recognition sequence. However, low reaction efficiency coupled with the requirement of costly enzymes and an additional purification step means that they are commonly retained (Jenny et al., 2003; Kielkopf et al., 2021). Yet, as indicated through this work, the utilization of a His_6 tag may be detrimental to determining the function of a protein, as the histidine residue may interact with an unintended epitope. The retention of these tags during experimental conditions can also change ligand binding dynamics. The two-dimensional infrared vibrational echo spectroscopy of His_6-myoglobin showed a significant change in the short time scale dynamics of binding carbon monoxide compared to native myoglobin, although there was no effect on the UV/VIS spectra (Thielges et al., 2011). The terminal placement (i.e., amino or carboxy) affects the product regiospecificity of the carbonyl reductase S1 from *Candida magnoliae* (Haas et al., 2017). With HupZ-His_6, the tag not only interacted with the bound heme but also promoted higher oligomeric states. Given histidine's propensity to affect protein dynamics and regiospecificity, along with their prominences in heme-binding pockets, they may not be suitable for heme-binding studies.

In summary, HupZ binds heme b and heme c and relies on exogenous imidazole for degradation *in vitro*. GAS mutants lacking *hupZ* can use heme iron albeit less efficiently. These observations, combined with the low turnover in heme b and MP-11 *in vitro* degradations, suggest that *in vivo* HupZ is likely a heme chaperone, or it contributes to heme detoxification by a yet-to-be-defined mechanism.

DATA AVAILABILITY STATEMENT

The raw data supporting the conclusions of this article will be made available by the authors, without undue reservation.

ETHICS STATEMENT

The animal study was reviewed and approved by Binghamton University Laboratory Animal Resources (LAR) and by the Binghamton Institutional Animal Care and Use Committee (IACUC) under protocols 803-18 and 857-21.

AUTHOR CONTRIBUTIONS

LT conducted the mouse model under the direction of LC. CO generated the tag-less HupZ and KL conducted the remaining experiments, both under the supervision of ZE. KL generated the figures and both she and ZE contributed equally to the generation of the manuscript. All authors contributed to the article and approved the submitted version.

FUNDING

KL received a Fellowship through the Georgia State University Molecular Basis of Disease program.

ACKNOWLEDGMENTS

Thank you to Dr. Nicholas Noinaj of Purdue University for providing the purified TEV protease and the pRK793 expression vector.

REFERENCES

Barnett, T. C., Bowen, A. C., and Carapetis, J. R. (2018). The Fall and Rise of Group A Streptococcus Diseases. *Epidemiol. Infect.* 147, E4. doi: 10.1017/S0950268818002285

Bates, C. S., Montanez, G. E., Woods, C. R., Vincent, R. M., and Eichenbaum, Z. (2003). Identification and Characterization of a Streptococcus Pyogenes Operon Involved in Binding of Hemoproteins and Acquisition of Iron. *Infect. Immun.* 71 (3), 1042–1055. doi: 10.1128/IAI.71.3.1042-1055.2003

Bates, C. S., Toukoki, C., Neely, M. N., and Eichenbaum, Z. (2005). Characterization of MtsR, a New Metal Regulator in Group A Streptococcus, Involved in Iron Acquisition and Virulence. *Infect. Immun.* 73 (9), 5743–5753. doi: 10.1111/j.1365-2958.2010.07157.x

CDC. Centers for Disease Control and Prevention (2019). Active Bacterial Core Surveillance Report, Emergin Infections Program Network, Group A Streptococcus, 2019. Available at: www.cdc.gov/abcs/downloads/GAS_Surveillance_Report_2019.pdf.

Chaffin, D. O., and Rubens, C. E. (1998). Blue/white Screening of Recombinant Plasmids in Gram-Positive Bacteria by Interruption of Alkaline Phosphatase Gene (phoZ) Expression. *Gene* (1998) 219 (1-2), 91–9. doi: 10.1016/s0378-1119(98)00396-5

Chatterjee, N., Cook, L. C. C., Lyles, K. V., Nguyen, H. A. T., Devlin, D. J., Thomas, L. S., et al. (2020). Novel Heme Transporter From the Energy Coupling Factor Family Is Vital for Group A Streptococcus Colonization and Infections. *A. J. Bacteriol.* 202 (14), e000205-20. doi: 10.1128/JB.00205-20

Cook, L. C. C., Chatterjee, N., Li, Y., Andrade, J., Federle, M. J., and Eichenbaum, Z. (2019). Transcriptomic Analysis of Streptococcus Pyogenes Colonizing the Vaginal Mucosa Identifies Hupy, an MtsR-Regulated Adhesin Involved in Heme Utilization. *mBio.* 10 (3), e00848-19. doi: 10.1128/mBio.00848-19

Cook, L., Hu, H., Maienschein-Cline, M., and Federle, M. (2018). A Vaginal Tract Signal Detected by the Group B Streptococcus SaeRS System Elicits Transcriptomic Changes and Enhances Murine Colonization. *Infect. Immun.* 86 (4), e00762–e00717. doi: 10.1128/IAI.00762-17

Davies, M. R., Holden, M. T., Coupland, P., Chen, J. H., Venturini, C., Barnett, T. C., et al. (2015). Emergence of Scarlet Fever Streptococcus Pyogenes Emm12 Clones in Hong Kong is Associated With Toxin Acquisition and Multidrug Resistance. *Nat. Genet.* 47 (1), 84–87. doi: 10.1038/ng.3147

de Ruyter, P. G., Kuipers, O. P., and de Vos, W. M. (1996). Controlled Gene Expression Systems for Lactococcus Lactis With the Food-Grade Inducer Nisin. *Appl. Environm. Microbiol.*, 62(10), 3662–3667. doi: doi: 10.1128/aem.62.10.3662-3667.1996

Giovannetti, R. (2012). "The Use of Spectropotometry UV-Vis for the Study of Porphyrins," in *Macro to Nano Spectroscopy*. Ed. J. Uddin (Croatia: InTech).

Haas, J., Hackh, M., Justus, V., Muller, M., and Ludeke, S. (2017). Addition of a Polyhistidine Tag Alters the Regioselectivity of Carbonyl Reductase S1 From Candida Magnoliae. *Org. Biomol. Chem.* 15 (48), 10256–10264. doi: 10.1039/C7OB02666H

Hannauer, M., Arifin, A. J., and Heinrichs, D. E. (2015). Involvement of Reductases IruO and NtrA in Iron Acquisition by Staphylococcus Aureus. *Mol. Microbiol.* 96 (6), 1192–1210. doi: 10.1111/mmi.13000

Hu, Y., Jiang, F., Guo, Y., Shen, X., Zhang, Y., Zhang, R., et al. (2011). Crystal Structure of HugZ, a Novel Heme Oxygenase From Helicobacter Pylori. *J. Biol. Chem.* 286 (2), 1537–1544. doi: 10.1074/jbc.m110.172007

Jenny, R. J., Mann, K. G., and Lundblad, R. L. (2003). A Critical Review of the Methods for Cleavage of Fusion Proteins With Thrombin and Factor Xa. *Protein Expr. Purif.* 31 (1), 1–11. doi: 10.1016/s1046-5928(03)00168-2

Kielkopf, C. L., Bauer, W., and Urbatsch, I. L. (2021). Expressing Cloned Genes for Protein Production, Purification, and Analysis. *Cold Spring Harb. Protoc.* 2021 (2), 43–69. doi: 10.1101/pdb.top102129

Kleerebezem, M., Beerthuyzen, M. M., Vaughan, E. E., De Vos, W. M., and Kuipers, O. P. (1997). Controlled Gene Expression Systems for Lactic Acid Bacteria: Transferable Nisin-Inducible Expression Cassettes for Lactococcus, Leuconostoc, and Lactobacillus Spp. *Applied and Environmental Microbiology*. (1997) 63 (11), 4581–4.

Kranz, R. G., Richard-Fogal, C., Taylor, J. S., and Frawley, E. R. (2009). Cytochrome C Biogenesis: Mechanisms for Covalent Modifications and Trafficking of Heme and for Heme-Iron Redox Control. *Microbiol. Mol. Biol. Rev.* 73 (3), 510–528. doi: 10.1128/MMBR.00001-09

Kudou, M., Yumioka, R., Ejima, D., Arakawa, T., and Tsumoto, K. (2011). A Novel Protein Refolding System Using Lauroyl-L-Glutamate as a Solubilizing Detergent and Arginine as a Folding Assisting Agent. *Protein Expr. Purif.* 75 (1), 46–54. doi: 10.1016/j.pep.2010.08.011

Li, S., Isiorho, E. A., Owens, V. L., Donnan, P. H., Odili, C. L., and Mansoorabadi, S. O. (2021). A Noncanonical Heme Oxygenase Specific for the Degradation of C-Type Heme. *J. Biol. Chem.* 296, 100666. doi: 10.1016/j.jbc.2021.100666

Lyles, K. V., and Eichenbaum, Z. (2018). From Host Heme To Iron: The Expanding Spectrum of Heme Degrading Enzymes Used by Pathogenic Bacteria. *Front. Cell Infect. Microbiol.* 8, 198. doi: 10.3389/fcimb.2018.00198

Marchetti, M., De Bei, O., Bettati, S., Campanini, B., Kovachka, S., Gianquinto, E., et al. (2020). Iron Metabolism at the Interface Between Host and Pathogen: From Nutritional Immunity to Antibacterial Development. *Int. J. Mol. Sci.* 21 (6), 1–44. doi: 10.3390/ijms21062145

Patras, K. A., and Doran, K. S. (2016). A Murine Model of Group B Streptococcus Vaginal Colonization. *J. Vis. Exp.* 117 (117), 54708. doi: 10.3791/54708

Porter, N. J., and Christianson, D. W. (2019). Preparation of a New Construct of Human Histone Deacetylase 8 for the Crystallization of Enzyme-Inhibitor Complexes. *Methods Enzymol.* 626, 561–585. doi: 10.1016/bs.mie.2019.06.029

Ratliff, M., Zhu, W., Deshmukh, R., Wilks, A., and Stojiljkovic, I. (2001). Homologues of Neisserial Heme Oxygenase in Gram-Negative Bacteria: Degradation of Heme by the Product of the pigA Gene of Pseudomonas Aeruginosa. *J. Bacteriol.* 183 (21), 6394–6403. doi: 10.1128/JB.183.21.6394-6403.2001

Sachla, A. J., Ouattara, M., Romero, E., Agniswamy, J., Weber, I. T., Gadda, G., et al. (2016). *In Vitro* Heme Biotransformation by the HupZ Enzyme From Group A Streptococcus. *Biometals.* 29 (4), 593–609. doi: 10.1007/s10534-016-9937-1

Saito, S., and Itano, H. A. (1982). Verdohemochrome IX Alpha: Preparation and Oxidoreductive Cleavage to Biliverdin IX Alpha. *Proc. Natl. Acad. Sci. U. S. A.* 79 (5), 1393–1397. doi: 10.1073/pnas.79.5.1393

Schmitt, M. P. (1997). Utilization of Host Iron Sources by Corynebacterium Diphtheriae: Identification of a Gene Whose Product is Homologous to Eukaryotic Heme Oxygenases and is Required for Acquisition of Iron From Heme and Hemoglobin. *J. Bacteriol.* 179 (3), 838–845. doi: 10.1128/jb.179.3.838-845.1997

Schneider, S., Marles-Wright, J., Sharp, K. H., and Paoli, M. (2007). Diversity and Conservation of Interactions for Binding Heme in B-Type Heme Proteins. *Nat. Prod. Rep.* 24 (3), 621–630. doi: 10.1039/B604186H

Skaar, E. P., Gaspar, A. H., and Schneewind, O. (2004). IsdG and IsdI, Heme-Degrading Enzymes in the Cytoplasm of Staphylococcus Aureus. *J. Biol. Chem.* 279 (1), 436–443. doi: 10.1074/jbc.M307952200

Sun, X., Ge, R., Zhang, D., Sun, H., and He, Q. Y. (2010). Iron-Containing Lipoprotein SiaA in SiaABC, the Primary Heme Transporter of Streptococcus Pyogenes. *J. Biol. Inorg. Chem.* 15 (8), 1265–1273. doi: 10.1007/s00775-010-0684-4

Tenhunen, R., Marver, H. S., and Schmid, R. (1969). Microsomal Heme Oxygenase. Characterization of the Enzyme. *J. Biol. Chem.* 244 (23), 6388–6394. doi: 10.1016/S0021-9258(18)63477-5

Thielges, M. C., Chung, J. K., Axup, J. Y., and Fayer, M. D. (2011). Influence of Histidine Tag Attachment on Picosecond Protein Dynamics. *Biochemistry.* 50 (25), 5799–5805. doi: 10.1021/bi2003923

Traore, E. S., Li, J., Chiura, T., Geng, J., Sachla, A. J., Yoshimoto, F., et al. (2021). Heme Binding to HupZ With a C-Terminal Tag From Group A Streptococcus. *Molecules* 26 (3), 1–19. doi: 10.3390/molecules26030549

Tripathi, S., O'Neill, M. J., Wilks, A., and Poulos, T. L. (2013). Crystal Structure of the Pseudomonas Aeruginosa Cytoplasmic Heme Binding Protein, Apo-PhuS. *J. Inorg. Biochem.* 128, 131–136. doi: 10.1016/j.jinorgbio.2013.07.030

Tropea, J. E., Cherry, S., and Waugh, D. S. (2009). Expression and Purification of Soluble His(6)-Tagged TEV Protease. *Methods Mol. Biol.* 498, 297–307. doi: 10.1007/978-1-59745-196-3_19

Vagenende, V., Yap, M. G., and Trout, B. L. (2009). Mechanisms of Protein Stabilization and Prevention of Protein Aggregation by Glycerol. *Biochemistry* 48 (46), 11084–11096. doi: 10.1021/bi900649t

Walker, M. J., Barnett, T. C., McArthur, J. D., Cole, J. N., Gillen, C. M., Henningham, A., et al. (2014). Disease Manifestations and Pathogenic Mechanisms of Group A Streptococcus. *Clin. Microbiol. Rev.* 27 (2), 264–301. doi: 10.1128/CMR.00101-13

Wang, A., Zeng, Y., Han, H., Weeratunga, S., Morgan, B. N., Moenne-Loccoz, P., et al. (2007). Biochemical and Structural Characterization of Pseudomonas Aeruginosa Bfd and FPR: Ferredoxin NADP+ Reductase and Not Ferredoxin is the Redox Partner of Heme Oxygenase Under Iron-Starvation Conditions. *Biochemistry* 46 (43), 12198–12211. doi: 10.1021/bi7013135

Watkins, D. A., Johnson, C. O., Colquhoun, S. M., Karthikeyan, G., Beaton, A., Bukhman, G., et al. (2017). Global, Regional, and National Burden of Rheumatic Heart Disease, 1990-2015. *N. Engl. J. Med.* 377 (8), 713–722. doi: 10.1056/NEJMoa1603693

Wilks, A., and Heinzl, G. (2014). Heme Oxygenation and the Widening Paradigm of Heme Degradation. *Arch. Biochem. Biophys.* 544, 87–95. doi: 10.1016/j.abb.2013.10.013

Wilks, A., and Ikeda-Saito, M. (2014). Heme Utilization by Pathogenic Bacteria: Not All Pathways Lead to Biliverdin. *Acc. Chem. Res.* 47 (8), 2291–2298. doi: 10.1021/ar500028n

Wissbrock, A., George, A. A. P., Brewitz, H. H., Kuhl, T., and Imhof, D. (2019). The Molecular Basis of Transient Heme-Protein Interactions: Analysis, Concept and Implementation. *Bioscience Rep.* 39, 1–11. doi: 10.1042/BSR20181940

Zhang, R., Zhang, J., Guo, G., Mao, X., Tong, W., Zhang, Y., et al. (2011). Crystal Structure of Campylobacter Jejuni ChuZ: A Split-Barrel Family Heme Oxygenase With a Novel Heme-Binding Mode. *Biochem. Biophys. Res. Commun.* 415 (1), 82–87. doi: 10.1016/j.bbrc.2011.10.016

Zhu, L., Olsen, R. J., Beres, S. B., Ojeda Saavedra, M., Kubiak, S. L., Cantu, C. C., et al. (2020). Genome-Wide Screens Identify Group A Streptococcus Surface Proteins Promoting Female Genital Tract Colonization and Virulence. *Am. J. Pathol.* 190 (4), 862–873. doi: 10.1016/j.ajpath.2019.12.003

Zhu, W., Wilks, A., and Stojiljkovic, I. (2000). Degradation of Heme in Gram-Negative Bacteria: The Product of the hemO Gene of Neisseriae is a Heme Oxygenase. *J. Bacteriol.* 182 (23), 6783–6790. doi: 10.1128/JB.182.23.6783-6790.2000

Conflict of Interest: The authors declare that the research was conducted in the absence of any commercial or financial relationships that could be construed as a potential conflict of interest.

Publisher's Note: All claims expressed in this article are solely those of the authors and do not necessarily represent those of their affiliated organizations, or those of the publisher, the editors and the reviewers. Any product that may be evaluated in this article, or claim that may be made by its manufacturer, is not guaranteed or endorsed by the publisher.

frontiers | Frontiers in Cellular and Infection Microbiology

REVIEW
published: 30 June 2022
doi: 10.3389/fcimb.2022.909888

Acclimation to Nutritional Immunity and Metal Intoxication Requires Zinc, Manganese, and Copper Homeostasis in the Pathogenic *Neisseriae*

Alexis Hope Branch[1], *Julie L. Stoudenmire*[1], *Kate L. Seib*[2] *and Cynthia Nau Cornelissen*[1]*

[1] Center for Translational Immunology, Institute for Biomedical Sciences, Georgia State University, Atlanta, GA, United States, [2] Institute for Glycomics, Griffith University, Gold Coast, QLD, Australia

OPEN ACCESS

Edited by:
Mauricio H. Pontes, The Pennsylvania State University, United States

Reviewed by:
Michael D. L. Johnson, University of Arizona, United States
Jacob P. Bitoun, Tulane University, United States

***Correspondence:**
Cynthia Nau Cornelissen
ccornelissen@gsu.edu

Specialty section:
This article was submitted to Bacteria and Host, a section of the journal Frontiers in Cellular and Infection Microbiology

Received: *31 March 2022*
Accepted: *18 May 2022*
Published: *30 June 2022*

Citation:
Branch AH, Stoudenmire JL, Seib KL and Cornelissen CN (2022) Acclimation to Nutritional Immunity and Metal Intoxication Requires Zinc, Manganese, and Copper Homeostasis in the Pathogenic Neisseriae. Front. Cell. Infect. Microbiol. 12:909888. doi: 10.3389/fcimb.2022.909888

Neisseria gonorrhoeae and *Neisseria meningitidis* are human-specific pathogens in the Neisseriaceae family that can cause devastating diseases. Although both species inhabit mucosal surfaces, they cause dramatically different diseases. Despite this, they have evolved similar mechanisms to survive and thrive in a metal-restricted host. The human host restricts, or overloads, the bacterial metal nutrient supply within host cell niches to limit pathogenesis and disease progression. Thus, the pathogenic *Neisseria* require appropriate metal homeostasis mechanisms to acclimate to such a hostile and ever-changing host environment. This review discusses the mechanisms by which the host allocates and alters zinc, manganese, and copper levels and the ability of the pathogenic *Neisseria* to sense and respond to such alterations. This review will also discuss integrated metal homeostasis in *N. gonorrhoeae* and the significance of investigating metal interplay.

Keywords: metal intoxication, nutritional immunity, *Neisseria gonorrhoeae*, *Neisseria meningitidis*, zinc, manganese, copper, integrated metal homeostasis

INTRODUCTION - PATHOGENIC *NEISSERIAE* CAUSE DEVASTATING YET DISTINCT DISEASES TO THE HUMAN HOST

Neisseria gonorrhoeae and *Neisseria meningitidis* are human-specific pathogens of significant public health concern. Despite high DNA and amino acid sequence identity, *N. gonorrhoeae* and *N. meningitidis* cause significantly different diseases (Tinsley and Nassif, 1996; Perrin et al., 2002).

N. gonorrhoeae is the causative agent of the second most common reportable infectious disease in the United States, gonorrhea, and predominantly colonizes the genital mucosal epithelium and oropharynx (CDC, 2019b). Symptomatic gonococcal infection presents as urethritis, cervicitis, salpingitis, pharyngitis or conjunctivitis (CDC, 2019b). However, gonorrhea can present asymptomatically as well. Asymptomatic infection in women is of great concern as it enables the pathogen to ascend to the upper reproductive tract, where it can cause pelvic inflammatory disease. Pelvic inflammatory disease can lead to ectopic pregnancy, scarring, infertility, and chronic pelvic

pain. In 2018, the incidence of gonococcal disease was 179.1 cases per 100,000, correlating with a total of 583,404 reported cases in the United States (CDC, 2019b).

N. meningitidis can inhabit the nasopharynx without eliciting symptoms; this carrier state can be found in 5-10% of the US population (CDC, 2019c). The carrier state can transition to symptomatic disseminated infection, sometimes referred to as invasive meningococcal disease (IMD), which is characterized by nausea, vomiting, rash, stiffness of neck, fever, and diarrhea (CDC, 2019c). While the incidence of meningococcal disease has decreased dramatically from ~1.50 per 100,000 in 1980 to ~0.2 per 100,000 in 2018, IMD remains a severe threat to infants. Incidence of IMD in children younger than 1 year has averaged around 1.20 per 100,000 in the past 10 years (CDC, 2019a). About 12% of infections result in death, and some survivors experience permanent brain damage, loss of limbs or hearing loss (Candrilli, 2019; CDC, 2019a).

While the pathogenic *Neisseriae* pose a direct threat to human health, they also represent a substantial economic burden in the United States. In 2018, gonorrhea infections resulted in an estimated $85 million in direct medical costs in the United States (Kumar et al., 2021). The estimated total cost of the response to an IMD outbreak at the University of Oregon Hospital (7 cases) and the Oregon State University Hospitals (6 cases) was $12.3 million (Candrilli, 2019).

During neisserial infection, the host limits bacterial proliferation by modulating metal availability through two related mechanisms: nutritional immunity and metal intoxication. Nutritional immunity is characterized by host sequestration of free metals from the bacterial nutrient supply, limiting metals required for enzymatic and metabolic functions (Hennigar and McClung, 2016). Metal intoxication is the process by which the host overloads pathogens with toxic metal concentrations (Becker and Skaar, 2014). Metal overload in bacteria contributes to reactive oxygen species (ROS) and reactive nitrogen species (RNS) cycling (Djoko et al., 2012), protein mismetallation (Veyrier et al., 2011), and subsequent stalling of respiration (Djoko and McEwan, 2013). Pathogenic bacteria have evolved mechanisms to access restricted metals as well as limit metal overload.

Metal availability within a biological niche dictates pathogen survival and the extent of pathogenesis. Although causing distinct disease presentations, pathogenic *Neisseria* share many mechanisms of responding to metal scarcity and overload to ensure survival and maintain virulence. This review aims to provide an overview of the neisserial response to nutritional immunity and metal intoxication with respect to zinc, manganese, and copper.

ZINC, MANGANESE, AND COPPER ARE ALLOCATED TO SPECIFIC HOST NICHES

Transition metals, such as zinc, manganese, and copper, are essential to many host processes, including oxidative stress resistance (Girotto et al., 2014; Jarosz et al., 2017; Ganini et al., 2018), cell signaling and metabolism (Maares et al., 2018), immune modulation (Hu Frisk et al., 2017), post-translational modifications (Braiterman et al., 2015; Tidball et al., 2015), and structural maintenance and enzymatic processing (Tidball et al., 2015; Ganini et al., 2018). These metals play similar roles in pathogens including *Neisseria meningitidis* (Persson et al., 2001; Pawlik et al., 2012; Hecel et al., 2018) and *Escherichia coli* (Kaur et al., 2017).

Zinc within the human body is primarily localized to the bone and skeletal muscle, with moderate concentrations found in the kidneys and liver (Jackson, 1989). Most zinc, however, is metabolically unavailable to the host due to slow zinc turnover with the exception being zinc found in the sperm (Baer and King, 1984). High levels of zinc-binding metallothioneins (Suzuki et al., 1994), which maintain zinc and copper homeostasis and limit heavy toxicity in host cells (Rahman and Karim, 2018), can be found in male secretions (Suzuki et al., 1992). It is feasible that zinc-binding metallothioneins help create a zinc limited environment for the gonococcus during male urethral infection. The majority of zinc within the host is not easily accessible to pathogens due to a limited pool of labile zinc (Brown et al., 2001), which can be further restricted during infection by production of calprotectin and other S100 proteins that act to sequester free zinc away from the pathogen (Yadav et al., 2020). Calprotectin makes up 45% of the protein content in neutrophils (Edgeworth et al., 1991) and is released following neutrophil death (Voganatsi et al., 2001) and Neutrophil Extracellular Trap (NET) formation (Urban et al., 2009). The zinc sequestering protein, S100A7, is enriched in lower genital tract epithelial cells (Mildner et al., 2010). In the case of mucosal infection by *N. gonorrhoeae*, a robust Th17 response results in the influx of neutrophils (Liu and Russell, 2011). Thus, S100A7 and calprotectin, which has been released by neutrophils, create a zinc limited environment for *N. gonorrhoeae* (Zackular et al., 2015). The remaining zinc is dispersed among the reproductive (Baer and King, 1984) and immune systems (Brown et al., 2001).

Within the human host, manganese exists as Mn^{2+} and Mn^{3+} (O'Neal and Zheng, 2015). Mn^{2+} is found in the blood bound to albumin, ß-globulin, bicarbonate, and citrate, and in the cytosolic content of neutrophils bound to calprotectin (O'Neal and Zheng, 2015; Zackular et al., 2015). Within the cell, Mn^{2+} is found at the highest concentrations in the endoplasmic reticulum and mitochondria, where it plays an antioxidant role through Mn-dependent superoxide dismutase (MnSOD) (Maynard and Cotzias, 1955; Ganini et al., 2018). In neurons, Mn^{2+} is required for signal transduction and enzymatic function (Gunter et al., 2013; Tidball et al., 2015). Excess Mn^{2+} accumulates in the liver, kidneys, bone, and pancreas, with higher levels bound to regulatory proteins in the brain and cerebrospinal fluid. Mn^{3+} can be bound to transferrin, which transports Mn^{3+} to neuronal cells in a mechanism similar to Fe^{3+} transport (Chen et al., 2001; Gunter et al., 2013). Many Gram-negative pathogens utilize Mn^{2+} (i.e. *Acinetobacter baumanii, Salmonella enterica, E. coli, Helicobacter pylori*, and *N. gonorrhoeae*), in the face of nutritional immunity, for oxidative stress resistance and metabolism (Tseng et al., 2001; Kehres et al., 2002b; Anjem et al., 2009; Lee et al., 2010; Diaz-Ochoa et al.,

2016; Juttukonda et al., 2016). During gonococcal infection of macrophages, the manganese transport protein Natural resistance-associated macrophage protein 1 (NRAMP1) (Jabado et al., 2000), is upregulated on the phagosomal membrane (Forbes and Gros, 2003; Zughaier et al., 2014). NRAMP1 shuttles manganese from the phagosomal compartment to the cell cytosol to restrict pathogen access to manganese. Consequently *N. gonorrhoeae* may experience manganese limitation in the endolysosomal compartment following phagocytosis by macrophages (Ivanov et al., 2022).

Copper is found primarily in the liver and plasma in free and ceruloplasmin-bound forms (Dunn et al., 1991). Ceruloplasmin facilitates copper transport through the vasculature and possesses the ferroxidase activity necessary for the oxidation of Fe^{2+} to Fe^{3+} and subsequent iron loading of transferrin (Ramos et al., 2016; Hyre et al., 2017). Ceruloplasmin is also transported to the urinary tract during human infection (Hyre et al., 2017). Thus, *N. gonorrhoeae* may experience ceruloplasmin-dependent copper limitation in addition to S100 protein-dependent zinc limitation at the mucosal surface. Copper can also be found within the cytosol of neutrophils, which are recruited to the gonococcal infection site (Johnson and Criss, 2011; Sintsova et al., 2014), following import by CTR1 on the neutrophil membrane (Zhou and Gitschier, 1997; Cichon et al., 2020).

METAL ACQUISITION BY THE PATHOGENIC *NEISSERIAE* IN METAL-RESTRICTED NICHES REQUIRES HIGHLY SPECIFIC METAL IMPORT

Metal import poses a particular challenge to Gram-negative bacteria, as it requires transport across a two-component cell wall. Outer membrane transport utilizes the proton motive force and requires energy transduction, *via* the Ton system, from the cytoplasmic membrane. Scarce metals (i.e., zinc, manganese, and copper) are transported into the cytoplasm in an ATP-driven mechanism, which is often tightly regulated to avoid metal overload, protein mismetallation, and oxidative stress. Highly specific metal transport is required in a host that uses metal sequestration to restrict microbial growth and pathogenesis.

In the human host, which allocates metals to specific niches, the pathogenic *Neisseria, N. gonorrhoeae and N. meningitidis*, have evolved mechanisms to acquire zinc, manganese, and copper in specific environments. Gonococcal TdfH and TdfJ are zinc-specific TonB-dependent transporters that pirate zinc from calprotectin (Kammerman et al., 2020) and S100A7 (Maurakis et al., 2019), respectively, to transport that zinc across the outer membrane to the periplasm (**Figure 1**). Gonococcal TdfH binds calprotectin through a high-affinity bimodal interaction. TdfH interacts with a tetramer of calprotectin, which itself is a heterodimer of S100A8 and S100A9 (Bera et al., 2022). Interestingly, gonococcal growth when calprotectin is the sole zinc source requires the presence of zinc in site 1 of calprotectin, the preferred zinc utilization site by gonococcal TdfH. Mutant calprotectin unable to bind zinc at site 2 fully supports gonococcal growth (Kammerman et al., 2020). The cryoEM structure of the calprotectin:TdfH complex has been

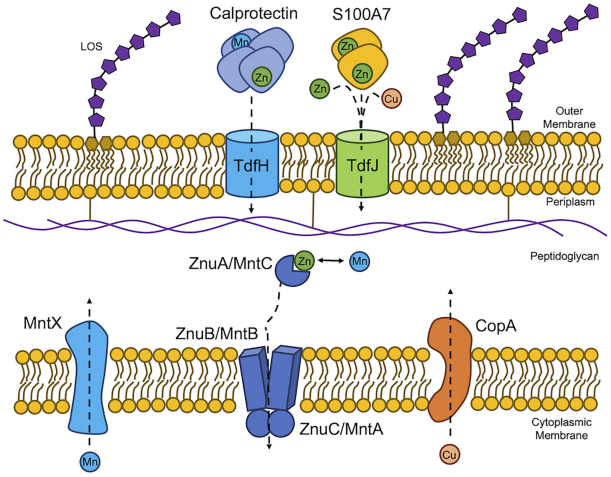

FIGURE 1 | *Neisseria gonorrhoeae* and *Neisseria meningitidis* experience host-driven nutritional immunity and metal intoxication. The host exerts nutritional immunity on the pathogenic *Neisseriae* by exposing the bacteria to calprotectin and S100A7. Calprotectin sequesters both zinc (Zn) and manganese (Mn) from the extracellular environment to limit Zn and Mn availability. *N. gonorrhoeae* in turn expresses TdfH, which has been shown to strip Zn from calprotectin and subsequently import the ion. TdfH is able bind Mn-loaded calprotectin suggesting a role for Mn import across the outer membrane. TdfH is referred to as CbpA in *N. meningitidis*. S100A7 also sequesters Zn from the extracellular environment. Gonococcal TdfJ binds S100A7 to pirate and import the Zn payload. Lipooligosaccharide (LOS) is shown in the outer membrane for reference. Once in the periplasm, Zn and Mn are chaperoned by the periplasmic binding protein, ZnuA (MntC) to the permease in the cytoplasmic membrane, ZnuB (MntB). Transport across the cytoplasmic membrane is energized by the ATPase, ZnuC (MntA). The host also exerts metal intoxication, specifically copper (Cu) intoxication on *N. gonorrhoeae* and Mn intoxication in *N. meningitidis* through unknown mechanisms. In response, these efflux proteins export excess cytoplasmic Cu or Mn from to the periplasmic space.

determined by Bera et al. (Bera et al., 2022). Since site 1 of calprotectin is capable of binding both zinc and manganese (Gagnon et al., 2015) and gonococcal TdfH is able to bind manganese-loaded calprotectin (Bera et al., 2022), it is feasible that TdfH may also be a manganese importer. The meningococcal TdfH homolog was renamed calprotectin-binding protein A (CbpA); this protein has been shown to bind to zinc- or manganese-loaded calprotectin (**Table 1**) with higher affinity than it does to unloaded calprotectin, demonstrating a preference for metalated calprotectin over the apo form (**Figure 1**) (Stork et al., 2013). Gonococcal TdfJ was shown to bind S100A7 with high specificity and to use the human protein as a zinc source (Maurakis et al., 2019). Similarly, the meningococcal homolog of TdfJ is a zinc-specific importer required for zinc import during zinc limitation (Stork et al., 2010).

After crossing the outer membrane, metals must be escorted across the periplasm to transporters in the cytoplasmic membrane. Metal chaperoning across the periplasm is often accomplished by periplasmic metal-binding proteins (PBP) of the Cluster A-I substrate-binding protein family. PBP transport precedes the ATP-dependent transport step through the cytoplasmic membrane (Dintilhac and Claverys, 1997;

TABLE 1 | *Neisseria gonorrhoeae* (Ng) and *Neisseria meningitidis* (Nm) express proteins which are potentially involved in integrated metal homeostasis.

Ng protein (Affinity [ligand])	Nm protein	Metals associated with ligand	Reference
TdfH (4 nM and 35 μM [calprotectin])	CbpA	Zn, Mn	(Pawlik et al., 2012; Stork et al., 2013; Jean et al., 2016; Kammerman et al., 2020)
TdfJ (nk, (S100A7))	ZnuD	Zn, Cu, Fe, Cd	(Jean et al., 2016; Hecel et al., 2019; Maurakis et al., 2019)
TbpB (7.4 nM [transferrin])	TbpB	Mn, Fe	(Cornelissen and Sparling, 1996; Ronpirin et al., 2001; Wu et al., 2010)
ZnuCBA/MntABC (100 ± 8 nM [Mn^{2+}]; 104 ± 5 nM [Zn^{2+}])	ZnuCBA/MntABC	Zn, Mn	(Chen and Morse, 2001; Tseng et al., 2001; Wu et al., 2006)
MntX (nk, [Mn^{2+}])	MntX	Mn, Fe	(Veyrier et al., 2011)
Zur/PerR (nk, [Mn^{2+}])	Zur	Zn, Mn	(Wu et al., 2006; Pawlik et al., 2012; Jean et al., 2016)

nk, (not known) indicates the affinity for that ligand is not known. These proteins have been shown to be regulated by or interact with multiple metals.

Berntsson et al., 2010). Precise metal transport across the periplasm is required for acclimation to the specific metal environments encountered by Gram-negative pathogens (Lewis et al., 1999; Ammendola et al., 2007; Davies and Walker, 2007; Lim et al., 2008; Davis et al., 2009; Desrosiers et al., 2010; Pederick et al., 2015). PBPs deliver specific metals to permeases in the cytoplasmic membrane, where an ATPase then hydrolyzes ATP to energize metal transport into the cytoplasm.

N. gonorrhoeae express a zinc import system encoded by *znuCBA* (NGO_0170-_0168) (accession number NC_002946) where the gene products, ZnuC, ZnuB, and ZnuA are the ATPase, permease, and PBP, respectively (**Figure 2** and **Table 1**). ZnuCBA transports zinc through the periplasm and across the cytoplasmic membrane. A *znuA* mutant was growth deficient in the presence of all supplemental metals (i.e. Mg^{2+}, Mn^{2+}, Cu^{2+}, Ni^{2+}, Fe^{2+}, Fe^{3+}, Ca^{2+}, and Cd^{2+}) except Zn^{2+}, demonstrating the specificity of this importer for zinc, over other metals, under these conditions (Chen and Morse, 2001). Growth only with supplemental zinc suggests that the gonococcus requires specific zinc import *via* ZnuA for cellular processes that cannot be completed with substituting metals under these conditions.

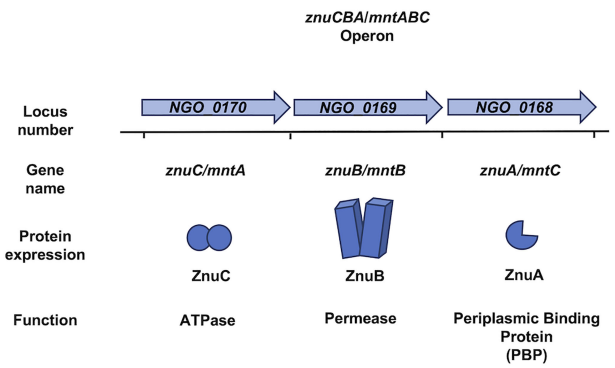

FIGURE 2 | The genome of *Neisseria gonorrhoeae* and *Neisseria meningitidis* encodes the *znuCBA/mntABC* operon. The *znuCBA* operon in *N. gonorrhoeae* is indicated by the locus numbers NGO_0170, NGO_0169, and NGO_0168. The operon is named in order of predicted transcriptional direction. NGO_0170 encodes an ATPase named ZnuC which provides energy from zinc (Zn) transport into the cytoplasm. NGO_0169 encodes a permease named ZnuB which serves as a channel for transporting Zn through the cytoplasmic membrane. NGO_0160 encodes ZnuA, which chaperones Zn from the periplasm and delivers it to ZnuB. A simplified image of the *znuCBA* gene products is depicted. The gene products of the NGO_0170, NGO_0169, and NGO_0168 have been implicated in both Zn and manganese (Mn) binding and transport. Thus, *znuCBA* is also referred to as *mntABC* in reference to Mn transport. *znuCBA* and *mntABC* are two different names to identify the same genetic sequence indicated by the locus numbers NGO_0170, NGO_0169, and NGO_0168. The *znuCBA* operon including the intergenic regions in *N. gonorrhoeae* is 92% identical to that in *N. meningitidis* (Accession number AE002098.2), in which *znuCBA* is also responsible for Zn and Mn import.

A manganese-specific outer membrane importer has not been identified in pathogenic *Neisseriae* despite the requirement for manganese, rather than zinc, cobalt, or magnesium, to resist oxidative killing (Tseng et al., 2001). However, the ability of TdfH to bind to manganese-loaded calprotectin suggests the possibility for highly specific manganese import across the outer membrane in the pathogenic *Neisseriae* (**Table 1**) (Bera et al., 2022).

The *znuCBA* operon is also referred to as *mntABC* in the context of manganese transport through the periplasm and across the cytoplasmic membrane (**Table 1**). MntA, MntB, and MntC are the ATPase, permease, and PBP, respectively. *znuCBA* and *mntABC* are different names for the same operon. *znuCBA* was used to describe the operon when the gene products were demonstrated to be involved in zinc import; somewhat confusingly, *mntABC* was deployed as the term to describe the operon when the gene products were involved in manganese import (**Figure 2**). The gene locus is the same for both systems and presumably encodes the proteins required for both manganese and zinc import.

ZnuA (**Figure 2**), from Ngo strain FA1090 (accession number NC_002946) shares 96% amino acid identity with a zinc ABC transport PBP encoded by *N. meningitidis*. This high sequence similarity suggests that *N. meningitidis* also requires a PBP for zinc and manganese transport through the periplasm. A gonococcal *mntC* mutant imports 500-fold less manganese than the wild type, demonstrating a dual metal-binding capacity (Tseng et al., 2001). MntC binds manganese and zinc with nearly equal affinity (100 ± 8 nM for Mn^{2+} and 104 ± 5 nM for Zn^{2+}), suggesting that the gonococcus occupies niches during infection that are limited in both metals (Chen and Morse, 2001; Lim et al., 2008). This import system may be required for growth and pathogenesis in *N. meningitidis* much like it is in *N. gonorrhoeae*.

Calmettes et al. showed that the meningococcal TdfJ homolog, ZnuD, crystalizes with zinc and cadmium (**Table 1**) at distinct binding sites in the absence of a chelator, suggesting the ability to bind both ions in their free form (Calmettes et al., 2015). Hecel et al. defined the metal binding specificity of the flexible loop responsible for ion capture by ZnuD (Hecel et al., 2019), noting that this flexible loop binds copper (**Figure 1**) with higher affinity and stability than it does zinc and that the loop undergoes a substantial conformational change upon copper binding (Hecel et al., 2019). The ability of ZnuD/TdfJ to bind copper suggests that this transporter may import copper in addition to zinc (**Figure 1**, **Table 1**).

A periplasmic copper chaperone has not yet been identified in the pathogenic *Neisseriae*. However, the ability of ZnuD to bind free copper suggests that copper could be imported through the outer membrane to the periplasm and may require a chaperone for delivery to the cytoplasmic membrane.

METAL AVAILABILITY SENSORS REGULATE METAL IMPORT GENES

Metal-dependent regulation in bacteria is often accomplished by the ferric uptake regulator (Fur) -family proteins (Taylor-Robinson et al., 1990). Fur-family metalloregulators include Fur, PerR, Mur, Nur, Zur, and Irr, which are responsible for regulating iron uptake, peroxide stress sensing, manganese uptake, nickel uptake, zinc uptake, and heme-dependent iron uptake (Fillat, 2014). These Fur-family regulators are responsible for sensing metal availability within microenvironments inhabited by pathogens and subsequently coordinating a transcriptional response.

Pathogenic *Neisseriae* express two well-characterized metal dependent regulators: Fur and Zur (Zur has also previously been called PerR) (Wu et al., 2006; Pawlik et al., 2012; Jean, 2015; Jean et al., 2016). In *N. gonorrhoeae*, Zur is hypothesized to repress zinc and manganese import genes in the presence of these metals and to de-repress zinc and manganese import genes in the absence of these metals (**Table 1**) (Chen and Morse, 2001; Wu et al., 2006). Production of gonococcal proteins TdfJ and TdfH is zinc-repressed in a Zur-depending manner (Jean et al., 2016). In the context of infection at mucosal surfaces and in neutrophils, *N. gonorrhoeae* requires a zinc sensor, such as Zur, to mount a transcriptional response to calprotectin- and S100A7- mediated zinc limitation. Zur de-represses expression of high-affinity metal importers, including *znuCBA, tdfJ*, and *tdfH*, so that the gonococcus can effectively and efficiently import Zn. Meningococcal Zur specifically binds to the promoter of *znuD* (P_{znuD}) in the presence of Zn^{2+}, but not Ca^{2+}, Co^{2+}, Cu^{2+}, Fe^{2+}, Mg^{2+}, Mn^{2+}, or Ni^{2+}. Zinc-dependent binding of Zur to P_{znuD} is abrogated with the addition of a zinc-specific chelator, N,N,N′, N′-tetrakis (2-pyridinylmethyl)-1,2-ethanediamine (TPEN) (Pawlik et al., 2012), suggesting that Zur is responsible for sensing zinc availability and coordinating a transcriptional response that allows for zinc acquisition. Microarray and RT-qPCR analyses also showed zinc-dependent regulation of 11 other genes, including *cbpA*, *znuCBA*, the high-affinity zinc ABC importer, and genes encoding multiple ribosomal proteins, nitrosative stress resistance proteins, and metabolic proteins (Pawlik et al., 2012; Stork et al., 2013).

Manganese-dependent regulation by gonococcal Zur (also referred to as PerR) was demonstrated by Tseng et al. and Wu et al. (**Table 1**) (Tseng et al., 2001; Seib et al., 2006; Wu et al., 2006). Wu et al. established that *znuCBA (mntABC)* is manganese-repressed in a Zur-dependent manner. Manganese has also been shown to upregulate many ribosomal proteins, pilus assembly proteins, adhesion proteins, outer membrane proteins, the multidrug efflux pump protein channel, MtrE, and many metabolic proteins (Wu et al., 2010). Interestingly, the iron-repressed transferrin-binding protein A (TbpA) and the transport protein ExbB were also manganese-repressed (Ronpirin et al., 2001; Wu et al., 2010). These data suggest that gonococcal Zur senses manganese limitation during infection where calprotectin and potentially other manganese-binding proteins sequester manganese.

Copper sensing and regulation in bacteria are often accomplished by CueR, which is absent from the gonococcal genome (accession number NC_002946; Arguello et al., 2013). The genome of *N. meningitidis* encodes a putative CueR regulator (accession number MBF1297094.1) that is 47.62% identical to that found in *E. coli* (accession number NP_415020). Although, it has not yet been empirically characterized as a copper-dependent regulator. Neisserial MisR (accession number WP_002214312.1), is homologous to CueR. MisR is the response regulator of theMisR-MisS two-component regulatory system and is known to be involved in cationic antimicrobial peptide resistance (Kandler et al., 2016). Interestingly, MisR is 36% identical and 58% similar to *Pseudomonas aeruginosa* CopR, which is involved in regulation of copper homeostasis (Novoa-Aponte et al., 2020).

Much work is needed to characterize the ability of pathogenic *Neisseriae* to sense and regulate copper, considering that ceruloplasmin is found in the serum, which is a meningococcal infection site (Osaki et al., 1966). Ceruloplasmin concentrations in the cerebrospinal fluid (0.8-2.2 μg/mL) are 100-500-fold lower than that in the serum (Irani, 2008). The gonococcus may also need to sense copper levels, considering the potential for copper to fluctuate following CTR1 protein expression within neutrophils.

TRANSITION METALS ARE REQUIRED FOR SURVIVAL AND VIRULENCE

Bacteria utilize scarce metals for several mechanisms related to survival and virulence, such as resistance to reactive oxygen species (ROS) and reactive nitrogen species (RNS), metabolism, maintenance of cell structural integrity, and proper protein structure and function.

Zn contributes to the function of biosynthetic pathways and virulence in *N. gonorrhoeae* and *N. meningitidis* as a cofactor for enzymes, enabling survival and virulence. For example, in both species, biosynthesis of lipid A, a potent immune activator

(Mandrell et al., 1988; Steimle et al., 2016), involves a putative zinc-dependent metalloamidase, UDP-3-O-(R-3-hydroxymyristoyl)-N-acetylglucosamine deacetylase (LpxC) (Barb and Zhou, 2008; Mochalkin et al., 2008; John et al., 2018). Lipid A anchors LOS into the bacterial membrane and can activate the immune system after its release from the bacterial cell wall (Steimle et al., 2016). Additionally, it can be directly recognized by host Lipid-A binding protein (LPB), which plays a role in sensing of pathogenic (Knapp et al., 2003) and commensal species (Steimle et al., 2016). Thus, LOS is a key virulence factor in *N. gonorrhoeae* and *N. meningitidis*. Similarly, the *N. meningitidis* protein, Ght, a zinc binding protein involved in LOS biogenesis, (Putker et al., 2014) is involved in LOS expression and outer membrane integrity (Putker et al., 2014). These observations implicate zinc in virulence and survival.

Manganese contributes to oxidative stress resistance in the pathogenic *Neisseriae* and thus contributes to survival during infection at highly oxidative sites (Tseng et al., 2001; Wu et al., 2006). Manganese in bacteria cycles between the Mn^{2+} and Mn^{3+} states during MnSOD processing of reactive oxygen species (Abreu and Cabelli, 2010). Interestingly, the pathogenic *Neisseria* do not express a MnSOD and instead use manganese directly as an ROS quencher (Seib et al., 2006). Wu et al. demonstrated a role for gonococcal *mntC* in the oxidative stress response under anaerobic rather than aerobic conditions (Wu et al., 2009). The vagina and cervix are normally oxygen-depleted, making anaerobic gonococcal growth conditions highly relevant (Hill et al., 2005). *In vitro*, growth of an *mntC* mutant under anaerobic conditions was inhibited by paraquat, an intracellular inducer of ROS, to an extent similar to that of the wild type (Wu et al., 2009). However, the *mntC* mutant was less competitive than the wild type during *in vivo* infection, which is characterized by both anaerobic and highly oxidative conditions (Wu et al., 2009). Reduced competition by the *mntC* mutant under anaerobic and oxidative conditions suggests that manganese is critical to gonococcal growth within the cervical niche. In contrast to the gonococcus, growth of the meningococcus in the presence of manganese does not enhance oxidative stress resistance (Seib et al., 2004).

N. meningitidis is able to grow on manganese concentrations 50-100 times higher (>100 mmol/L) than *N. gonorrhoeae*, which suggests that manganese homeostasis differs between these species (Tseng et al., 2001; Seib et al., 2004). Despite the non-restorative effect of manganese during oxidative conditions in the meningococcus, manganese is a vital cofactor in biosynthetic pathways within the bacterium. Meningococcal sialic acid synthase, NeuB, was shown to crystalize best with the addition of manganese, suggesting that this enzyme also requires a manganese cofactor (Tseng et al., 2001; Gunawan et al., 2005). NeuB is involved in sialylated capsule formation (Gunawan et al., 2005), and the sialylated surface of *N. meningitidis* has been shown to protect the bacterium from complement deposition (van Emmerik et al., 1994) through molecular mimicry of host cell surface proteins (Mandrell et al., 1988). Due to the potential involvement of manganese in NeuB activity, and consequently capsule formation, the metal may play a role in protection from host complement deposition and thus in immune evasion. This mechanism of innate immune evasion is particularly useful to the pathogen during infection of the vasculature, a niche that is complement is enriched.

In the pathogenic *Neisseria*, copper plays a role in resistance to extracellular RNS (Mellies et al., 1997; Boulanger and Murphy, 2002; Seib et al., 2006). *N. gonorrhoeae* (Gotschlich and Seiff, 1987) and *N. meningitidis* (Woods et al., 1989) possess a surface-exposed lipid-modified azurin (Desrosiers et al. 2010), which is a putative electron donor to peroxidases (Seib et al., 2006). This biological function is particularly relevant to macrophage infection because they are known to increase the expression of nitric oxide synthase (NOS) upon stimulation with LOS (Blondiau et al., 1994; Iovine et al., 2008). *N. gonorrhoeae* can survive in the harsh environment of macrophage phagosomes, potentially through a mechanism involving copper-bound Laz (Château and Seifert, 2016; Quillin and Seifert, 2018). Interestingly, the gonococcal genome encodes a putative peptidase with a PepSy domain (Accession number WP_003702955.1). This peptidase is 34% identical and 51% similar to that produced by *P. aeruginosa* (NCBI Reference Sequence: NP_252478.1). The peptidase in *P. aeruginosa* has been shown to be copper-repressed (Quintana et al., 2017). A similar putative peptidase is predicted to be produced by the meningococcus (Accession number WP_079889394.1) and is 36% identical and 50% similar to that from *P. aeruginosa*. The role of copper in the regulation and function of this peptidase in *N. gonorrhoeae* and *N. meningitidis* is a potential focus of future investigation.

THE RESPONSE TO METAL OVERLOAD REQUIRES SENSING AND EXPORT OF INTOXICATING METALS

The host applies metal intoxication strategies to limit bacterial growth and survival. Metal intoxication is the process by which the host floods the bacterial nutrient supply with metals. The consequences of metal intoxication for bacteria include electron transport chain (ETC) inhibition, protein mismetallation, and ROS and RNS accumulation (Chandrangsu et al., 2017). To limit these consequences, bacteria utilize mechanisms that store or export excess metal and repress metal import systems (Chandrangsu et al., 2017). Metal toxicity in *N. gonorrhoeae* has also been shown in reference to Mn^{2+}, Co^{2+}, Ni^{2+}, and Zn^{2+} (Odugbemi et al., 1978; Veyrier et al., 2011). However, specific responses to overload of each metal remain poorly characterized.

While macrophages have not been shown to exert metal intoxication upon the pathogenic *Neisseria* species, these immune cells have demonstrated the ability to increase the concentration of zinc in the cytosol and the phagocytic vacuole *via* the SLC39A transporters (Begum et al., 2002; Stafford et al., 2013; Chandrangsu et al., 2017) suggesting that host-induced zinc toxicity may be relevant to pathogenic *Neisseria* infection. Macrophages have been shown to increase phagosomal zinc concentrations to apply metal stress on invading *Mycobacterium* species (Wagner et al., 2005; Lefrançois et al., 2019). In *Streptococcus pneumoniae*, excess zinc competes with

manganese for binding to pneumococcal surface antigen A (PsaA), resulting in reduced manganese uptake, reduced oxidative stress resistance, and reduced resistance to PMN killing (McDevitt et al., 2011). In *E. coli*, high levels of manganese correlate with reduced levels of Fe^{2+}, iron-containing enzymes in the ETC and TCA cycle (iron-sulfur clusters and heme-containing enzymes), and consequently, reduced levels of NADH and ATP (Kaur et al., 2017).

Although not empirically tested in the gonococcus, manganese intoxication has been tested and shown to be relevant to meningococcal growth. Excess manganese in *N. meningitidis* results in protein mismetalation and subsequent dysregulation of Fur-regulated genes (**Table 1**) (Veyrier et al., 2011). Under excess manganese conditions, the meningococcus expresses *mntX*, the gene encoding a manganese export protein, which is critical to survival under high manganese conditions. MntX contains predicted transmembrane domains suggesting that this protein transports manganese from the cytoplasm to the periplasm (Veyrier et al., 2011). The *mntX* mutant exhibited a reduced ability to survive in the blood of infected mice relative to the wild-type strain (Veyrier et al., 2011). Additionally, the *mntX* mutant showed reduced resistance to human serum (Veyrier et al., 2011). Taken together, these data suggest that the meningococcus senses high manganese during septicemic infection and responds by expressing *mntX*. It is also feasible that the meningococcus requires a manganese exporter during infection in the cerebrospinal fluid. The blood and cerebrospinal fluid are body sites that are manganese-enriched and may be a hostile environment for a pathogen lacking a Mn exporter. Metal toxicity in *N. meningitidis* has also been shown in reference to Cu^{2+}, Co^{2+}, Ni^{2+}, and Zn^{2+} (Odugbemi et al., 1978). Conversely, *mntX* is frameshifted in 66% of sequenced *N. gonorrhoeae* strains. A *N. gonorrhoeae* strain, which was sensitive to manganese in this way, could be rescued through complementation with meningococcal *mntX* (Veyrier et al., 2011). Expression of *mntX* in certain gonococcal strains may enable dissemination to the blood and meninges.

Copper intoxication is used by the host to limit bacterial infection. For example, copper influx into the phagosomal compartment of macrophages results in increased killing of an *E. coli* strain deficient in a copper efflux protein, CopA, relative to the wild type (White et al., 2009). The gonococcus also produces a copper efflux protein, CopA, in the cytoplasmic membrane (Djoko et al., 2012). CopA likely transports copper from the cytoplasm to the periplasm. A *copA* mutant exhibited higher concentrations of internal copper and was growth impaired under high copper conditions (Djoko et al., 2012). Following copper supplementation, the *copA* mutant was limited in its ability to associate with and invade primary human cervical epithelial cells; it was also less resistant to killing by nitrite and *S*-nitrosoglutathione (GSNO), a nitric oxide generator (Djoko et al., 2012). This data suggest *N. gonorrhoeae* experiences copper overload within cervical epithelial cells. Djoko and McEwan showed that high levels of copper increase gonococcal sensitivity to the RNS generator, sodium nitrite and suggested that copper-dependent inactivation of hemoproteins involved in intracellular RNS detoxification results in RNS-dependent killing of *N. gonorrhoeae* (Djoko and McEwan, 2013).

While the concept of nutritional immunity has been thoroughly studied, the concept of metal intoxication requires further exploration. Expanded application of this concept to pathogenic *Neisseriae* infection will broaden our understanding of metal homeostasis and its role in pathogenesis.

NEXT STEPS - COMPREHENSIVE CHARACTERIZATION OF NUTRITIONAL IMMUNITY AND METAL INTOXICATION REQUIRES INSIGHT INTO INTEGRATED METAL HOMEOSTASIS

Pathogens possess mechanisms of defense against metal starvation and metal intoxication exerted by the host, as these metals play integral roles in metabolism, maintenance of cell structural integrity, and ROS and RNS resistance. Metal involvement in these processes is often studied in isolation, meaning only one metal (i.e., zinc, manganese, or copper) is considered at a time. However, it is improbable that pathogens encounter a single type of metal depletion or stress during infection of a host whose metal allocations and concentrations are heterogeneous.

One of the most thoroughly investigated examples of metal interplay is that between manganese and zinc in *S. pneumoniae*. Cell-associated manganese in wild-type *S. pneumoniae* is substantially reduced in the presence of excess zinc, and zinc depletion of cellular manganese could be restored by the addition of excess manganese (Jacobsen et al., 2011). Under high zinc conditions, zinc competes with and inhibits manganese binding to the manganese importer, PsaA, resulting in manganese starvation and zinc toxicity (Jacobsen et al., 2011; Eijkelkamp et al., 2014). Zinc-induced manganese starvation leads to increased sensitivity to oxidative stress (Eijkelkamp et al., 2014). Another example of metal interplay has been investigated in *S.enterica* Serovar Typhimurium. In this bacterium, *mntH* encodes a manganese importer that is iron-repressed in a Fur-dependent manner and manganese-repressed in a manganese transport repressor (MntR) -dependent manner (Kehres et al., 2002a). Kehres et al. hypothesized that co-regulation of *mntH* maintains an equilibrated Mn^{2+}/Fe^{2+} ratio in *Salmonella* (Kehres et al., 2002a). The genomes of *N. gonorrhoeae* and *N. meningitidis* encode a MntH homolog; however, the functions of this Fe^{2+}/Mn^{2+} symporter in manganese or iron import have yet to be tested in the *Neisseriae*. *Helicobacter pylori* expresses a metal efflux system, CznABC, which interacts with cadmium, zinc, and nickel and confers resistance to intoxicating levels of all three metals (Stähler et al., 2006). *Acinetobacter baumannii*, when grown in the presence of calprotectin that is able to simultaneously chelate zinc and manganese, exhibits reduced intracellular manganese and zinc but increased iron levels (Hood et al., 2012). In this case, calprotectin treatment not only resulted in altered zinc,

manganese, and iron homeostasis but also in reduced growth (Hood et al., 2012). In *Klebsiella pneumoniae*, the zinc efflux protein, ZntA, is responsible for exporting zinc from the cytoplasm (Maunders Eve et al., 2022). The *zntA* mutant was shown to accumulate more manganese in addition to zinc and less iron than the wild type when subject to high zinc conditions, demonstrating integrated zinc, manganese, and iron homeostasis in wild type *K. pneumoniae* (Maunders Eve et al., 2022).

Pathogenic *Neisseriae* sense metal concentrations in the environment and respond by altering the expression of metal import or export systems and allocating these metals to metabolic and biosynthetic processes to allow for survival and virulence. *N. gonorrhoeae* and *N. meningitidis* are similar pathogens, which respond similarly to metal limitation and overload within the same host, despite causing different physiological symptoms. It is unlikely that the pathogenic *Neisseria* experience zinc, manganese, and copper starvation or intoxication in isolation from other metals. Interaction with multiple metals by neisserial proteins suggests the need for complex and integrated metal homeostasis (**Table 1**). This is evidenced by the ZnuCBA manganese import system in *N. gonorrhoeae*, which is manganese-regulated in a Zur-dependent manner but is also responsible for zinc import (**Table 1**) (Chen and Morse, 2001; Tseng et al., 2001; Wu et al., 2006). More work needs to be done to characterize Zur metal sensing when zinc and manganese are present together. Gonococcal TdfJ is zinc-repressed in a Zur-dependent manner and is iron-induced (Jean et al., 2016). The zinc to iron ratio required for optimal TdfJ expression in the presence of S100A7 should be addressed in future studies. Gonococcal TbpA (**Table 1**) is both iron- (Ronpirin et al., 2001; Vélez Acevedo et al., 2014) and manganese-repressed (Wu et al., 2010). TbpA is an iron-repressed (Ronpirin et al., 2001; Vélez Acevedo et al., 2014) TonB-dependent transporter that pirates iron from human transferrin and transports it across the outer membrane (Noto and Cornelissen, 2008; Cash et al., 2015). Considering that TbpA is also manganese-repressed and that transferrin can bind manganese in a manner similar to iron, it would be interesting to determine whether TbpA can pirate manganese from manganese-loaded transferrin. Additionally, studies regarding the application of this potential manganese transport system to a host niche would be informative. The manganese export protein, MntX, in *N. meningitidis* is required for survival under high manganese and low iron conditions, and the absence of the gene encoding this system results in mis-regulation of iron-regulated genes (**Table 1**) (Veyrier et al., 2011). It would be informative to discern the exact manganese to iron ratio required for optimal *mntX* expression and consequent serum resistance in *N. meningitidis*. In-frame MntX is only present in a subset of gonococcal strains (Veyrier et al., 2011).

The evolution of complex metal regulatory and import mechanisms suggests that the pathogenic *Neisseriae* possess a need for multifactorial metal homeostasis. Instances of overlap in different metal-related processes imply that the pathogenic *Neisseriae* may specifically require the integration of manganese and iron homeostasis and zinc and copper homeostasis. The exact mechanisms of integrated metal homeostasis and the host conditions under which they are relevant have not yet been fully deciphered. Further investigation into the complex metal environment sensed by the bacteria in the host could broaden our understanding of mixed metal homeostasis and the neisserial response to nutritional immunity and metal intoxication.

AUTHOR CONTRIBUTIONS

AHB completed the literature review and manuscript drafting and editing based on JLS, KSL, and CNC comments. JLS reviewed and proofread the manuscript multiples times before review by KLS. CNC then reviewed and proofread the manuscript and acquired funding. All authors contributed to the article and approved the submitted version.

FUNDING

This work was funded by the National Institute of Allergy and Infectious Diseases, award numbers U19AI144182, R01AI127793, and R01AI125421 to CC. The funder had no role in data collection, synthesis, analysis, interpretation, or management of the data presented in this review. The funder had no role in review generation and revision, or in the decision to submit this review for publication.

REFERENCES

Abreu, I. A., and Cabelli, D. E. (2010). Superoxide Dismutases—A Review of the Metal-Associated Mechanistic Variations. *Biochim. Biophys. Acta (BBA) - Proteins Proteomics* 1804 (2), 263–274. doi: 10.1016/j.bbapap.2009.11.005

Ammendola, S., Pasquali, P., Pistoia, C., Petrucci, P., Petrarca, P., Rotilio, G., et al. (2007). High-Affinity Zn^{2+} Uptake System ZnuABC Is Required for Bacterial Zinc Homeostasis in Intracellular Environments and Contributes to the Virulence of *Salmonella Enterica*. *Infect. Immun.* 75 (12), 5867. doi: 10.1128/IAI.00559-07

Anjem, A., Varghese, S., and Imlay, J. A. (2009). Manganese Import is a Key Element of the OxyR Response to Hydrogen Peroxide in *Escherichia Coli*. *Mol. Microbiol.* 72 (4), 844–858. doi: 10.1111/j.1365-2958.2009.06699.x

Arguello, J., Raimunda, D., and Padilla-Benavides, T. (2013). Mechanisms of Copper Homeostasis in Bacteria. *Front. Cell. Infect. Microbiol.* 3 (73). doi: 10.3389/fcimb.2013.00073

Baer, M. T., and King, J. C. (1984). Tissue Zinc Levels and Zinc Excretion During Experimental Zinc Depletion in Young Men. *Am. J. Clin. Nutr.* 39 (4), 556–570. doi: 10.1093/ajcn/39.4.556

Barb, A. W., and Zhou, P. (2008). Mechanism and Inhibition of LpxC: An Essential Zinc-Dependent Deacetylase of Bacterial Lipid A Synthesis. *Curr. Pharm. Biotechnol.* 9 (1), 9–15. doi: 10.2174/138920108783497668

Becker, K. W., and Skaar, E. P. (2014). Metal Limitation and Toxicity at the Interface Between Host and Pathogen. *FEMS Microbiol. Rev.* 38 (6), 1235–1249. doi: 10.1111/1574-6976.12087

Begum, N. A., Kobayashi, M., Moriwaki, Y., Matsumoto, M., Toyoshima, K., and Seya, T. (2002). *Mycobacterium Bovis* BCG Cell Wall and Lipopolysaccharide

Induce a Novel Gene, BIGM103, Encoding a 7-TM Protein: Identification of a New Protein Family Having Zn-Transporter and Zn-Metalloprotease Signatures. *Genomics* 80 (6), 630–645. doi: 10.1006/geno.2002.7000

Bera, A. K., Wu, R., Harrison, S., Cornelissen, C. N., Chazin, W. J., and Noinaj, N. (2022). TdfH Selectively Binds Metal-Loaded Tetrameric Calprotectin for Zinc Import. *Commun. Biol.* 5 (1), 103. doi: 10.1038/s42003-022-03039-y

Berntsson, R. P. A., Smits, S. H. J., Schmitt, L., Slotboom, D.-J., and Poolman, B. (2010). A Structural Classification of Substrate-Binding Proteins. *FEBS Lett.* 584 (12), 2606–2617. doi: 10.1016/j.febslet.2010.04.043

Blondiau, C., Lagadec, P., Lejeune, P., Onier, N., Cavaillon, J.-M., and Jeannin, J.-F. (1994). Correlation Between the Capacity to Activate Macrophages *In Vitro* and the Antitumor Activity *In Vivo* of Lipopolysaccharides From Different Bacterial Species. *Immunobiology* 190 (3), 243–254. doi: 10.1016/S0171-2985(11)80272-X

Boulanger, M. J., and Murphy, M. E. P. (2002). Crystal Structure of the Soluble Domain of the Major Anaerobically Induced Outer Membrane Protein (AniA) From Pathogenic *Neisseria*: A New Class of Copper-Containing Nitrite Reductases. *J. Mol. Biol.* 315 (5), 1111–1127. doi: 10.1006/jmbi.2001.5251

Braiterman, L. T., Gupta, A., Chaerkady, R., Cole, R. N., and Hubbard, A. L. (2015). Communication Between the N and C Termini is Required for Copper-Stimulated Ser/Thr Phosphorylation of Cu(I)-ATPase (ATP7B). *J. Biol. Chem.* 290 (14), 8803–8819. doi: 10.1074/jbc.M114.627414

Brown, K. H., Wuehler, S. E., and Peerson, J. M. (2001). The Importance of Zinc in Human Nutrition and Estimation of the Global Prevalence of Zinc Deficiency. *Food Nutr. Bull.* 22 (2), 113–125. doi: 10.1177/156482650102200201

Calmettes, C., Ing, C., Buckwalter, C. M., El Bakkouri, M., Chieh-Lin Lai, C., Pogoutse, A., et al. (2015). The Molecular Mechanism of Zinc Acquisition by the Neisserial Outer-Membrane Transporter ZnuD. *Nat. Commun.* 6 (1), 7996. doi: 10.1038/ncomms8996

Candrilli, S., and Kurosky, S. (2019). The Response to and Cost of Meningococcal Disease Outbreaks in University Campus Settings: A Case Study in Oregon, United States. *Res. Triangle Park (NC): RTI Press)*. doi: 10.3768/rtipress.2019.rr.0034.1910

Cash, D. R., Noinaj, N., Buchanan, S. K., and Cornelissen, C. N. (2015). Beyond the Crystal Structure: Insight Into the Function and Vaccine Potential of TbpA Expressed by Neisseria Gonorrhoeae. *Infect. Immun.* 83 (11), 4438–4449. doi: 10.1128/IAI.00762-15

CDC. (2019a). *Enhanced Meningococcal Disease Surveillance Report, 2018*. Atlanta, GA: National Center for Immunization and Respiratory Diseases Office of Infectious Disease.

CDC. (2019b). *Sexually transmitted disease surveillance 2018*. Atlanta, GA: U.S. Department of Health and Human Services Centers for Disease Control and Prevention National Center for HIV/AIDS, Viral Hepatitis, STD, and TB Prevention Division of STD.

CDC. (2019c). *VPD Surveillance Manual 8 Meningococcal Disease: Chapter 8.1*. Atlanta, GA: National Center for Immunization and Respiratory Diseases Office of Infectious Disease.

Chandrangsu, P., Rensing, C., and Helmann, J. D. (2017). Metal Homeostasis and Resistance in Bacteria. *Nat. Rev. Microbiol.* 15 (6), 338–350. doi: 10.1038/nrmicro.2017.15

Château, A., and Seifert, H. S. (2016). *Neisseria Gonorrhoeae* Survives Within and Modulates Apoptosis and Inflammatory Cytokine Production of Human Macrophages. *Cell. Microbiol.* 18 (4), 546–560. doi: 10.1111/cmi.12529

Chen, C.-Y., and Morse, S. A. (2001). Identification and Characterization of a High-Affinity Zinc Uptake System in *Neisseria Gonorrhoeae*. *FEMS Microbiol. Lett.* 202 (1), 67–71. doi: 10.1111/j.1574-6968.2001.tb10781.x

Chen, J. Y., Tsao, G. C., Zhao, Q., and Zheng, W. (2001). Differential Cytotoxicity of Mn(II) and Mn(III): Special Reference to Mitochondrial [Fe-S] Containing Enzymes. *Toxicol. Appl. Pharmacol.* 175 (2), 160–168. doi: 10.1006/taap.2001.9245

Cichon, I., Ortmann, W., Bednarz, A., Lenartowicz, M., and Kolaczkowska, E. (2020). Reduced Neutrophil Extracellular Trap (NET) Formation During Systemic Inflammation in Mice With Menkes Disease and Wilson Disease: Copper Requirement for NET Release. *Front. Immunol.* 10 (3021). doi: 10.3389/fimmu.2019.03021

Cornelissen, C. N., and Sparling, P. F. (1996). Binding and Surface Exposure Characteristics of the Gonococcal Transferrin Receptor are Dependent on Both Transferrin-Binding Proteins. *J. bacteriol.* 178 (5), 1437–1444. doi: 10.1128/jb.178.5.1437-1444.1996

Davies, B. W., and Walker, G. C. (2007). Disruption of *sitA* Compromises *Sinorhizobium Meliloti* for Manganese Uptake Required for Protection Against Oxidative Stress. *J. Bacteriol.* 189 (5), 2101. doi: 10.1128/JB.01377-06

Davis, L. M., Kakuda, T., and DiRita, V. J. (2009). A *Campylobacter Jejuni znuA* Orthologue Is Essential for Growth in Low-Zinc Environments and Chick Colonization. *J. Bacteriol.* 191 (5), 1631. doi: 10.1128/JB.01394-08

Desrosiers, D. C., Bearden, S. W., Mier, I., Abney, J., Paulley, J. T., Fetherston, J. D., et al. (2010). Znu Is the Predominant Zinc Importer in *Yersinia Pestis* During *In Vitro* Growth But Is Not Essential for Virulence. *Infect. Immun.* 78 (12), 5163. doi: 10.1128/IAI.00732-10

Diaz-Ochoa, V. E., Lam, D., Lee, C. S., Klaus, S., Behnsen, J., Liu, J. Z., et al. (2016). *Salmonella* Mitigates Oxidative Stress and Thrives in the Inflamed Gut by Evading Calprotectin-Mediated Manganese Sequestration. *Cell Host Microbe* 19 (6), 814–825. doi: 10.1016/j.chom.2016.05.005

Dintilhac, A., and Claverys, J. P. (1997). The *Adc* Locus, Which Affects Competence for Genetic Transformation in *Streptococcus Pneumoniae*, Encodes an ABC Transporter With a Putative Lipoprotein Homologous to a Family of Streptococcal Adhesins. *Res. Microbiol.* 148 (2), 119–131. doi: 10.1016/S0923-2508(97)87643-7

Djoko, K. Y., Franiek, J. A., Edwards, J. L., Falsetta, M. L., Kidd, S. P., Potter, A. J., et al. (2012). Phenotypic Characterization of a *copA* Mutant of *Neisseria Gonorrhoeae* Identifies a Link Between Copper and Nitrosative Stress. *Infect. Immun.* 80 (3), 1065–1071. doi: 10.1128/IAI.06163-11

Djoko, K. Y., and McEwan, A. G. (2013). Antimicrobial Action of Copper Is Amplified *via* Inhibition of Heme Biosynthesis. *ACS Chem. Biol.* 8 (10), 2217–2223. doi: 10.1021/cb4002443

Dunn, M. A., Green, M. H., and Leach, R. M.Jr (1991). Kinetics of Copper Metabolism in Rats: A Compartmental Model. *Am. J. Physiol.* 261 (1 Pt 1), E115–E125. doi: 10.1152/ajpendo.1991.261.1.E115

Edgeworth, J., Gorman, M., Bennett, R., Freemont, P., and Hogg, N. (1991). Identification of P8,14 as a Highly Abundant Heterodimeric Calcium Binding Protein Complex of Myeloid Cells. *J. Biol. Chem.* 266 (12), 7706–7713. doi: 10.1016/S0021-9258(20)89506-4

Eijkelkamp, B. A., Morey, J. R., Ween, M. P., Ong, C.-l., McEwan, A. G., Paton, J. C., et al. (2014). Extracellular Zinc Competitively Inhibits Manganese Uptake and Compromises Oxidative Stress Management in *Streptococcus Pneumoniae*. *PLos One* 9 (2), e89427. doi: 10.1371/journal.pone.0089427

Fillat, M. F. (2014). The FUR (Ferric Uptake Regulator) Superfamily: Diversity and Versatility of Key Transcriptional Regulators. *Arch. Biochem. Biophys.* 546, 41–52. doi: 10.1016/j.abb.2014.01.029

Forbes, J. R., and Gros, P. (2003). Iron, Manganese, and Cobalt Transport by Nramp1 (Slc11a1) and Nramp2 (Slc11a2) Expressed at the Plasma Membrane. *Blood* 102 (5), 1884–1892. doi: 10.1182/blood-2003-02-0425

Gagnon, D. M., Brophy, M. B., Bowman, S. E. J., Stich, T. A., Drennan, C. L., Britt, R. D., et al. (2015). Manganese Binding Properties of Human Calprotectin Under Conditions of High and Low Calcium: X-Ray Crystallographic and Advanced Electron Paramagnetic Resonance Spectroscopic Analysis. *J. Am. Chem. Soc.* 137 (8), 3004–3016. doi: 10.1021/ja512204s

Ganini, D., Santos, J. H., Bonini, M. G., and Mason, R. P. (2018). Switch of Mitochondrial Superoxide Dismutase Into a Prooxidant Peroxidase in Manganese-Deficient Cells and Mice. *Cell Chem. Biol.* 25 (4), 413–425.e416. doi: 10.1016/j.chembiol.2018.01.007

Girotto, S., Cendron, L., Bisaglia, M., Tessari, I., Mammi, S., Zanotti, G., et al. (2014). DJ-1 is a Copper Chaperone Acting on SOD1 Activation. *J. Biol. Chem.* 289 (15), 10887–10899. doi: 10.1074/jbc.M113.535112

Gotschlich, E. C., and Seiff, M. E. (1987). Identification and Gene Structure of an Azurin-Like Protein With a Lipoprotein Signal Peptide in *Neisseria Gonorrhoeae*. *FEMS Microbiol. Lett.* 43 (3), 253–255. doi: 10.1111/j.1574-6968.1987.tb02153.x

Gunawan, J., Simard, D., Gilbert, M., Lovering, A. L., Wakarchuk, W. W., Tanner, M. E., et al. (2005). Structural and Mechanistic Analysis of Sialic Acid Synthase NeuB From *Neisseria Meningitidis* in Complex With Mn^{2+}, Phosphoenolpyruvate, and N-Acetylmannosaminitol. *J. Biol. Chem.* 280 (5), 3555–3563. doi: 10.1074/jbc.M411942200

Gunter, T. E., Gerstner, B., Gunter, K. K., Malecki, J., Gelein, R., Valentine, W. M., et al. (2013). Manganese Transport *via* the Transferrin Mechanism. *Neurotoxicology* 34, 118–127. doi: 10.1016/j.neuro.2012.10.018

Hecel, A., Rowińska-Żyrek, M., and Kozłowski, H. (2019). Copper(II)-Induced Restructuring of ZnuD, A Zinc(II) Transporter From *Neisseria Meningitidis*. *Inorganic Chem.* 58 (9), 5932–5942. doi: 10.1021/acs.inorgchem.9b00265

Hecel, A., Watly, J., Rowinska-Zyrek, M., Swiatek-Kozlowska, J., and Kozlowski, H. (2018). Histidine Tracts in Human Transcription Factors: Insight Into Metal Ion Coordination Ability. *JBIC J. Biol. Inorg. Chem.* 23 (1), 81. doi: 10.1007/s00775-017-1512-x

Hennigar, S. R., and McClung, J. P. (2016). Nutritional Immunity: Starving Pathogens of Trace Minerals. *Am. J. lifestyle Med.* 10 (3), 170–173. doi: 10.1177/1559827616629117

Hill, D. R., Brunner, M. E., Schmitz, D. C., Davis, C. C., Flood, J. A., Schlievert, P. M., et al. (2005). *In Vivo* Assessment of Human Vaginal Oxygen and Carbon Dioxide Levels During and Post Menses. *J. Appl. Physiol.* 99 (4), 1582–1591. doi: 10.1152/japplphysiol.01422.2004

Hood, M. I., Mortensen, B. L., Moore, J. L., Zhang, Y., Kehl-Fie, T. E., Sugitani, N., et al. (2012). Identification of an Acinetobacter Baumannii Zinc Acquisition System That Facilitates Resistance to Calprotectin-Mediated Zinc Sequestration. *PLos Pathog.* 8 (12), e1003068. doi: 10.1371/journal.ppat.1003068

Hu Frisk, J. M., Kjellén, L., Kaler, S. G., Pejler, G., and Öhrvik, H. (2017). Copper Regulates Maturation and Expression of an MITF:Tryptase Axis in Mast Cells. *J. Immunol.* 199 (12), 4132–4141. doi: 10.4049/jimmunol.1700786

Hyre, A. N., Kavanagh, K., Kock, N. D., Donati, G. L., and Subashchandrabose, S. (2017). Copper Is a Host Effector Mobilized to Urine During Urinary Tract Infection To Impair Bacterial Colonization. *Infect. Immun.* 85 (3), e01041–e01016. doi: 10.1128/IAI.01041-16

Iovine, N. M., Pursnani, S., Voldman, A., Wasserman, G., Blaser, M. J., and Weinrauch, Y. (2008). Reactive Nitrogen Species Contribute to Innate Host Defense Against *Campylobacter Jejuni*. *Infect. Immun.* 76 (3), 986. doi: 10.1128/IAI.01063-07

Irani, D. N. (2008). *Cerebrospinal Fluid in Clinical Practice* (Philadephia, PA: saunders elsevier).

Ivanov, S. S., Castore, R., Juarez Rodriguez, M. D., Circu, M., and Dragoi, A.-M. (2022). Neisseria Gonorrhoeae Subverts Formin-Dependent Actin Polymerization to Colonize Human Macrophages. *PLos Pathog.* 17 (12), e1010184. doi: 10.1371/journal.ppat.1010184

Jabado, N., Jankowski, A., Dougaparsad, S., Picard, V., Grinstein, S., and Gros, P. (2000). Natural Resistance to Intracellular Infections: Natural Resistance-Associated Macrophage Protein 1 (Nramp1) Functions as a pH-Dependent Manganese Transporter at the Phagosomal Membrane. *J. Exp. Med.* 192 (9), 1237–1248. doi: 10.1084/jem.192.9.1237

Jackson, M. J. (1989). *"Physiology of Zinc: General Aspects," in Zinc in Human Biology, Ed* (C.F. Mills: London: Springer London), 1–14.

Jacobsen, F. E., Kazmierczak, K. M., Lisher, J. P., Winkler, M. E., and Giedroc, D. P. (2011). Interplay Between Manganese and Zinc Homeostasis in the Human Pathogen *Streptococcus Pneumoniae*. *Metallomics* 3 (1), 38–41. doi: 10.1039/c0mt00050g

Jarosz, M., Olbert, M., Wyszogrodzka, G., Młyniec, K., and Librowski, T. (2017). Antioxidant and Anti-Inflammatory Effects of Zinc. Zinc-Dependent NF-κb Signaling. *Inflammopharmacology* 25 (1), 11–24. doi: 10.1007/s10787-017-0309-4

Jean, S. (2015). *Characterizarion of the Regulation and Function of Neisseria Gonorrhoeae TonB-Dependent Transporters: TdfG, TdfH and TdfJ* (Virginia Commonwealth University: Doctor of Philosophy).

Jean, S., Juneau, R. A., Criss, A. K., and Cornelissen, C. N. (2016). *Neisseria Gonorrhoeae* Evades Calprotectin-Mediated Nutritional Immunity and Survives Neutrophil Extracellular Traps by Production of TdfH. *Infect. Immun.* 84 (10), 2982–2994. doi: 10.1128/IAI.00319-16

John, C. M., Feng, D., and Jarvis, G. A. (2018). Treatment of Human Challenge and MDR Strains of *Neisseria Gonorrhoeae* With LpxC Inhibitors. *J. Antimicrob. Chemother.* 73 (8), 2064–2071. doi: 10.1093/jac/dky151

Johnson, M. B., and Criss, A. K. (2011). Resistance of Neisseria Gonorrhoeae to Neutrophils. *Front. Microbiol.* 2. doi: 10.3389/fmicb.2011.00077

Juttukonda, L. J., Chazin, W. J., and Skaar, E. P. (2016). *Acinetobacter Baumannii* Coordinates Urea Metabolism With Metal Import To Resist Host-Mediated Metal Limitation. *mBio* 7 (5), e01475–e01416. doi: 10.1128/mBio.01475-16

Kammerman, M. T., Bera, A., Wu, R., Harrison, S. A., Maxwell, C. N., Lundquist, K., et al. (2020). Molecular Insight Into TdfH-Mediated Zinc Piracy From Human Calprotectin by *Neisseria Gonorrhoeae*. *mBio* 11 (3), e00949–e00920. doi: 10.1128/mBio.00949-20

Kandler, J. L., Holley, C. L., Reimche, J. L., Dhulipala, V., Balthazar, J. T., Muszyński, A., et al. (2016). The MisR Response Regulator Is Necessary for Intrinsic Cationic Antimicrobial Peptide and Aminoglycoside Resistance in Neisseria Gonorrhoeae. *Antimicrob. Agents chemother.* 60 (8), 4690–4700. doi: 10.1128/AAC.00823-16

Kaur, G., Kumar, V., Arora, A., Tomar, A., Sur, R., Dutta, D., et al. (2017). Affected Energy Metabolism Under Manganese Stress Governs Cellular Toxicity. *Sci. Rep.* 7 (1), 11645–11645. doi: 10.1038/s41598-017-12004-3

Kehres, D. G., Janakiraman, A., Slauch, J. M., and Maguire, M. E. (2002a). Regulation of *Salmonella Enterica* Serovar Typhimurium mntH Transcription by H_2O_2, Fe^{2+}, and Mn^{2+}. *J. Bacteriol.* 184 (12), 3151–3158. doi: 10.1128/jb.184.12.3151-3158.2002

Kehres, D. G., Janakiraman, A., Slauch, J. M., and Maguire, M. E. (2002b). SitABCD is the Alkaline Mn^{2+} Transporter of *Salmonella Enterica* Serovar Typhimurium. *J. bacteriol.* 184 (12), 3159–3166. doi: 10.1128/jb.184.12.3159-3166.2002

Knapp, S., de Vos Alex, F., Florquin, S., Golenbock Douglas, T., and van der Poll, T. (2003). Lipopolysaccharide Binding Protein Is an Essential Component of the Innate Immune Response to *Escherichia Coli* Peritonitis in Mice. *Infect. Immun.* 71 (12), 6747–6753. doi: 10.1128/IAI.71.12.6747-6753.2003

Kumar, S., Chesson, H., and Gift, T. L. (2021). Estimating the Direct Medical Costs and Productivity Loss of Outpatient Chlamydia and Gonorrhea Treatment. *Sex Transm. Dis.* 48 (2), e18–e21. doi: 10.1097/olq.0000000000001240

Lee, M.-J., Chien-Liang, L., Tsai, J.-Y., Sue, W.-T., Hsia, W.-S., and Huang, H. (2010). Identification and Biochemical Characterization of a Unique Mn^{2+}-Dependent UMP Kinase From *Helicobacter Pylori*. *Arch. Microbiol.* 192 (9), 739–746. doi: 10.1007/s00203-010-0600-x

Lefrançois, L. H., Kalinina, V., Cardenal-Muñoz, E., Hanna, N., Koliwer-Brandl, H., Appiah, J., et al. (2019). Zn^{2+} Intoxication of *Mycobacterium Marinum* During Dictyostelium Discoideum Infection Is Counteracted by Induction of the Pathogen Zn^{2+} Exporter CtpC. *bioRxiv* 575217. doi: 10.1101/575217

Lewis, D. A., Klesney-Tait, J., Lumbley, S. R., Ward, C. K., Latimer, J. L., Ison, C. A., et al. (1999). Identification of the *znuA*-Encoded Periplasmic Zinc Transport Protein of *Haemophilus Ducreyi*. *Infect. Immun.* 67 (10), 5060–5068. doi: 10.1128/IAI.67.10.5060-5068.1999

Lim, K. H. L., Jones, C. E., vanden Hoven, R. N., Edwards, J. L., Falsetta, M. L., Apicella, M. A., et al. (2008). Metal Binding Specificity of the MntABC Permease of *Neisseria Gonorrhoeae* and Its Influence on Bacterial Growth and Interaction With Cervical Epithelial Cells. *Am. Soc. Microbiol. J. Infect. Immun.* doi: 10.1128/IAI.01725-07

Liu, Y., and Russell, M. W. (2011). Diversion of the Immune Response to *Neisseria Gonorrhoeae* From Th17 to Th1/Th2 by Treatment With Anti-Transforming Growth Factor β Antibody Generates Immunological Memory and Protective Immunity. *mBio* 2 (3), e00095–e00011. doi: 10.1128/mBio.00095-11

Maares, M., Keil, C., Koza, J., Straubing, S., Schwerdtle, T., and Haase, H. (2018). *In Vitro* Studies on Zinc Binding and Buffering by Intestinal Mucins. *Int. J. Mol. Sci.* 19 (9), 2662. doi: 10.3390/ijms19092662

Mandrell, R. E., Griffiss, J. M., and Macher, B. A. (1988). Lipooligosaccharides (LOS) of *Neisseria Gonorrhoeae* and *Neisseria Meningitidis* Have Components That are Immunochemically Similar to Precursors of Human Blood Group Antigens. Carbohydrate Sequence Specificity of the Mouse Monoclonal Antibodies That Recognize Crossreacting Antigens on LOS and Human Erythrocytes. *J. Exp. Med.* 168 (1), 107–126. doi: 10.1084/jem.168.1.107

Maunders Eve, A., Ganio, K., Hayes Andrew, J., Neville Stephanie, L., Davies Mark, R., Strugnell Richard, A., et al. (2022). The Role of ZntA in *Klebsiella Pneumoniae* Zinc Homeostasis. *Microbiol. Spectr.* 10 (1), e01773–e01721. doi: 10.1128/spectrum.01773-21

Maurakis, S., Keller, K., Maxwell, C. N., Pereira, K., Chazin, W. J., Criss, A. K., et al. (2019). The Novel Interaction Between *Neisseria Gonorrhoeae* TdfJ and Human S100A7 Allows Gonococci to Subvert Host Zinc Restriction. *PLos Pathog.* 15 (8), e1007937–e1007937. doi: 10.1371/journal.ppat.1007937

Maynard, L. S., and Cotzias, G. C. (1955). The Partition of Manganese Among Organs and Intracellular Organelles of the Rat. *J. Biol. Chem.* 214 (1), 489–495. doi: 10.1016/S0021-9258(18)70986-1

McDevitt, C. A., Ogunniyi, A. D., Valkov, E., Lawrence, M. C., Kobe, B., McEwan, A. G., et al. (2011). A Molecular Mechanism for Bacterial Susceptibility to Zinc. *PLos Pathog.* 7 (11), e1002357–e1002357. doi: 10.1371/journal.ppat.1002357

Mellies, J., Jose, J., and Meyer, T. F. (1997). The *Neisseria Gonorrhoeae* Gene *aniA* Encodes an Inducible Nitrite Reductase. *Mol. Gen. Genet.* 256 (5), 525–532. doi: 10.1007/s004380050597

Mildner, M., Stichenwirth, M., Abtin, A., Eckhart, L., Sam, C., Gläser, R., et al. (2010). Psoriasin (S100A7) is a Major *Escherichia Coli*-Cidal Factor of the Female Genital Tract. *Mucosal Immunol.* 3 (6), 602–609. doi: 10.1038/mi.2010.37

Mochalkin, I., Knafels, J. D., and Lightle, S. (2008). Crystal Structure of LpxC From *Pseudomonas Aeruginosa* Complexed With the Potent BB-78485 Inhibitor. *Protein Sci.* 17 (3), 450–457. doi: 10.1110/ps.073324108

Noto, J. M., and Cornelissen, C. N. (2008). Identification of TbpA Residues Required for Transferrin-Iron Utilization by Neisseria Gonorrhoeae. *Infect. Immun.* 76 (5), 1960–1969. doi: 10.1128/IAI.00020-08

Novoa-Aponte, L., Xu, C., Soncini, F. C., and Argüello, J. M. (2020). The Two-Component System CopRS Maintains Subfemtomolar Levels of Free Copper in the Periplasm of Pseudomonas Aeruginosa Using a Phosphatase-Based Mechanism. *mSphere* 5 (6), e01193–e01120. doi: 10.1128/mSphere.01193-20

O'Neal, S. L., and Zheng, W. (2015). Manganese Toxicity Upon Overexposure: A Decade in Review. *Curr. Environ. Health Rep.* 2 (3), 315–328. doi: 10.1007/s40572-015-0056-x

Odugbemi, T., McEntegart, M., and Hafiz, S. (1978). Effects of Various Divalent Cations on the Survival of *Neisseria Gonorrhoeae* in Liquid Media. *Br. J. Vener Dis.* 54 (4), 239–242. doi: 10.1136/sti.54.4.239

Osaki, S., Johnson, D. A., and Frieden, E. (1966). The Possible Significance of the Ferrous Oxidase Activity of Ceruloplasmin in Normal Human Serum. *J. Biol. Chem.* 241 (12), 2746–2751. doi: 10.1016/S0021-9258(18)96527-0

Pawlik, M.-C., Hubert, K., Joseph, B., Claus, H., Schoen, C., and Vogel, U. (2012). The Zinc-Responsive Regulon of *Neisseria Meningitidis* Comprises 17 Genes Under Control of a Zur Element. *J. Bacteriol.* 194 (23), 6594 LP–6603. doi: 10.1128/JB.01091-12

Pederick, V. G., Eijkelkamp, B. A., Begg, S. L., Ween, M. P., McAllister, L. J., Paton, J. C., et al. (2015). ZnuA and Zinc Homeostasis in *Pseudomonas Aeruginosa*. *Sci. Rep.* 5 (1), 13139. doi: 10.1038/srep13139

Perrin, A., Bonacorsi, S., Carbonnelle, E., Talibi, D., Dessen, P., Nassif, X., et al. (2002). Comparative Genomics Identifies the Genetic Islands That Distinguish *Neisseria Meningitidis*, the Agent of Cerebrospinal Meningitis, From Other *Neisseria* Species. *Infect. Immun.* 70 (12), 7063. doi: 10.1128/IAI.70.12.7063-7072.2002

Persson, K., Ly, H. D., Dieckelmann, M., Wakarchuk, W. W., Withers, S. G., and Strynadka, N. C. (2001). Crystal Structure of the Retaining Galactosyltransferase LgtC From *Neisseria Meningitidis* in Complex With Donor and Acceptor Sugar Analogs. *Nat. Struct. Biol.* 8 (2), 166–175. doi: 10.1038/84168

Putker, F., Grutsch, A., Tommassen, J., and Bos, M. P. (2014). Ght Protein of *Neisseria Meningitidis* Is Involved in the Regulation of Lipopolysaccharide Biosynthesis. *J. Bacteriol.* 196 (4), 780. doi: 10.1128/JB.00943-13

Quillin, S., and Seifert, H. (2018). *Neisseria Gonorrhoeae* Host Adaptation and Pathogenesis. *Springer Nat.* 16, 226–240. doi: 10.1038/nrmicro.2017.169

Quintana, J., Novoa-Aponte, L., and Argüello, J. M. (2017). Copper Homeostasis Networks in the Bacterium Pseudomonas Aeruginosa. *J. Biol. Chem.* 292 (38), 15691–15704. doi: 10.1074/jbc.M117.804492

Rahman, M. T., and Karim, M. M. (2018). Metallothionein: A Potential Link in the Regulation of Zinc in Nutritional Immunity. *Biol. Trace Element Res.* 182 (1), 1–13. doi: 10.1007/s12011-017-1061-8

Ramos, D., Mar, D., Ishida, M., Vargas, R., Gaite, M., Montgomery, A., et al. (2016). Mechanism of Copper Uptake From Blood Plasma Ceruloplasmin by Mammalian Cells. *PLos One* 11 (3), e0149516–e0149516. doi: 10.1371/journal.pone.0149516

Ronpirin, C., Jerse, A. E., and Cornelissen, C. N. (2001). Gonococcal Genes Encoding Transferrin-Binding Proteins A and B are Arranged in a Bicistronic Operon But are Subject to Differential Expression. *Infect. Immun.* 69 (10), 6336–6347. doi: 10.1128/IAI.69.10.6336-6347.2001

Seib, K. L., Tseng, H.-J., McEwan, A. G., Apicella, M. A., and Jennings, M. P. (2004). Defenses Against Oxidative Stress in *Neisseria Gonorrhoeae* and *Neisseria Meningitidis:* Distinctive Systems for Different Lifestyles. *J. Infect. Dis.* 190 (1), 136–147. doi: 10.1086/421299

Seib, K. L., Wu, H.-J., Kidd, S. P., Apicella, M. A., Jennings, M. P., and McEwan, A. G. (2006). Defenses Against Oxidative Stress in *Neisseria Gonorrhoeae*: A System Tailored for a Challenging Environment. *Microbiol. Mol. Biol. Rev.* 70 (2), 344–361. doi: 10.1128/MMBR.00044-05

Sintsova, A., Sarantis, H., Islam, E. A., Sun, C. X., Amin, M., Chan, C. H. F., et al. (2014). Global Analysis of Neutrophil Responses to *Neisseria Gonorrhoeae* Reveals a Self-Propagating Inflammatory Program. *PLos Pathog.* 10 (9), e1004341–e1004341. doi: 10.1371/journal.ppat.1004341

Stafford, S. L., Bokil, N. J., Achard, M. E. S., Kapetanovic, R., Schembri, M. A., McEwan, A. G., et al. (2013). Metal Ions in Macrophage Antimicrobial Pathways: Emerging Roles for Zinc and Copper. *Biosci. Rep.* 33 (4). doi: 10.1042/BSR20130014

Stähler, F. N., Odenbreit, S., Haas, R., Wilrich, J., Van Vliet, A. H. M., Kusters, J. G., et al. (2006). The Novel Helicobacter Pylori CznABC Metal Efflux Pump Is Required for Cadmium, Zinc, and Nickel Resistance, Urease Modulation, and Gastric Colonization. *Infect. Immun.* 74 (7), 3845–3852. doi: 10.1128/IAI.02025-05

Steimle, A., Autenrieth, I. B., and Frick, J.-S. (2016). Structure and Function: Lipid A Modifications in Commensals and Pathogens. *Int. J. Med. Microbiol.* 306 (5), 290–301. doi: 10.1016/j.ijmm.2016.03.001

Stork, M., Bos, M. P., Jongerius, I., de Kok, N., Schilders, I., Weynants, V. E., et al. (2010). An Outer Membrane Receptor of *Neisseria Meningitidis* Involved in Zinc Acquisition With Vaccine Potential. *PLos Pathog.* 6 (7), e1000969. doi: 10.1371/journal.ppat.1000969

Stork, M., Grijpstra, J., Bos, M. P., Mañas Torres, C., Devos, N., Poolman, J. T., et al. (2013). Zinc Piracy as a Mechanism of *Neisseria Meningitidis* for Evasion of Nutritional Immunity. *PLos Pathog.* 9 (10), e1003733–e1003733. doi: 10.1371/journal.ppat.1003733

Suzuki, T., Suzuki, K., Nakajima, K., Otaki, N., and Yamanaka, H. (1994). Metallothionein in Human Seminal Plasma. *Int. J. Urol.* 1 (4), 345–348. doi: 10.1111/j.1442-2042.1994.tb00062.x

Suzuki, T., Yamanaka, H., Nakajima, K., Suzuki, K., Kanatani, K., Kimura, M., et al. (1992). Immunohistochemical Study of Metallothionein in Human Seminal Vesicles. *Tohoku J. Exp. Med.* 167 (2), 127–134. doi: 10.1620/tjem.167.127

Taylor-Robinson, D., Furr, P. M., and Hetherington, C. M. (1990). *Neisseria Gonorrhoeae* Colonises the Genital Tract of Oestradiol-Treated Germ-Free Female Mice. *Microbial. Pathogen.* 9 (5), 369–373. doi: 10.1016/0882-4010(90)90071-W

Tidball, A. M., Bryan, M. R., Uhouse, M. A., Kumar, K. K., Aboud, A. A., Feist, J. E., et al. (2015). A Novel Manganese-Dependent ATM-P53 Signaling Pathway is Selectively Impaired in Patient-Based Neuroprogenitor and Murine Striatal Models of Huntington's Disease. *Hum. Mol. Genet.* 24 (7), 1929–1944. doi: 10.1093/hmg/ddu609

Tinsley, C. R., and Nassif, X. (1996). Analysis of the Genetic Differences Between *Neisseria Meningitidis* and *Neisseria Gonorrhoeae*: Two Closely Related Bacteria Expressing Two Different Pathogenicities. *Proc. Natl. Acad. Sci. U. S. A.* 93 (20), 11109–11114. doi: 10.1073/pnas.93.20.11109

Tseng, H. J., Srikhanta, Y., McEwan, A. G., and Jennings, M. P. (2001). Accumulation of Manganese in *Neisseria Gonorrhoeae* Correlates With Resistance to Oxidative Killing by Superoxide Anion and is Independent of Superoxide Dismutase Activity. *Mol. Biol.* 40 (5), 1175–1186. doi: 10.1046/j.1365-2958.2001.02460.x

Urban, C. F., Ermert, D., Schmid, M., Abu-Abed, U., Goosmann, C., Nacken, W., et al. (2009). Neutrophil Extracellular Traps Contain Calprotectin, a Cytosolic Protein Complex Involved in Host Defense Against *Candida Albicans*. *PLos Pathog.* 5 (10), e1000639. doi: 10.1371/journal.ppat.1000639

van Emmerik, L. C., Kuijper, E. J., Fijen, C. A., Dankert, J., and Thiel, S. (1994). Binding of Mannan-Binding Protein to Various Bacterial Pathogens of Meningitis. *Clin. Exp. Immunol.* 97 (3), 411–416. doi: 10.1111/j.1365-2249.1994.tb06103.x

Vélez Acevedo, R. N., Ronpirin, C., Kandler, J. L., Shafer, W. M., and Cornelissen, C. N. (2014). Identification of Regulatory Elements That Control Expression of the *tbpBA* Operon in *Neisseria Gonorrhoeae*. *J. Bacteriol.* 196 (15), 2762–2774. doi: 10.1128/JB.01693-14

Veyrier, F. J., Boneca, I. G., Cellier, M. F., and Taha, M.-K. (2011). A Novel Metal Transporter Mediating Manganese Export (MntX) Regulates the Mn to Fe Intracellular Ratio and *Neisseria Meningitidis* Virulence. *PLos Pathog.* 7 (9), e1002261–e1002261. doi: 10.1371/journal.ppat.1002261

Voganatsi, A., Panyutich, A., Miyasaki, K. T., and Murthy, R. K. (2001). Mechanism of Extracellular Release of Human Neutrophil Calprotectin Complex. *J. Leukocyte Biol.* 70 (1), 130–134. doi: 10.1189/jlb.70.1.130

Wagner, D., Maser, J., Lai, B., Cai, Z., Barry, C. E., Höner zu Bentrup, K., et al. (2005). Elemental Analysis of *Mycobacterium Avium*, *Mycobacterium Tuberculosis*, and *Mycobacterium Smegmatis* Containing Phagosomes Indicates Pathogen-Induced Microenvironments Within the Host Cell's Endosomal System. *J. Immunol.* 174 (3), 1491. doi: 10.4049/jimmunol.174.3.1491

White, C., Lee, J., Kambe, T., Fritsche, K., and Petris, M. J. (2009). A Role for the ATP7A Copper-Transporting ATPase in Macrophage Bactericidal Activity. *J. Biol. Chem.* 284 (49), 33949–33956. doi: 10.1074/jbc.M109.070201

Woods, J. P., Dempsey, J. F., Kawula, T. H., Barritt, D. S., and Cannon, J. G. (1989). Characterization of the Neisserial Lipid-Modified Azurin Bearing the H.8 Epitope. *Mol. Microbiol.* 3 (5), 583–591. doi: 10.1111/j.1365-2958.1989.tb00205.x

Wu, H.-J., Seib, K. L., Srikhanta, Y. N., Edwards, J., Kidd, S. P., Maguire, T. L., et al. (2010). Manganese Regulation of Virulence Factors and Oxidative Stress Resistance in *Neisseria Gonorrhoeae*. *J. Proteomics* 73 (5), 899–916. doi: 10.1016/j.jprot.2009.12.001

Wu, H.-J., Seib, K., Srikhanta, Y., Kidd, S., Edwards, J., Maguire, T., et al. (2006). PerR Controls Mn-Dependent Resistance to Oxidative Stress in *Neisseria Gonorrhoeae*. *Mol. Biol.* 60 (2), 401–416. doi: 10.1111/j.1365-2958.2006.05079.x

Wu, H., Soler-García, A. A., and Jerse, A. E. (2009). A Strain-Specific Catalase Mutation and Mutation of the Metal-Binding Transporter Gene *mntC* Attenuate *Neisseria Gonorrhoeae In Vivo* But Not by Increasing Susceptibility to Oxidative Killing by Phagocytes. *Infect. Immun.* 77 (3), 1091–1102. doi: 10.1128/IAI.00825-08

Yadav, R., Noinaj, N., Ostan, N., Moraes, T., Stoudenmire, J., Maurakis, S., et al. (2020). Structural Basis for Evasion of Nutritional Immunity by the Pathogenic *Neisseriae*. *Front. Microbiol.* 10. doi: 10.3389/fmicb.2019.02981

Zackular, J. P., Chazin, W. J., and Skaar, E. P. (2015). Nutritional Immunity: S100 Proteins at the Host-Pathogen Interface. *J. Biol. Chem.* 290 (31), 18991–18998. doi: 10.1074/jbc.R115.645085

Zhou, B., and Gitschier, J. (1997). *Hctr1*: A Human Gene for Copper Uptake Identified by Complementation in Yeast. *Proc. Natl. Acad. Sci.* 94 (14), 7481. doi: 10.1073/pnas.94.14.7481

Zughaier, S. M., Kandler, J. L., and Shafer, W. M. (2014). Neisseria Gonorrhoeae Modulates Iron-Limiting Innate Immune Defenses in Macrophages. *PLos One* 9 (1), e87688. doi: 10.1371/journal.pone.0087688

Conflict of Interest: The authors declare that the research was conducted in the absence of any commercial or financial relationships that could be construed as a potential conflict of interest.

Publisher's Note: All claims expressed in this article are solely those of the authors and do not necessarily represent those of their affiliated organizations, or those of the publisher, the editors and the reviewers. Any product that may be evaluated in this article, or claim that may be made by its manufacturer, is not guaranteed or endorsed by the publisher.

frontiers | Frontiers in Cellular and Infection Microbiology

ORIGINAL RESEARCH
published: 13 July 2022
doi: 10.3389/fcimb.2022.898796

The Innate Immune Protein Calprotectin Interacts With and Encases Biofilm Communities of *Pseudomonas aeruginosa* and *Staphylococcus aureus*

Jiwasmika Baishya[1], *Jake A. Everett*[2], *Walter J. Chazin*[3,4,5], *Kendra P. Rumbaugh*[2,6,7] *and Catherine A. Wakeman*[1]*

[1] Department of Biological Sciences, Texas Tech University, Lubbock, TX, United States, [2] Department of Surgery, Texas Tech University Health Sciences Center, Lubbock, TX, United States, [3] Department of Biochemistry, Vanderbilt University, Nashville, TN, United States, [4] Department of Chemistry, Vanderbilt University, Nashville, TN, United States, [5] Center for Structural Biology, Vanderbilt University, Nashville, TN, United States, [6] Department of Immunology and Molecular Microbiology, Texas Tech University Health Sciences Center, Lubbock, TX, United States, [7] Texas Tech University Health Sciences Center Surgery Burn Center of Research Excellence, Texas Tech University Health Sciences Center, Lubbock, TX, United States

OPEN ACCESS

Edited by:
Mauricio H Pontes,
The Pennsylvania State University, United States

Reviewed by:
Thomas H Hampton,
Dartmouth College, United States
Chelsie Armbruster,
University at Buffalo, United States

***Correspondence:**
Catherine A. Wakeman
catherine.wakeman@ttu.edu

Specialty section:
This article was submitted to Bacteria and Host, a section of the journal Frontiers in Cellular and Infection Microbiology

Received: 17 March 2022
Accepted: 09 June 2022
Published: 13 July 2022

Citation:
Baishya J, Everett JA, Chazin WJ, Rumbaugh KP and Wakeman CA (2022) The Innate Immune Protein Calprotectin Interacts With and Encases Biofilm Communities of Pseudomonas aeruginosa and Staphylococcus aureus. Front. Cell. Infect. Microbiol. 12:898796. doi: 10.3389/fcimb.2022.898796

Calprotectin is a transition metal chelating protein of the innate immune response known to exert nutritional immunity upon microbial infection. It is abundantly released during inflammation and is therefore found at sites occupied by pathogens such as *Pseudomonas aeruginosa* and *Staphylococcus aureus*. The metal limitation induced by this protein has previously been shown to mediate *P. aeruginosa* and *S. aureus* co-culture. In addition to the transition metal sequestration role of calprotectin, it has also been shown to have metal-independent antimicrobial activity *via* direct cell contact. Therefore, we sought to assess the impact of this protein on the biofilm architecture of *P. aeruginosa* and *S. aureus* in monomicrobial and polymicrobial culture. The experiments described in this report reveal novel aspects of calprotectin's interaction with biofilm communities of *P. aeruginosa* and *S. aureus* discovered using scanning electron microscopy and confocal laser scanning microscopy. Our results indicate that calprotectin can interact with microbial cells by stimulating encapsulation in mesh-like structures. This physical interaction leads to compositional changes in the biofilm extracellular polymeric substance (EPS) in both *P. aeruginosa* and *S. aureus*.

Keywords: calprotectin, *Pseudomonas aeruginosa*, *Staphylococcus aureus*, biofilm architecture, extracellular polymeric substance (EPS), nutritional immunity

INTRODUCTION

Multiple pathogenic and commensal microbial species can colonize the human body. These microbial species often form highly adaptable, monomicrobial or polymicrobial communities called biofilms. Biofilms are encased in a matrix called the extracellular polymeric substance, or the EPS, that is typically produced by the microbes living within the biomass (Costerton et al., 1999). Microbial biofilms exhibit altered gene expression compared to their planktonic counterparts and

have been shown to protect cells from environmental stresses such as antibiotics and phagocytosis (Römling and Balsalobre, 2012) (Stewart and Franklin, 2008; Flemming et al., 2016). The presence of the EPS as a physical barrier of drug penetration also provides antimicrobial resistance to biofilm-forming polymicrobial communities (Ren et al., 2019) and aids survival in harsh environmental conditions (Goltermann and Tolker-Nielsen, 2017). Additionally, the probability of exchange of DNA molecules containing antibiotic-resistance genes is also very high within cells in a biofilm (Águila-Arcos et al., 2017, Balcázar et al., 2015).

Most chronic infections such as cystic fibrosis (CF), chronic wound infections, periodontitis, chronic prostatitis, otitis media, *etc*. are associated with microbial biofilms (Donlan, 2002). According to the National Institutes of Health, biofilms account for almost 80% of all chronic microbial infections (James et al., 2008). *Pseudomonas aeruginosa* is a ubiquitous nosocomial pathogen particularly notable for the ability to form robust biofilms upon infection (Goltermann and Tolker-Nielsen, 2017).

To prevent colonization by pathogens, the host's innate and adaptive immune responses possess various pattern-recognition receptors (PRRs), which detect microbial-associated molecular patterns (MAMPs) and trigger intracellular and intercellular signaling pathways (Medzhitov, 2007; Tan et al., 2018). The innate immune response is the first line of defense against bacterial infections. Its recognition of MAMPs is mediated by germline encoded PRRs, each of which can detect molecular structures unique to microorganisms (Janeway, 1989; Kubelkova and Macela, 2019). The PRRs have broad specificity and can often bind to many molecules with a common structural motif or pattern (Medzhitov, 2007). In addition to defending the host tissues *via* MAMP recognition-mediated phagocytosis, innate immune cells have other processes to inhibit invasion of tissues by pathogenic species. For example, host neutrophils have been shown to exert nutritional immunity on microbial pathogens such as *Pseudomonas aeruginosa* and *Staphylococcus aureus* (Corbin et al., 2008; Kehl-Fie et al., 2011; Zygiel et al., 2019). Nutritional immunity refers to withholding essential metals, such as iron, zinc, manganese, *etc*., from pathogens to hinder invasion and colonization (Hood and Skaar, 2012). Sequestration of transition metals is an effective antimicrobial strategy as these metals often serve as co-factors for essential enzymes in pathogens (Hood and Skaar, 2012; Ma et al., 2015). Transition metal-sequestering proteins are released from immune cells to bind free metal ions and decrease their concentration at infection sites. Calprotectin (CP) is one such metal-sequestering innate immune protein known for its ability to limit microbial access to multiple transition metal nutrients (Damo et al., 2013; Zygiel et al., 2019).

CP is a hetero-dimer of two S100 EF-hand Ca(II)-binding proteins, S100A8 (10.8 kDa) and S100A9 (13.2 kDa) that form an integrated structural unit with four EF-hand motifs. The CP heterodimer has two transition metal binding sites at the S100A8/S100A9 interface: a His3Asp motif (site 1) that chelates Zn(II) and Cu(II) and a His6 motif (site 2) that chelates these and other divalent metal ions, including Mn(II), Fe(II) and Ni(II) (Korndorfer et al., 2007; Damo et al., 2013; Nakashige et al., 2016; Gilston et al., 2016). The binding of Ca(II) or transition metals by CP promotes formation of a heterotetrameric dimer of dimers, and ultimately, higher order oligomeric states. All metal binding sites are energetically coupled, so binding of Ca(II) in the EF-hands increases the binding affinities at the transition metal site and vice versa (Obisesan et al., 2021).

In standard laboratory culture, *P. aeruginosa* is known to interact competitively with *S. aureus* (Mashburn et al., 2005; Beaume et al., 2015; Nguyen and Oglesby-Sherrouse, 2016). Typically, this competition results in *P. aeruginosa* dominating and outcompeting *S. aureus* growth. However, during infection, these two microbes are often found to coexist and exhibit a spectrum of microbial interactions ranging from competitive to cooperative depending on environmental context (Limoli and Hoffman, 2019). For example, CP exposure and zinc limitation has been shown to suppress competitive phenotypes in *P. aeruginosa* and permit coexistence with *S. aureus* (Wakeman et al., 2016; Vermilyea et al., 2021). Specifically, CP-mediated zinc limitation leads to repression of *P. aeruginosa* virulence factors such as pyocyanin and alkyl quinolones, which can promote co-infection with *S. aureus* in the murine lung (Wakeman et al., 2016). This suggests that the host immune protein CP can alter interactions between these pathogens.

In addition to the physiological effects of CP exposure mediated by transition metal sequestration, CP has been shown to interact with the surface of some pathogens to achieve an antimicrobial effect that is independent of metal starvation (Besold et al., 2018). Due to the ability of CP to impact bacterial cells in both a metal-dependent and contact-dependent manner, we sought to better understand the role that CP can play in the biofilm community structure of both mono- and polymicrobial communities of *S. aureus* and *P. aeruginosa*. We hypothesized that the surface interactions of CP associating to microbial cells could directly influence biofilm community extracellular polymeric substance (EPS) in a manner independent of zinc starvation. To test this hypothesis, we studied *S. aureus* and *P. aeruginosa* biofilm community structure in the presence and absence of CP using scanning electron microscopy (SEM) and confocal laser scanning microscopy (CLSM). Using these methods, we indeed observed direct interactions between CP and the cell surface of both Gram-positive and Gram-negative microbes and found that this interaction influenced biofilm EPS composition.

MATERIALS AND METHODS

Bacterial Strains and Media

The *P. aeruginosa* strain used in the experiments is UCBPP-PA14, a highly virulent strain originally isolated from a wound infection (Rahme et al., 1995). The *S. aureus* strain used in the experiments is USA300 JE2, a laboratory-adapted strain derived from the parental strain, USA300, which was isolated from skin

and soft tissue infection (Rahme et al., 1995). Both the strains were stored as glycerol stocks at -80°C and grown overnight at 37°C in Tryptic soy broth (TSB) for conducting any of the experiments described in this paper. The *P. aeruginosa* strain used in the *in vivo* infections is PAO1, a wild-type strain originally isolated from wound and is capable of producing exopolysaccharides such as Psl, Pel and alginate (Holloway, 1955).

Chemicals and Reagents

All chemicals used to perform experiments were purchased from Sigma-Aldrich unless otherwise indicated. Wild-type human CP was expressed in *E. coli* and purified by ion exchange followed by size-exclusion chromatography as described previously (Kehl-Fie et al., 2011; Damo et al., 2013). Fixative solutions used to process biofilms for SEM and CLSM were purchased from Electron Microscopy Sciences (https://www.emsdiasum.com/microscopy/).

Antibodies and Fluorescent Dyes

Human CP in culture media was detected by binding of the primary antibody, S100A8 Polyclonal Antibody (catalog number: PA5-82881, Invitrogen™) and mouse CP in chronic wound infections was detected by binding of the primary antibody, S100A8 Polyclonal Antibody (catalog number: BS-2696R, Invitrogen™). These were, in turn, bound by the fluorescently tagged secondary antibody, Goat anti-Rabbit IgG (H+L) Secondary Antibody, Alexa Fluor 488-10 nm colloidal gold (catalog number: A-31566, Invitrogen™). Microbial cell viability in *in vitro* samples was checked by staining biofilms with the cell-permeant dye, Hoechst 33342 Solution (20 mM) (catalog number: 62249, Thermo Scientific™). Microbial presence in *in vivo* samples was detected by labelling with the primary antibody, Anti-*Pseudomonas aeruginosa* antibody (catalog number: ab74980, abcam), coupled to a red-fluorescent secondary antibody, Goat Anti-Chicken IgY H&L (Alexa Fluor® 594) preadsorbed (catalog number: ab150176, abcam). The biofilm EPS matrix components such as extracellular DNA (eDNA), matrix proteins, and carbohydrates such as α-mannopyranosyl and α-glucopyranosyl residues were detected by the fluorescent dyes, TOTO™-3 Iodide (642/660) (catalog number: T3604, Invitrogen™); FilmTracer™ SYPRO™ Ruby Biofilm Matrix Stain (catalog number: F10318, Invitrogen™); and Concanavalin A, Tetramethylrhodamine Conjugate (catalog number: C860, Invitrogen™), respectively. Fluorescently stained coverslips were mounted on glass slides using the ProLong™ Diamond Antifade Mountant (catalog number: P36961, Invitrogen™).

In Vitro Co-Culture

Co-culture assays were performed in 50 mL conical tubes containing co-culture media (60% TSB; 40% calprotectin buffer [100 mM NaCl, 3 mM $CaCl_2$, 10 mM β-mercaptoethanol, 20 mM Tris, pH 7.5)]. In the presence of CP and +zinc conditions, co-culture media was supplemented with 0.25 mg/mL WT calprotectin and 10 μM $ZnCl_2$, respectively. The 50 mL conical tube co-cultures were seeded with 1:100 dilutions of the metal-limited *P. aeruginosa* and/or *S. aureus* monocultures and grown for 42 hours statically at 37°C. The metal-limited monocultures *P. aeruginosa* and *S. aureus* used to seed the co-cultures were first grown overnight in glucose-supplemented low nutrient broth (GLNB) (2 g l–1 tryptic soy broth, 2 g l–1 glucose) at 37°C with shaking at 180 r.p.m. The next morning, cultures were metal-restricted by pelleting and suspending samples in Chelex 100-treated GLNB supplemented with 100 μM $CaCl_2$ and 1 mM $MgCl_2$. These cultures were grown at 37°C with shaking at 180 r.p.m. for 1.5 hours. Cultures were then pelleted, suspended in fresh metal-restricted GLNB, and grown for an additional 1.5 hours to produce metal-limited samples used for co-culture inoculation. Culture assays with Bovine serum albumin (BSA) were performed similarly in 50 mL conical tubes containing 0.25 mg/mL BSA added to TSB growth media.

Murine Chronic Wound Infection Model

Adult female, non-diabetic Swiss Webster mice were anesthetized and depilated prior to administering full-thickness surgically excised wounds as previously described (Watters et al., 2013). To establish infection, 10^5 CFU/mL of PAO1 was administered onto the wound bed. Wound-only groups were mock-infected with sterile phosphate-buffered saline. Uninjured mice were anesthetized, depilated, but not wounded. Mice were euthanized at 12-days post-injury and an approximately 2.5 cm^2 area of the superficial murine dorsa, including wound bed and surrounding intact tissues, were resected for histology. Tissues were fixed with 10% neutral buffered formalin, embedded in paraffin and cut into sections.

Scanning Electron Microscopy

For SEM, static cultures of *P. aeruginosa* and *S. aureus* were grown in 50 mL conical tubes with circular glass coverslips partially submerged in 1 mL of media. Coverslip samples were handled and processed as described previously (Gaddy et al., 2009). Briefly, cells on coverslips were fixed at room temperature for 1 hour using a primary fixative (2.5% glutaraldehyde, 2% paraformaldehyde solution in 0.05M sodium cacodylate buffer, pH 7.4). Fixed cells were then washed with 0.05 M sodium cacodylate to prevent sample dehydration. The coverslips were then incubated in 1% osmium tetroxide for 30 minutes, followed by a series of ethanol dehydration with increasing ethanol concentrations starting from 25% to 100%. Finally, cells were dried using liquid CO_2 at critical point temperature and pressure. Processed samples were gold-palladium coated before imaging using a Hitachi S-4300 scanning electron microscope.

Confocal Laser Scanning Microscopy

For CLSM, *P. aeruginosa* and *S. aureus* static cultures were grown in 50 mL conical tubes with rectangular glass coverslips partially submerged in 3 mL of media. Post 42-hour incubation, coverslips were washed with phosphate-buffered saline to remove planktonic cells and fixed at room temperature for 1 hour using 4% paraformaldehyde solution. Fixed cells were washed with phosphate-buffered saline and blocked using 10% normal goat serum at room temperature for 1 hour. Blocked coverslips were incubated with S100A8 primary antibody and Goat anti-Rabbit

Alexa Fluor 488 for 1 hour each to detect CP. To detect EPS matrix components, coverslips were incubated with either 2 μM TOTO-3 iodide for 20 minutes, or 200 μL of FilmTracer™ SYPRO™ Ruby Biofilm Matrix Stain for 30 minutes, or 200 μg/mL Concanavalin A, Tetramethylrhodamine Conjugate (TRITC Con A) for 1 hour. Coverslips were counterstained with the 20 μg/mL Hoechst 33342 for 15 minutes. Fluorescently labeled coverslips were mounted on glass slides and imaged at 100X magnification using the Olympus FV3000 Scanning Confocal Microscope.

Confocal Imaging of Infected Mouse Wound Tissue

Tissue sections were de-paraffinized by washing them first with pure xylene twice (3 minutes each) and then with xylene mixed with 100% ethanol in a 1:1 ratio (3 minutes wash). Following this, tissue sections were treated twice with 100% ethanol and once each with 95%, 70% and 50% ethanol for 3 minutes each in the order mentioned and then submerged in cold tap water. Tris-EDTA buffer (10 mM Tris base, 1 mM EDTA solution, 0.05% Tween 20, pH 9.0) was used to perform heat-induced epitope retrieval on de-paraffinized sections. Briefly, the antigen retrieval buffer was heated to a temperature of ~98°C for 20 minutes on a hot plate. Tissue sections were placed inside 50 mL conical tubes containing the hot buffer solution and boiled for 20 minutes while being submerged within this solution. Post 20 minutes, tissue sections were rinsed with running cold tap water for 10 minutes and then blocked using 10% normal goat serum at room temperature for 1 hour. Blocked sections were incubated with the S100A8 and the Chicken anti-*P. aeruginosa* primary antibodies overnight at 4°C. The following morning, sections were incubated with the Goat anti-Rabbit Alexa Fluor 488 and the Goat Anti-Chicken IgY H&L (Alexa Fluor® 594) secondary antibodies simultaneously for 1 hour, each to detect CP and PAO1, respectively (Fleming et al., 2022). Labelled sections were finally counterstained with 2 μg/mL Hoechst 33342 for 15 minutes and imaged at 100X magnification using the Olympus FV3000 Scanning Confocal Microscope.

Image Analyses

Image analyses were done using ImageJ for EPS quantification and CellSens for colocalization quantification. For EPS quantification, images were analyzed by splitting each image into RGB channels. Fluorescence integrated density values for TOTO-3 iodide/SYPRO Ruby/TRITC Con-A stains were collected from the red channel and for Hoechst 33342 stain from the blue channel. All fluorescence integrated density values were normalized based on the area and respective backgrounds. Average density values of each image were calculated and data was recorded as a ratio of TOTO-3 iodide/SYPRO Ruby/TRITC Con-A signals relative to Hoechst 33342 signals. Finally, the trimmed averages from each replicate (trimmed average represents the average of a dataset calculated by excluding the highest and lowest values of the set) were graphed using GraphPad Prism. For qualitative purposes, the brightness and contrast have been adjusted equally for all confocal images.

Statistical Analyses

Statistical analyses were performed using GraphPad Prism 9.0 (GraphPad Software, Inc., San Diego, CA). Unpaired t-test (two-tailed) was used to calculate statistical significances.

RESULTS

CP Leads to Encapsulation of *Pseudomonas aeruginosa* and *Staphylococcus aureus* in a Mesh-Like Structure

The interaction of pathogenic microorganisms with host immune molecules can play a significant role in their survival and colonization in human tissues (Baishya and Wakeman, 2019). Research conducted with CP and the causative agent of Lyme disease, *Borreliella (Borrelia) burgdorferi*, has shown that CP can inhibit the growth of *B. burgdorferi via* a mechanism that involves physical association of the protein with the bacteria (Besold et al., 2018). Additionally, exposure to CP has been shown to repress the production of anti-staphylococcal molecules within metal-deplete portions of *P. aeruginosa* biofilm and promote interaction between *P. aeruginosa* and *S. aureus* (Wakeman et al., 2016). Given these findings, we wanted to visualize the interaction of CP with *P. aeruginosa* and *S. aureus* biofilm communities in monoculture and co-culture using SEM.

Our SEM images of cultures grown in presence of 0.25 mg/mL CP, a physiologically relevant levels of this protein (Kehl-Fie et al., 2011), revealed the presence of a large and distinctive mesh-like structure that appeared to be encapsulating both *P. aeruginosa* and *S. aureus* cells (**Figure 1**). The structure was seen in both the monoculture conditions (**Figures 1A, B**) as well as the co-culture condition (**Figure 1C**). The observation that the formation of the mesh was not microbial species specific indicated that the enormous structure is likely not a bacterial EPS component but rather composed of an aggregation of the CP protein. However, to verify that the mesh formation in the presence of CP was not a cellular adaptation to CP-induced metal starvation, excess zinc was supplemented into the cultures to determine if the mesh-like structure was abolished by reversal of metal starvation. Since CP contains two metal binding sites, one known to be zinc/copper specific and one known to generally bind to multiple transition metals (Damo et al., 2013), saturation of these two sites with excess zinc is likely to generally alleviate CP-induced metal starvation. Supplementation with excess zinc did not reverse the formation of the mesh (**Supplementary Figures 1A–C**), indicating that the mesh is not simply an EPS adaptation to CP-induced metal restriction. Since cell surface contact between CP and microbial cells has previously been shown to be important (Besold et al., 2018), these mesh-like structures could be associated with the contact-based antimicrobial mechanism of CP.

Alternatively, these structures could represent a general aggregation phenotype of proteins added at high concentrations. To assess this possibility, we tested whether bovine serum albumin (BSA) will aggregate and cause a similar mesh structure at 0.25 mg/mL in the presence of biofilms. In this control experiment, the mesh

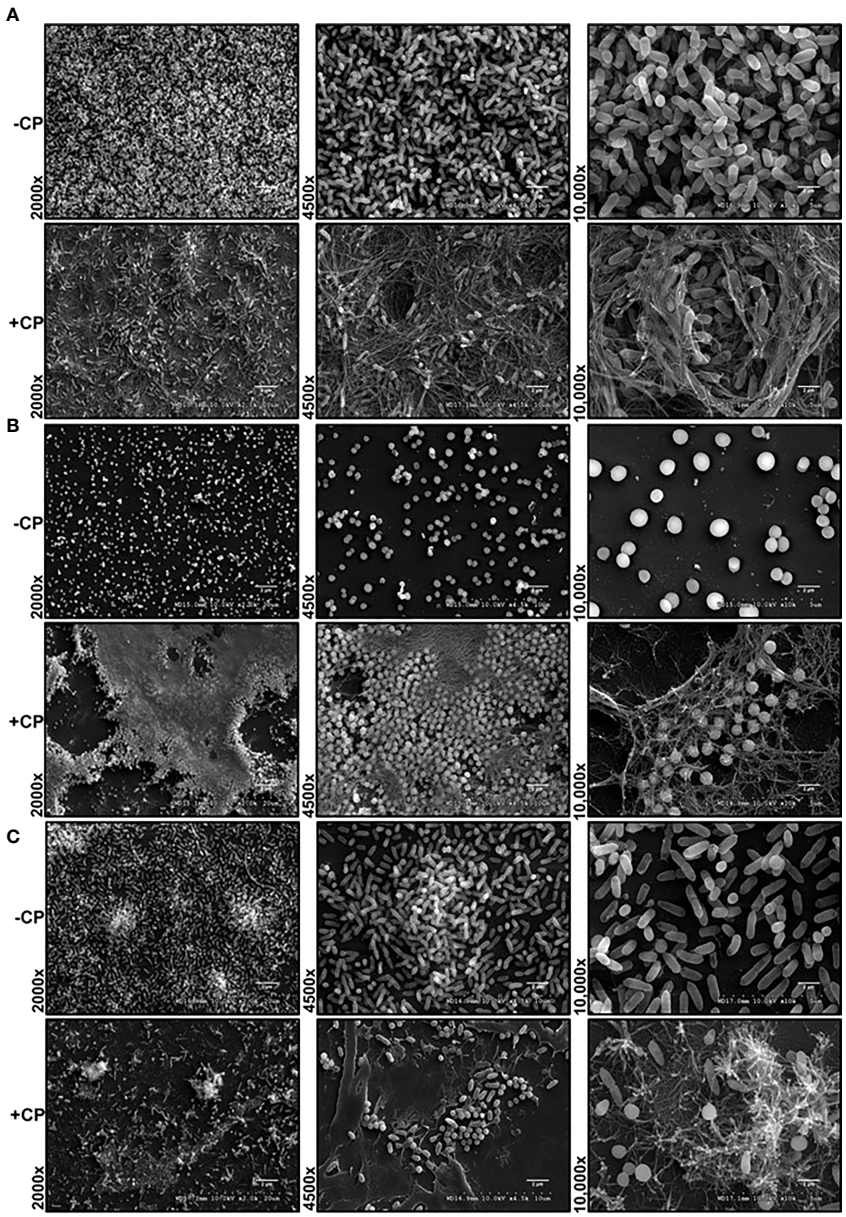

FIGURE 1 | Addition of CP to growth media leads to encapsulation of *P. aeruginosa* and *S. aureus* in a mesh-like structure. SEM images of *P. aeruginosa* and *S. aureus* biofilms grown as mono and co-cultures in +/- CP conditions- **(A)** *P. aeruginosa* monoculture **(B)** *S. aureus* monoculture **(C)** *P. aeruginosa-S. aureus* co-culture. Images show 2000X, 4500X, and 10,000X magnification and are representative of three independent experiments.

structure was only observed in CP treated but not BSA treated biofilms (**Supplementary Figure 2**) suggesting that the structure observed in presence of CP may be unique to this protein.

The Mesh-Like Structure Encasing Biofilms Contains Substantial Amounts of CP

After detecting the presence of a mesh-like structure in *P. aeruginosa* and/or *S. aureus* biofilm cultures containing the antimicrobial protein, CP, we wanted to confirm this structure contains CP. Therefore, we used immunofluorescence with a S100A8 Polyclonal primary antibody to directly detect CP presence in the biofilm structures. Our confocal images showed that in monocultures and co-culture of *P. aeruginosa* and/or *S. aureus*, only microbial cells were detected in the absence of CP, whereas both microbial cells as well as CP were detected in the presence of CP treatment (**Figures 2A–C**). Additionally, the signals denoting CP resembled the structure of the mesh seen in our SEM images where the CP-induced mesh appeared to be encapsulating *P. aeruginosa* and/or *S. aureus* cells within it. Thus, these results indicate that the mesh-like structure around microbial cells contains substantial amounts of CP and likely

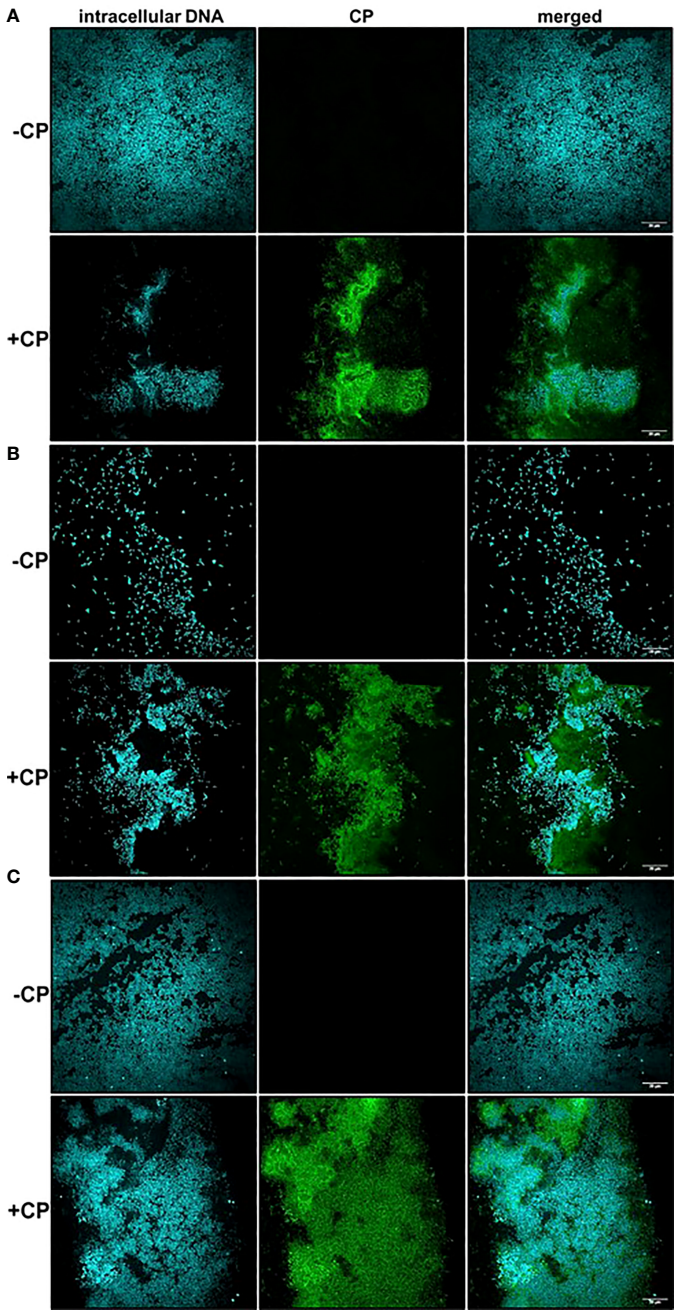

FIGURE 2 | Calprotectin is a major component of the mesh-like structure that encapsulates *P. aeruginosa* and *S. aureus* biofilms. Intracellular DNA of microbial cells was detected by staining with the cell-permeant nucleic acid dye, Hoechst 33342; CP was detected by staining with Alexa fluor 488-tagged Goat anti-Rabbit antibody. **(A)** *P. aeruginosa* monoculture **(B)** *S. aureus* monoculture **(C)** *P. aeruginosa-S. aureus* co-culture. Images show 100X magnification and were processed using ImageJ.

plays a role in CP's interaction with microorganisms through a contact-based mechanism.

A striking and consistent observation from our CLSM images was that *S. aureus* monoculture biofilms grown in the absence of CP contained very few cells unlike the *P. aeruginosa* monoculture and the co-culture biofilms. Addition of CP led to an increase in *S. aureus* cells when grown as biofilms under static conditions at 37°C (**Figure 2B**). We were able to demonstrate that, while the growth conditions used in these studies did lead to a reduction in *P. aeruginosa* numbers, *S. aureus* viability was unaffected by our CP treatments (**Supplemental Figure 3**). Even though CP treatment was not toxic to *S. aureus* in our experimental conditions, it is surprising and interesting that a growth condition known to elicit zinc

limitation would induce *S. aureus* biofilm formation given the fact that certain biofilm-associated proteins of *S. aureus* such as SasG have been shown to require zinc for biofilm formation (Formosa-Dague et al., 2016). Of note, it is known that *S. aureus* preferentially forms biofilms on substrates treated with host components such as human plasma (Chen et al., 2012; Cardile et al., 2014; Watters et al., 2016). These data indicate that, in *S. aureus* biofilms, CP-stimulated mesh-like structures might represent another host-derived substrate that can promote surface colonization, at least at sublethal concentrations of this protein.

Accumulation of CP Around *P. aeruginosa* Occurs in Murine Chronic Wound Infections

To check if CP interacted with *P. aeruginosa* infecting host tissues *via* a similar mechanism involving mesh formation and encapsulation as seen under *in vitro* conditions, we stained PAO1-infected murine wound tissue sections using a mouse CP antibody and a *P. aeruginosa* staining antibody. The CLSM images from the prepared tissue sections from 12 day murine chronic wound infections revealed multiple areas consisting of an overlap of CP and PAO1 signals and an apparent encasement of PAO1 cells within CP-containing structures (**Figure 3**). The CP-stimulated structures detected in these more complex *in vivo* samples are not identical to the ones we showed in our *in vitro* samples (**Figure 2**), possibly due to the increased sample complexity or the additional processing required to remove the paraffin embedding matrix on the murine samples. However, the CP and *P. aeruginosa* aggregates in the *in vivo* samples do display enough similarities to our *in vitro* data to indicate that these findings might be relevant to structures occurring naturally during infection.

The Carbohydrate Component of the EPS Is Enriched in the CP-Induced Matrix of *P. aeruginosa* and *S. aureus* Biofilms

As CP was directly interacting with microbial biofilms, we hypothesized that this contact might influence the production and localization of biofilm EPS components. To test this, we used fluorescent dyes to stain three major components of *P. aeruginosa* and *S. aureus* biofilm matrix, namely: eDNA; proteins; and carbohydrates. We first quantified the eDNA levels of the EPS in the presence or absence of CP. We hypothesized that the contact-mediated antimicrobial action of CP might result in increased eDNA release. Instead, we observed relatively small overall impacts on eDNA release relative to cell number in any of the conditions tested. If any trends could be inferred, it would be the opposite of what was hypothesized, with subtle trends towards a CP-mediated decrease in eDNA release per biomass in some cultures (**Figure 4**). Quantification of this data confirmed that no apparent trends were statistically significant (**Figure 4D**). We also compared the colocalization of eDNA in the biofilm matrix of both *P. aeruginosa* and *S. aureus* with cells and CP. Our results show no to minimal correlation with the distribution of eDNA signal with cell signal and/or CP signal in any tested conditions (**Figure 4E**).

Next, we determined the impact of CP on protein component of the EPS using SYPRO ruby staining. These data indicate subtle trends in increased protein EPS component in cultures containing *P. aeruginosa* (**Figures 5A–C**). However, due to high variability in the data, these trends display no statistical significance (**Figure 5D**). Furthermore, this stain is a very general stain that can associate with CP. Therefore, it was especially important that we demonstrate that the SYPRO staining is not simply co-localizing with the CP signal. Some degree of co-localization of the CP signal and the general protein signal was observed, but this co-localization did not exceed what was observed for the correlation between the protein and cell signals (**Figure 5E**).

Finally, we determined the impact of CP on carbohydrate molecules present in the biofilm EPS of *P. aeruginosa* and *S. aureus*. Our data indicate trends of CP-mediated increases of carbohydrate EPS components (specifically, α-mannopyranosyl and α-glucopyranosyl-containing ones based on the known staining preference of the concanavalin A dye) in all culture conditions (**Figure 6**); however, only the CP-induced increase seen in *P. aeruginosa* monoculture was determined to be statistically significant (**Figure 6D**). Colocalization data for carbohydrates in the biofilm matrix of both *P. aeruginosa* and *S. aureus* with cells and CP showed higher colocalization of CP with carbohydrates compared to cells for all culture conditions (**Figure 6E**), indicating a potential role of carbohydrate EPS molecules in combating CP-mediated antibacterial stresses. Overall, these data indicate that addition of CP can lead to alterations in the carbohydrate composition of *P. aeruginosa* and *S. aureus*'s biofilm matrix. These alterations are interesting and might be associated with microbial responses to the host environment.

DISCUSSION

Microorganisms are ubiquitous and exhibit physiological changes that allow them to adapt and survive in varying environments. These adaptations allow microorganisms to sustain life and multiply by utilizing the resources/factors unique to each environment. For example, biofilm communities of *P. aeruginosa* have been shown to exhibit temperature-specific adaptations in the human host versus in an industrial/environmental (i.e., soil/root associated or aquatic) surrounding (Bisht et al., 2021). Similarly, pathogenic microbial species rely on different biological processes when grown in laboratory conditions compared to when they infect and attempt to colonize human hosts (Cornforth et al., 2018; Ibberson and Whiteley, 2019). Colonization and survival in the human host environment can be different from lab conditions as it requires microbial species to counteract and overcome the host-associated antimicrobial molecules (Baishya and Wakeman, 2019). Therefore, studying the interactions between the human host immune components and pathogenic biofilm communities, at the host-pathogen interface, is a critical element for the discovery of unique and/or new targets for antimicrobial drugs and therapies.

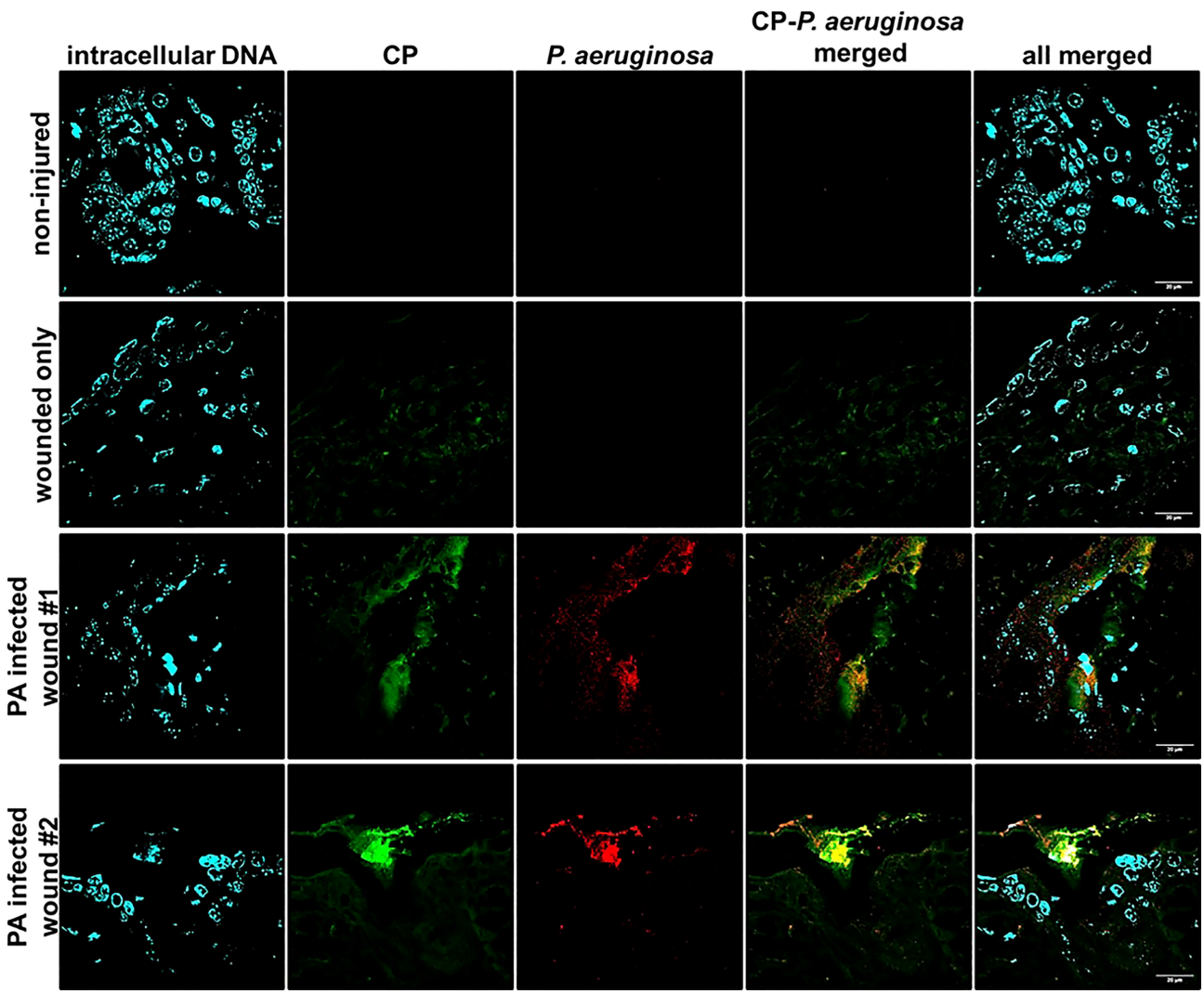

FIGURE 3 | Mouse CP signals overlap with bacterial signals in paraffin-embedded dorsal tissue sections. Non-injured skin control collected 12 days post-depilation display no background CP or bacterial signal, 12-day uninfected wound only data reveals minimal CP signal and no background bacterial signal. Duplicate samples of 12-day PAO1-infected wounds reveal both CP and bacterial signals. CP was detected by staining with Alexa fluor 488-tagged Goat anti-Rabbit antibody, PAO1 was detected by staining with Alexa fluor 594-tagged Goat Anti- Chicken antibody and nuclei were detected by staining with the cell-permeant dye, Hoechst 33342. Images are shown at 100X magnification and processed using ImageJ.

CP is a human host innate immune protein that has been studied extensively for its metal sequestering properties (Kehl-Fie et al., 2011; Wakeman et al., 2016; Zygiel et al., 2019) and stimulation of inflammatory receptors including TLR4 and RAGE (Chen et al., 2013; Wang et al., 2018). CP is a heterodimer of the S100A8 and S100A9 proteins and is abundantly found within neutrophils, comprising approximately 50% of its cytoplasmic protein content (Edgeworth et al., 1991). In infected tissues, CP has been shown to sequester transition metals, such as zinc, from infecting pathogens to starve them, a phenomenon termed as nutritional immunity (Hood and Skaar, 2012). Since the role of CP is so critical to prevent microbial infections in humans, we wanted to explore the antimicrobial functions of CP in further detail, especially in the context of infections caused by the opportunistic and nosocomial pathogens, *P. aeruginosa* and *S. aureus*.

In this study, we have described experiments that were designed to investigate the interaction of CP with biofilm communities of *P. aeruginosa* and *S. aureus* using light microscopy (CLSM) as well as electron microscopy (SEM). Our SEM micrographs showed that presence of a mesh-like structure was seen around microbial cells grown in presence of CP (**Figure 1**). The mesh structure was confirmed to contain substantial amounts of CP by CLSM images where we detected strong fluorescence signals from CP-antibody complexes in the

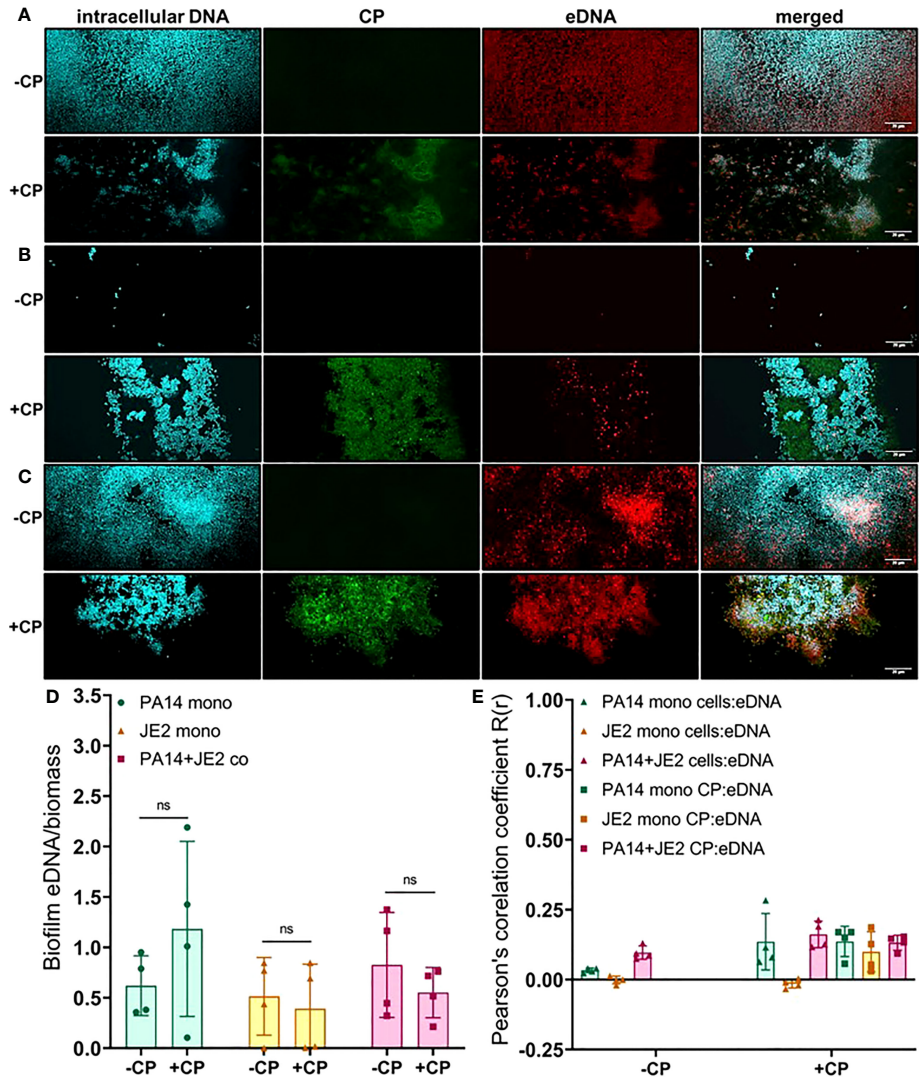

FIGURE 4 | Addition of CP minimally impacts the relative abundance of eDNA in biofilm matrices of *P. aeruginosa* and *S. aureus*. This figure depicts confocal images that represent abundance of eDNA in *P. aeruginosa* and/or *S. aureus* biofilm communities in presence or absence of CP conditions. The fluorescence dyes Hoechst 33342, Alexa 488, and TOTO-3 iodide correspond to intracellular DNA of microbial cells, CP, and eDNA in the biofilm EPS matrix of- **(A)** *P. aeruginosa* monoculture **(B)** *S. aureus* monoculture **(C)** *P. aeruginosa*-*S. aureus* co-culture. **(D)** Quantification of eDNA per biomass in *P. aeruginosa* and *S. aureus* biofilms in presence or absence of CP. **(E)** Colocalization analysis of eDNA signals with cells and CP show minimal correlation of distribution of eDNA with cells and/or CP. Images show 100X magnification and were processed using ImageJ. Bars represent the mean of four biological replicates performed on two independent days. Error bars represent the standard error of mean of the biological replicates. Unpaired t-test (two-tailed) was used to measure statistical significance. Comparisons marked ns denote changes that were not found to be statistically significant.

presence of CP cultures only (**Figure 2**). Additionally, accumulation of CP around *P. aeruginosa* was seen in CLSM images of mouse tissues infected by the pathogen (**Figure 3**). As CP is a metal chelating protein, we sought to investigate next if these mesh-like structures only form when the cells are starved for metals. However, we still observed the formation of this structure when excess exogenous $ZnCl_2$ was added (**Supplementary Figure 1**). Given the extensive interaction of CP with the biofilm matrix, the fact that EPS composition changes in each biofilm type remained relatively subtle was surprising. Analysis of our confocal images exhibited a shift to a carbohydrate-rich composition of the EPS matrix in both *P. aeruginosa* and *S. aureus* (**Figure 6**). The carbohydrate component of the EPS seemed to preferentially co-localize with the CP signal as opposed to the cell-specific signal (**Figure 6E**). Finally, a general trend of increased ability for *S. aureus* to colonize non-human surfaces in the presence of the human protein CP was consistently observed in all CSLM data (**Figures 2B**, **4B**, **5B**, **6B**).The results from our experiments indicate that interaction of microbial species with the

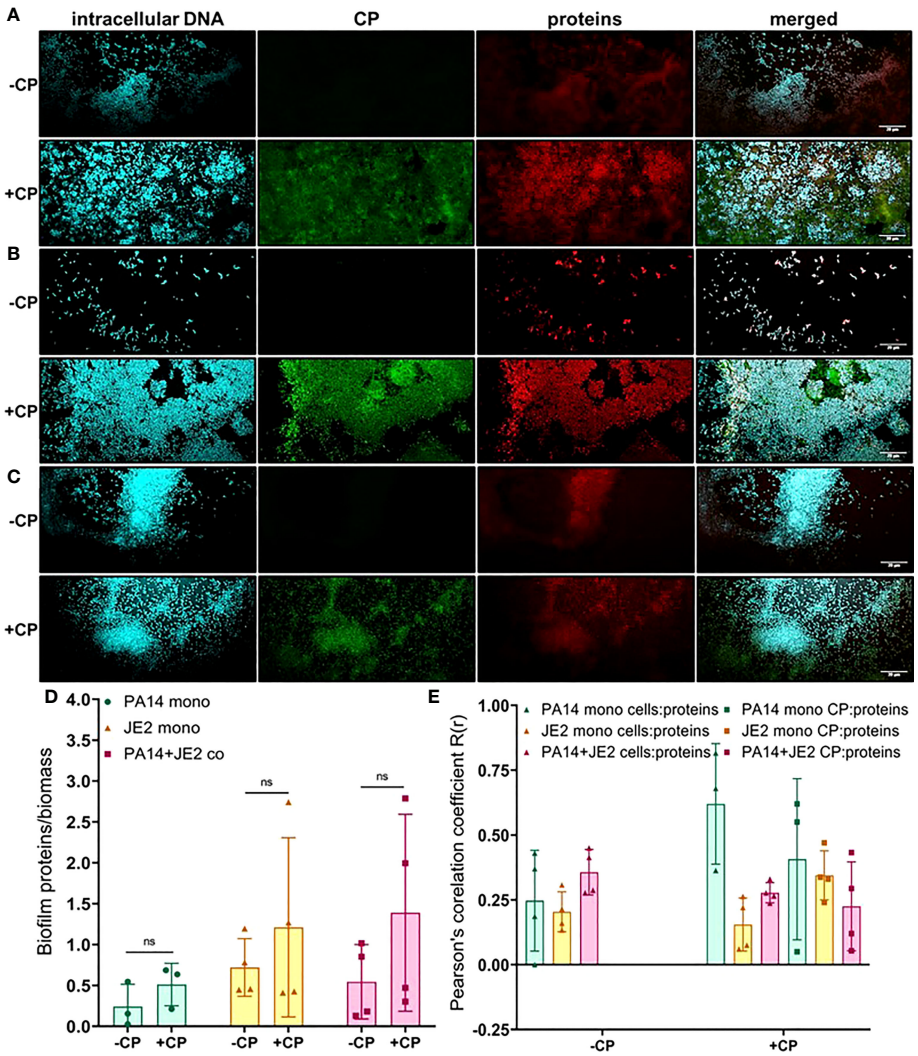

FIGURE 5 | Addition of CP correlates with subtle increase in the protein component of biofilm matrices. This figure depicts confocal images that represent abundance of proteins in *P. aeruginosa* and/or *S. aureus* biofilm communities in presence or absence of CP conditions. The fluorescence dyes Hoechst 33342, Alexa 488, and SYPRO Ruby correspond to intracellular DNA of microbial cells, CP, and matrix proteins in the biofilm EPS of- **(A)** *P. aeruginosa* monoculture **(B)** *S. aureus* monoculture **(C)** *P. aeruginosa*-*S. aureus* co-culture. **(D)** Quantification of proteins per biomass in *P. aeruginosa* and *S. aureus* biofilms in presence or absence of CP. **(E)** Colocalization analysis of protein signals with cells and CP show similar distribution of protein signals around cell signals and CP signals. Images show 100X magnification and were processed using ImageJ. Bars represent the mean of four biological replicates performed on two independent days. Error bars represent the standard error of mean of the biological replicates. Unpaired t-test (two-tailed) was used to measure statistical significance. Comparisons marked ns denote changes that were not found to be statistically significant.

environment they are seeking to colonize play a significant role in the nature of the infection. As such, when colonizing the human hosts, interactions with the antimicrobial and immune components are crucial for infecting pathogens to be able to colonize the environment and establish an infection. Hence, exploring these interactions are crucial to the discovery and identification of key molecules and processes affecting the infecting microorganisms that may be useful for developing antibiotics. For example, our confocal results have shown that a shift in the EPS composition occurs in *P. aeruginosa* and *S. aureus* biofilms in presence of CP, an innate immune protein (**Figure 6**). This shift could be a result of adaptations by the microbial species in response to CP and can be, potentially, targeted by antibiotics and/or other therapeutics. In fact, targeting of *P. aeruginosa*'s EPS matrix components, specifically carbohydrates, by degrading enzymes such as glycoside hydrolases (GH) has recently been shown as an alternative to classical chronic infection treatments (Fleming and Rumbaugh, 2018; Redman et al., 2020; Kovach et al., 2020). EPS carbohydrates serve as the major EPS structural component in many pathogenic species and also play roles in the biofilm's surface/cell-cell adhesion, aggregate formation,

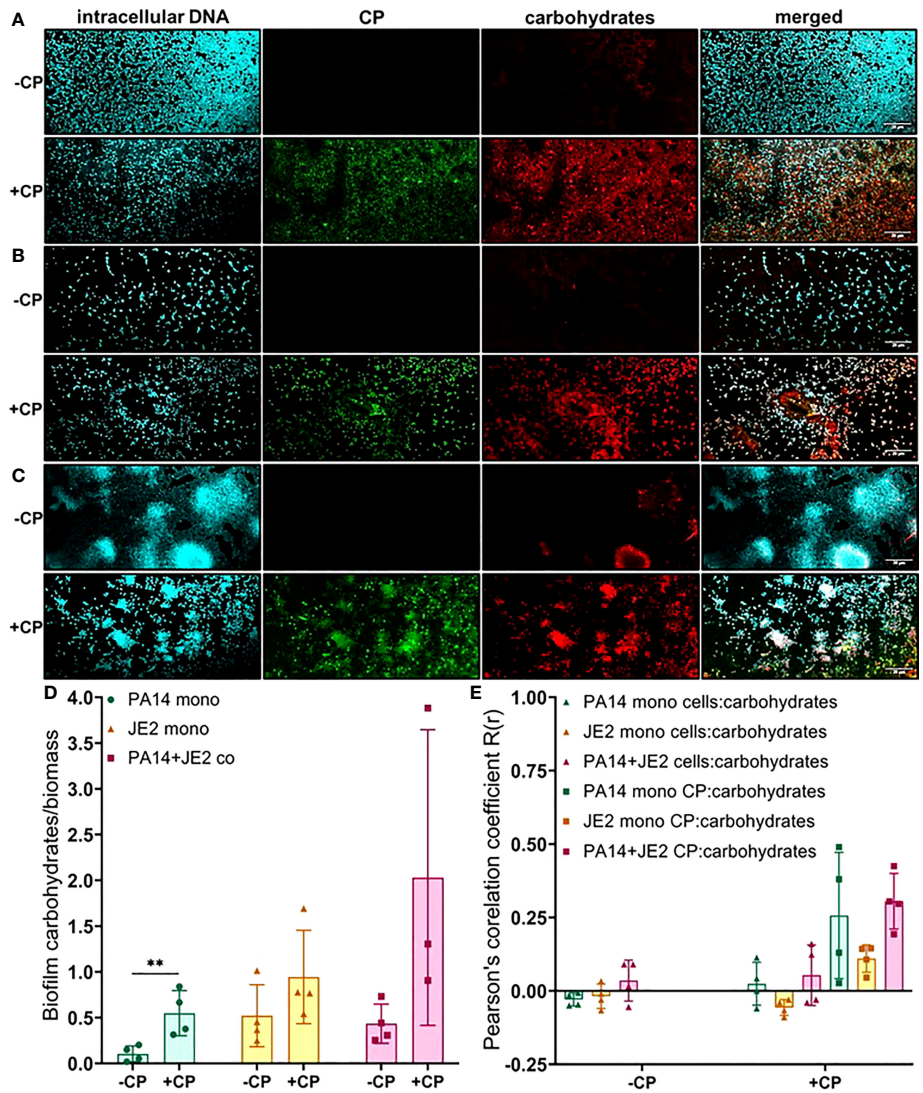

FIGURE 6 | Addition of CP leads to an increase in EPS carbohydrates in *P. aeruginosa* monoculture biofilms. This figure depicts confocal images that represent abundance of carbohydrates in *P. aeruginosa* and/or *S. aureus* biofilm communities in presence or absence of CP conditions. The fluorescence dyes Hoechst 33342, Alexa 488, and TRITC ConA correspond to intracellular DNA of microbial cells, CP, and carbohydrates in the biofilm EPS of- **(A)** *P. aeruginosa* monoculture **(B)** *S. aureus* monoculture **(C)** *P. aeruginosa-S. aureus* co-culture. **(D)** Quantification of carbohydrates per biomass in *P. aeruginosa* and *S. aureus* biofilms in presence or absence of CP. **(E)** Colocalization analysis of carbohydrate signals with cells and CP signals show higher correlation with CP compared to cells. Images show 100X magnification and were processed using ImageJ. Bars represent the mean of four biological replicates performed on two independent days. Error bars represent the standard error of mean of the biological replicates. Unpaired t-test (two-tailed) was used to measure statistical significance. **p≤ 0.01.

tolerance to desiccation, nutrient sorption, binding of enzymes and protection from antimicrobials and phagocytic cells (Flemming and Wingender, 2010; Yang et al., 2011).

P. aeruginosa produces three main types of carbohydrates/exopolysaccharides namely, Pel, Psl and alginate (Ma et al., 2009; Yang et al., 2011) and *S. aureus* mainly produces the poly N-acetyl glucosamine (PIA/PNAG) polysaccharide (Arciola et al., 2015). Active degradation of these EPS molecules *via* enzymes such as GHs could effectively break-up the pathogenic biofilms and disperse cells and in turn increase their susceptibility to antimicrobials and/or host immune cells (Fleming et al., 2017; Fleming and Rumbaugh, 2018). Thus, data from our research adds to this new pool of information that can lead to discovery of new and more effective methods of treating microbial infections with minimum off target effects.

While such alternative therapies are promising for treating biofilm-associated infections that are multi-drug resistant and recalcitrant, a large-scale dispersal of pathogenic cells within a living host can hyperactivate its immune system, causing dissemination of the infection and possibly lethal septicemia (Koo et al., 2017). Additionally, the biofilm composition of *P. aeruginosa* and *S. aureus* within the host-environment could

differ significantly, and degrading enzymes would need to break up biofilms present in various physiologically distinct microenvironments that have differing nutritional profiles, oxygen levels, pHs, microbial community, etc. Hence, further studies exploring the biofilm composition of *P. aeruginosa* and/or *S. aureus in vivo* and the effect of CP on them is anticipated to enhance understanding of how host factors alter the communal biofilms in infected tissues and generate insights for the development of new antimicrobial therapeutics.

DATA AVAILABILITY STATEMENT

The raw data supporting the conclusions of this article will be made available by the authors, without undue reservation.

ETHICS STATEMENT

The animal study was reviewed and approved by Institutional Animal Care and Use Committee of Texas Tech University Health Sciences Center (protocol number: 07044).

AUTHOR CONTRIBUTIONS

JB contributed to project design, data generation, data analysis, and manuscript writing. JAE performed the mouse infections and processed tissue samples. WC contributed to resource generation and manuscript editing. KPR contributed to design of the mouse infection experiments and manuscript editing. CW contributed to project design, data interpretation, and manuscript writing. All authors contributed to the article and approved the submitted version.

FUNDING

Work in the Wakeman lab was supported by NIH/NIGMS (R15GM128072). Calprotectin research in the Chazin lab is supported by NIH/NIAID (R01 AI118089 and R01 AI127793). JB was supported by the Doctoral Dissertation Completion Fellowship granted from Texas Tech University Graduate School. JB received a publication award from Tech American Society for Microbiology (Tech ASM).

ACKNOWLEDGMENTS

We would like to thank Hafij Al Mahmud, Jayc Waller and Siddiqur Md Rahman from the Wakeman Lab for their critical reading of this manuscript. A special thanks to Brittany Herrin and John Mark Stevenson for some of their early observations with CP-treated SEM images in the lab. We would also like to thank Dr. Peter Keyel, Minal Engavale and Roshan Thapa from the Biology department at Texas Tech University for their advice and suggestions in operating the Olympus FV3000 Scanning Confocal Microscope. Finally, we would like to thank the College of Arts & Sciences Microscopy for their assistance on sample preparation and the use of the Hitachi S-4300 Scanning Electron Microscope.

SUPPLEMENTARY MATERIAL

The Supplementary Material for this article can be found online at: https://www.frontiersin.org/articles/10.3389/fcimb.2022.898796/full#supplementary-material

Supplementary Figure 1 | Addition of zinc to CP-treated biofilm cultures of *P. aeruginosa* and *S. aureus* does not reverse and/or prevent the formation of the mesh. SEM images of biofilms grown in presence or absence of CP and +/-zinc conditions- **(A)**. *P. aeruginosa* monoculture **(B)**. *S. aureus* monoculture **(C)**. *P. aeruginosa-S. aureus* co-culture. Images show 4500X magnification and are representative of three independent experiments.

Supplementary Figure 2 | Addition of equivalent concentration of BSA, a common host protein, to growth media does not lead to formation of the mesh structure that is seen around *P. aeruginosa* biofilms grown in presence of CP. SEM images of *P. aeruginosa* monoculture biofilms grown in presence of CP or BSA at 4500X magnification are shown. Due to a broken critical point dryer at the time these images were collected, the protocol for SEM sample processing was modified in the following manner, resulting in lower quality images: after standard biofilm growth on coverslips, cells were fixed at room temperature for 1 hour using 4% paraformaldehyde solution. Fixed samples were washed three times with distilled water and frozen as being submerged in distilled water at -80°C. Frozen samples were dehydrated via freeze drying overnight, then gold-palladium coated and subsequently image using a Hitachi S-4300 Scanning Electron Microscope.

Supplementary Figure 3 | Cell viability following CP treatment in biofilm cultures of *P. aeruginosa* or *S. aureus*. Biofilms were grown in 0.25 mg/mL CP mimicking the growth conditions for the SEM and confocal cultures. These conditions resulted in a decrease in viability of *P. aeruginosa* but no change in *S. aureus* cell viability as determined by colony forming units (cfus). Data was generated on two independent days. Error bars represent standard deviation and * denotes statistical significance as determined by a two tailed Student's t-test.

REFERENCES

Águila-Arcos, S., Álvarez-Rodríguez, I., Garaiyurrebaso, O., Garbisu, C., Grohmann, E., and Alkorta, I. (2017). Biofilm-Forming Clinical Staphylococcus Isolates Harbor Horizontal Transfer and Antibiotic Resistance Genes. *Front. Microbiol.* doi: 10.3389/fmicb.2017.02018

Arciola, C. R., Campoccia, D., Ravaioli, S., and Montanaro, L. (2015). Polysaccharide Intercellular Adhesin in Biofilm: Structural and Regulatory Aspects. *Front. Cell Infect. Microbiol.* 5, 7. doi: 10.3389/fcimb.2015.00007

Baishya, J., and Wakeman, C. A. (2019). Selective Pressures During Chronic Infection Drive Microbial Competition and Cooperation. *NPJ Biofilms. Microbiomes.* 5, 16. doi: 10.1038/s41522-019-0089-2

Balcázar, J. L., Subirats, J., and Borrego, C. M. (2015). The Role of Biofilms as Environmental Reservoirs of Antibiotic Resistance. *Front. Microbiol.* doi: 10.3389/fmicb.2015.01216

Beaume, M., Kohler, T., Fontana, T., Tognon, M., Renzoni, A., and Van Delden, C. (2015). Metabolic Pathways of *Pseudomonas aeruginosa* Involved in Competition With Respiratory Bacterial Pathogens. *Front. Microbiol.* 6, 321. doi: 10.3389/fmicb.2015.00321

Besold, A. N., Culbertson, E. M., Nam, L., Hobbs, R. P., Boyko, A., Maxwell, C. N., et al. (2018). Antimicrobial Action of Calprotectin That Does Not Involve Metal Withholding. *Metallomics* 10, 1728–1742. doi: 10.1039/C8MT00133B

Bisht, K., Moore, J. L., Caprioli, R. M., Skaar, E. P., and Wakeman, C. A. (2021). Impact of Temperature-Dependent Phage Expression on Pseudomonas

aeruginosa Biofilm Formation. *NPJ Biofilms. Microbiomes.* 7, 22. doi: 10.1038/s41522-021-00194-8

Cardile, A. P., Sanchez, C. J., JR., Samberg, M. E., Romano, D. R., Hardy, S. K., Wenke, J. C., et al. (2014). Human Plasma Enhances the Expression of Staphylococcal Microbial Surface Components Recognizing Adhesive Matrix Molecules Promoting Biofilm Formation and Increases Antimicrobial Tolerance *In Vitro*. *BMC Res. Notes* 7, 457. doi: 10.1186/1756-0500-7-457

Chen, P., Abercrombie, J. J., Jeffrey, N. R., and Leung, K. P. (2012). An Improved Medium for Growing *Staphylococcus aureus* Biofilm. *J. Microbiol. Methods* 90, 115–118. doi: 10.1016/j.mimet.2012.04.009

Chen, X., Eksioglu, E. A., Zhou, J., Zhang, L., Djeu, J., Fortenbery, N., et al. (2013). Induction of Myelodysplasia by Myeloid-Derived Suppressor Cells. *J. Clin. Invest.* 123, 4595–4611. doi: 10.1172/JCI67580

Corbin, B. D., Seeley, E. H., Raab, A., Feldmann, J., Miller, M. R., Torres, V. J., et al. (2008). Metal Chelation and Inhibition of Bacterial Growth in Tissue Abscesses. *Science* 319, 962–965. doi: 10.1126/science.1152449

Cornforth, D. M., Dees, J. L., Ibberson, C. B., Huse, H. K., Mathiesen, I. H., Kirketerp-Moller, K., et al. (2018). *Pseudomonas aeruginosa* Transcriptome During Human Infection. *Proc. Natl. Acad. Sci. U.S.A.* 115, E5125–E5134. doi: 10.1073/pnas.1717525115

Costerton, J. W., Stewart, P. S., and Greenberg, E. P. (1999). Bacterial Biofilms: A Common Cause of Persistent Infections. *Science* 284, 1318–1322. doi: 10.1126/science.284.5418.1318

Damo, S. M., Kehl-Fie, T. E., Sugitani, N., Holt, M. E., Rathi, S., Murphy, W. J., et al. (2013). Molecular Basis for Manganese Sequestration by Calprotectin and Roles in the Innate Immune Response to Invading Bacterial Pathogens. *Proc. Natl. Acad. Sci. U.S.A.* 110, 3841–3846. doi: 10.1073/pnas.1220341110

Donlan, R. M. (2002). Biofilms: Microbial Life on Surfaces. *Emerging. Infect. Dis.* 8, 881. doi: 10.3201/eid0809.020063

Edgeworth, J., Gorman, M., Bennett, R., Freemont, P., and Hogg, N. (1991). Identification of P8,14 as a Highly Abundant Heterodimeric Calcium Binding Protein Complex of Myeloid Cells. *J. Biol. Chem.* 266, 7706–7713. doi: 10.1016/S0021-9258(20)89506-4

Fleming, D., Chahin, L., and Rumbaugh, K. (2017). Glycoside Hydrolases Degrade Polymicrobial Bacterial Biofilms in Wounds. *Antimicrob. Agents Chemother.* 61, 1–9. doi: 10.1128/AAC.01998-16

Fleming, D., Niese, B., Redman, W., Vanderpool, E., Gordon, V., and Rumbaugh, K. P. (2022). Contribution of *Pseudomonas aeruginosa* Exopolysaccharides Pel and Psl to Wound Infections. *Front. Cell Infect. Microbiol.* 12, 835754. doi: 10.3389/fcimb.2022.835754

Fleming, D., and Rumbaugh, K. (2018). The Consequences of Biofilm Dispersal on the Host. *Sci. Rep.* 8, 10738. doi: 10.1038/s41598-018-29121-2

Flemming, H. C., and Wingender, J. (2010). The Biofilm Matrix. *Nat. Rev. Microbiol.* 8, 623–633. doi: 10.1038/nrmicro2415

Flemming, H. C., Wingender, J., Szewzyk, U., Steinberg, P., Rice, S. A., and Kjelleberg, S. (2016). Biofilms: An Emergent Form of Bacterial Life. *Nat. Rev. Microbiol.* 14, 563–575. doi: 10.1038/nrmicro.2016.94

Formosa-Dague, C., Speziale, P., Foster, T. J., Geoghegan, J. A., and Dufrene, Y. F. (2016). Zinc-Dependent Mechanical Properties of *Staphylococcus aureus* Biofilm-Forming Surface Protein SasG. *Proc. Natl. Acad. Sci. U.S.A.* 113, 410–415. doi: 10.1073/pnas.1519265113

Gaddy, J. A., Tomaras, A. P., and Actis, L. A. (2009). The Acinetobacter Baumannii 19606 OmpA Protein Plays a Role in Biofilm Formation on Abiotic Surfaces and in the Interaction of This Pathogen With Eukaryotic Cells. *Infect. Immun.* 77, 3150–3160. doi: 10.1128/IAI.00096-09

Gilston, B. A., Skaar, E. P., and Chazin, W. J. (2016). Binding of Transition Metals to S100 Proteins. *Sci. China Life Sci.* 59, 792–801. doi: 10.1007/s11427-016-5088-4

Goltermann, L., and Tolker-Nielsen, T. (2017). Importance of the Exopolysaccharide Matrix in Antimicrobial Tolerance of *Pseudomonas aeruginosa* Aggregates. *Antimicrobial. Agents Chemotherapy.* 61, 1–7. doi: 10.1128/AAC.02696-16

Holloway, B. W. (1955). Genetic Recombination in *Pseudomonas aeruginosa*. *J. Gen. Microbiol.* 13, 572–581. doi: 10.1099/00221287-13-3-572

Hood, M. I., and Skaar, E. P. (2012). Nutritional Immunity: Transition Metals at the Pathogen-Host Interface. *Nat. Rev. Microbiol.* 10, 525–537. doi: 10.1038/nrmicro2836

Ibberson, C. B., and Whiteley, M. (2019). The *Staphylococcus aureus* Transcriptome During Cystic Fibrosis Lung Infection. *mBio*, 1–14 10. doi: 10.1128/mBio.02774-19

James, G. A., Swogger, E., Wolcott, R., Pulcini, E. D., Secor, P., Sestrich, J., et al. (2008). Biofilms in Chronic Wounds. *Wound Repair Regeneration* 16, 37–44. doi: 10.1111/j.1524-475X.2007.00321.x

Janeway, C. A., JR. (1989). Approaching the Asymptote? Evolution and Revolution in Immunology. *Cold Spring Harb. Symp. Quant. Biol.* 54 Pt 1, 1–13. doi: 10.1101/sqb.1989.054.01.003

Kehl-Fie, T. E., Chitayat, S., Hood, M. I., Damo, S., Restrepo, N., Garcia, C., et al. (2011). Nutrient Metal Sequestration by Calprotectin Inhibits Bacterial Superoxide Defense, Enhancing Neutrophil Killing of *Staphylococcus aureus*. *Cell Host Microbe* 10, 158–164. doi: 10.1016/j.chom.2011.07.004

Koo, H., Allan, R. N., Howlin, R. P., Stoodley, P., and Hall-Stoodley, L. (2017). Targeting Microbial Biofilms: Current and Prospective Therapeutic Strategies. *Nat. Rev. Microbiol.* 15, 740–755. doi: 10.1038/nrmicro.2017.99

Korndorfer, I. P., Brueckner, F., and Skerra, A. (2007). The Crystal Structure of the Human (S100A8/S100A9)2 Heterotetramer, Calprotectin, Illustrates How Conformational Changes of Interacting Alpha-Helices Can Determine Specific Association of Two EF-Hand Proteins. *J. Mol. Biol.* 370, 887–898. doi: 10.1016/j.jmb.2007.04.065

Kovach, K. N., Fleming, D., Wells, M. J., Rumbaugh, K. P., and Gordon, V. D. (2020). Specific Disruption of Established *Pseudomonas aeruginosa* Biofilms Using Polymer-Attacking Enzymes. *Langmuir* 36, 1585–1595. doi: 10.1021/acs.langmuir.9b02188

Kubelkova, K., and Macela, A. (2019). Innate Immune Recognition: An Issue More Complex Than Expected. *Front. Cell Infect. Microbiol.* 9, 241. doi: 10.3389/fcimb.2019.00241

Limoli, D. H., and Hoffman, L. R. (2019). Help, Hinder, Hide and Harm: What Can We Learn From the Interactions Between *Pseudomonas aeruginosa* and *Staphylococcus aureus* During Respiratory Infections? *Thorax* 74, 684–692. doi: 10.1136/thoraxjnl-2018-212616

Ma, L., Conover, M., Lu, H., Parsek, M. R., Bayles, K., and Wozniak, D. J. (2009). Assembly and Development of the *Pseudomonas aeruginosa* Biofilm Matrix. *PLoS Pathog.* 5, e1000354. doi: 10.1371/journal.ppat.1000354

Mashburn, L. M., Jett, A. M., Akins, D. R., and Whiteley, M. (2005). *Staphylococcus aureus* Serves as an Iron Source for *Pseudomonas aeruginosa* During *In Vivo* Coculture. *J. Bacteriol.* 187, 554–566. doi: 10.1128/JB.187.2.554-566.2005

Ma, L., Terwilliger, A., and Maresso, A. W. (2015). Iron and Zinc Exploitation During Bacterial Pathogenesis. *Metallomics* 7, 1541–1554. doi: 10.1039/C5MT00170F

Medzhitov, R. (2007). Recognition of Microorganisms and Activation of the Immune Response. *Nature* 449, 819–826. doi: 10.1038/nature06246

Nakashige, T. G., Stephan, J. R., Cunden, L. S., Brophy, M. B., Wommack, A. J., Keegan, B. C., et al. (2016). The Hexahistidine Motif of Host-Defense Protein Human Calprotectin Contributes to Zinc Withholding and Its Functional Versatility. *J. Am. Chem. Soc.* 138, 12243–12251. doi: 10.1021/jacs.6b06845

Nguyen, A. T., and Oglesby-Sherrouse, A. G. (2016). Interactions Between *Pseudomonas aeruginosa* and *Staphylococcus aureus* During Co-Cultivations and Polymicrobial Infections. *Appl. Microbiol. Biotechnol.* 100, 6141–6148. doi: 10.1007/s00253-016-7596-3

Obisesan, A. O., Zygiel, E. M., and Nolan, E. M. (2021). Bacterial Responses to Iron Withholding by Calprotectin. *Biochemistry* 60, 3337–3346. doi: 10.1021/acs.biochem.1c00572

Rahme, L. G., Stevens, E. J., Wolfort, S. F., Shao, J., Tompkins, R. G., and Ausubel, F. M. (1995). Common Virulence Factors for Bacterial Pathogenicity in Plants and Animals. *Science* 268, 1899–1902. doi: 10.1126/science.7604262

Redman, W. K., Welch, G. S., and Rumbaugh, K. P. (2020). Differential Efficacy of Glycoside Hydrolases to Disperse Biofilms. *Front. Cell Infect. Microbiol.* 10, 379. doi: 10.3389/fcimb.2020.00379

Ren, Z., Kim, D., Paula, A. J., Hwang, G., Liu, Y., Li, J., et al. (2019). Dual-Targeting Approach Degrades Biofilm Matrix and Enhances Bacterial Killing. *J. Dent. Res.* 98, 322–330. doi: 10.1177/0022034518818480

Römling, U., and Balsalobre, C. (2012). Biofilm Infections, Their Resilience to Therapy and Innovative Treatment Strategies. *J. Internal Med.* 272, 541–561. doi: 10.1111/joim.12004

Stewart, P. S., and Franklin, M. J. (2008). Physiological Heterogeneity in Biofilms. *Nat. Rev. Microbiol.* 6, 199–210. doi: 10.1038/nrmicro1838

Tan, X., Sun, L., Chen, J., and Chen, Z. J. (2018). Detection of Microbial Infections Through Innate Immune Sensing of Nucleic Acids. *Annu. Rev. Microbiol.* 72, 447–478. doi: 10.1146/annurev-micro-102215-095605

Vermilyea, D. M., Crocker, A. W., Gifford, A. H., and Hogan, D. A. (2021). Calprotectin-Mediated Zinc Chelation Inhibits *Pseudomonas aeruginosa* Protease Activity in Cystic Fibrosis Sputum. *J. Bacteriol.* 203, e0010021. doi: 10.1128/JB.00100-21

Wakeman, C. A., Moore, J. L., Noto, M. J., Zhang, Y., Singleton, M. D., Prentice, B. M., et al. (2016). The Innate Immune Protein Calprotectin Promotes *Pseudomonas aeruginosa* and *Staphylococcus aureus* Interaction. *Nat. Commun.* 7, 11951. doi: 10.1038/ncomms11951

Wang, S., Song, R., Wang, Z., Jing, Z., Wang, S., and Ma, J. (2018). S100A8/A9 in Inflammation. *Front. Immunol.* 9, 1298. doi: 10.3389/fimmu.2018.01298

Watters, C. M., Burton, T., Kirui, D. K., and Millenbaugh, N. J. (2016). Enzymatic Degradation of *In Vitro Staphylococcus aureus* Biofilms Supplemented With Human Plasma. *Infect. Drug Resist.* 9, 71–78. doi: 10.2147/IDR.S103101

Watters, C., Deleon, K., Trivedi, U., Griswold, J. A., Lyte, M., Hampel, K. J., et al. (2013). Pseudomonas aeruginosa Biofilms Perturb Wound Resolution and Antibiotic Tolerance in Diabetic Mice. *Med. Microbiol. Immunol.* 202, 131–141. doi: 10.1007/s00430-012-0277-7

Yang, L., Hu, Y., Liu, Y., Zhang, J., Ulstrup, J., and Molin, S. (2011). Distinct Roles of Extracellular Polymeric Substances in Pseudomonas aeruginosa Biofilm Development. *Environ. Microbiol.* 13, 1705–1717. doi: 10.1111/j.1462-2920.2011.02503.x

Zygiel, E. M., Nelson, C. E., Brewer, L. K., Oglesby-Sherrouse, A. G., and Nolan, E. M. (2019). The Human Innate Immune Protein Calprotectin Induces Iron Starvation Responses in *Pseudomonas aeruginosa*. *J. Biol. Chem.* 294, 3549–3562. doi: 10.1074/jbc.RA118.006819

Conflict of Interest: The authors declare that the research was conducted in the absence of any commercial or financial relationships that could be construed as a potential conflict of interest.

Publisher's Note: All claims expressed in this article are solely those of the authors and do not necessarily represent those of their affiliated organizations, or those of the publisher, the editors and the reviewers. Any product that may be evaluated in this article, or claim that may be made by its manufacturer, is not guaranteed or endorsed by the publisher.

frontiers | Frontiers in Cellular and Infection Microbiology

TYPE Mini Review
PUBLISHED 15 September 2022
DOI 10.3389/fcimb.2022.1017348

OPEN ACCESS

EDITED BY
Mauricio H Pontes,
College of Medicine, The Pennsylvania State University, United States

REVIEWED BY
Jennifer Angeline Gaddy,
Vanderbilt University Medical Center, United States

*CORRESPONDENCE
Cynthia Nau Cornelissen
ccornelissen@gsu.edu

SPECIALTY SECTION
This article was submitted to Bacteria and Host, a section of the journal Frontiers in Cellular and Infection Microbiology

RECEIVED 11 August 2022
ACCEPTED 30 August 2022
PUBLISHED 15 September 2022

CITATION
Stoudenmire JL, Greenawalt AN and Cornelissen CN (2022) Stealthy microbes: How *Neisseria gonorrhoeae* hijacks bulwarked iron during infection.
Front. Cell. Infect. Microbiol.
12:1017348.
doi: 10.3389/fcimb.2022.1017348

Stealthy microbes: How *Neisseria gonorrhoeae* hijacks bulwarked iron during infection

Julie Lynn Stoudenmire, Ashley Nicole Greenawalt and Cynthia Nau Cornelissen*

Center for Translational Immunology, Institute for Biomedical Sciences, Georgia State University, Atlanta, GA, United States

Transition metals are essential for metalloprotein function among all domains of life. Humans utilize nutritional immunity to limit bacterial infections, employing metalloproteins such as hemoglobin, transferrin, and lactoferrin across a variety of physiological niches to sequester iron from invading bacteria. Consequently, some bacteria have evolved mechanisms to pirate the sequestered metals and thrive in these metal-restricted environments. *Neisseria gonorrhoeae*, the causative agent of the sexually transmitted infection gonorrhea, causes devastating disease worldwide and is an example of a bacterium capable of circumventing human nutritional immunity. *Via* production of specific outer-membrane metallotransporters, *N. gonorrhoeae* is capable of extracting iron directly from human innate immunity metalloproteins. This review focuses on the function and expression of each metalloprotein at gonococcal infection sites, as well as what is known about how the gonococcus accesses bound iron.

KEYWORDS

transferrin, hemoglobin, lactoferrin, *Neisseria gonorrhoeae*, iron, nutritional immunity, siderophore

Introduction

Neisseria gonorrhoeae (Ngo) is an obligate human pathogen responsible for the sexually-transmitted disease, gonorrhea (Unemo et al., 2019). Gonococcal infections are on the rise; in 2020, the World Health Organization (WHO) estimates an approximate 82.4 million people were newly infected with Ngo and the Centers for Disease Control and Prevention (CDC) reported 677,769 new cases in the United States (WHO, 2021; CDC, 2021). As antibiotic resistance increases, Ngo is a high priority for many agencies to monitor as an urgent threat pathogen (Ohnishi et al., 2011; WHO, 2021; Fifer et al., 2021). In December 2020 the CDC modified the recommended treatment of uncomplicated gonococcal infection, from dual therapy with ceftriaxone and

azithromycin, to a higher dose of monotherapy ceftriaxone (Sancta St. Cyr et al., 2020). Prior infection does not provide protective immunity against reinfection and currently there is no effective vaccine, so at-risk individuals are often reinfected (Schmidt et al., 2001; Liu et al., 2011).

Ngo colonizes mucosal sites including the genital tract, rectum, conjunctiva, or oropharynx; genital infections often begin as urethritis in men and cervicitis in women (Schmidt et al., 2001; Walker and Sweet, 2011; Unemo et al., 2019). An estimated 80% of cases in women are asymptomatic, thus delaying treatment. Belated treatment may allow the infection to ascend the reproductive tract causing severe secondary sequalae in men and women (Portnoy et al., 1974; Walker and Sweet, 2011). Disseminated gonococcal infection (DGI) occurs when Ngo invades the bloodstream, sometimes due to delayed treatment; DGIs historically occur in less than 3% of cases, are more common in individuals less than 40, and occur more frequently in women than men (Rice, 2005; Walker and Sweet, 2011; Unemo et al., 2019; Li and Hatcher, 2020; Springer and Salen, 2020). In recent years, the numbers of DGI infections, particularly in men, have increased with no known link among cases (Belkacem et al., 2013).

Pathogens require metals for metabolism; therefore, there is a constant tug-of-war between host sequestration and pathogen acquisition for essential metals. Nutritional immunity is a host defense against infection where metalloproteins sequester essential nutrients away from pathogens (Figure 1A) (Hood and Skaar, 2012). Upon infection by Ngo, PMNs (Polymorphonuclear monocytes) are recruited to the site of infection, often forming NETs (Neutrophil Extracellular Traps), whereby the bacteria are exposed to the intracellular contents of the neutrophil, including several metal sequestration proteins [reviewed in (Criss and Seifert, 2012)]. Some Gram-negative pathogens have evolved ways to acquire iron directly from host metalloproteins, including transferrin (Tf), lactoferrin (Lf), and hemoglobin (Hb), using dedicated outer-membrane transporters [for a recent review see (Yadav et al., 2019)].

Access to, and availability of, metals in biological niches dictates the success and extent of infection by a pathogen. This review focuses on the roles of metalloproteins in regulating iron homeostasis in key gonococcal infection sites and how the gonococcus obtains the required iron for successful infection.

Iron requirements and sequestration proteins in the human host

Iron is the most abundant metal in humans and is essential for metabolism in most aerobic organisms (Brock, 1999; Pantopoulos et al., 2012; Nairz et al., 2014; Golonka et al., 2019). During metabolism, iron acts as a cofactor in iron-sulfur (Fe-S) cluster proteins and heme-containing proteins, aiding in heme synthesis, oxygen transport, and DNA synthesis (Pantopoulos et al., 2012; Ganz and Nemeth, 2015). Iron is also important for proliferation of immune cells including T-lymphocytes and neutrophils (Brock, 1999; Weiss, 1999). Iron levels are stringently regulated in humans; iron overload is cytotoxic due to the generation of reactive oxygen species (ROS) and oxidative stress (Brock, 1999; Golonka et al., 2019). Hemochromatosis, or iron overload, can be caused by inherited genetic mutations, blood transfusions, or excessive dietary intake of iron, and may lead to increased susceptibility to infections and accelerated death (Khan et al., 2007; McDowell et al., 2022).

To prevent the toxic effects of free iron, over 99.9% of excess mammalian iron is sequestered intracellularly, either *via* ferritin or heme, and extracellular iron is bound to metalloproteins including Hb, Lf, and Tf (Pantopoulos et al., 2012; Andreini et al., 2018). Approximately 2% of the human genome encodes iron-containing proteins, of which, more than half of the proteins have a catalytic function (Andreini et al., 2018). Upon inflammation or infection by a pathogen, the liver secretes a peptide hormone, hepcidin, which modifies an iron exporter ferroportin, thereby trapping iron intracellularly (Nemeth et al., 2004b). By solubilizing iron, making iron bioavailable, chelating iron, and protecting the host from ROS, Fe-containing metalloproteins play essential roles in humans.

Hb, found within erythrocytes, is the most abundant protein in blood; Hb sequesters heme, which is a heterocyclic porphyrin ring that binds centrally-coordinated ferrous iron (Fe^{2+}) (Baldwin, 1975). Hb is a globular protein consisting of α- and β-globulin chains, and inside erythrocytes, Hb stores approximately 75% of all the iron in the body and the remaining 25% is stored by ferritin in liver, spleen, and bone marrow (Brock, 1999; Delaby et al., 2005; Ganz and Nemeth, 2015). Hemoproteins, including hemopexin, Hb, and Hb complexed with haptoglobin (Hp), each bind heme strongly at one or two of the free iron-coordination sites located perpendicularly to the porphyrin ring (Hare, 2017). Erythrocytes spontaneously lyse, releasing up to 3 μM free Hb in healthy patients (Na et al., 2005). In serum, tetrameric Hb dissociates into dimers, which are rapidly sequestered by Hp, and the Hb-Hp complex is recycled by macrophages (Kristiansen et al., 2001). Hb may release heme spontaneously, particularly after oxidation to ferric Hb, or because of bacterial proteases (Na et al., 2005; Kassa et al., 2016; Hare, 2017).

Tf and Lf are glycoproteins of similar structure and function, sharing 60% sequence identity (Baker et al., 2002). Tf and Lf both contain a C-lobe and an N-lobe, with one Fe^{3+} ion bound to coordinating residues on each lobe (Aisen et al., 1978; Baker et al., 2002). Both Tf and Lf bind iron with nM affinity, and, notably, Lf maintains high affinity iron binding at low pH, down to pH 3.0, whereas Tf releases bound iron below pH 6.5 (Aisen et al., 1978; Baker and Baker, 2004).

Tf, at 80 kDa, is synthesized by hepatocytes and secreted into the serum where it solubilizes ferric iron, sequesters iron to prevent toxicity, and delivers iron into cells (Andrews and Ganz, 2019). Tf is naturally found at approximately 30% iron-

saturation in serum (Ganz and Nemeth, 2015; Andrews and Ganz, 2019). While inflammation increases hepcidin concentrations, serum Tf concentrations decrease due to the decreased iron in circulation, causing a syndrome called anemia of infection (Ganz and Nemeth, 2009).

Lf, at 82 kDa is synthesized by neutrophils and exocrine glands and is primarily located in human milk and mucosal secretions (Masson and Heremans, 1968; Cohen et al., 1987; Kruzel et al., 2000; Rageh et al., 2016). Lf is antimicrobial and anti-inflammatory (Broekhuyse, 1974; Flanagan and Willcox, 2009; Okubo et al., 2016; Lepanto et al., 2019). Lf has been implicated as a regulator of inflammation (Baker and Baker, 2004; Alexander et al., 2012; Valenti et al., 2018). Lf is secreted by cervical and epithelial cells and found in secondary granules of human neutrophils (Lewis-Jones et al., 1985; Nuijens et al., 1992; Alexander et al., 2012; Valenti et al., 2018). Lf levels change in mucosal secretions at different stages of the menstrual cycle; Lf levels are lowest in the days before menstruation and highest proceeding menstruation when the cervix is more open, to prevent pathogenesis (Cohen et al., 1987). The fluctuation of Lf levels is likely hormone driven, as women taking oral contraceptives do not demonstrate an increase in Lf levels during menses, which could lead to higher infection rates (Cohen et al., 1987).

Humans produce siderocalins of the lipocalin family that chelate siderophores (Correnti and Strong, 2012; Sia et al., 2013; Page, 2019). Most Gram-negative bacteria produce siderophores, which scavenge environmental iron (Guerinot, 1994; Rohde and Dyer, 2003; Wandersman and Delepelaire, 2004; Miethke and Marahiel, 2007). Siderophores have such a high affinity and specificity for iron that they can pirate iron directly from Tf, Lf, but not heme (Raymond et al., 2003). By sequestering the bacterially produced siderophores, siderocalins can inhibit bacterial growth.

Lipocalin 2 (Lcn2) was first discovered as a neutrophil granule component and tightly binds bacterial catecholate ferric siderophores, including enterobactin; however, Lcn2 can also sequester some carboxylates (Kjeldsen et al., 2000; Goetz et al., 2002; Chakraborty et al., 2012). Mammalian catechols, often secreted in the urine, and the mammalian siderophore 2, 5-DHBA also bind to Lcn2; mammalian catechols may be derived from foods and 2,5-DHBA is produced from a gene with a bacterial homolog for the production of enterobactin (Bao et al., 2010; Devireddy et al., 2010). Lcn2 is produced by neutrophils, macrophages, hepatocytes, epithelial cells and adipocytes; therefore, it is present at mucosal sites at the initial stages of gonococcal infection and colonization (Kjeldsen et al., 2000; Chakraborty et al., 2012; Xiao et al., 2017).

Acquisition of iron by *Neisseria*

TonB-dependent transporters (TDTs) are important for iron acquisition by Ngo and *Neisseria meningitidis*. TDTs are produced by most *Neisseria* strains and are highly conserved, suggesting TDTs play a significant survival role (Cornelissen et al., 1997a; Cornelissen et al., 2000; Cornelissen, 2008; Cornelissen and Hollander, 2011; Yadav et al., 2019). In Gram-negative bacteria, TDTs pirate iron, zinc, and other metals directly from host metalloproteins (Schryvers and Stojiljkovic, 1999; Cornelissen, 2018; Maurakis et al., 2019; Kammerman et al., 2020). TDTs are beta-barrels embedded in the outer membrane of the bacterium (Noinaj et al., 2013; Noinaj and Buchanan, 2014; Noinaj and Buchanan, 2018). With the help of TonB, TDTs extract metals, including iron and zinc, from host metalloproteins (Noinaj et al., 2012b; Cash et al., 2015; Maurakis et al., 2019; Kammerman et al., 2020).

The mechanism of metal import through TDTs is still being characterized. However, studies on TbpA suggest that a helical structure in the extracellular loops of the TDT may physically force the metal out upon binding of the ligand (Cash et al., 2015; Duran and Özbil, 2021). The extracted metal is immediately exposed to the plug domain of the TDT located in the pore of the beta-barrel, which may have a higher affinity for the metal than the ligand; thus, the metal ion relocates to the plug domain (Noto and Cornelissen, 2008). TonB is hypothesized to move the plug domain out of the barrel towards the periplasm, the metal ion is then exposed to a periplasmic binding protein that will ferry it to an ABC transporter, upon which the metal is imported into the cytoplasm, where it can then be used for essential metabolic processes, including replication within humans (Cornelissen et al., 1997b; Noinaj et al., 2010; Noinaj et al., 2012a; Noinaj et al., 2012b; Noinaj and Buchanan, 2014; Cash et al., 2015; Noinaj et al., 2017).

Several TDTs have been identified for their role in iron acquisition (Table 1; Figure 1B). Transferrin binding protein A (TbpA) is repressed by the ferric uptake regulator (Fur) under iron replete conditions (Agarwal et al., 2005). TbpA binds to hTf with an affinity of ~10 nM and is required for iron utilization from hTf (Cornelissen et al., 1992; Cornelissen and Sparling, 1996; Gray-Owen and Schryvers, 1996; Renauld-Mongénie et al., 2004; Noto and Cornelissen, 2008). Utilizing the human male model of gonococcal infection, a TbpAB knockout mutant was unable to establish an infection, suggesting essentiality of the system (Cornelissen et al., 1998). TbpA is a highly conserved 100 kDa, 22-stranded β-barrel outer-membrane receptor and TbpB is a more variable 85 kDa lipoprotein, which facilitates TbpA binding to iron loaded host Tf (Cornelissen and Sparling, 1996; Noinaj and Buchanan, 2014; Cash et al., 2015; Noinaj et al., 2017; Yadav et al., 2019). In Ngo, or *N. meningitidis* strains containing the type 2 variants of *tbpB*, TbpB is not essential for iron acquisition from Tf, but instead increases the rate iron uptake from hTf (Anderson et al., 1994; Renauld-Mongénie et al., 2004). *N. meningitidis* strains containing type 1 variants of *tbpB*, however, do require both proteins to bind hTf (Irwin et al., 1993). TbpA binds iron-saturated Tf or apo-Tf at similar rates (Tsai et al., 1988; Blanton et al., 1990; Anderson et al., 1994; Retzer et al., 1998).

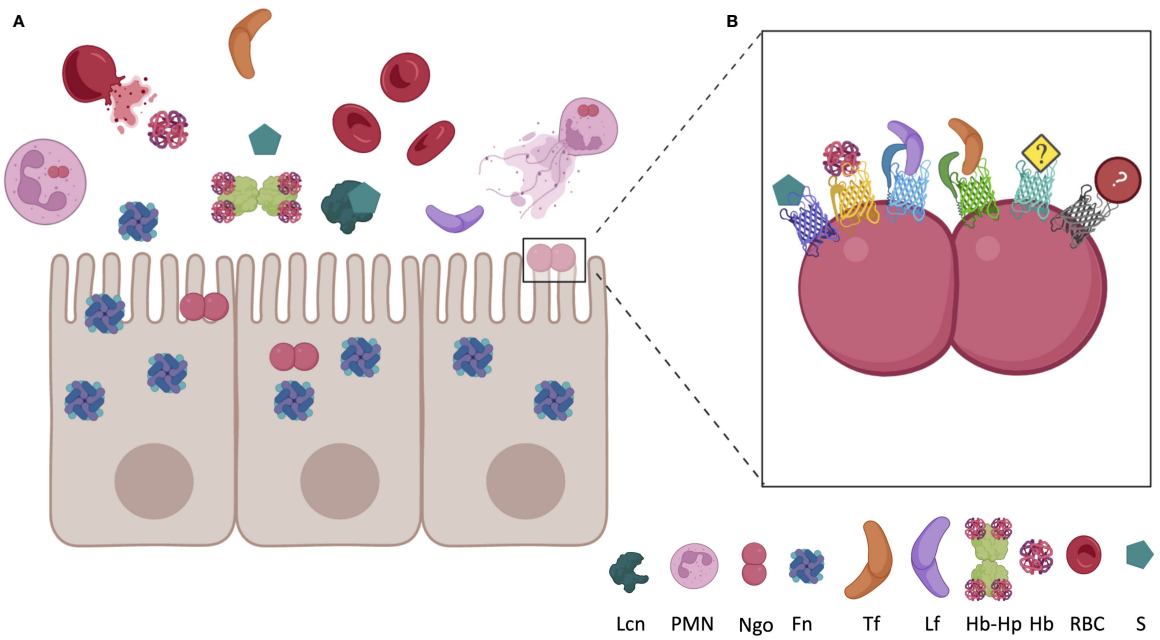

FIGURE 1
Localization of host nutritional immunity proteins near epithelial cell surface during inflammation and *Neisseria gonorrhoeae* (Ngo) infection. **(A)** In a healthy environment, iron is almost entirely bound to intracellular ferritin (Fn), erythrocyte bound haptoglobin, or sequestered in circulating transferrin (Tf). Under inflammatory conditions, Fn may be released from epithelial cells and hemoglobin (Hb) may be released from red blood cells (RBC). Haptoglobin (Hp) almost immediately binds to the newly circulating Hb, forming the Hb-Hp complex. Infection by Ngo recruits PMNs, which can expel their cellular contents in an innate immune response, which includes lactoferrin (Lf). Coinfection with other bacteria, or presence of commensals, may lead to circulation of siderophores (S). Siderophores produced by bacteria, or the mammalian siderophore 2,5-DHBA, may also be present at the site of infection bound to circulating lipocalin (Lcn). **(B)** Ngo has evolved mechanisms to cope with the nutritional immunity evoked by the host. TonB-dependent proteins bind many of the host Fe-chelating proteins, permitting Ngo to grow in these metal-restricted environments. FetA binds to S, HpuAB bind to Hb or Hb-Hp, TbpA binds to Tf, LbpA binds to Lf, and TdfF and TdfG are both iron regulated, but the host ligand has yet to be identified. Utilization of iron from ferritin and lipocalin should be investigated due to the close proximity to Ngo during infection. Figure not to scale and generated with BioRender.com.

Lactoferrin-binding protein A (LbpA) binds to and extracts iron from human Lf (Schryvers and Morris, 1988; Pettersson et al., 1994; Biswas and Sparling, 1995; Anderson et al., 2003). LbpA is present in approximately 50% of gonococcal strains and all meningococcal strains and is Fur-repressed in high-iron environments and subjected to phase variation (Mickelsen and Sparling, 1981; Biswas and Sparling, 1995; Biswas et al., 1999; Anderson et al., 2003). Among the Ngo LbpA producers, only 30% express the lipoprotein LbpB, suggesting that LbpB is not required for Lf utilization (Bonnah and Schryvers, 1998; Biswas et al., 1999; Anderson et al., 2003; Cornelissen and Hollander, 2011). Similar to TbpB, LbpB binds primarily to holo-Lf (Yadav

TABLE 1 *Neisseria* express TonB-dependent transporters in response to iron limitation, which allow for the utilization of host nutritional immunity proteins as metal sources.

Neisseria gene(s)	Expression profile	Host protein	References
tbpA/tbpB	Fur-repressed	Human Transferrin	(Cornelissen et al., 1992; Agarwal et al., 2005)
lbpA/lbpB	Fur-repressed; found in approximately 50% of Ngo, 100% of *N. meningitidis*	Human Lactoferrin	(Schryvers and Morris, 1988; Biswas et al., 1999)
hpuB/hpuA	Fur-repressed; phase variable	Hemoglobin/hemoglobin: haptoglobin	(Lewis et al., 1997; Lewis et al., 1999)
fetA	Indirect Fur regulation; MpeR induced; phase variable	Bacterially produced siderophores	(Carson et al., 1999; Jackson et al., 2010; Hollander et al., 2011)
tdfF	Unknown regulation	Unknown	(Jackson et al., 2010)
tdfG	Unknown/potentially indirect Fur regulation	Unknown	(Jackson et al., 2010)

et al., 2021). While the presence of LbpAB increases competitive fitness over strains expressing the Tbp system alone, LbpAB is not essential for infection (Anderson et al., 2003).

Both TDTs TbpA and LbpA are capable of binding to, and extracting iron from, their human ligand in the absence of their respective lipoprotein partner; however, the TDT HpuB requires the lipoprotein HpuA to utilize the iron or heme from Hb and Hb-Hp complexes (Lewis et al., 1997; Lewis et al., 1998; Lewis et al., 1999; Rohde et al., 2002; Rohde and Dyer, 2004). HpuB (85 kDa) is the outer-membrane receptor (Postle, 1993; Klebba et al., 1993) and HpuA (35 kDa) is the lipoprotein partner (Lewis et al., 1997; Lewis et al., 1999; Rohde et al., 2002; Anzaldi and Skaar, 2010). In *N. meningitidis*, HpuAB binds to Hb, Hb-Hp, and apo-haptoglobin (Lewis et al., 1999). *hpuAB* undergoes phase variation due to slipped-strand mispairing, resulting in a frameshifted non-functional protein (Lewis et al., 1997; Chen et al., 1998; Lewis et al., 1999). Further, *hpuAB* is Fur repressed under iron replete conditions. (Lewis et al., 1997). Gonococcal isolates collected from women in the first two weeks of their menstrual cycle are more likely to express HpuAB, suggesting that when Hb and Hp are abundant, Ngo producing HpuAB is under selective pressure to be expressed (Chen et al., 1998; Anderson et al., 2001).

Ngo is unable to synthesize siderophores; however, the gonococcus can use siderophores produced by other bacteria, including salmochelin, enterobactin, and dihydroxybenzoylserine acid through the TDT FetA (West and Sparling, 1987; Carson et al., 1999; Strange et al., 2011). FetA is an 80 kDa outer membrane transporter that is iron repressed and induced by MpeR, an AraC-like regulator, under iron-deplete conditions (Hollander et al., 2011). FetA is phase variable *via* slipped-strand mispairing (Carson et al., 1999). Additionally, MpeR is regulated by Fur and is pathogen specific, suggesting FetA is potentially upregulated as a virulence factor under iron limiting conditions (Snyder and Saunders, 2006; Marri et al., 2010; Jackson et al., 2010).

Repressed under iron replete conditions, both TDTs, TdfF and TdfG, have been implicated in iron acquisition by Ngo. TdfF, an 80 kDa outer membrane protein, is produced exclusively by the pathogenic *Neisseria*, which could suggest importance as a virulence factor (Turner et al., 2001). While no ligand has been identified to interact with TdfF, in some strains of Ngo, TdfF does contribute to intracellular survival in a TonB-dependent way (Hagen and Cornelissen, 2006). Utilizing the FA1090 Ngo sequence for bioinformatic analysis, the largest of the TDTs at 136 kDa, TdfG is exclusive to Ngo and *Neisseria elongota* (Turner et al., 2001; Marri et al., 2010). Like TdfF, no ligand has been identified for TdfG and little more is known about how TdfG contributes to Ngo growth or survival in humans. Thus far, little is known about the regulation of gene expression for either TdfF or TdfG, though a Fur-independent mechanism has been proposed for TdfG regulation (Jackson et al., 2010).

Host iron cycling: Infection and inflammation

Bacterial infection and inflammation act as signals for the host to deplete iron by activating an acute phase response and/or upregulating nutrient sequestration mechanisms (Weinberg, 1975; Ganz and Nemeth, 2015; Cornelissen, 2018; Golonka et al., 2019). Low blood iron during the first 24 hours of infection in patients was first described in the 1940s (Cartwright et al., 1946). Cytokines and tissue damage from inflammation are known to induce hepcidin production in the liver, promoting iron, heme, and Hb sequestration by macrophages and other iron-storage cells (Nemeth et al., 2004a; Armitage et al., 2011; Ganz and Nemeth, 2015; Ross, 2017). As serum iron levels dip below physiological levels of 10 to 30 μM, erythropoiesis, or the synthesis of erythrocytes, is inhibited freeing the iron for other processes (Ganz and Nemeth, 2015).

Ngo can invade cells, including macrophages and neutrophils which are the first immune cells to arrive at the site of infection (Zughaier et al., 2014). Iron retention in macrophages could be particularly beneficial for gonococcal infection, as iron retention in macrophages inhibits nitric oxide formation which aids in killing of intracellular bacteria (Nairz et al., 2014). Interestingly, upon infection of monocytes and macrophages, Ngo can upregulate hepcidin and downregulate ferroportin, resulting in an overall increase of iron retention (Zughaier et al., 2014). Ngo and *N. meningitidis* reduce expression of the host transferrin receptor in infected epithelial cells (Bonnah et al., 2000; Bonnah et al., 2004). The gene expression profiles of gonococcal or meningococcal infected cells mimic cells propagated in a low-iron environment, suggesting infection of these cells either shuttles all available iron to the infecting pathogens, generating a low-iron environment for the eukaryotic cells, or a signal from the pathogens may alter the regulatory network (Bonnah et al., 2004).

Perspectives: Potential pathways for treatment and prevention

TDTs have been suggested as vaccine candidates because they are highly conserved, present in pathogenic *Neisseria*, and most are not subject to high-frequency antigenic variation (Cornelissen et al., 2000; Cornelissen, 2008; Martinez-Martinez et al., 2011; Noinaj et al., 2012a; Cash et al., 2015; Frandoloso et al., 2015; Martínez-Martínez et al., 2016; Martinez-Martinez et al., 2016; Rice et al., 2017; Chan et al., 2018; Russell et al., 2019). This review summarizes the important iron metalloproteins and tissue specialization involved in neisserial pathogenesis. TbpA is essential for infection; LbpA, aids in pathogenesis; HpuAB is upregulated in females during the first half of their menstrual cycle; and TdfF is essential

for intracellular survival. Consequently, these iron-regulated TDTs are also attractive targets for future therapeutics.

Neisseria species have the ability to capitalize on many mammalian nutritional immunity tactics by utilizing the iron from these chelating proteins. TbpA and LbpA bind only the human versions of transferrin and lactoferrin, respectively, suggesting a tightly co-evolved system of nutrient acquisition. Some potential iron sinks have not been assessed for their ability to support neisserial growth. For example, no evidence is available on whether *Neisseria* are capable of exploiting Lcn2, ferritin, or NRAMP-1, all of which are upregulated at infection sites in response to infection/inflammation. Human calprotectin is found in high concentrations in PMNs, and recently, calprotectin has been described as binding iron with high affinity (Urban et al., 2009; Nakashige et al., 2015). Further, the TDT, TdfH, binds to and utilizes the Zn bound to calprotectin (Jean et al., 2016). Thus, calprotectin is in close proximity to Ngo during infection and the interaction between calprotectin and Ngo has been described; however, calprotectin binds Fe(II) with high affinity, whereas all known Ngo iron sources are Fe(III), making calprotectin an unlikely source of iron for Ngo (Nakashige et al., 2015). It is possible that TDTs can bind to and utilize metals from multiple iron sources, thus it is important to assess potential metal sources in an unbiased way.

Author contributions

JS and AG completed the literature review and manuscript drafting. JS edited based on comments by CC. CC reviewed and proofread the manuscript and acquired funding. All authors contributed to the article and approved the submitted version.

Funding

This work was funded by the National Institute of Allergy and Infectious Diseases, award numbers U19AI144182, R01AI127793, and R01AI125421 to CC. The funder had no role in data collection, synthesis, analysis, interpretation, or management of the data presented in this review. The funder had no role in review generation and revision, or in the decision to submit this review for publication.

Acknowledgments

We thank the support from the Institute for Biomedical Sciences at Georgia State University.

Conflict of interest

The authors declare that the research was conducted in the absence of any commercial or financial relationships that could be construed as a conflict of interest.

Publisher's note

All claims expressed in this article are solely those of the authors and do not necessarily represent those of their affiliated organizations, or those of the publisher, the editors and the reviewers. Any product that may be evaluated in this article, or claim that may be made by its manufacturer, is not guaranteed or endorsed by the publisher.

References

Agarwal, S., King, C. A., Klein, E. K., Soper, D. E., Rice, P. A., Wetzler, L. M., et al. (2005). The gonococcal fur-regulated *tbpA* and *tbpB* genes are expressed during natural mucosal gonococcal infection. *Infect. Immun.* 73, 4281–4287. doi: 10.1128/IAI.73.7.4281-4287.2005

Aisen, P., Leibman, A., and Zweier, J. (1978). Stoichiometric and site characteristics of the binding of iron to human transferrin. *J. Biol. Chem.* 253, 1930–1937. doi: 10.1016/S0021-9258(19)62337-9

Alexander, D. B., Iigo, M., Yamauchi, K., Suzui, M., and Tsuda, H. (2012). Lactoferrin: An alternative view of its role in human biological fluids. *Biochem. Cell Biol.* 90, 279–306. doi: 10.1139/o2012-013

Anderson, J. E., Hobbs, M. M., Biswas, G. D., and Sparling, P. F. (2003). Opposing selective forces for expression of the gonococcal lactoferrin receptor. *Mol. Microbiol.* 48, 1325–1337. doi: 10.1046/j.1365-2958.2003.03496.x

Anderson, J. E., Leone, P. A., Miller, W. C., Chen, C., Hobbs, M. M., and Sparling, P. F. (2001). Selection for expression of the gonococcal hemoglobin receptor during menses. *J. Infect. Dis.* 184, 1621–1623. doi: 10.1086/324564

Anderson, J. E., Sparling, P. F., and Cornelissen, C. N. (1994). Gonococcal transferrin-binding protein 2 facilitates but is not essential for transferrin utilization. *J. Bacteriol.* 176, 3162–3170. doi: 10.1128/jb.176.11.3162-3170.1994

Andreini, C., Putignano, V., Rosato, A., and Banci, L. (2018). The human iron-proteome. *Metallomics* 10, 1223–1231. doi: 10.1039/c8mt00146d

Andrews, N. C., and Ganz, T. (2019). *The molecular basis of iron metabolism* (Oxford, UK: John Wiley & Sons, Ltd).

Anzaldi, L. L., and Skaar, E. P. (2010). Overcoming the heme paradox: Heme toxicity and tolerance in bacterial pathogens. *Infect. Immun.* 78, 4977–4989. doi: 10.1128/IAI.00613-10

Armitage, A. E., Eddowes, L. A., Gileadi, U., Cole, S., Spottiswoode, N., Selvakumar, T. A., et al. (2011). Hepcidin regulation by innate immune and infectious stimuli. *Blood* 118, 4129–4139. doi: 10.1182/blood-2011-04-351957

Baker, H. M., and Baker, E. N. (2004). Lactoferrin and iron: Structural and dynamic aspects of binding and release. *Biometals* 17, 209–216. doi: 10.1023/B:BIOM.0000027694.40260.70

Baker, E. N., Baker, H. M., and Kidd, R. D. (2002). Lactoferrin and transferrin: Functional variations on a common structural framework. *Biochem. Cell Biol.* 80, 27–34. doi: 10.1139/o01-153

Baldwin, J. M. (1975). Structure and function of haemoglobin. *Prog. Biophys. Mol. Biol.* 29, 225–320. doi: 10.1016/0079-6107(76)90024-9

Bao, G., Clifton, M., Hoette, T. M., Mori, K., Deng, S.-X., Qiu, A., et al. (2010). Iron traffics in circulation bound to a siderocalin (Ngal)-catechol complex. *Nat. Chem. Biol.* 6, 602–609. doi: 10.1038/nchembio.402

Belkacem, A., Caumes, E., Ouanich, J., Jarlier, V., Dellion, S., Cazenave, B., et al. (2013). Changing patterns of disseminated gonococcal infection in France: cross-

sectional data 2009-2011. *Sex Transm. Infect.* 89, 613–615. doi: 10.1136/sextrans-2013-051119

Biswas, G. D., Anderson, J. E., Chen, C. J., Cornelissen, C. N., and Sparling, P. F. (1999). Identification and functional characterization of the *Neisseria gonorrhoeae lbpB* gene product. *Infect. Immun.* 67, 455–459. doi: 10.1128/IAI.67.1.455-459.1999

Biswas, G. D., and Sparling, P. F. (1995). Characterization of *lbpA*, the structural gene for a lactoferrin receptor in *Neisseria gonorrhoeae*. *Infect. Immun.* 63, 2958–2967. doi: 10.1128/iai.63.8.2958-2967.1995

Blanton, K. J., Biswas, G. D., Tsai, J., Adams, J., Dyer, D. W., Davis, S. M., et al. (1990). Genetic evidence that *Neisseria gonorrhoeae* produces specific receptors for transferrin and lactoferrin. *J. Bacteriol.* 172, 5225–5235. doi: 10.1128/jb.172.9.5225-5235.1990

Bonnah, R. A., Lee, S. W., Vasquez, B. L., Enns, C. A., and So, M. (2000). Alteration of epithelial cell transferrin-iron homeostasis by *Neisseria meningitidis* and *Neisseria gonorrhoeae*. *Cell Microbiol.* 2, 207–218. doi: 10.1046/j.1462-5822.2000.00042.x

Bonnah, R. A., Muckenthaler, M. U., Carlson, H., Minana, B., Enns, C. A., Hentze, M. W., et al. (2004). Expression of epithelial cell iron-related genes upon infection by *Neisseria meningitidis*. *Cell Microbiol.* 6, 473–484. doi: 10.1111/j.1462-5822.2004.00376.x

Bonnah, R. A., and Schryvers, A. B. (1998). Preparation and characterization of *Neisseria meningitidis* mutants deficient in production of the human lactoferrin-binding proteins LbpA and LbpB. *J. Bacteriol.* 180, 3080–3090. doi: 10.1128/JB.180.12.3080-3090.1998

Brock, J. H. (1999). Benefits and dangers of iron during infection. *Curr. Opin. Clin. Nutr. Metab. Care* 2, 507–510. doi: 10.1097/00075197-199911000-00013

Broekhuyse, R. M. (1974). Tear lactoferrin: A bacteriostatic and complexing protein. *Invest. Ophthalmol.* 13, 550–554.

Carson, S. D., Klebba, P. E., Newton, S. M., and Sparling, P. F. (1999). Ferric enterobactin binding and utilization by *Neisseria gonorrhoeae*. *J. Bacteriol.* 181, 2895–2901. doi: 10.1128/JB.181.9.2895-2901.1999

Cartwright, G. E., Lauritsen, M. A., Jones, P. J., Merrill, I. M., and Wintrobe, M. M. (1946). The anemia of infection, hypoferremia, hypercupremia, and alterations in porphyrin metabolism in patients. *J. Clin. Invest.* 25, 65–80. doi: 10.1172/JCI101690

Cash, D. R., Noinaj, N., Buchanan, S. K., and Cornelissen, C. N. (2015). Beyond the crystal structure: Insight into the function and vaccine potential of TbpA expressed by *Neisseria gonorrhoeae*. *Infect. Immun.* 83, 4438–4449. doi: 10.1128/IAI.00762-15

CDC (2021). Incidence, prevalence and cost of sexually transmitted infections in the united states.

Chakraborty, S., Kaur, S., Guha, S., and Batra, S. K. (2012). The multifaceted roles of neutrophil gelatinase associated lipocalin (NGAL) in inflammation and cancer. *Biochim. Biophys. Acta* 1826, 129–169. doi: 10.1016/j.bbcan.2012.03.008

Chan, C., Andisi, V. F., Ng, D., Ostan, N., Yunker, W. K., and Schryvers, A. B. (2018). Are lactoferrin receptors in gram-negative bacteria viable vaccine targets? *Biometals* 31, 381–398. doi: 10.1007/s10534-018-0105-7

Chen, C. J., Elkins, C., and Sparling, P. F. (1998). Phase variation of hemoglobin utilization in *Neisseria gonorrhoeae*. *Infect. Immun.* 66, 987–993. doi: 10.1128/IAI.66.3.987-993.1998

Cohen, M. S., Britigan, B. E., French, M., and Bean, K. (1987). Preliminary observations on lactoferrin secretion in human vaginal mucus: Variation during the menstrual cycle, evidence of hormonal regulation, and implications for infection with *Neisseria gonorrhoeae*. *Am. J. Obstet. Gynecol.* 157, 1122–1125. doi: 10.1016/S0002-9378(87)80274-0

Cornelissen, C. N. (2008). Identification and characterization of gonococcal iron transport systems as potential vaccine antigens. *Future Microbiol.* 3, 287–298. doi: 10.2217/17460913.3.3.287

Cornelissen, C. N. (2018). Subversion of nutritional immunity by the pathogenic *Neisseriae*. *Pathog. Dis.* 76. doi: 10.1093/femspd/ftx112

Cornelissen, C. N., Anderson, J. E., Boulton, I. C., and Sparling, P. F. (2000). Antigenic and sequence diversity in gonococcal transferrin-binding protein a. *Infect. Immun.* 68, 4725–4735. doi: 10.1128/IAI.68.8.4725-4735.2000

Cornelissen, C. N., Anderson, J. E., and Sparling, P. F. (1997a). Characterization of the diversity and the transferrin-binding domain of gonococcal transferrin-binding protein 2. *Infect. Immun.* 65, 822–828. doi: 10.1128/iai.65.2.822-828.1997

Cornelissen, C. N., Anderson, J. E., and Sparling, P. F. (1997b). Energy-dependent changes in the gonococcal transferrin receptor. *Mol. Microbiol.* 26, 25–35. doi: 10.1046/j.1365-2958.1997.5381914.x

Cornelissen, C. N., Biswas, G. D., Tsai, J., Paruchuri, D. K., Thompson, S. A., and Sparling, P. F. (1992). Gonococcal transferrin-binding protein 1 is required for transferrin utilization and is homologous to TonB-dependent outer membrane receptors. *J. Bacteriol.* 174, 5788–5797. doi: 10.1128/jb.174.18.5788-5797.1992

Cornelissen, C. N., and Hollander, A. (2011). TonB-dependent transporters expressed by *Neisseria gonorrhoeae*. *Front. Microbiol.* 2, 117. doi: 10.3389/fmicb.2011.00117

Cornelissen, C. N., Kelley, M., Hobbs, M. M., Anderson, J. E., Cannon, J. G., Cohen, M. S., et al. (1998). The transferrin receptor expressed by gonococcal strain FA1090 is required for the experimental infection of human male volunteers. *Mol. Microbiol.* 27, 611–616. doi: 10.1046/j.1365-2958.1998.00710.x

Cornelissen, C. N., and Sparling, P. F. (1996). Binding and surface exposure characteristics of the gonococcal transferrin receptor are dependent on both transferrin-binding proteins. *J. Bacteriol.* 178, 1437–1444. doi: 10.1128/jb.178.5.1437-1444.1996

Correnti, C., and Strong, R. K. (2012). Mammalian siderophores, siderophore-binding lipocalins, and the labile iron pool. *J. Biol. Chem.* 287, 13524–13531. doi: 10.1074/jbc.R111.311829

Criss, A. K., and Seifert, H. S. (2012). A bacterial siren song: Intimate interactions between *Neisseria* and neutrophils. *Nat. Rev. Microbiol.* 10, 178–190. doi: 10.1038/nrmicro2713

Cyr, S. St., Barbee, L., Workowski, K. A., Bachmann, L. H., Pham, C., Schlanger, K., et al. (2020). Update to CDC's treatment guidelines for gonococcal infection, 2020. *Morb. Mortality Weekly Rep.* 69, 1911–6. doi: 10.15585/mmwr.mm6950a6

Delaby, C., Pilard, N., Hetet, G., Driss, F., Grandchamp, B., Beaumont, C., et al. (2005). A physiological model to study iron recycling in macrophages. *Exp. Cell Res.* 310, 43–53. doi: 10.1016/j.yexcr.2005.07.002

Devireddy, L. R., Hart, D. O., Goetz, D. H., and Green, M. R. (2010). A mammalian siderophore synthesized by an enzyme with a bacterial homolog involved in enterobactin production. *Cell* 141, 1006–1017. doi: 10.1016/j.cell.2010.04.040

Duran, G. N., and Özbil, M. (2021). Structural rearrangement of *Neisseria meningitidis* transferrin binding protein a (TbpA) prior to human transferrin protein (hTf) binding. *Turkish J. Chem.* 45, 1146–1154. doi: 10.3906/kim-2102-25

Fifer, H., Livermore, D. M., Uthayakumaran, T., Woodford, N., and Cole, M. J. (2021). What's left in the cupboard? Older antimicrobials for treating gonorrhoea. *J. Antimicrob. Chemother.* 76, 1215–20. doi: 10.1093/jac/dkaa559

Flanagan, J. L., and Willcox, M. D. (2009). Role of lactoferrin in the tear film. *Biochimie* 91, 35–43. doi: 10.1016/j.biochi.2008.07.007

Frandoloso, R., Martinez-Martinez, S., Calmettes, C., Fegan, J., Costa, E., Curran, D., et al. (2015). Nonbinding site-directed mutants of transferrin binding protein b exhibit enhanced immunogenicity and protective capabilities. *Infect. Immun.* 83, 1030–1038. doi: 10.1128/IAI.02572-14

Ganz, T., and Nemeth, E. (2009). Iron sequestration and anemia of inflammation. *Semin. Hematol.* 46, 387–393. doi: 10.1053/j.seminhematol.2009.06.001

Ganz, T., and Nemeth, E. (2015). Iron homeostasis in host defence and inflammation. *Nat. Rev. Immunol.* 15, 500–510. doi: 10.1038/nri3863

Goetz, D. H., Holmes, M. A., Borregaard, N., Bluhm, M. E., Raymond, K. N., and Strong, R. K. (2002). The neutrophil lipocalin NGAL is a bacteriostatic agent that interferes with siderophore-mediated iron acquisition. *Mol. Cell* 10, 1033–1043. doi: 10.1016/S1097-2765(02)00708-6

Golonka, R., Yeoh, B. S., and Vijay-Kumar, M. (2019). The iron tug-of-War between bacterial siderophores and innate immunity. *J. Innate Immun.* 11, 249–262. doi: 10.1159/000494627

Gray-Owen, S. D., and Schryvers, A. B. (1996). Bacterial transferrin and lactoferrin receptors. *Trends Microbiol.* 4, 185–191. doi: 10.1016/0966-842X(96)10025-1

Guerinot, M. L. (1994). Microbial iron transport. *Annu. Rev. Microbiol.* 48, 743–772. doi: 10.1146/annurev.mi.48.100194.003523

Hagen, T. A., and Cornelissen, C. N. (2006). *Neisseria gonorrhoeae* requires expression of TonB and the putative transporter TdfF to replicate within cervical epithelial cells. *Mol. Microbiol.* 62, 1144–1157. doi: 10.1111/j.1365-2958.2006.05429.x

Hare, S. A. (2017). Diverse structural approaches to haem appropriation by pathogenic bacteria. *Biochim. Biophys. Acta Proteins Proteom.* 1865, 422–433. doi: 10.1016/j.bbapap.2017.01.006

Hollander, A., Mercante, A. D., Shafer, W. M., and Cornelissen, C. N. (2011). The iron-repressed, AraC-like regulator MpeR activates expression of *fetA* in *Neisseria gonorrhoeae*. *Infect. Immun.* 79, 4764–4776. doi: 10.1128/IAI.05806-11

Hood, M. I., and Skaar, E. P. (2012). Nutritional immunity: transition metals at the pathogen-host interface. *Nat. Rev. Microbiol.* 10, 525–537. doi: 10.1038/nrmicro2836

Irwin, S. W., Averil, N., Cheng, C. Y., and Schryvers, A. B. (1993). Preparation and analysis of isogenic mutants in the transferrin receptor protein genes, *tbpA* and *tbpB*, from *Neisseria meningitidis*. *Mol. Microbiol.* 8, 1125–1133. doi: 10.1111/j.1365-2958.1993.tb01657.x

Jackson, L. A., Ducey, T. F., Day, M. W., Zaitshik, J. B., Orvis, J., and Dyer, D. W. (2010). Transcriptional and functional analysis of the *Neisseria gonorrhoeae* fur regulon. *J. Bacteriol.* 192, 77–85. doi: 10.1128/JB.00741-09

Jean, S., Juneau, R. A., Criss, A. K., and Cornelissen, C. N. (2016). *Neisseria gonorrhoeae* evades calprotectin-mediated nutritional immunity and survives neutrophil extracellular traps by production of TdfH. *Infect. Immun.* 84, 2982–2994. doi: 10.1128/IAI.00319-16

Kammerman, M. T., Bera, A., Wu, R., Harrison, S. A., Maxwell, C. N., Lundquist, K., et al. (2020). Molecular insight into TdfH-mediated zinc piracy from human calprotectin by *Neisseria gonorrhoeae*. *mBio* 11, 00949-20. doi: 10.1128/mBio.00949-20

Kassa, T., Jana, S., Meng, F., and Alayash, A. I. (2016). Differential heme release from various hemoglobin redox states and the upregulation of cellular heme oxygenase-1. *FEBS Open Bio* 6, 876–884. doi: 10.1002/2211-5463.12103

Khan, F. A., Fisher, M. A., and Khakoo, R. A. (2007). Association of hemochromatosis with infectious diseases: Expanding spectrum. *Int. J. Infect. Dis.* 11, 482–487. doi: 10.1016/j.ijid.2007.04.007

Kjeldsen, L., Cowland, J. B., and Borregaard, N. (2000). Human neutrophil gelatinase-associated lipocalin and homologous proteins in rat and mouse. *Biochim. Biophys. Acta* 1482, 272–283. doi: 10.1016/S0167-4838(00)00152-7

Klebba, P. E., Rutz, J. M., Liu, J., and Murphy, C. K. (1993). Mechanisms of TonB-catalyzed iron transport through the enteric bacterial cell envelope. *J. Bioenerg. Biomembr.* 25, 603–611. doi: 10.1007/bf00770247

Kristiansen, M., Graversen, J. H., Jacobsen, C., Sonne, O., Hoffman, H. J., Law, S. K., et al. (2001). Identification of the haemoglobin scavenger receptor. *Nature* 409, 198–201. doi: 10.1038/35051594

Kruzel, M. L., Harari, Y., Chen, C. Y., and Castro, G. A. (2000). Lactoferrin protects gut mucosal integrity during endotoxemia induced by lipopolysaccharide in mice. *Inflammation* 24, 33–44. doi: 10.1023/A:1006935908960

Lepanto, M. S., Rosa, L., Paesano, R., Valenti, P., and Cutone, A. (2019). Lactoferrin in aseptic and septic inflammation. *Molecules* 24. doi: 10.3390/molecules24071323

Lewis, L. A., Gipson, M., Hartman, K., Ownbey, T., Vaughn, J., and Dyer, D. W. (1999). Phase variation of HpuAB and HmbR, two distinct haemoglobin receptors of *Neisseria meningitidis* DNM2. *Mol. Microbiol.* 32, 977–989. doi: 10.1046/j.1365-2958.1999.01409.x

Lewis, L. A., Gray, E., Wang, Y. P., Roe, B. A., and Dyer, D. W. (1997). Molecular characterization of *hpuAB*, the haemoglobin-haptoglobin-utilization operon of *Neisseria meningitidis*. *Mol. Microbiol.* 23, 737–749. doi: 10.1046/j.1365-2958.1997.2501619.x

Lewis-Jones, D. I., Lewis-Jones, M. S., Connolly, R. C., Lloyd, D. C., and West, C. R. (1985). Sequential changes in the antimicrobial protein concentrations in human milk during lactation and its relevance to banked human milk. *Pediatr. Res.* 19, 5. doi: 10.1203/00006450-198506000-00012

Lewis, L. A., Sung, M. H., Gipson, M., Hartman, K., and Dyer, D. W. (1998). Transport of intact porphyrin by HpuAB, the hemoglobin-haptoglobin utilization system of *Neisseria meningitidis*. *J. Bacteriol.* 180, 6043–6047. doi: 10.1128/JB.180.22.6043-6047.1998

Li, R., and Hatcher, J. D. (2020). *Gonococcal arthritis* (Treasure Island (FL: StatPearls Publishing). Copyright © 2020, StatPearls Publishing LLC.

Liu, Y., Feinen, B., and Russell, M. W. (2011). New concepts in immunity to *Neisseria gonorrhoeae*: Innate responses and suppression of adaptive immunity favor the pathogen, not the host. *Front. Microbiol.* 2, 52. doi: 10.3389/fmicb.2011.00052

Marri, P. R., Paniscus, M., Weyand, N. J., Rendón, M. A., Calton, C. M., Hernández, D. R., et al. (2010). Genome sequencing reveals widespread virulence gene exchange among human *Neisseria* species. *PloS One* 5, e11835. doi: 10.1371/journal.pone.0011835

Martinez-Martinez, S., Frandoloso, R., Gutierrez-Martin, C. B., Lampreave, F., Garcia-Iglesias, M. J., Perez-Martinez, C., et al. (2011). Acute phase protein concentrations in colostrum-deprived pigs immunized with subunit and commercial vaccines against glässer's disease. *Vet. Immunol. Immunopathol.* 144, 61–67. doi: 10.1016/j.vetimm.2011.07.002

Martínez-Martínez, S., Frandoloso, R., Rodríguez-Ferri, E.-F., García-Iglesias, M.-J., Pérez-Martínez, C., Álvarez-Estrada, Á., et al. (2016). A vaccine based on a mutant transferrin binding protein b of *Haemophilus parasuis* induces a strong T-helper 2 response and bacterial clearance after experimental infection. *Vet. Immunol. Immunopathol.* 179, 18–25. doi: 10.1016/j.vetimm.2016.07.011

Martinez-Martinez, S., Rodriguez-Ferri, E. F., Frandoloso, R., Garrido-Pavon, J. J., Zaldivar-Lopez, S., Barreiro, C., et al. (2016). Molecular analysis of lungs from pigs immunized with a mutant transferrin binding protein b-based vaccine and challenged with *Haemophilus parasuis*. *Comp. Immunol. Microbiol. Infect. Dis.* 48, 69–78. doi: 10.1016/j.cimid.2016.08.005

Masson, P. L., and Heremans, J. F. (1968). Metal-combining properties of human lactoferrin (red milk protein). *Eur. J. Biochem.* 6, 579–584. doi: 10.1111/j.1432-1033.1968.tb00484.x

Maurakis, S., Keller, K., Maxwell, C. N., Pereira, K., Chazin, W. J., Criss, A. K., et al. (2019). The novel interaction between *Neisseria gonorrhoeae* TdfJ and human S100A7 allows gonococci to subvert host zinc restriction. *PloS Pathog.* 15, e1007937. doi: 10.1371/journal.ppat.1007937

McDowell, L. A., Kudaravalli, P., and Sticco, K. L. (2022). Iron overload. *StatPearls*.

Mickelsen, P. A., and Sparling, P. F. (1981). Ability of *Neisseria gonorrhoeae*, *Neisseria meningitidis*, and commensal *Neisseria* species to obtain iron from transferrin and iron compounds. *Infect. Immun.* 33, 555–564. doi: 10.1128/iai.33.2.555-564.1981

Miethke, M., and Marahiel, M. A. (2007). Siderophore-based iron acquisition and pathogen control. *Microbiol. Mol. Biol. Rev.* 71, 413–451. doi: 10.1128/MMBR.00012-07

Nairz, M., Haschka, D., Demetz, E., and Weiss, G. (2014). Iron at the interface of immunity and infection. *Front. Pharmacol.* 5, 152. doi: 10.3389/fphar.2014.00152

Nakashige, T. G., Zhang, B., Krebs, C., and Nolan, E. M. (2015). Human calprotectin is an iron-sequestering host-defense protein. *Nat. Chem. Biol.* 11, 765–771. doi: 10.1038/nchembio.1891

Na, N., Ouyang, J., Taes, Y. E., and Delanghe, J. R. (2005). Serum free hemoglobin concentrations in healthy individuals are related to haptoglobin type. *Clin. Chem.* 51, 1754–1755. doi: 10.1373/clinchem.2005.055657

Nemeth, E., Rivera, S., Gabayan, V., Keller, C., Taudorf, S. , Pedersen, B. K., et al. (2004a). IL-6 mediates hypoferremia of inflammation by inducing the synthesis of the iron regulatory hormone hepcidin. *J. Clin. Invest.* 113, 1271–1276. doi: 10.1172/JCI200420945

Nemeth, E., Tuttle, M. S., Powelson, J., Vaughn, M. B., Donovan, A. , Ward, D. M., et al. (2004b). Hepcidin regulates cellular iron efflux by binding to ferroportin and inducing its internalization. *Science* 306, 2090–2093. doi: 10.1126/science.1104742

Noinaj, N., and Buchanan, S. K. (2014). Structural insights into the transport of small molecules across membranes. *Curr. Opin. Struct. Biol.* 27, 8–15. doi: 10.1016/j.sbi.2014.02.007

Noinaj, N., and Buchanan, S. (2018). Editorial overview: Membranes and their embedded molecular machines. *Curr. Opin. Struct. Biol.* 51, vii–viii. doi: 10.1016/j.sbi.2018.10.005

Noinaj, N., Buchanan, S. K. , and Cornelissen, C. N. (2012a). The transferrin-iron import system from pathogenic *Neisseria* species. *Mol. Microbiol.* 86, 246–257. doi: 10.1111/mmi.12002

Noinaj, N., Cornelissen, C. N., and Buchanan, S. K. (2013). Structural insight into the lactoferrin receptors from pathogenic *Neisseria*. *J. Struct. Biol.* 184, 83–92. doi: 10.1016/j.jsb.2013.02.009

Noinaj, N., Easley, N. C., Oke, M., Mizuno, N., Gumbart, J. , Boura, E., et al. (2012b). Structural basis for iron piracy by pathogenic *Neisseria*. *Nature* 483, 53–58. doi: 10.1038/nature10823

Noinaj, N., Guillier, M., Barnard, T. J., and Buchanan, S. K. (2010). TonB-dependent transporters: regulation, structure, and function. *Annu. Rev. Microbiol.* 64, 43–60. doi: 10.1146/annurev.micro.112408.134247

Noinaj, N., Gumbart, J. C., and Buchanan, S. K. (2017). The beta-barrel assembly machinery in motion. *Nat. Rev. Microbiol.* 15, 197–204. doi: 10.1038/nrmicro.2016.191

Noto, J. M., and Cornelissen, C. N. (2008). Identification of TbpA residues required for transferrin-iron utilization by *Neisseria gonorrhoeae*. *Infect. Immun.* 76, 1960–1969. doi: 10.1128/IAI.00020-08

Nuijens, J. H., Abbink, J. J., Wachtfogel, Y. T., Colman, R. W., Eerenberg, A. J., Dors, D., et al. (1992). Plasma elastase alpha 1-antitrypsin and lactoferrin in sepsis: evidence for neutrophils as mediators in fatal sepsis. *J. Lab. Clin. Med.* 119, 159–168.

Ohnishi, M., Golparian, D., Shimuta, K., Saika, T., Hoshina, S., Iwasaku, K., et al. (2011). Is *Neisseria gonorrhoeae* initiating a future era of untreatable gonorrhea?: Detailed characterization of the first strain with high-level resistance to ceftriaxone. *Antimicrob. Agents Chemother.* 55, 3538–3545. doi: 10.1128/AAC.00325-11

Okubo, K., Kamiya, M., Urano, Y., Nishi, H., Herter, J. M., Mayadas, T., et al. (2016). Lactoferrin suppresses neutrophil extracellular traps release in inflammation. *EBioMedicine* 10, 204–215. doi: 10.1016/j.ebiom.2016.07.012

Page, M. G. P. (2019). The role of iron and siderophores in infection, and the development of siderophore antibiotics. *Clin. Infect. Dis.* 69, S529–s537. doi: 10.1093/cid/ciz825

Pantopoulos, K., Porwal, S. K., Tartakoff, A., and Devireddy, L. (2012). Mechanisms of mammalian iron homeostasis. *Biochemistry* 51, 5705–5724. doi: 10.1021/bi300752r

Pettersson, A., Maas, A., and Tommassen, J. (1994). Identification of the *iroA* gene product of *Neisseria meningitidis* as a lactoferrin receptor. *J. Bacteriol.* 176, 1764–1766. doi: 10.1128/jb.176.6.1764-1766.1994

Portnoy, J., Mendelson, J., Clecner, B., and Heisler, L. (1974). Asymptomatic gonorrhea in the male. *Can. Med. Assoc. J.* 110, 169.

Postle, K. (1993). TonB protein and energy transduction between membranes. *J. Bioenerg. Biomembr.* 25, 591–601. doi: 10.1007/bf00770246

Rageh, A. A., Ferrington, D. A., Roehrich, H., Yuan, C., Terluk, M. R., Nelson, E. F., et al. (2016). Lactoferrin expression in human and murine ocular tissue. *Curr. Eye Res.* 41, 883–889. doi: 10.3109/02713683.2015.1075220

Raymond, K. N., Dertz, E. A., and Kim, S. S. (2003). Enterobactin: An archetype for microbial iron transport. *Proc. Natl. Acad. Sci.* 100, 3584–3588. doi: 10.1073/pnas.0630018100

Renauld-Mongénie, G., Poncet, D., Mignon, M., Fraysse, S., Chabanel, C., Danve, B., et al. (2004). Role of transferrin receptor from a *Neisseria meningitidis tbpB* isotype II strain in human transferrin binding and virulence. *Infect. Immun.* 72, 3461–3470. doi: 10.1128/IAI.72.6.3461-3470.2004

Retzer, M. D., Yu, R., Zhang, Y., Gonzalez, G. C., and Schryvers, A. B. (1998). Discrimination between apo and iron-loaded forms of transferrin by transferrin binding protein b and its n-terminal subfragment. *Microb. Pathog.* 25, 175–180. doi: 10.1006/mpat.1998.0226

Rice, P. A. (2005). Gonococcal arthritis (disseminated gonococcal infection). *Infect. Dis. Clin. North Am.* 19, 853–861. doi: 10.1016/j.idc.2005.07.003

Rice, P. A., Shafer, W. M., Ram, S., and Jerse, A. E. (2017). *Neisseria gonorrhoeae*: Drug resistance, mouse models, and vaccine development. *Annu. Rev. Microbiol.* 71, 665–686. doi: 10.1146/annurev-micro-090816-093530

Rohde, K. H., and Dyer, D. W. (2003). Mechanisms of iron acquisition by the human pathogen *Neisseria meningitidis* and *Neisseria gonorrhoeae*. *Front. Biosci.* 33. doi: 10.2741/1133

Rohde, K. H., and Dyer, D. W. (2004). Analysis of haptoglobin and hemoglobin-haptoglobin interactions with the *Neisseria meningitidis* TonB-dependent receptor HpuAB by flow cytometry. *Infect. Immun.* 72, 2494–2506. doi: 10.1128/IAI.72.5.2494-2506.2004

Rohde, K. H., Gillaspy, A. F., Hatfield, M. D., Lewis, L. A., and Dyer, D. W. (2002). Interactions of haemoglobin with the *Neisseria meningitidis* receptor HpuAB: The role of TonB and an intact proton motive force. *Mol. Microbiol.* 43, 335–354. doi: 10.1046/j.1365-2958.2002.02745.x

Ross, A. C. (2017). Impact of chronic and acute inflammation on extra- and intracellular iron homeostasis. *Am. J. Clin. Nutr.* 106, 1581s–1587s. doi: 10.3945/ajcn.117.155838

Russell, M. W., Jerse, A. E. , and Gray-Owen, S. D. (2019). Progress toward a gonococcal vaccine: The way forward. *Front. Immunol.* 10, 2417. doi: 10.3389/fimmu.2019.02417

Schmidt, K. A., Schneider, H., Lindstrom, J. A., Boslego, J. W., Warren, R. A., Van De Verg, L., et al. (2001). Experimental gonococcal urethritis and reinfection with homologous gonococci in male volunteers. *Sex Transm. Dis.* 28, 555–564. doi: 10.1097/00007435-200110000-00001

Schryvers, A. B., and Morris, L. J. (1988). Identification and characterization of the human lactoferrin-binding protein from *Neisseria meningitidis*. *Infect. Immun.* 56, 1144–1149. doi: 10.1128/iai.56.5.1144-1149.1988

Schryvers, A. B., and Stojiljkovic, I. (1999). Iron acquisition systems in the pathogenic *Neisseria*. *Mol. Microbiol.* 32, 1117–1123. doi: 10.1046/j.1365-2958.1999.01411.x

Sia, A. K., Allred, B. E., and Raymond, K. N. (2013). Siderocalins: Siderophore binding proteins evolved for primary pathogen host defense. *Curr. Opin. Chem. Biol.* 17, 150–157. doi: 10.1016/j.cbpa.2012.11.014

Snyder, L. A., and Saunders, N. J. (2006). The majority of genes in the pathogenic *Neisseria* species are present in non-pathogenic *Neisseria lactamica*, including those designated as 'virulence genes'. *BMC Genomics* 7, 128. doi: 10.1186/1471-2164-7-128

Springer, C., and Salen, P. (2020). *Gonorrhea* (Treasure Island (FL: StatPearls Publishing). Copyright © 2020, StatPearls Publishing LLC.

Strange, H. R., Zola, T. A., and Cornelissen, C. N. (2011). The *fbpABC* operon is required for ton-independent utilization of xenosiderophores by *Neisseria gonorrhoeae* strain FA19. *Infect. Immun.* 79, 267–278. doi: 10.1128/IAI.00807-10

Tsai, J., Dyer, D. W., and Sparling, P. F. (1988). Loss of transferrin receptor activity in *Neisseria meningitidis* correlates with inability to use transferrin as an iron source. *Infect. Immun.* 56, 3132–3138. doi: 10.1128/iai.56.12.3132-3138.1988

Turner, P. C., Thomas, C. E., Stojiljkovic, I., Elkins, C., Kizel, G., Ala'aldeen, D. A. A., et al. (2001). Neisserial TonB-dependent outer-membrane proteins: Detection, regulation and distribution of three putative candidates identified from the genome sequences. *Microbiol. (Reading)* 147, 1277–1290. doi: 10.1099/00221287-147-5-1277

Unemo, M., Seifert, H. S., Hook, E. W., Hawkes, S., Ndowa, F., and Dillon, J. R. (2019). Gonorrhoea. *Nat. Rev. Dis. Primers* 5, 79. doi: 10.1038/s41572-019-0128-6

Urban, C. F., Ermert, D., Schmid, M., Abu-Abed, U., Goosmann, C., Nacken, W., et al. (2009). Neutrophil extracellular traps contain calprotectin, a cytosolic protein complex involved in host defense against *Candida albicans*. *PloS Pathog.* 5, e1000639. doi: 10.1371/journal.ppat.1000639

Valenti, P., Rosa, L., Capobianco, D., Lepanto, M. S., Schiavi, E., Cutone, A., et al. (2018). Role of lactobacilli and lactoferrin in the mucosal cervicovaginal defense. *Front. Immunol.* 9, 376. doi: 10.3389/fimmu.2018.00376

Walker, C. K., and Sweet, R. L. (2011). Gonorrhea infection in women: Prevalence, effects, screening, and management. *Int. J. Womens Health* 3, 197–206. doi: 10.2147/ijwh.S13427

Wandersman, C., and Delepelaire, P. (2004). Bacterial iron sources: from siderophores to hemophores. *Annu. Rev. Microbiol.* 58, 611–647. doi: 10.1146/annurev.micro.58.030603.123811

Weinberg, E. D. (1975). Nutritional immunity. host's attempt to withold iron from microbial invaders. *Jama* 231, 39–41. doi: 10.1001/jama.1975.03240130021018

Weiss, G. (1999). Iron and anemia of chronic disease. *Kidney Int. Suppl.* 69, S12–S17. doi: 10.1046/j.1523-1755.1999.055Suppl.69012.x

West, S. E., and Sparling, P. F. (1987). Aerobactin utilization by *Neisseria gonorrhoeae* and cloning of a genomic DNA fragment that complements *Escherichia coli fhuB* mutations. *J. Bacteriol.* 169, 3414–3421. doi: 10.1128/jb.169.8.3414-3421.1987

WHO (2021). Sexually transmitted infections (STIs).

Xiao, X., Yeoh, B. S., and Vijay-Kumar, M. (2017). Lipocalin 2: An emerging player in iron homeostasis and inflammation. *Annu. Rev. Nutr.* 37, 103–130. doi: 10.1146/annurev-nutr-071816-064559

Yadav, R., Govindan, S., Daczkowski, C., Mesecar, A., Chakravarthy, S., and Noinaj, N. (2021). Structural insight into the dual function of LbpB in mediating neisserial pathogenesis. *Elife* 10, e71683. doi: 10.7554/eLife.71683.sa2

Yadav, R., Noinaj, N., Ostan, N., Moraes, T., Stoudenmire, J., Maurakis, S., et al. (2019). Structural basis for evasion of nutritional immunity by the pathogenic *Neisseriae*. *Front. Microbiol.* 10, 2981. doi: 10.3389/fmicb.2019.02981

Zughaier, S. M., Kandler, J. L., and Shafer, W. M. (2014). *Neisseria gonorrhoeae* modulates iron-limiting innate immune defenses in macrophages. *PloS One* 9, e87688. doi: 10.1371/journal.pone.0087688

Frontiers in
Cellular and Infection Microbiology

Investigates how microorganisms interact with their hosts

Explores bacteria, fungi, parasites, viruses, endosymbionts, prions and all microbial pathogens as well as the microbiota and its effect on health and disease in various hosts.

Discover the latest Research Topics

See more →

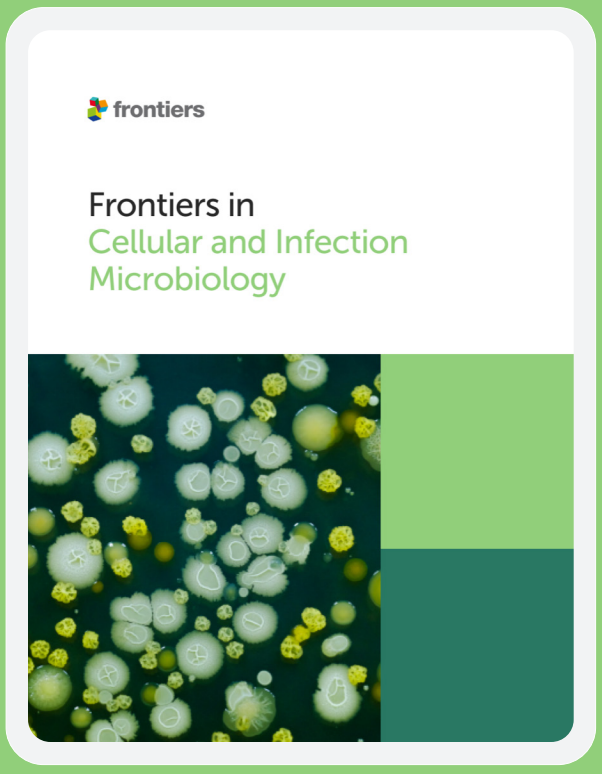

Frontiers

Avenue du Tribunal-Fédéral 34
1005 Lausanne, Switzerland
frontiersin.org

Contact us

+41 (0)21 510 17 00
frontiersin.org/about/contact